

Aus
der Augenklinik und Poliklinik
Ludwig-Maximilians-Universität München
(Direktor: Prof. Dr. med. Anselm Kampik)
und
dem Institut für Entwicklungsgenetik, Helmholtz Zentrum München
Deutsches Forschungszentrum für Gesundheit und Umwelt
(Direktor: Prof. Dr. rer. nat. Wolfgang Wurst)

The role of *Peroxidasin* and *Bmpr1b* in eye development and diseases



Dissertation
zum Erwerb des Doktorgrades der Humanbiologie
an der Medizinischen Fakultät der
Ludwig-Maximilians-Universität zu München

vorgelegt von

Xiaohe Yan

aus
Anhui, China

2014

Mit Genehmigung der Medizinischen Fakultät
der Universität München

Berichterstatter: Prof. Dr. med. Anselm Kampik

Mitberichterstatter: Prof. Dr. rer. nat. Anja Horn-Bochtler
Prof. Dr. med. Michael Meyer

Mitbetreuung durch den
promovierten Mitarbeiter: Prof. Dr. rer. nat. Jochen Graw

Dekan: Prof. Dr. med. Dr. h.c. Maximilian Reiser, FACR, FRCR

Tag der mündlichen Prüfung: 20.02.2014

Declaration

I declare that the thesis hereby submitted for the academic degree of Dr. rer. biol. hum. in the Faculty of Medicine has not been submitted for any other degrees in this or any other university. This thesis is independently performed by myself under the supervision of Prof. Dr. Jochen Graw in the Institute of Developmental Genetics, Helmholtz Center Munich from May, 2011 till May, 2013.

Contents

1	Summary	1
1.1	Summary	1
1.2	Zusammenfassung.....	3
2	Introduction.....	5
2.1	Eye development.....	5
2.1.1	General introduction to eye development	5
2.1.2	Anterior segment development (except lens)	5
2.1.3	Lens development	6
2.1.4	Molecular pathways during anterior segment development	8
2.1.5	Retinal development	12
2.2	Eye diseases in the study.....	14
2.2.1	Anterior segment dysgenesis (ASD).....	14
2.2.2	Retinal gliosis.....	16
2.2.3	Optic nerve coloboma/hypoplasia.....	18
2.2.4	Microphthalmia.....	19
2.3	Two proteins in eye development and diseases	19
2.3.1	Peroxidasin.....	19
2.3.2	Bmpr1b	21
2.4	Two new ENU-induced mouse mutants with different eye phenotypes.....	24
1.4.1	<i>KTA48</i> : ENU-induced <i>peroxidasin</i> -mutant mice.....	24
1.4.2	<i>Ali030</i> : ENU-induced <i>Bmpr1b</i> -mutant mice	25
3	Aims of the study	28
3.1	<i>KTA48</i> project	28
3.2	<i>Ali030</i> project.....	28
4	Materials and Methods.....	29
4.1	Materials	29
4.2	Methods.....	39
4.2.1	Animal experiments	39

4.2.2	Clinical samples	42
4.2.3	Histology.....	43
4.2.4	Molecular biology technology	49
4.2.5	Cell culture techniques.....	56
4.2.6	Protein techniques	57
4.2.7	<i>In vivo</i> retinal imaging and electrophysiology.....	58
4.2.8	Statistics	59
5	Results.....	60
5.1	Part I: <i>Peroxidasin</i> is essential for eye development	60
5.1.1	The expression of peroxidasin in the developing and postnatal eye.....	60
5.1.2	The point mutation in <i>peroxidasin</i> causes loss of function of peroxidasin..	65
5.1.3	Anterior segment and eye size are severely affected in <i>KTA48</i> mutant embryos during eye development	66
5.1.4	Reduced proliferation and aberrant differentiation of the lens during eye development in <i>KTA48</i> mutants.....	71
5.1.5	The defects in peroxidasin may affect eye development through regulation of Pax6 and Tgfb β 1 expression and increased inflammation	79
5.1.6	Axon guidance from optic disc to optic tract is not affected in <i>KTA48</i> mutant embryos at E15.5	83
5.1.7	<i>KTA48</i> is a new mouse model of anterior segment dysgenesis particularly Peters anomaly associated with microphthalmia and early-onset glaucoma.....	84
5.2	Part II: <i>Bmpr1b</i> is essential for optic nerve and ventral retinal development	92
5.2.1	Mis-splicing of exon 10 in <i>Ali030</i> homozygous mutants	92
5.2.2	Optic nerve head hypoplasia and ventral retinal gliosis without lens phenotypes in <i>Ali030</i> mutants.....	93
5.2.3	Activated glial cells in the optic nerve head and in the ventral retina, and hypodevelopment of the optic nerve in <i>Ali030</i> mutants	97
5.2.4	Loss of ventral retinal ganglion cells, axon misguidance in ventral retina and defective axons in the optic nerve in <i>Ali030</i> mutants	102
5.2.5	Retinal dysgenesis is associated with reactive gliosis in <i>Ali030</i> mutants..	104

5.2.6	Regular ERG response in <i>Ali030</i> aged mutants.....	106
5.2.7	Glial-like cells expressing Sox2, Pax2 and Nestin but not Pax6 are found in the ventral retinal gliosis and they are proliferating in <i>Ali030</i> mutants	108
5.2.8	Mis-splicing of <i>Bmpr1b</i> may not play a role in the activation of retinal Müller cells <i>in vitro</i>	117
5.2.9	A delayed retinal development, ectopical expression of Pax2 and congenital ventral retinal gliosis in <i>Ali030</i> mutants during eye development	118
5.2.10	Glial-like cells expressing Sox2, Pax2 and Nestin are found in the epiretinal membranes and in the inner limiting membranes in patients with retinal gliosis.....	122
6	Discussion.....	129
6.1	Peroxidasin is essential for eye development	129
6.2	Bmpr1b is essential for optic nerve and ventral retinal development.....	137
7	References.....	143
8	Abbreviations.....	170
9	Acknowledgements.....	175

1. Summary

1.1 Summary

Many studies demonstrated that transcription factors are critical for eye development, such as Pax6, Pax2, Sox2 and Foxe3. However, the roles of other proteins rather than transcription factors in eye development are largely unknown. Here, I focus on the role of two fascinating and conserved proteins rather than transcription factors in eye development, one is peroxidasin and the other one is Bmpr1b.

Peroxidasin is an extracellular peroxidase combining with multiple domains found in extracellular matrix molecules. The manifestations of patients with *peroxidasin (PXDN)* mutations seem to be confined to the eyes including corneal opacity, congenital cataract and developing glaucoma. However, the function of peroxidasin in higher organisms is still largely unknown. Here, I explored the role of peroxidasin in eye development using an ENU-induced *peroxidasin (Pxdn)* mutant mouse line (with the point mutation in the peroxidase domain). Peroxidasin is expressed in the lens vesicle, developing lens and vitreous nucleated cells and the inner part of the retina. In *peroxidasin*-mutant mice, the anterior segment and eye size are severely affected which starts from embryonic stages, especially at E15.5. Moreover, the proliferation and differentiation of the lens is disrupted in association with aberrant expression of transcription factor genes (*Pax6* and *Foxe3*) and *Tgfb1* during eye development. In addition, it is also involved in the consolidation of basement membrane in the mammalian eyes. Lens matrix including γ -crystallin in the anterior chamber due to local lens ruptures is a secondary damage to the anterior segment development. Further, the mutant eyes are associated with up-regulated expression of inflammation markers (TNF- α and IL-1 β) during eye development. Early-onset glaucoma was detected in the *Pxdn* mutants in the postnatal periods and it develops progressively. Thus, this study has shown that peroxidasin has multiple roles in eye development, including cell proliferation and differentiation, basement membrane consolidation and regulation of the inflammation.

The other protein, Bmpr1b (Bmp receptor type 1b), is a receptor for Bmp signaling. In previous studies, Bmpr1b was found to be involved in retinal axon guidance, and ablation of *Bmpr1a* and

Bmpr1b causes defects in retinal neurogenesis and dorso-ventral patterning in mice. Here, I further investigated the role of *Bmpr1b* in eye development using a mutant mouse line caused by a splice donor site mutation in intron 10 of *Bmpr1b*. This point mutation results in RNA mis-splicing (skipping of exon 10), which is predicted to affect the cytoplasmic domain including the conserved serine/threonine kinase activity. Then this event further has caused delayed closure of ventral optic fissure and dysregulated the expression of Pax2 during embryonic retinal development, leading to optic nerve hypoplasia and congenital ventral retinal gliosis in association with retinal dysplasia in mice. The ventral retinal gliosis is proliferative and dominated by activated astrocytes but not retinal Müller cells. Interestingly, some of activated glial cells seem to be from retinal neurons (retinal ganglion cells and bipolar cells). These activated glial cells express some progenitor cell markers such as Sox2, Pax2 and Nestin, but not Pax6. Consistent with this result, similar activated glial cells were also found in epiretinal membranes (ERMs) and inner limiting membranes (ILMs) from patients with retinal gliosis. Moreover, the axons in the optic nerve are disorganized in association with decreased number of Sox2-positive precursor cells in mutants, indicating a maldevelopment of the optic nerve. In addition, axon guidance is disrupted in the ventral retina in mutants. This study demonstrated that *Bmpr1b* is essential for ventral retinal and optic nerve development, and the activated glial cells expressing progenitor cell markers may play a general role in the pathogenesis of retinal gliosis in mice and humans.

1.2 Zusammenfassung

Viele Studien zeigen, dass Transkriptionsfaktoren (Pax6, Pax2, Sox2 und Foxe3) entscheidend für die Entwicklung des Auges sind. Die Funktion anderer Proteingruppen ist dagegen weitgehend unbekannt. Zu diesen Gruppen zählen unter anderem Peroxidasin und BMPR1B, deren Rolle in der Augenentwicklung im Rahmen dieser Arbeit untersucht wurde.

Peroxidasin ist eine extrazelluläre Peroxidase, die mit mehreren Domänen von extrazellulären Matrix-Molekülen interagiert. Patienten mit Peroxidasin - Mutationen scheinen ausschließlich im Auge betroffen zu sein, wobei Hornhauttrübungen, kongenitale Katarakte und Glaukome auftreten. Allerdings ist die Funktion von Peroxidasin in höheren Organismen noch weitgehend unbekannt. Im Rahmen dieser Arbeit wird die Rolle von Peroxidasin in der Entwicklung des Auges mit Hilfe einer ENU - induzierten Peroxidasin (*Pxdn*) - Mausmutante untersucht, die eine Punktmutation in der Peroxidase-Domäne trägt. Peroxidasin wird in frühen Entwicklungsstadien in der Linsenplakode exprimiert. Zu späteren Zeitpunkten findet sich eine Expression vor allem im Bereich der vorderen Linse, in mesenchymalen Zellen und in der inneren Retina. In den Peroxidasin-Mutanten sind die vorderen Augensegmente und die Augengröße stark betroffen. Diese Auswirkungen treten bereits in embryonalen Stadien auf, vor allem ab dem Zeitpunkt E15.5. Darüber hinaus sind während der Augenentwicklung Proliferation und Differenzierung der Linse betroffen in Verbindung mit irregulärer Expression von Transkriptionsfaktoren (Pax6 und Foxe3) und TGF β 1. Weiterhin ist Peroxidasin auch an der Entwicklung der Basalmembran im Säugetierauge beteiligt. Linsenaufbrüche und der damit verbundene Eintritt von Linsenmaterial in die vordere Augenkammer (einschließlich γ -Kristallin) stellen sekundäre pathologische Effekte während der vorderen Augenentwicklung dar. Darüber hinaus ist in den betroffenen Augen die Expression von Entzündungsmarkern (TNF- α und IL-1 β) während der Entwicklung hochreguliert. In den *Pxdn* - Mutanten traten Glaukome schon in frühen postnatalen Stadien auf und zeigten einen progressiven Verlauf. Im Rahmen dieser Studie wurde gezeigt, dass Peroxidasin verschiedene Funktionen während der Augenentwicklung übernimmt. Dies schließt eine Beteiligung an der Zellproliferation und Differenzierung, an der Entwicklung der Basalmembran sowie an der Regulation von Entzündungsreaktionen mit ein.

BMPR1B (BMP-Rezeptor Typ 1 b) ist ein Rezeptorprotein des BMP-Signalwegs. In früheren

Studien wurde gezeigt, dass BMPR1B an der Orientierung der retinalen Nervenfasern beteiligt ist. Die Deletion von BMPR1A und BMPR1B führt zu einer fehlerhaften retinalen Neurogenese sowie zu einer inkorrekten Ausbildung des dorso-ventralen Musters in Mäusen. Im Rahmen dieser Arbeit wurde die Rolle von BMPR1B in der Entwicklung des Auges mit Hilfe einer mutierten Mauslinie untersucht, die durch eine Mutation in der Spleißdonorstelle des Introns 10 von *Bmpr1b* charakterisiert ist. Diese Punktmutation führt zu einem irregulären Spleißen der mRNA mit einem Ausschluss von Exon 10, das voraussichtlich für die Zytoplasma-Domäne einschließlich der konservierten Serin/Threonin-Kinase-Aktivität kodiert. Dies führt zu einer verzögerten Schließung der ventralen optischen Naht sowie zu einer irregulären Pax2 Expression während der embryonalen Retinaentwicklung. Letztendlich kommt es zu einer Hypoplasie des Sehnervs sowie zu einer ventralen retinalen Gliose in Verbindung mit einer Retinadysplasie in den betroffenen Mäusen. Die ventrale retinale Gliose ist sehr ausgeprägt und scheint durch aktivierte Astrozyten, aber nicht durch retinale Müller Zellen dominiert zu werden. Interessanterweise scheinen einige der aktivierten Gliazellen von Netzhautneuronen (retinale Ganglienzellen und bipolar Zellen) zu stammen. Diese aktivierten Gliazellen exprimieren einige Marker für Vorläuferzellen wie Sox2, Pax2 und Nestin, nicht jedoch Pax6. In Übereinstimmung mit diesem Ergebnis wurden ähnliche aktivierte Gliazellen auch in epiretinalen Membranen (ERM) und in inneren Grenzmembranen (ILM) von Patienten mit retinaler Gliose gefunden. Darüber hinaus sind in Mutanten die Sehnervaxone fehlerhaft organisiert in Verbindung mit einer verringerten Anzahl von Sox2-positiven Vorläuferzellen. Dies deutet auf eine fehlerhafte Entwicklung des Sehnervs hin. Darüber hinaus ist in Mutanten die Axonausrichtung innerhalb der ventralen Retina gestört. In dieser Arbeit wurde gezeigt, dass BMPR1B für die Entwicklung der ventralen Retina und des Sehnervs essentiell ist. Ferner könnten die aktivierten Gliazellen, die Marker für Vorläuferzellen exprimieren, eine allgemeine Rolle während der Pathogenese der retinalen Gliose in Mäusen und Menschen spielen.

2. Introduction

2.1 Eye development

2.1.1 General introduction to eye development

Eye development is a complex developmental process involving different molecular signaling interactions within and from different tissues (mainly cornea, lens, vitreous and retina (Figure 1.1, A)). The eye development originates from three different tissues during early development, neuroectoderm, surface ectoderm and periocular mesenchyme. The neuroectoderm gives rise to the retina, the epithelium of the iris and ciliary body, the smooth muscle of the iris and optic nerve. The surface ectoderm gives rise to the corneal epithelium, lens, eyelids and lacrimal apparatus. The periocular mesenchyme migrates into the eye during the optic cup formation and gives rise to the stroma and endothelium of the cornea, iris and ciliary body, trabecular meshwork, choroid and the vessel of the eyes.

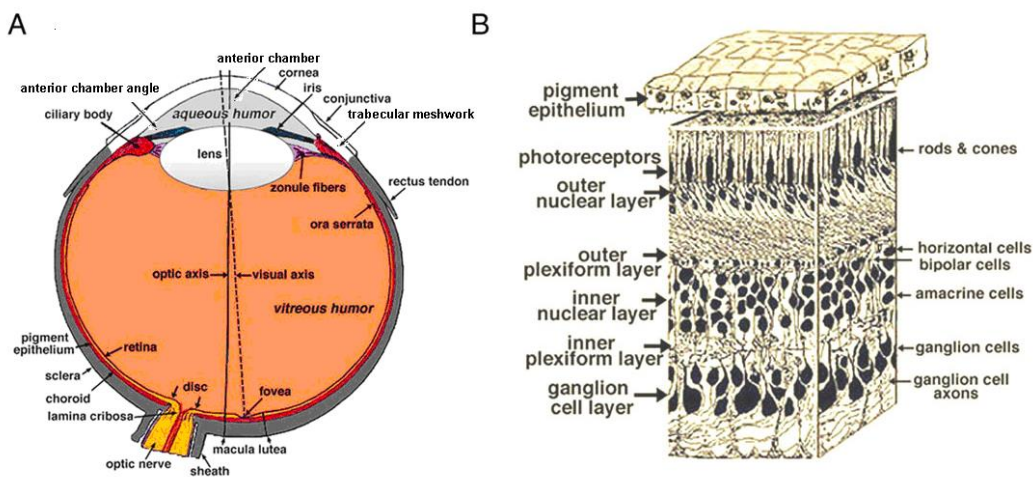


Figure 1.1 The anatomy of the eye. (A) Anterior segment of the eye comprises the structure before the front face of the vitreous and mainly include cornea, anterior chamber, iris, ciliary body, anterior chamber angle, trabecular meshwork and lens. Posterior segment of the eye contains vitreous, retina, retinal pigment epithelium and optic nerve. (B) A section of retina. The retina is composed of different layers of neurons and glial cells, including retinal pigment epithelium, photoreceptor, outer nuclear layer, outer plexiform layer, inner nuclear layer, inner plexiform layer, retinal ganglion cell layer outside to inside. The outside of the retina is covered with internal limiting membrane. (The picture from webvision.med.utah.edu.cn)

2.1.2 Anterior segment development (except lens)

Anterior segment contains the front part of the eye, including cornea, anterior chamber, iris, ciliary body, anterior chamber angle, trabecular meshwork and lens (Figure 1.1, A). The anterior segment

development is coordinated by interactions between lens vesicle, surface ectoderm and ocular mesenchymal cells. Ocular mesenchymal cells play a key role in the anterior segment development. In general, corneal development starts from the stage that lens vesicle makes contact with the overlying surface ectoderm. Then the single cell layer of surface ectoderm proliferate and form 3-4 cell layers of corneal epithelium. Shortly after the lens vesicle is separated from lens surface ectoderm, the mesenchymal cells of neural crest origin in the space between corneal epithelium and lens differentiate into corneal stromal keratocytes and endothelium (Figure 1.2, A-B). The mesenchymal cells in the anterior chamber angle also contribute to the formation of the iris and ciliary body and trabecular meshwork (Figure 1.2, C-D).

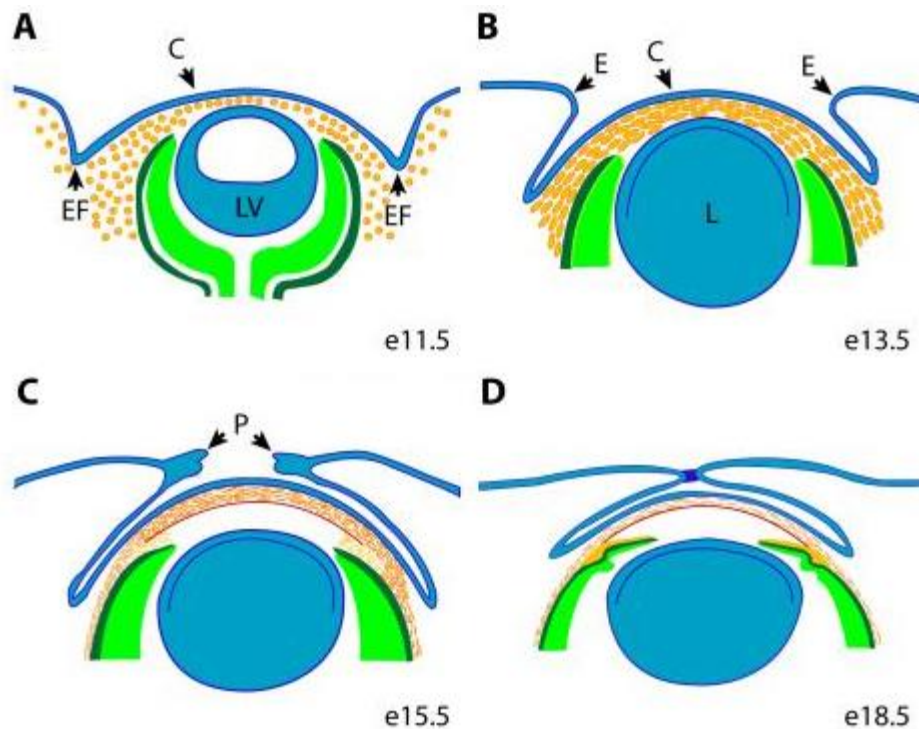


Figure 1.2 The development of ocular mesenchymal cells during anterior segment development. (A) In the early eye development, mesenchymal cells (yellow, round) migrate into the front part of the eye between surface ectoderm (blue) and lens vesicle (LV) at E11.5. (B-D) The mesenchymal cells aggregate in organized layers at E13.5 and differentiate into corneal stromal cells and endothelial cells around E13.5-E15.5 and further differentiate into the iris and form proper corneal-iris angle after E17.5. C, cornea; EF, eyelid folds; E, eyelid; P, periderm (The picture from Gage and Zacharias, 2009)

2.1.3 Lens development

The first step of lens morphogenesis is that surface ectoderm thickens to form the lens placode (Figure 1.3, A-B). Then the surface ectoderm invaginates and further forms the optic vesicle,

followed by the separation of the optic vesicle from surface ectoderm, and thus lens vesicle is formed (Figure 1.3, C-D). The epithelial cells in the posterior part of the lens vesicle begin to proliferate and further differentiate into primary lens fiber cells; these lens fiber cells elongate and fill up the lens vesicle (Figure 1.3, E). The epithelial cells around the lens equator still proliferate and have the capacity to differentiate into the fiber cells throughout life of the organisms. These newly-formed fiber cells elongate in the anterior-posterior direction and form secondary fiber cells, which are laid down around the primary lens fiber cells. Both, the primary and secondary lens fiber cells lose their cytoplasmic organelles including nucleus, mitochondria and endoplasmic reticulum, and become transparent forming an organelle-free zone in the lens center. The innermost part of the lens is made up of primary lens fibers surrounded by secondary fiber cells and newly-formed secondary fiber cells. The lens development is a complex process involving cell proliferation, cell differentiation, cell migration and organelle degradation. The anterior epithelial cells of the lens remain active. The lens capsule is detected at E11.5 after the lens vesicle is separated from surface ectoderm. Then the lens capsule thickens and has also the permeability to make some molecules selectively diffuse into the lens, such as growth factors and nutrients. The lens epithelium and fiber cells secrete some basement membrane molecules which are involved in the formation and consolidation of the lens capsule. The capsule is also necessary for lens epithelium survival (Danysh and Duncan, 2009).

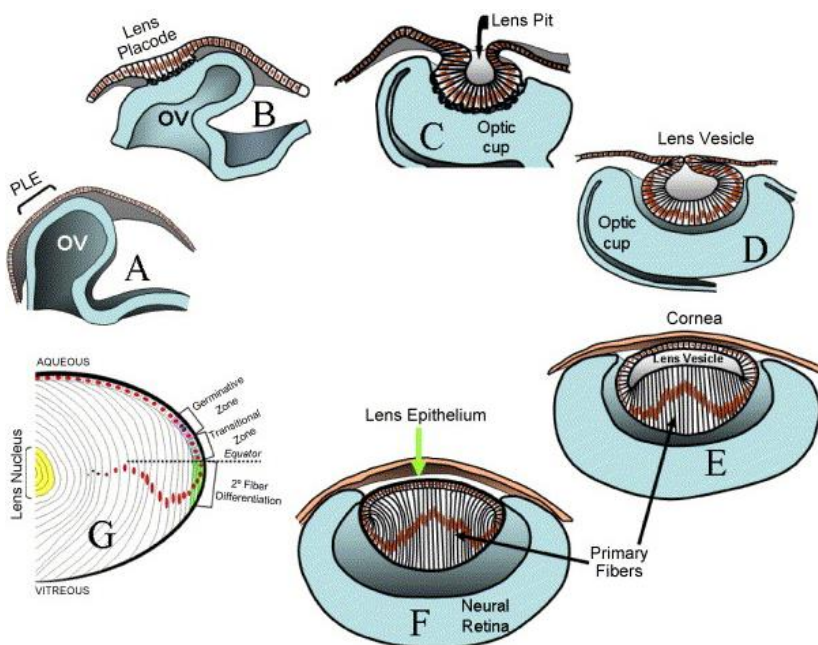


Figure 1.3 Lens development. (A-B) At the earliest stage of eye development, the surface ectoderm thickens to form lens placode once it contacts with optic vesicle (OV). (C-D) Then the placode invaginates and forms the lens vesicle followed by its separation from the lens placode. (E) The posterior lens epithelial cells proliferate and differentiate into the lens fiber cells, which elongate to fill the lens vesicle, which are called primary fibers. (F-G) The lens epithelium in the equator of the lens proliferates and differentiates into the secondary lens fibers. PLE: presumptive lens ectoderm; OV: optic vesicle. (The picture from Robinson, 2006)

2.1.4 Molecular pathway during anterior segment development

Transcription factors

Pax6 (Paired box gene 6)

Pax6 is a “master control” and highly-conserved gene for eye development. The canonical Pax6 consists of an N-terminal paired domain, a linker region to a paired-type homeodomain, and a proline/serine/threonine (P/S/T)-rich C-terminal domain. The paired domain and paired-type homeodomain have DNA-binding capacity and the P/S/T-rich domain contains the transactivation activity. Pax6 has three isoforms, the canonical Pax6, Pax6 (5a), and Pax6 (Δ PD). Pax6 (5a) contains a 14 amino acid insertion in the paired domain due to alternative splicing of exon 5a, resulting in a low capacity of DNA binding. Pax6 (Δ PD) or paired-less isoform encodes from an alternative translate start codon of the paired domain. Thus, Pax6 (Δ PD) has no DNA binding capacity.

Patients with heterozygous *PAX6* mutations manifest variable phenotypes, including aniridia, coloboma of the iris and choroid, or anterior segment malformations (Lin et al., 2011) and aniridia and cataract (Cai et al., 2010). Some patients with *PAX6* mutations also showed Peters anomaly (Jia et al., 2010; Nanjo et al., 2004), Rieger syndrome (Riise et al., 2001) and autosomal dominant keratitis (Mirzayans et al., 1995). Some mutations lead to congenital nystagmus, foveal hypoplasia, iris hypoplasia or atypical coloboma (Vincent et al., 2004) and ocular anterior segment anomalies including uveal ectropion of the iris, invasion of the conjunctival epithelia into the cornea, and posterior embryotoxon caused by a missense mutation of the *PAX6* gene (Azuma and Yamada, 1998). But another study showed that *PAX6* is not affected in most patients with Peters anomaly (Churchill et al., 1998). In mice, homozygous mutations in *Pax6* lead to anophthalmia (no eyes) and embryo lethality (Hill et al., 1991; Puk et al., 2013). Heterozygous mutations in *Pax6* causes a wide spectrum of anterior segment abnormalities including Peters anomaly in mice (Baulmann et al., 2002; Hanson et al., 1994) and corneal opacity including thinner corneal epithelium and thicker corneal stroma and microphthalmia (smaller eyes) (Ramaesh et al., 2003), which are similar to the symptoms observed in the patients. Interestingly, overexpression of Pax6 also causes microphthalmia and anterior segment dysgenesis (Schedl et al., 1996; Manuel et al., 2008).

Foxc1 (Forkhead box C1)

Interestingly, mutations in *FOXC1* cause a similar phenotype, including Axenfeld-Rieger syndrome (Panicker et al., 2002), Peters anomaly and iris hypoplasia. Global or neural crest-specific *Foxc1* null mutant mice exhibit corneal neovascularization and excessive growth of lymphatic vessels which is associated with aberrant extracellular matrix and up-regulation of matrix metalloproteinase (MMP) (Seo et al., 2012). A zebrafish study showed that vascular basement membrane is disrupted caused by loss of FoxC1 (Skarie and Link, 2009), suggesting a possible role of FoxC1 in glaucoma development. Haploinsufficiency of *Foxc1* also results in anterior segment dysgenesis in mice, which is similar to human patients (Smith et al., 2000). Further work demonstrated that FGF19 is a direct target of FOXC1 in corneal and mesenchymal cells (Tamimi et al., 2006) which provide a mechanism for the role of FOXC1 in the anterior segment development.

Foxe3 (Forkhead box protein E3)

The manifestations of patients with *FOXE3* mutations are variable. Some patients showed a variable phenotype of anterior segment dysgenesis including Peters anomaly (Doucette et al., 2011), while others showed sclerocornea, aphakia, microphthalmia and optic nerve coloboma (Ali et al., 2010), congenital aphakia (Anjum et al., 2010), microphthalmia associated with aphakia and/or corneal defects without systemic diseases (Reis et al., 2010) and anterior segment dysgenesis and microphthalmia (Semina et al., 2001).

Foxe3 is a key transcription factor for lens development and *Foxe3* is mapped to the short arm of chromosome 4 in mice. It can be detected in the developing eye at E9.5, the earliest stage for eye development in mice, and later it is only expressed in the lens epithelial cells in the eyes during the embryonic and postnatal periods. The first study on Foxe3 and lens development in the mouse is that mutants *dysgenetic lens (dyl)* with the mutation in *Foxe3* exhibit reduced proliferation of the lens epithelium and persistent lens-corneal adhesion, suggesting that it is necessary for lens proliferation and closure of the lens vesicle (Blixt et al., 2000). *Foxe3*-null mice exhibit the anterior segments including iris, cornea, ciliary body and trabecular meshwork are malformed (Blixt et al., 2007), and the *Foxe3*-null mice are regarded as a model of Peters anomaly (Ormestad et al., 2002), and in these mutant mice, the proliferation and differentiation of the lens epithelial cells are also affected (Medina-Martinez et al., 2005). In addition, persistent activation of Foxe3 causes a partial

epithelialization of lens fiber cells (Landgren et al., 2008). A few studies investigated the upstream regulator of *Foxe3* *in vivo* and *in vitro*. Recent data from our lab strongly supports that *Pitx3* is a direct upstream regulator of *Foxe3* in mice, which explains the eye phenotype of aphakia and dysgenetic lens in *Pitx3* mutants (Naffees Ahmed, PhD dissertation, Technical University of Munich, 2011). In addition, *Msx-2* (*Msh* homeobox 2) is regarded as another upstream molecule regulating *Foxe3*, since the expression of *Foxe3* is greatly reduced in the lens epithelium of the *Msx-2* knockout mice (Zhao et al., 2012).

Pitx2 and *Pitx3*

Pitx2 (Paired-like homeodomain transcription factor 2)

Mutations in *PITX2* also can cause anterior segment dysgenesis in humans including Axenfeld-Rieger syndrome (Idrees et al., 2006; Vieira et al., 2006; Li et al., 2008; Footz et al., 2009). The neural crest-specific *Pitx2* knockout mice exhibit anophthalmia and severe optic nerve defects (Evans and Gage, 2005). The upstream and downstream regulators of *Pitx2* are largely unknown. *Gpr48* (G protein-coupled receptor 48) was found to be an upstream regulator of *Pitx2* (Weng et al., 2008). *Pitx2* is found to be a responsive gene for retinoic acid during eye development (Matt et al., 2008). Recently, retinoic acid was found to be a key upstream molecule regulator of *Pitx2* during eye and craniofacial development in a zebrafish model of Axenfeld-Rieger syndrome (Bohnsack et al., 2012). In addition, *Pitx2* also regulates the morphogenesis of extraocular muscles (Kitamura et al., 1999; Diehl et al., 2006).

Pitx3 (Paired-like homeodomain transcription factor 3)

Pitx3 is expressed in the lens epithelium and midbrain dopaminergic neurons (Dutta et al., 2005; Korotkova et al., 2005). Mutations in *PITX3* causes microphthalmia and aphakia in mice and congenital cataract with anterior segment dysgenesis (ASD) in humans (Semina et al., 1998). Similar to humans, two deletions in *Pitx3* also causes severe abnormal lens development in *aphakia* mice (Semina et al., 2000; Rieger et al., 2001). A point mutation in *Pitx3* also causes microphthalmia in mice (Rosemann et al., 2010). The development and differentiation of the lens in *Pitx3*-mutants is severely disrupted (Medina-Martinez et al., 2009). In addition, *Pitx3* also plays a role in Parkinson's disease (Li et al., 2009; Rosemann et al., 2010). The direct target of *Pitx3* is still unclear, but recently it was shown that *Pax6*, *Crybb1* (β B1-Crystallin), *Hes 7.1* (*Hes*, Hairy

and enhancer of split), and *Hes4* are likely to be direct targets of Pitx3 based on microarray identification (Hooker et al., 2012). The data from our lab strongly supports that Pitx3 is a direct upstream regulator of *Foxe3* in mice (Naffees Ahmed, PhD dissertation, Technical University of Munich, 2011).

BMP (Bone morphogenetic protein) signaling

Overexpression of *Tgfb1* (Transforming growth factor beta 1) with β B-crystallin promoter causes severe anterior segment dysgenesis without microphthalmia in the transgenic mice (Flügel-Koch et al., 2002). Another *Tgfb1* transgenic mouse line with α A-crystallin promoter showed subcapsular cataract formation (Banh et al., 2006), but corneal-lens adhesion and disorganized lens matrix can be found from the histology picture although the authors did not mention it in the text. In consistency with this study, overexpression of *Beta ig-h3* (Transforming growth factor-beta-induced protein ig-h3) also causes anterior segment dysgenesis in mice (Kim et al., 2007). In addition, *Bmp4*, another member of the Bmp family, is also important for anterior segment development. Lens induction is defective and the lens cannot be formed in *Bmp4* homozygous null mutant mice (Furuta and Hogan, 1998), and haploinsufficiency of *Bmp4* results in anterior segment dysgenesis and elevated ocular pressure (Chang et al., 2001). These data showed that Bmp signaling is important for eye development. The role of Bmp receptors in eye development will be discussed later (2.3.2).

Extracellular matrix (ECM)

ECM is a complex network of extracellular macromolecules surrounding most of the cells in the multicellular organisms. ECM interactions play essential roles during organ development and many pathological processes. Several studies showed that extracellular matrix molecules are essential for anterior segment development (Hopfer et al., 2005; Van Agtmael et al., 2005; Rødahl et al., 2013). Collagen IV is a main component of the basement membrane. Patients with a *COL4A1* (*Collagen 4A1*) mutation manifest variable anterior segment phenotypes with corneal clouding, anterior synechiae, iris hypoplasia, posterior embryotoxon, corectopia (displacement of the pupil) and early cataract (Rødahl et al., 2013). In mice, mutations in *Col4a1* causes anterior segment dysgenesis including buphthalmos (enlarged eye increased by intraocular pressure), corneal

opacity, iris-corneal adhesion and vacuolar cataracts which are associated with the defects of the basement membrane (Van Agtmael et al., 2005). A point mutation in *Col8a2* (*Collagen 8a2*) showed increased anterior chamber depth, extended axial length and reduced thickness of corneal layers but without reduced visual acuity in mice (Puk et al., 2009). Further studies showed that this mutant line seems to be resistant to the retinal ganglion cells damage induced by ocular pressure (Steinhart et al., 2012). Also, targeted inactivation of *Col8a1* (*Collagen 8a1*) and *Col8a2* causes thinner corneal stroma and Descemet's membrane, and decreased proliferation of corneal endothelial cells (Hopfer et al., 2005). Compared with *Col8a1* and *Col8a2*, *Col4a1* showed more important roles in the development of anterior segment. These findings suggest that ECM plays a novel and specific role during anterior segment development.

Other genes

G protein-coupled receptor 48 (Gpr48)

Gpr48, also known as LGR4, is a member of G protein-coupled receptors (GPCRs). It consists of leucine-rich repeats in the N-terminal and several transmembrane domains. The ligand of Gpr48 is unknown. Deletion of *Gpr48* leads to a broad spectrum of anterior segment dysgenesis in mice, including microphthalmia, iris hypoplasia, iris-cornea angle malformation, corneal dysgenesis and cataract and early-onset glaucoma and *Pitx2* was found to be a direct target of Gpr48 (Weng et al., 2008). This study suggests that the signaling receptors are also very important for eye development.

2.1.5 Retinal development

In general, there are seven layers in the mammalian retina including retina pigmental epithelium (RPE), outer segment of the photoreceptors (OS), outer nuclear layer (ONL), outer plexiform layer (OPL), inner nuclear layer (INL), inner plexiform layer (IPL), retinal ganglion cell layer (GCL) from outside to inner part (Figure 1.1). There is a nerve fiber layer on the surface of the retinal ganglion cell (RGC) layer which consists of axons from RGCs. The first six layers are usually called neuroretina, which is separated from RPE by a tiny space called subretinal space. The neuroretina contains six types of retinal neurons including rod and cone photoreceptors, amacrine cells, horizontal cells, bipolar cells, retinal ganglion cells and one type of glial cells (retinal Müller cells). There are also retinal astrocytes whose origin is from a distinct progenitor in the optic stalk and optic nerve during eye development (Stone and Dreher, 1987; Ling and Stone, 1988; Watanabe

and Raff, 1988). The photoreceptor layer consists of the outer segment (OS) of rod and cone photoreceptors. The outer nuclear layer contains the cell bodies from rod and cone photoreceptors. The inner nuclear layer consists of the cell bodies of bipolar cells, horizontal cells and amacrine cells. The axons from retinal ganglion cells comprise the retinal nerve fiber layer. The outer plexiform layer is composed of the axons and synapses between photoreceptor cells, horizontal cells and bipolar cells, and the inner plexiform layer contains the axons and synapses between amacrine cells, bipolar cells and retinal ganglion cells.

In the early retinal development, progenitor cells are multi-potent with the ability to differentiate into all the types of retinal cells. As they divide symmetrically, one begins to differentiate into a specific type of retina cell, and the other one still keep its multi-potent competence, but they receive different signals, such as signaling through lateral inhibition, to restrict them to produce the same type of retinal cells (Agathocleous and Harris, 2009; Reese, 2011). Thus, the retinal cells are generated in a defined sequence: retinal ganglion cells generate firstly followed by cone photoreceptors, horizontal cells and amacrine cells during embryonic stages, and rod photoreceptors, bipolar cells and Müller glia are generated after birth in mice (Agathocleous and Harris, 2009; Reese, 2011). However, retinal astrocytes are regarded to come from a distinct progenitor in the optic stalk and optic nerve during eye development (Stone and Dreher, 1987; Ling and Stone, 1988; Watanabe and Raff, 1988).

There are a number of genes encoding transcription factors which regulate retinal development. Multiple basic helix-loop-helix (bHLH) genes are well studied and they play a key role in regulating differentiation of the retinal progenitor cells (Ohsawa and Kageyama, 2008), and these different types of bHLH genes cross-regulate each other to specify the retinal neuronal subtypes (Akagi et al., 2004). Math 5 (Helix-loop-helix protein mATH-5) is critical for retinal ganglion cell development and deletions of Math5 or Ath5 (Ath5 in zebrafish equals Math5 in mouse) causes dramatic loss of retinal ganglion cells (Brown et al., 2001; Kay et al., 2001). But the following study traced the fate of Math5-expressing progenitor cells during retinal development and found they can differentiate into multiple types of retinal neurons, indicating that Math5 defines the competence of the retinal ganglion cell progenitors but it is not a final determinant of retinal ganglion cells (Yang et al., 2003). The member of Brn3 (POU-domain transcription factors) family

also plays a key role for retinal ganglion cell development. Deletions of *Brn3* also greatly reduced the number of retinal ganglion cells (Erkman et al., 1996; Gan et al., 1996). *Ath5* was found to function upstream of *Brn3* to regulate retinal ganglion cell development (Liu et al., 2001). It appears that amacrine cells and horizontal cells have common regulators (Graw, 2010). *Foxn4* (Forkhead box N4) controls the genesis of retinal amacrine cells and horizontal cells. Disruption of *Foxn4* causes greatly decreased number of retinal amacrine cells and completely loss of horizontal cells, whereas overexpression of *Foxn4* promotes the fate of amacrine cells (Li et al., 2004). *Barhl2* (BarH-like homeobox 2) is another key factor for amacrine cells development. In *Barhl2*-deficient mice, the number of glycinergic and GABAergic amacrine cells is decreased, whereas the number of cholinergic amacrine cells is increased (Ding et al., 2009). *Mash1* (Mammalian achaete-scute complex homolog-1) and *Math3* (Helix-loop-helix protein *mATH-3*) are required for the fate determination of retinal bipolar cells. Either *Mash1* or *Math3* mutants showed very weak defects, whereas *Mash1* and *Math3* double mutants exhibit a lack of retinal bipolar cells, and these bipolar cells become retinal Müller cells (Tomita et al., 2000). The photoreceptor cells fate is controlled by *Otx2* (Orthodenticle homeobox 2) and *Crx* (Cone-rod homeobox transcription factor), and deletion of either gene causes loss of photoreceptors but generates more amacrine cells instead (Graw, 2010). *p27Xic1*, a *Xenopus* cyclin dependent kinase inhibitor, is key for retinal Müller cell differentiation. Overexpression of *p27Xic1* promotes early differentiation of retinal Müller cells in *Xenopus* (Ohnuma et al., 1999). *Sox2* (SRY(Sex determining region Y)-box 2 transcription factor) was found to be essential for postnatal Müller glial cells differentiation, and conditional knockout of *Sox2* in mice causes disrupted morphology and cell cycle quiescence of retinal Müller cells, leading to depletion of retinal Müller glia and retinal degeneration (Surzenko et al., 2013). In addition, Notch signalling is important for retinal Müller cells development. Inactivation of Notch-Delta signalling leads to the defect of retinal Müller cell differentiation, whereas the differentiation of retinal neurons is not affected in zebrafish (Bernardos et al., 2005).

2.2 Eye diseases in this study

2.2.1 Anterior segment dysgenesis (ASD)

Anterior segment dysgenesis is a broad manifestation of failures during anterior segment

development, including cornea, lens, iris, corneal-iris angle and trabecular meshwork. Clinically, it is usually characterized by corneal opacity, cataract, glaucoma, aniridia and microphthalmia. In patients with corneal opacity, the most common manifestation of ASD is Peters anomaly and Axenfeld-Rieger syndrome representing 80% of those patients (Shigeyasu et al., 2012).

Peters anomaly: it is characterized by persistent corneal-lens adhesion and central/peripheral corneal opacity. It is often associated with glaucoma, cataract and microphthalmia. There are several mutations in these genes found in patients with Peters anomaly, such as *PAX6* (Azuma et al., 1998), *FOXC1* (Honkanen et al., 2003; Weisschuh et al., 2008) and *FOXE3* (Docette et al., 2010).

Axenfeld-Rieger syndrome: The most common manifestations of the disease are the iris correctopia/atrophy and posterior embryotoxon (A congenital eye malformation characterized by a prominent displaced Schwalbe's line). But the cornea is clear and there is no corneal-lens adhesion in this disease compared with Peters anomaly. It is also often associated with glaucoma. *PITX2* (Idrees et al., 2006; Vieira et al., 2006; Li et al., 2008; Footz et al., 2009) and *FOXC1* (Honkanen et al., 2003; Weisschuh et al., 2008) are found to be mutant genes for the disease.

We still know less about the mechanisms of ASD although there are a number of mutant genes found in the patients. The majority of the mutant genes associated with ASD are transcription factors, such as *PAX6*, *FOXC1*, *PITX2*, *PITX3*, *FOXE3*, *AP2 α* (Reis and Semina, 2011). These transcription factors were found to regulate the mesenchymal cells to differentiate into distinct anterior segment tissues, and these developmental processes are also sensitive to the dose of these transcription factors (Sowden, 2007). The complex interactions between transcription factors may be one reason for phenotype variability of anterior segment dysgenesis (Sowden, 2007). Recently, there are several extracellular matrix molecules which are found to be related to anterior segment dysgenesis, such as Collagen4 A1 (Rødahl et al., 2013; Van Agtmael et al., 2005) and heparan sulfate (Iwao et al., 2009). Collagen4 A1 has been discussed in 2.1.4. Heparan sulfate is a glycosaminoglycan component of the extracellular matrix. Ablation of *Exostosin 1* (an enzyme indispensable for heparan sulfate synthesis) in neural crest cells causes the disruption of Tgf β 2 signaling and further down-regulates the expression of Foxc1 and Pitx2, leading to anterior

segment dysgenesis (Peters anomaly) in mice (Iwao et al., 2009). These studies suggest that ECM molecules play a critical role in anterior segment development as well as transcription factors.

2.2.2 Retinal gliosis

Gliosis is a process of glial scar formation caused by activated glial cells in the neural system which usually occur after injury. It is characterized by activated and/or proliferating glial cells and up-regulation of intermediate filament expression (Glial fibrillary acidic protein, GFAP) in the gliosis region. We often called gliosis induced by injury as reactive gliosis which is due to the properties of reactive cell process. In the retina, retinal Müller cells are the main glial cells, but the other cell types of glial cells including astrocytes and microglia cells were found to come from a distinct progenitor in the optic stalk and optic nerve during eye development (Stone and Dreher, 1987; Ling and Stone, 1988; Watanabe and Raff, 1988). Retinal reactive gliosis is characterized by the activation of retinal Müller cells and astrocytes. There are a number of studies showing that retinal Müller cells are involved in reactive gliosis induced by injury or other retinal diseases (Bringmann et al., 2009; 2012). Deficiency of transcription factors also leads to retinal reactive gliosis, suggesting that gliosis can also be controlled by genetic factors. Mice lacking *p27Kip1*, a tumor suppressor gene, showed retinal reactive gliosis which results in the retinal dysplasia and abnormal vessels (Dyer and Cepko, 2000). In consistency with this study, retinal reactive gliosis occurs in *P27* knock-out mice, but retinal function and visual acuity are not affected in the mutants (Vázquez-Chona et al., 2011). Conditional knock-out mice of *Lhx2*, a LIM homeodomain transcription factor, showed hypertrophic reactive gliosis in retina under the conditional ablation of *Lhx2* in mature Müller glia (de Melo et al., 2012). These studies showed that retinal gliosis is not only induced by injury or degeneration but also caused by intrinsic factors such as gene regulation.

In the human retina, gliosis is usually found in the pre-retina area. For example, the epiretinal membrane (ERM), a thin sheet of glial scar, can be found on the surface of the retina in patients with diabetic retinopathy, retinal detachment, ocular inflammation such as uveitis, etc. It also occurs on the front surface of the macula which is the small center region of the retina responsible for central vision. Sometimes it is associated with vitreous traction but without obvious other diseases and called idiopathic retinal gliosis. The exact cause, initial events, the progression and

the recurrent reasons of retinal epiretinal membrane remains largely unknown. But we still get some insights about the ERMs based on the morphological observations by different histology methods. The main cells of ERMs are glial cells, which are initially found based on the observation of 8 enucleated eyes with ERMs and it seems that the glial cells migrate out of the retina through the ruptured inner limiting membrane (ILM) and contribute to ERMs (Foos, 1974). The subsequent work found that the cell components of the epiretinal membranes are not only the glial cells, but also fibroblasts, myofibroblasts and macrophages based on morphology by electron microscopy (Kampik et al., 1981; Gandorfer et al., 2002; 2005). Then glial cells as well as hyalocytes may be predominant cells in the ILMs from patients with idiopathic macular hole, which were analyzed by immunostaining of cell markers and electron microscopy (Schumann et al., 2011). Growth factors may contribute to the pathogenesis of ERMs, because the expression level of some growth factors such as TGF β 2 and NGF (Nerve growth factor) is elevated in the vitreous from patients with idiopathic epiretinal membranes (Iannetti et al., 2011). In addition, in patients with macular holes, ERMs can be found on the surface of the macula with or without vitreous traction. But whether the vitreous detachment is a cause or effect of the ERMs remains unclear.

Interestingly, Nestin, a marker for neural stem cells, is also expressed in the epiretinal membranes (Mayer et al., 2003). Recently, glial cells were found in the vitreous from patients with diabetic retinopathy, and these cells can co-express neural stem/progenitor cell markers, such as Nestin (Johnsen et al., 2012), but whether these cells are involved in the ERM formation is still unknown. As the main glial cell type in retina, retinal Müller cells may have the properties of neural stem cells. One evidence is that, MIO-M1 (Moorfields/Institute of Ophthalmology-Müller 1), a retinal Müller cell line derived from postmortem adult human neural retina, exhibited the characteristics of neural stem cells. The cell lines can express the markers for neural stem cells, such as Sox2, Pax6, Chx10 and Notch1, in the presence of growth factors such as FGF-2 or retinoic acid (Lawrence et al., 2007). Moreover, adult retinal Müller cells have the ability to differentiate into rod photoreceptors (Giannelli et al., 2011). And a further study demonstrated that Wnt and Notch pathways are involved in activating the neural stem cell properties of retinal Müller cells (Das et al., 2006). Sonic hedgehog (Shh) signaling also can induce retinal Müller cells to dedifferentiate and promote their neurogenic potential to photoreceptor cells (Wan et al., 2007). These studies suggest that the retinal Müller cells as the main glial cells in retina showed characteristics of neural

stem cells. We can imagine that retinal Müller cells may play a unique role in the pathogenesis of the retinal gliosis because of their stem cell properties.

2.2.3 Optic nerve coloboma/hypoplasia

Optic nerve coloboma is a developmental disorder which is characterized by a demarcated bowl-shaped excavation in the optic disc (Dutton, 2004). It usually causes poor vision from moderate to severe blindness. It is often associated with other eye diseases, such as microphthalmos, cyst, microcornea, retinal detachment and abnormal retinal vessels. The cause and pathogenesis of the disease are not completely known. There are also some mutant genes found in patients with optic nerve coloboma, such as *PAX2* (Sanyanusin et al., 1995; Schimmenti et al., 2003), *PAX6* (Shukla and Mishra, 2011), *FOXE3* (Ali et al., 2010), *TMEM126A* (Transmembrane protein 126A) (Meyer et al., 2010) and *TUBA8* (alpha-tubulin 8) (Abdollahi et al., 2009).

Because the relationship of Pax2 and optic nerve coloboma is well studied, here I focus on the role of Pax2 during optic nerve development and coloboma. Pax2 (Paired box gene 2) is a transcription factor which is critical for embryonic morphogenesis. Pax2 also plays an important role in kidney development (Harshmann et al., 2012) and a variety of cancers (Ordóñez, 2012). In mouse eyes, Pax2 is expressed in the ventral optic cup and stalk in early eye development and then restricted to the optic nerve-retina junction and optic nerve (Otteson et al., 1998). Pax2 is a regulator for neuron-glial cell fate determination in the optic nerve, and if Pax2 is down-regulated, the cells in the optic nerve turn to generate neurons. If Pax2 is overexpressed, it will trigger glial cells differentiation of the optic nerve precursors (Soukkaieh et al., 2007). A frameshift mutation in *Pax2* causes misguidance of the optic nerve during eye development and a coloboma in the optic nerve head in mice (Favor et al., 1996). In consistency with this study, a missense mutation in *Pax2* also causes the congenital excavation of the optic nerve head but with retinal rosette formation and this mutation results in the changes in protein localization, transactivation and DNA binding (Alur et al., 2010). Like loss of function of Pax2, overexpression or ectopical expression of Pax2 appears to cause similar coloboma (failure of choroid fissure closure) during chicken eye development (Sehgal et al., 2008). There are a few studies demonstrating the pathway regulating the expression of Pax2. The earlier study showed that c-Jun NH2-terminal kinase (JNK) initiates Bmp4 and Shh signaling which induces Pax2 expression (Weston et al., 2003). Another study

showed that BMP7 and SHH (Sonic hedgehog) can regulate Pax2 in the retinal astrocytes through relieving TLX (an orphan nuclear receptor) repression (Sehgal et al., 2009). In addition, Grg4 (a Groucho/TLE family protein) can specifically interact with Pax2 to suppress transactivation (phosphorylation of the Pax2 active domain) (Cai et al., 2003). Nevertheless, the upstream regulation pathway of Pax2 is not completely understood.

2.2.4 Microphthalmia

Microphthalmia is a congenital manifestation of reduced eye size. It is usually associated with other congenital eye diseases, such as anterior segment dysgenesis (Peters anomaly and Axenfeld-Rieger syndrome) and eye coloboma. As well as anterior segment dysgenesis, there are a number of genes found to be associated with microphthalmia. Besides transcription factor genes such as *MITF* (Microphthalmia-associated transcription factor), *PAX6*, *SOX2*, *OTX2* and *FOXE3* (Bardakjian and Schneider, 2011), there are several other mutated genes found recently which cause microphthalmia, such as *ALDH1A3* (Aldehyde dehydrogenase family 1, subfamily A3) (Yahyavi et al., 2013), *c12orf57* (chromosome 12 open reading frame 57) (Zahrani et al., 2013), *ODZ3* (odd Oz/ten-m homolog 3, a transmembrane protein) (Aldahmesh et al., 2012). In addition, mutations in *ALDH1A3* (Yahyavi et al., 2013) or *ODZ3* (Aldahmesh et al., 2012) can also cause anophthalmia (the absence of the eye). These studies suggest that there is a more complex molecular network regulating eye size and growth including transcription factors. The other genes such as given above are as important as the transcription factors.

2.3 Two novel protein molecules in eye development and diseases

2.3.1 Peroxidasin (Pxdn)

Peroxidasin is also known as P53-responsive gene 2, Melanoma-associated gene 50 (MG50) or Vascular peroxidase 1 (VPO1). Peroxidasin is a conserved molecule combining multiple domains (leucine rich repeats, immunoglobulin domains and a von Willebrand factor domain) found in other extracellular matrix proteins and a peroxidase domain. It is also regarded as extracellular peroxidase. The coding sequence of *Pxdn* mRNA is around 4.5 kb and the protein size is around 165 kDa.

Although the function of peroxidasin is still largely unknown, several studies showed that peroxidasin may play multiple roles in extracellular matrix formation, development, homeostasis and host defense. Peroxidasin was firstly identified in *Drosophila*; it is expressed by hemocytes and involved in the formation of the extracellular matrix (Nelson et al., 1994). Furthermore, an *in vitro* study demonstrates that peroxidasin can be secreted from myofibroblasts and incorporated into the extracellular matrix and this process can be stimulated by TGF- β 1 but seems not mediated by the peroxidase enzyme activity (Péterfi et al., 2009). Further, disrupted extracellular matrix was also found in *C. elegans* with *peroxidasin* (*PXN*) mutations by electron microscopy (Gotenstein et al., 2010). Recently, it was known that peroxidasin crosslinks with collagen IV, and the expression of collagen IV is aberrant in *Drosophila* with a *peroxidasin* mutation (Bhave et al., 2012). On the other hand, peroxidasin is not only involved in the extracellular matrix, but also essential for embryonic development in lower organisms. In *C. elegans*, mutations in *peroxidasin* can cause embryonic and larval lethality, and variable epidermal morphology phenotypes, suggesting that it is essential for embryonic development and further experiments showed that these phenotypes are dependent on the peroxidase activity (Gotenstein et al., 2010).

Moreover, peroxidasin is highly expressed in the heart and vascular wall (Cheng, et al, 2008). It plays a role in promoting oxidative stress, and its function as an extracellular matrix molecule seems independent of its peroxidase activity in cardiovascular systems (Ma et al., 2013). Peroxidasin also can form sulfilimine chemical bonds using hypohalous acids (Bhave et al., 2012; Li et al., 2012) and also can generate hypochlorous acid, a reagent with microbicidal activity, and may further play a role in host defense in human plasma (Li et al., 2012). In addition, it is up-regulated in the P53-dependent apoptotic cells (Horikoshi et al., 1999). It may be involved in ox-LDL-induced (ox-LDL, oxidized low-density lipoprotein) endothelial cell apoptosis (Bai et al., 2011) and also in tumor pathogenesis since peroxidasin is highly expressed in melanoma cell lines (Mitchell et al., 2000).

Interestingly, mutations in *PXDN* gene (one affects the leucine-rich repeats domain and the other two affect the peroxidase domain) cause severe anterior segment dysgenesis in humans including corneal opacity, developmental glaucoma and congenital cataract, and the phenotypes of these patients are mainly present in the eyes (Khan et al., 2011) (Figure 1.4), suggesting that peroxidasin

plays an important role during eye development. Other work about peroxidase and eye research is only confined to the expression pattern analysis in lower animals. In *Xenopus tropicalis*, peroxidase can be detected in the eye-forming region, especially in the developing lens by *in-situ* hybridization (Tindall et al., 2005). Another *in-situ* hybridization study showed that peroxidase is expressed in the lens vesicle and in the retina, especially in the lens at E10 in mice (Homma et al., 2009). However, the role of peroxidase during eye development is still unknown.

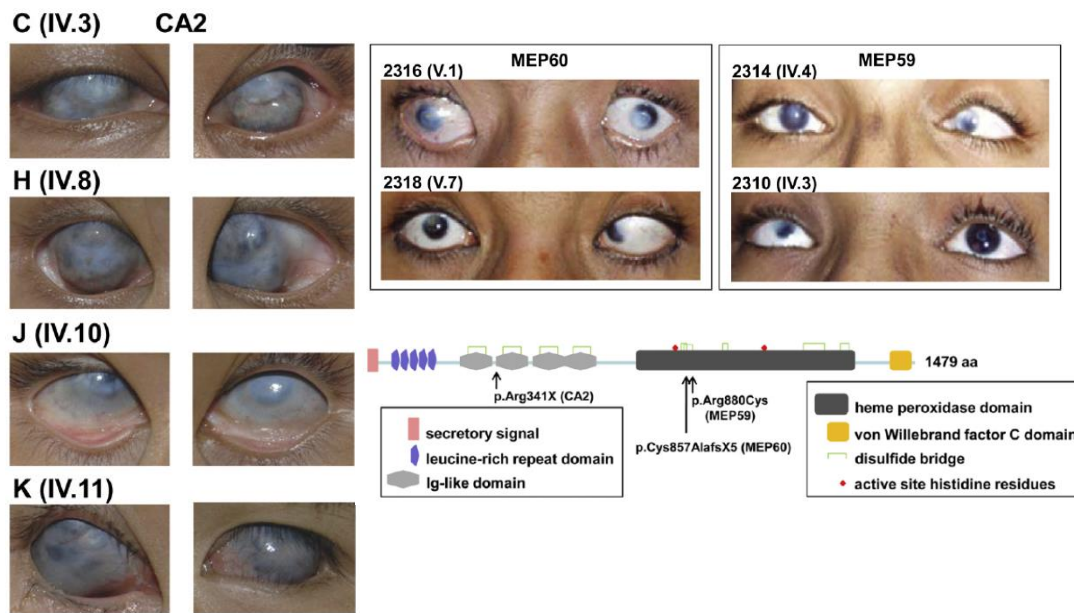


Figure 1.4 The clinical manifestations of patients with *PXDN* mutations. The point mutation of CA2 family is located at the leucine-rich repeats domain (p.Arg341X). The point mutations of MEP60 and MEP59 families are located at the peroxidase domains, one is Cys857AlafsX5 (MEP60) and the other is p.Arg880Cys (MEP59). The manifestations of patients in CA2 families is more severe and whole cornea opacity, whereas the patients in MEP60 and MEP59 families showed similar phenotype, including partial central/peripheral corneal opacity. Congenital cataract and developmental glaucoma are also found in these patients (The picture from Khan et al., 2011)

2.3.2 Bmpr1b

BMP receptors are a family of transmembrane serine/threonine kinases, which consist of an N-terminal signal sequence, a transmembrane domain and a serine/threonine kinase in the cytoplasm. There are three types of BMP receptors, Bmpr1a (Bmp receptor type 1a), Bmpr1b (Bmp receptor type 1b) and Bmpr2 (Bmp receptor 2). These three receptors may dynamically form different receptor complexes. In the absence of a Bmp ligand, the heteromeric and homomeric complexes of Bmp receptors (BR) are formed in living cells including BR-II/BR-Ia, BR-II/BR-Ib, BR-II/BR-II, BR-Ia/BR-Ia, BR-Ib/BR-Ib and BR-Ia/BR-Ib, whereas in the presence of Bmp2, the hetero- and

homo-oligomerization is increased (Gilboa et al., 2000). Here I focus on the expression and function of Bmpr1b.

Bmpr1b is highly conserved between human and mice. It is widely expressed in different types of cells and involved in multiple processes including proliferation, apoptosis and differentiation. It is expressed in neurons, astrocytes, oligodendrocytes, ependymal cells and microglia in the spinal cord (Miyagi et al., 2012). It also can be detected in embryonic stem cells during early development (Roelen et al., 1997), in the neural precursor cells in the dorsal region of the neural tube (Panchision et al., 2001) and in the proximal mesenchymal cells at the onset of mouse limb bud development (Barna et al., 2005). In addition, it is highly expressed in different malignant tumors, such as malignant glioma (Yamada et al., 1996), prostate cancer tissue (Ide et al., 1997; Kim et al., 2000) and epithelial ovarian cancer tissue (Ma et al., 2010), indicating that it may play a role in the pathogenesis of malignant tumors. In the eyes, Bmpr1b is expressed in the corneal epithelial and stromal cells (You et al., 1999). During early eye development, *Bmpr1b* mRNA is expressed in the optic vesicle at E9.0-E9.5 (Danesh et al., 2009; Faber et al., 2002), and it is mainly expressed in the ventral retina during E10.5-E11.5 by *in-situ* hybridization (Faber et al., 2002; Figure 1.5). Moreover, it is highly expressed in the embryonic retina at E13.5 and then its expression is decreased after E13.5 revealed by western blot, and its mRNA is detected in retinal progenitor cells at E14.5 by RT-PCR (Du et al., 2010). In adult mouse retina, Bmpr1b is expressed in the retinal ganglion cell layer (Du et al., 2010). In the chick retina, Bmpr1b is much less expressed in the retina and choroid compared to Bmpr1a and Bmpr2, and it is not detected in RPE by real-time PCR (Zhang et al., 2012).

Most studies about the role of Bmpr1b in development are from bone and ovarian research. Bmpr1b is required for distal limb development in the mouse (Baur et al., 2000; Kobayashi et al., 2005). In the truncated-*Bmpr1b* (lacking of Bmpr1b kinase domain) transgenic mouse, Bmp signaling is blocked and bone formation is reduced during postnatal periods (Zhao et al., 2002). In humans, mutations in *BMPR1B* lead to Brachydactyly type A2 and whether the serine/threonine kinase activity is affected according to different mutations (Lehmann et al., 2003) and acromesomelic chondrodysplasia with genital anomalies (Demirhan et al., 2005). Mutations in *GDF-5* (Growth differentiation factor 5, a ligand of Bmpr1b (Nishitoh et al., 1996; Nickel et al.,

2005)) also cause Brachydactyly type A2 which is similar to the phenotype caused by *Bmpr1b* mutations (Seemann et al., 2005; Kjaer et al., 2006). At the cellular level, it plays a role in cell apoptosis and terminal differentiation (Panchision et al., 2001). For example, *Bmpr1b* can induce apoptosis in osteoblastic cells (Haÿ et al., 2004). Overexpression of mutant *Bmpr1b* (truncated *Bmpr1b*) leads to the block of *Bmp2*-induced osteoblast differentiation *in vitro* (Chen et al., 1998). In addition, *Bmpr1b* is important for ovarian development (Souza et al., 2002; Shimasaki et al., 2003; Reader et al., 2012; Pulkki et al., 2012).

Bmpr1b plays a role in the pathogenesis of gliosis. *Bmpr1a* conditional knockout mice (ablation of *Bmpr1a* in GFAP-expressing cells) exhibit defects in hyperactive glial cells, reduced gliosis and inflammatory cell infiltration in the spinal cords after injury, whereas *Bmpr1b* knockout mice showed that glial cells appear to be more active and attenuated glial is formed after injury. The gliosis phenotypes can be relieved by *Bmpr1a/Bmpr1b* double knock-out mice (Sahni et al., 2010). These also indicate that both the receptors function coordinately in a different way. Moreover, *Bmpr1b* is a major mediator of glial cell differentiation in the cultured hippocampus progenitor cells (Brederlau et al., 2004).

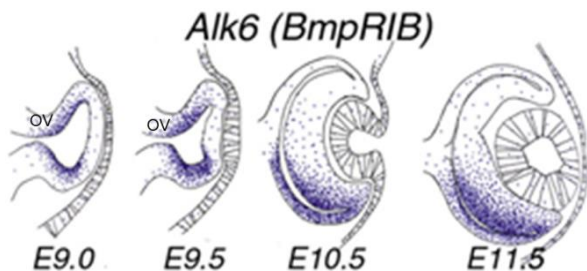


Figure 1.5 The expression of *Bmpr1b* mRNA during early eye development by *in-situ* hybridization. The expression of *Bmpr1b* mRNA starts from E9.5, the earliest stage of eye development in mice and it is expressed in the optic vesicle. From E10.5 to E11.5, *Bmpr1b* is mainly expressed in the ventral retina. OV: optic vesicle. (The picture from Faber et al., 2002)

A few studies demonstrate functional redundancy of *Bmpr1* receptors. This means that either deletion of *Bmpr1a* or *Bmpr1b* does not cause any defects but deletion of *Bmpr1a* and *Bmpr1b* lead to severe phenotypes. For examples, deletions of *Bmpr1a* or *Bmpr1b* in cartilage are able to form intact cartilaginous elements in mice, whereas double mutants develop a severe generalized chondrodysplasia (Yoon et al., 2005). Similar to this condition, either *Bmpr1a* or *Bmpr1b* knock-out mice does not exhibit any cerebellar defects, but *Bmpr1a/Bmpr1b* knock-out mice exhibit severe defects in cerebellar patterning and reduced size of cerebella (Qin et al., 2006). In addition, *Bmpr1a/Bmpr1b* knock-out mice showed that the development of two different types of

interneuron cell (D1 and D2) is defective in the dorsal spinal cord: D1 interneurons are absent and D2 interneurons are significantly reduced (Wine-Lee et al., 2004).

However, there are very few studies focusing on the role of *Bmpr1b* in eye development. From previous very limited studies, *Bmpr1b* also seems important for eye development. In *Bmpr1b* knockout mice, some retinal axons are misguided in the optic nerve head at E15.5 - E16.5, and apoptosis may be increased in the retina (Liu et al., 2003). Interestingly, *Bmpr1a* knockout mice have normal eye development, whereas *Bmpr1a/Bmpr1b* double knockout mice showed severe retinal defects including retinal growth and neurogenesis (Murali et al., 2005), suggesting that *Bmpr1b* may interact with *Bmpr1a* and function coordinately. In addition, primary lens fiber cell differentiation is defect in the lenses of *Bmpr1b* transgenic mice (Faber et al., 2002).

2.4 Two new ENU-induced mouse mutants with different eye phenotypes

2.4.1 *KTA48*: ENU-induced *peroxidasin*-mutant mice

In the past, the *in vivo* functions of peroxidasin were investigated in lower organisms such as *Drosophila* and *C. elegans*. Mammalian animal models with peroxidasin defects are lacking. *KTA48*, to the best of my knowledge, is the first *peroxidasin*-mutant mouse line and also the first mammalian model with a peroxidasin mutation. ENU (N-ethyl-N-nitrosourea) is an alkylating agent by which the ethyl group can be transferred to the oxygen and nitrogen atoms of the nucleotide base in the genomic DNA and it causes point mutations in the spermatogonial stem cells with a high frequency in mice (Justice et al., 1999). ENU is widely used for generating mouse mutants, followed by a phenotype-driven screening and the identification and confirmation of gene mutations. The ENU-induced *peroxidasin* mutant mice have an appearance of microphthalmia, white spots on the coat and kinky tail (Figure 1.6). The *KTA48* mutation was identified and found to be located at T3816A (cDNA) in exon 19 of *Pxdn* mRNA (coding sequence, from start codon to the stop codon) by linkage analysis, positional candidate approach, haplotype analysis and sequencing (unpublished work by Dr. Sibylle Sabrautzki, Dr. Helmut Fuchs and Dr. Jochen Graw, HMGU (Helmholtz Center Munich or German Research Center for Environmental Health)). It is predicted to cause a premature stop codon (Figure 1.7) and thereby leads to a partial loss of function of peroxidasin in the mutant mice.

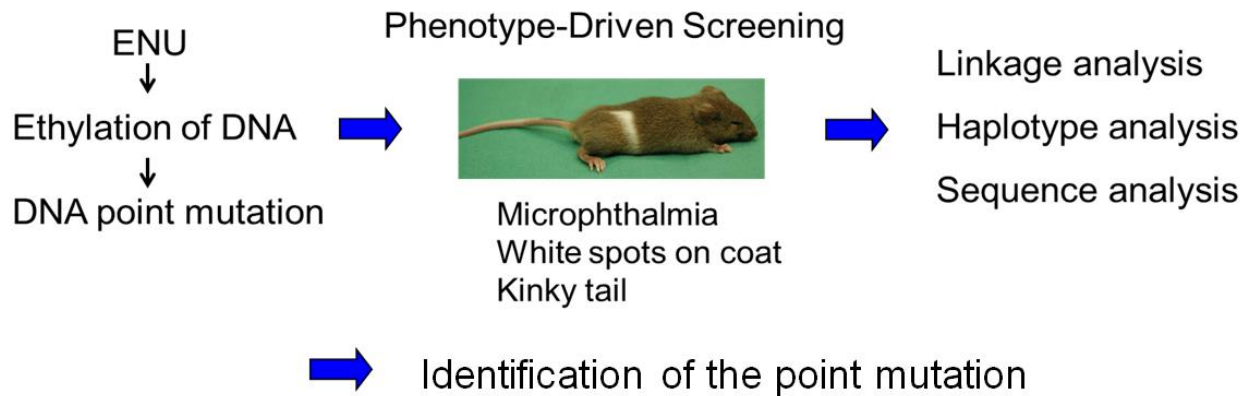


Figure 1.6 The procedure for identification of the point mutation in *KTA48*. *KTA48* homozygous mice exhibited microphthalmia, white spots on coat and kinky tail due to a point mutation induced by ENU. Linkage analysis, haplotype analysis and sequence analysis have been used to identify the point mutation (The picture taken by Ms. Erika Bürkle and Ms. Monika Stadler, HMGU).

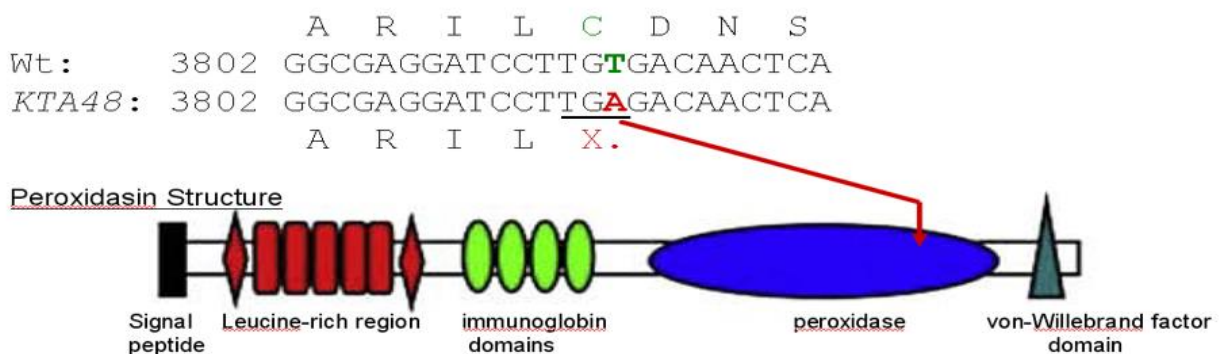


Figure 1.7 The point mutation of *KTA48* mutant mice. The point mutation in *KTA48* mutants is located at T3816A (Exon 19 of *Pxdn* mRNA, coding sequence from start codon to the stop codon) and it produces a new restriction site for *Alw26I* and a new stop codon (TGA, underlined). (Performed by Dr. Sibylle Sabrautzki, Dr. Helmut Fuchs and Dr. Jochen Graw, HMGU) (The figure of peroxidase structure from Cheng et al., 2008, modified).

2.4.2 *Ali030*: ENU-induced *Bmpr1b*-mutant mice

Ali030 is another ENU-induced mutant mouse line characterized by a point mutation in the *Bmpr1b* gene (Figure 1.8, A). *Ali030* mutant mice have an appearance of severe brachydactyly (Figure 1.8, B). The mutation was identified by similar genetic methods used for *KTA48* mutants, including linkage analysis, positional candidate approach, haplotype analysis and sequencing. This point mutation in *Ali030* mutants is located at the second base pair in intron 10 of *Bmpr1b* gene (Figure 1.8, A) and it is predicted that it may influence the alternative pre-mRNA splicing. The

identification of the point mutation in *Ali030* mutant mice was performed by Dr. Sibylle Sabrautzki (unpublished work). The mutant mice were sent to GMC (German mouse clinic) for initial eye screening by AC master (a special equipment used to measure anterior chamber depth, lens thickness and eye size (Puk et al., 2006)), funduscopy and optokinetic drum. There is a big hole in the optic nerve head (Figure 1.8, C) and the vision acuity was reduced (Figure 1.8, D) in *Ali030* homozygous mice, and larger axial eye length was found in mutants which may be due to the enlarged optic nerve head, but the lens size and transparency are not changed in these mutants (*Ali030* GMC report, unpublished). In addition, the global retinal function is not changed in *Ali030* mutant mice at 10 weeks, because they exhibit regular electrical activity of the retina response to flash light (12,500 cd/m²) by ERG (Electroretinogram), and there are no obvious differences between wild types and mutants (Figure 1.8, E, performed by Susanne Weber, unpublished).

A

Bmpr1b gene (Blue: exon 10 Green: intron10)

Wt 5'...CATTCCCAATCGATGGAGCAGTGATGAGGTAAGGCTAGGCTTAGGGAAGGG...3'

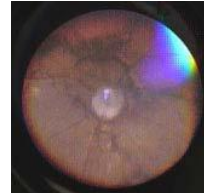
Ali030 5'...CATTCCCAATCGATGGAGCAGTGATGAGGGAAGGCTAGGCTTAGGGAAGGG...3'

B



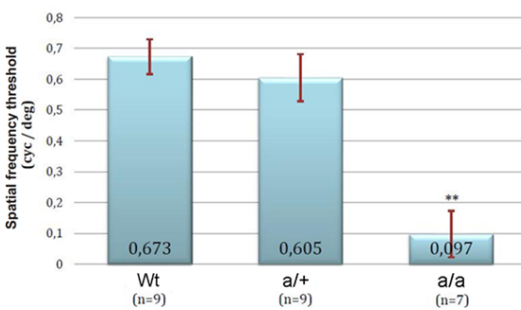
Brachydactyly

C



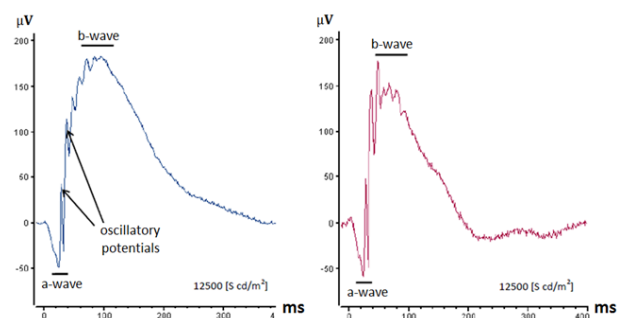
A coloboma in the optic nerve head

D



Visual acuity in *Ali030* mice

E



ERG in *Ali030* mice

Figure 1.8 A point gene mutation, brachydactyly, the hole in the optic nerve head and reduced visual acuity in *Ali030* mutants. (A) A point mutation was found in the second base pair of intron 10 of *Bmpr1b* in *Ali030* mutants (From Dr. Sibylle Sabrautzki, HMGU). (B-C) The distal limb showed a phenotype of Brachydactyly (B) and the optic nerve head coloboma (C) by fundoscopy (performed by Dr. Claudia Dalke, HMGU). (D) The visual acuity was measured by optokinetic drum and it is significantly reduced in *Ali030* homozygous mutants compared to wild types and heterozygous, but no difference in visual acuity was found between wild types and heterozygous (performed by Susanne Weber, HMGU). (E) *Ali030* mutant mice exhibit regular electrical activity of the retina response to flash light (12,500 cd/m²) at 10 weeks (performed by Susanne Weber, HMGU).

3 Aims of the study

3.1 *KTA48* project

The role of peroxidasin in eye development is largely unknown. Here, I investigated the role of peroxidasin in eye development using the ENU-induced *KTA48* mutant mice, in which the eye phenotype is highly similar to the manifestations in patients with *PXDN* mutations. The first question is the expression pattern of peroxidasin and morphological phenotypes of peroxidasin-mutant eyes during embryonic eye development and postnatal periods. The second question is to identify possible cellular and molecular mechanism of peroxidasin in eye development based on *in-situ* hybridization, BrdU assay, immunostaining and real-time PCR.

3.2 *Ali030* project

Very limited studies showed that *Bmpr1b* may play roles in retinal growth, neurogenesis and axon guidance. The roles of *Bmpr1b* in retinal development are still not clear. In this study, ENU-induced *Ali030* mutant mice were used to investigate the role of *Bmpr1b* during retinal and optic nerve development. Specifically, the first question is to analyze how this point mutation affects RNA splicing process. The second question is to find and analyze the detailed ocular phenotypes in mutants and to investigate the role of *Bmpr1b* in retinal development *in vivo* and *in vitro*. Finally, clinical samples (epiretinal and inner limiting membranes) from patients with different types of retinal gliosis were analyzed.

4 Materials and Methods

4.1 Materials

4.1.1 Equipment

Equipment	Manufacturer
Balance (TE 1502S)	Sartorius AG, Germany
Cell culture incubator (CO ₂ -Teco 20)	Selutec GmbH, Germany
Light microscope camera (Axiocam)	Zeiss, Germany
Cell counting chamber	Paul Marienfeld GmbH, Germany
Centrifuge (Eppendorf 5415D)	Eppendorf, Germany
Centrifuge (Sigma 3K18)	Sigma, Germany
Centrifuge (Eppendorf 5415R)	Eppendorf, Germany
Centrifuge (Biofuge)	Heraeus, Germany
Centrifuge (SD2 20)	Car Roth GmbH, Germany
Fume hood	Waldner Laboreinrichtungen GmbH, Germany
Gel electrophoresis apparatus	Biorad, Germany
Gel documentation system (Argus X1)	Biostep GmbH, Germany
Incubator	Memmert, Germany
Laminar flow	Gelaire Pty Ltd, Australia
Microwave	Samsung, Germany
Fluorescence microscopy (DMI 6000B)	Leica, Germany
Confocal microscopy (Olympus 8934)	Olympus, Japan
Microtome (RM 2050)	Leica, Germany
Microtome (Cryotome)	Leica, Germany
pH meter (761 calimetic)	Knick, Germany
Pipette	Eppendorf, Germany
Refrigerators	Liebherr, Germany
Shaker (Polymax 1040)	Heidolph Instruments GmbH, Germany
Shaker (Rotamax 120)	Heidolph Instruments GmbH, Germany
Shaker (Centromat S)	Braun Melsungen AG, Germany
Spectrophotometer (Nanodrop: ND1000)	PeQlab Bioehcnology GmbH, Germany
Thermal cycle (PTC-225)	MJ Research, Germany
Stereomicroscope	Zeiss, Germany
Vortex (G-560E)	Scientific Industries, USA
Water bath	LTF labortechnik GmbH, Germany
Water purification sytem (MilliQ biocel)	Millipore, Germany
Heating plate (Ikamag)	Ludwig Empgenzeder, Germany
Thermomixer (7410)	Bachofer, Germany

4.1.2 Consumables

Consumables	Manufacturer
96-well optical well adhesive film	ABI, Germany
48-well optical well adhesive film	ABI, Germany
Petri dishes	Greiner Bio-One GmbH, Germany

Cell culture plates (96-well)	Becton Dickinson, France
Cover glass	Roth, Germany
Coverslips	Roth, Germany
Disposable cuvettes	Eppendorf, Germany
Glass slides	Gerhard Menzel Gmbh, Germany
Parafilm	Carl Roth GmbH, Germany
Pipette tips	Biozym, Germany
Reaction tubes (1.5 ml, 2 ml)	Eppendorf, Germany
Gloves	Meditrade GmbH, Germany
Syringes	Braun, Germany
Needles (27G)	Henke sass, wolf GmbH, Germany
Reaction tubes (15 ml, 50 ml)	BD Falcon, Germany
SuperFrost® Plus microscope slides	Menzel, Germany
Pipetman (2µl 10µl 20µl 200µl 1ml)	Gilson, France
96-well plates for luminometer	Thermo Fisher Scientific, Denmark

4.1.3 Chemicals

Chemical	Catalogue number	Manufacturer
Acetic acid	1.00063	Merk, Germany
Agarose	840004	Biozyme, Germany
Aqua Poly Mount	18606	Polysciences, Germany
Ampicillin	K029.1	Carl Roth GmbH, Germany
5-Bromo-2'-Deoxyuridine	B5002	Sigma-Aldrich, Germany
BMP-2	A gift from Prof. Sebald Walter, Würzburg, Germany	
Citric acid	X863.2	Carl Roth GmbH, Germany
4',6-diamidino-2-phenylindole (DAPI)	D9564	Sigma-Aldrich, Germany
Diethyl pyrocarbonate (DEPC)	18835	Serva Electrophoresis GmbH, Germany
DMEM with low glucose	E15-806	PAA Laboratories GmbH, Austria
DMEM with high glucose and sodium pyruvate	E15-843	PAA Laboratories GmbH, Austria
DiI	D-282	Invitrogen, Germany
DiO	D-275	Invitrogen, Germany
dNTPs	R0241	Fermentas GmbH, Germany
Eosin	A gift from Mr. Shen Chi from Institute of Experimental Genetics, HGMU	
Ethylenediaminetetraacetic acid (EDTA)	8043.2	Carl Roth GmbH, Germany
Ethanol	2246.2500	Th. Geyer GmbH and Co. KG Renningen, Germany
Ethidiumbromid	A1152	Applichem GmbH, Germany
Eukitt quick hardening mounting medium	03989	Fluka, Germany
Fetal bovine serum	A15-104	PAA GmbH, Austria
Formamide	P040.1	Carl Roth GmbH, Austria
Formamide (37%)	4979.1	Carl Roth GmbH, Germany
GDF-5 (recombinant murine)	315-24	Peptotech, Germany
25% Glutaraldehyde	G5882	Sigma-Aldrich, Germany
Glycerol	1.04093	Merk KgaA, Germany
Glycine	G7126	Sigma-Aldrich, Germany

Hydrochloric acid (HCl)	1.00319	Merk KGaA, Germany
Isopropylthio- β -galactoside (IPTG)	2316.3	Carl Roth GmbH and Co. KG, Germany
Levamisole	31742	Sigma-Aldrich, Germany
Mayer's hematoxylin	MHS16	Sigma-Aldrich, Germany
2-Mercaptoethanol	M7522	Sigma-Aldrich, Germany
Methanol	1.06009	Merk KGaA, Germany
MgCl ₂	2189.1	Carl Roth, Germany
NaAc	1.06268	Merk KGaA, Germany
OCT Compound Tissue Tek	4583; 1200600006	Sakura Finetek, USA
Osmium tetroxide solution (2%)	23310-10	Polysciences, Germany
100 \times Penicillin/streptomycin	P11.010	PAA GmbH, Austria
Paraformaldehyde (PFA)	0335.3	Carl Roth, Germany
2-Propanol	9866.1	Carl Roth, Germany
Phenethyl acetate	290580	Sigma-Aldrich, Germany
Precision Plus Protein™ Dual Color Standards	161-0374	BIO-RAD, Germany
Potassium chloride (KCl)	4936	Merk, Germany
RNase Zap	R2020	Sigma-Aldrich, Germany
Roti-Histol	6640	Carl Roth GmbH and Co. KG, Germany
Roti-Mount	HP-19	Carl Roth GmbH and Co. KG, Germany
Sodium chloride (NaCl)	1.06404	Merk KGaA, Germany
Sodium citrate	3580.1	Carl Roth GmbH, Germany
Sodium deoxycholate	D6750	Sigma-Aldrich, Germany
Sodium dodecyl sulfate (SDS)	20760	Serva Feinbiochemica GmbH and KG, Germany
Sodium hydroxide (NaOH)	1.06482	Merk KGaA, Germany
Sodium phosphate dibasic	1.06580	Merk KGaA, Germany
Sodium phosphate monobasic	1.06346	Merk KGaA, Germany
Sucrose	4621.1	Carl Roth GmbH and Co. KG, Germany
Toluidine blue	A gift from Institute of Pathology, HG MU	
0.05% Trypsin-EDTA	L11-004	PAA, Germany
Trypan blue	L6323	Biochrom, Germany
Tween-20	9127.1	Carl Roth GmbH and Co. KG, Germany
X-gal	R0404	Fermentas GmbH, Germany
Xylene	1.08685	Merk KGaA, Germany

DiI: 1,1'-dioctadecyl-3,3',3'-tetramethylindocarbocyanine perchlorate

DiO: 3,3'-Dioctadecyloxycarbocyanine perchlorate

4.1.4 Enzymes

Enzymes	Catalogue number	Company
<i>Alw36I</i>	ER0031	Fermentas GmbH, Germany
Dream Taq Green PCR Master Mix	K1082	Fermentas GmbH, Germany
<i>HindIII</i>	ER0501	Fermentas GmbH, Germany
Phusion® High-Fidelity DNA Polymerase	M0530S	New England Biolabs, Germany

SP6 polymerase	EP0131	Fermentas GmbH, Germany
T7 polymerase	EP0111	Fermentas GmbH, Germany
<i>Taq</i> DNA Polymerase	18038	Invitrogen, Germany
<i>Xho</i> I	742929	Boehringer Mannheim, Germany

4.1.5 Commercial kits

Kits	Catalogue number	Manufacturer
Anti-Digoxigenin-Ap Fab fragments	11093274910	Roche Dignostics GmbH, Germany
BM purple Ap substrat	11442074001	Roche Dignostics GmbH, Germany
DH5 α competent cells	18258012	Invitrogen, Germany
DIG RNA labeling mixture	11277073N5P12	Roche Dignostics GmbH, Germany
DNA Midi preparation Kit	12143	Qiagen, Germany
DNA Mini preparation Kit (NucleoSpin $^{\text{®}}$ Plasmid)	740588.50	Macherey-Nagel, Germany
DreamTaq Green PCR Master Mix	K1082	Fermentas, Germany
Embed-It $^{\text{TM}}$ Low Viscosity Epoxy Kit	24300-1	Polysciences, Germany
5x HOT FIREPol $^{\text{®}}$ EvaGreen $^{\text{®}}$ qPCR Mix Plus (ROX)	08-24-00001	Solis BioDyne, Estonia
JB-4 $^{\text{®}}$ Embedding Kit	00226-1	Polysciences, Germany
Lipofectamine $^{\text{®}}$ 2000 Transfection Reagent	11668-027	Invitrogen, Germany
NucleoSpin $^{\text{®}}$ Gel and PCR Clean-up	740609.50	Macherey-Nagel, Germany
pcDNA $^{\text{TM}}$ 3.1 Directional TOPO $^{\text{®}}$ Expression Kit	K4900-01	Invitrogen, Germany
Phusion $^{\text{®}}$ High-Fidelity DNA Polymerase	M0530S	New England Biolabs, Germany
Ready-To-Go T-primed First-stand Kit	GEHE27-9263-01	Amsterdam Biosciences, Germany
RNeasy Mini Kit	74104	Qiagen, Germany
1kb DNA ladder marker	SM0311	Fermentas GmbH, Germany

4.1.6 Softwares and tools

Softwares and tools	Website
BioEdit software 9.0	http://www.mbio.ncsu.edu/bioedit/bioedit.html
DNA sequence and gene analysis	http://www.ensembl.org
ImageJ	http://rsb.info.nih.gov/ij/
Microsoft office 2010	http://www.microsoft.com
NCBI	http://www.ncbi.nlm.nih.gov/
Olympus FluoView 1.7a	http://www.olympusconfocal.com/
Primer premier 5.0	http://primer-premier.softpedia.com/
StepOne $^{\text{TM}}$ Real-Time PCR Systems	http://www.appliedbiosystems.com/

4.1.7 Primers

Table 4.1 Primers for genotyping

Primer	Sequence	Annealing temperature (°C)	Product size (bp)
Pxdn-Ex19-L1	5'-CCTTGTGGCTGACATTCTCCC-3'	55	356
Pxdn-Ex19-R1	5'-CACTTTCCCCGTTCTCAGGC-3'		
AliCR	5'-CAGGAGGTTGTGAGCTAGGAAA-3'	62	see below
AliCF	5'-GGAATGTAACCAGGAGATGAGG-3'		
AliWtF	5'-CGATGGAGCAGTGATGAGGT-3'		
AliMtF	5'-CGATGGAGCAGTGATGATGG-3'		

Product size (*Ali030* genotyping):

WT	AliCR and AliWtF 291 bp	AliCF and AliWtF 376 bp
	AliCR and AliMtF 291 bp	AliCF and AliMtF 0 bp
Homozygous	AliCR and AliWtF 291 bp	AliCF and AliWtF 0 bp
	AliCR and AliMtF 291 bp	AliCF and AliMtF 373 bp
Heterozygous	AliCR and AliWtF 291 bp	AliCF and AliWtF 376 bp
	AliCR and AliMtF 291 bp	AliCF and AliMtF 373 bp

Table 4.2 Primers for cloning of *Bmpr1b* cDNA

Primer	Sequence	Annealing temperature (°C)	Product size (bp)
Bmpr1b-cDNA-CACCL1	5'-CACCATGCTCTTACGAAGCT-3'	55	1509
Bmpr1b-cDNA-R1 SC	5'-TCAGAGTTTAATGTCCTGGG-3'		

Table 4.3 Primers for cloning of riboprobes for *in-situ* hybridization

Primer	Sequence	Annealing temperature (°C)	Product size (bp)
Pax6-forward	5'-GGGAGTGCCCTTCCATCT-3'	62	885
Pax6-reverse	5'-CCCATGGGCTGACTGTTC-3'		

Table 4.4 Primers for real-time RT-PCR

Gene	Primer	Sequence
<i>Pax6</i>	Pax6-qF	5'-GTTCTTCGCAACCTGGCTA-3'
	Pax6-qR	5'-TGAGCTTCATCCGAGTCTTCT-3'
<i>TGFβ1</i>	TGFβ1_FW	5'-TGACGTCACTGGAGTTGTACG-3'
	TGFβ1_RV	5'-GGTTCATGTCATGGATGGTGC-3'

<i>TNF-α</i>	TNF α _2F TNF α _2R	5'-CACCACGCTCTTCTGTCT-3' 5'-GGCTACAGGCTTGCTCACTC-3'
<i>IL-1β</i>	IL-1 β _FW IL-1 β _RV	5'-CAACCAACAAGTATTCTCCATG-3' 5'-GATCCACACTCTCCAGCTGCA-3'
<i>Tubea</i>	TubeaF TubeaR	5'-CCAGATGCCAAGTGACAAGA-3' 5'-GTGGGTTCAGGTCTACGAA-3'

4.1.8 Buffers and solutions

DNA preparation and PCR

Lysis buffer	Tris pH 8.0	500 μ l
	5M NaCl	1 ml
	0.5M EDTA pH8.0	1 ml
	10% SDS	2.5 ml
	Add H ₂ O to 50 ml	

dNTP mix	dATP	2.5 mM
	dTTP	2.5 mM
	dGTP	2.5 mM
	dCTP	2.5 mM
	in dd H ₂ O	

Tissue preparation

0.2 M Phosphate buffer	Sodium phosphate monobasic	16.56 g/l
	Sodium phosphate dibasic	65.70 g/l
	Disolve in H ₂ O	
4% Paraformaldehyde	Paraformaldehyd(PFA)	40 g/l
	Dissolve in 1xPBS	
30% Sucrose solution	Sucrose	15 g
	dd H ₂ O	50 ml

In-situ hybridization

1M Tris-Cl	Tris-base Dissolve in H ₂ O adjust PH 7.4 with HCl	121.4 g/l
Hybe buffer	Deionized formamide 20X SSC Heparin solution Tween-20 dd H ₂ O Adjust pH to 6.0 with 1M Citric acid	10 g/l 10 g/l 5 µl 10 µl 2.05 ml
Hybridization solution	50x Denhardt's 100mg/ml baker yeast tRNA 20x SCC form amide Fill up to 50 ml with dd H ₂ O	5 ml 125 ul 12.5 ml 25 ml
20X SSC	NaCl Sodium citrate Add dd H ₂ O and adjust pH to 7.0 and autoclave	175.3 g 88.2 g
MAB	Maleic acid NaCl Add 800 ml dd H ₂ O Adjust pH to 7.5 with NaOH Add to 1L with dd H ₂ O	11.6 g 8.8 g
MABT	MAB + 0.1% Tween-20	
NTE	5M NaCl 1M Tris/HCl pH 7.0 0.5M EDTA	100ml 10 ml

Add to 1L with dd H₂O 10 ml

NTMT

5M NaCl 20 ml
1M Tris/HCl pH 9.5 100 ml
1M Mg₂Cl 50 ml
0.1% Tween-20
Add to 1L with dd H₂O

PBS:

5M NaCl 30 ml
1M Na-phosphate buffer pH7.3 15 ml
Add to 1L with dd H₂O

Immunofluorescence staining

0.2 M Phosphate buffer:

Sodium phosphate monobasic 16.56 g/l
Sodium phosphate dibasic 65.70 g/l
Dissolve in H₂O

Blocking solution:

(for sections)

Fetal bovine serum 3%
TritonX-100 0.25%
In 1X PBS

Blocking solution:

(for whole-mount)

Fetal bovine serum 3%
TritonX-100 0.25%
In 1X PBS

2M HCl:

(for BrdU sections)

100% HCl 16.95 ml
Add d H₂O to 100 ml

2M HCl in PBST:

(for BrdU sections)

	37% HCl	2 ml
	Add d PBS/0.1%TritonX-100 to 12 ml	
4M HCl: (for BrdU sections)	37% HCl	4 ml
	Add d H2O to 12 ml	
Borate buffer:	Boric acid	6.183 g
	Dissolved in 1L H ₂ O and adjust pH to 8.5	
Sodium citrate (1M):	Sodium citrate * 2H ₂ O	129.1 g
	Add d H ₂ O to 500 ml	
	Total volume 1L	
Histology		
Methylene blue and Basic fuchsin solution	Methylene Blue Stock	
	Methylene blue	0.5 g
	Distilled water	400 ml
	Basic Fuchsin Stock	
	Basic fuchsin	0.5 g
	Distilled water	400 ml
	Working solution	
	Working solution	
	Methylene Blue stock	12 ml
	Basic Fuchsin stock	12 ml
	0.2M PBS pH 7.2	21 ml
	95% Ethnol	15 ml
Sorensen's buffer (0.133 M, pH 7.2)	0.133 M Na ₂ HPO ₄	35.76g Na ₂ HPO ₄ / 1L dH ₂ O
	0.133 M KH ₂ PO ₄	9.08g KH ₂ PO ₄ / 0.5L dH ₂ O

71.5 mL 0.133 M Na₂HPO₄ and
 28.5 mL 0.133 M KH₂PO₄ pH 7.2

Davidson' solution

95% Ethanol	28.5. ml
37% Formadehyde	20 ml
Acetic acid	10 ml
Distilled water	31.5 ml

1% Toluidine blue solution

Toluidine blue	1.0 g
Distilled water	100 ml

Western blot

RIPA

5M NaCl	15 ml
NP40	5 ml
10% SDS	2.5 ml
0.5M EDTA	1 ml
1M Tris-HCl pH 8.0	25 ml
10% Deoxycholate	25 ml
Add dd H ₂ O to 500 ml	

4X loading dye

2-Mercaptoethanol	1.6 ml
Glycerin	5 ml
20% SDS	8 ml
1M Tris HCl pH 8.5	2 ml
Bromphenol blue	50 mg
dd H ₂ O	3.4 ml

4.2 Methods

4.2.1 Animal experiments

4.2.1.1 Mouse strains

All animal care and experimental procedures were conducted in accordance with the German Law for Animal Protection and the corresponding rules in Helmholtz Center Munich. The mouse lines in the studies were as follows:

KTA48 mouse line: a point mutation (Exon 19, T3816A, coding sequence) within the peroxidase domain of peroxidase with the background of C3H or C57BL/6J. The control mice used were littermates or C3H or C57BL/6J wild-type mice at the same age.

Ali030 mouse line: a point mutation (a T->G transversion in the second base pair of intron 10) in *Bmpr1b* with the background of C57BL/6J. The control mice used were littermates or C57BL/6J mice with the same age.

4.2.1.2 BrdU labelling

The thymidine analog, 5-bromo-2-deoxyuridine (BrdU), can incorporate itself into newly synthesized DNA during the S-phase of the cells. It is used to label proliferating cells in mice and it is widely used in the study of neurogenesis (Abrous et al., 2005). Timed pregnant mice were intraperitoneally injected with BrdU (0.1mg/g, dissolved in 0.09% NaCl solution) and sacrificed after 2 hours. The embryos were collected and tails were used for genotyping.

In order to investigate the proliferation of ventral glial cells in postnatal *Ali030* mice (P21), BrdU was intraperitoneally injected (0.05mg/g, dissolved in 0.09% NaCl solution) and the mice were sacrificed at 24 hours after injection.

4.2.1.3 Embryo and tissue preparation

Embryo preparation

The noon of the day on which the presence of the vaginal plug is regarded as day 0.5 of pregnancy

(E0.5). At noon next day the embryo is regarded as E1.5, and so on. For embryonic eyes, timed pregnant females were sacrificed by CO₂ asphyxiation and embryos were dissected and collected from uterus.

For cryosections or paraffin sections, the embryo heads were fixed in 4% PFA/0.1M PBS for at least two hours at room temperature, followed by washing in PBS and transferring in 30% sucrose until they sink to the bottom of the tubes. For cryosections, they were embedded in Tissue-Tek O.C.T (Sakura Finetek, USA) and stored at -80 °C. For paraffin sections, they were dehydrated in graded ethanol series (25%, 50% and 75% ethanol) for 10 minutes each and embedded in paraffin and stored at -20 °C.

For plastic sections, the embryos were fixed in Davidson's solution overnight, and then dehydrated in 100% ethanol for 3 times, with each for 15 minutes, followed by fixation in JB-4 solution (Polysciences, Germany), and then embedded in JB-4 plastic medium and stored at room temperature in dark.

Postnatal tissue preparation

For cryosections of whole postnatal eyes, mice were sacrificed by CO₂ asphyxiation or cervical dislocation and fresh eyes were immediately embedded in Tissue-Tek O.C.T and stored at -80 °C.

For the cryosections from postnatal retinal tissues, the mice were sacrificed by CO₂ asphyxiation or cervical dislocation, followed by dissection of the eyes. Further preparation was done in ice-cold PBS under the microscope. Briefly, the cornea was excised and the lens was removed. Then the retina and optic nerve were fixed in 4% PFA/PBS for 30 minutes at 4°C, followed by wash in PBS and then cryoprotection in 30% sucrose overnight at 4°C. The samples were embedded in Tissue-Tek O.C.T. Compound and stored at -80 °C before further processing.

For plastic sections, the procedure is the same as the method used in embryo preparation. The JB-4 plastic block holders were stored at room temperature in dark.

For the semithin section of the optic nerve, the procedure is the same as the method used in electron

microscopy sample preparation. Briefly, the samples were immersed in 2% PFA/2.5% glutaraldehyde in 0.133 M Sorensen's buffer, pH=7.2 for 24-48 hours at 4 °C. Then the samples were washed in 0.133 M Sorensen's buffer, pH=7.2 for three times. After that, the samples were stained with 2% OsO₄ in 0.133 M Sorensen's buffer for 1 – 1.5 h, followed by washing the samples in 0.1 M 0.133 M Sorensen's buffer, pH 7.2 for three times. Then the tissues were dehydrated in 50% ethanol, 50% ethanol, 70% ethanol, 90% ethanol and 95% ethanol for 10 minutes, respectively. The samples were infiltrated and embedded in *Embed-It* Low Viscosity Epoxy Resin using Embed-It™ Low Viscosity Epoxy Kit (Polysciences, Germany). Finally place the samples in the mold and let them polymerise in 60°C oven for 24-48 hours.

Eye tissue preparation for gene expression analysis

For real time PCR experiments, two eyes from each embryo or one eye from each postnatal mouse as one group were or was collected and stored at -80 °C for further experiments. The tail tissues were collected and stored at -20 °C for genotyping.

Eye tissue preparation for protein analysis

For Western blot experiments for embryonic eyes, twelve eyes from six E15.5 embryos as one group (wild types and mutants, respectively) were collected and stored at -80 °C for further experiments.

For Western blot experiments for 1 month eyes, four eyes from two mice were collected as one group (wild types and mutants, respectively). The eyes were stored at -80 °C for further experiments.

Sectioning of eyes

For the cryosections, the eyes were cut at 10 µm (embryonic eyes) or 12 µm (postnatal eyes or retina) using a Cryostat (Leica Microsystems, Germany) at -20 °C, and a series of sagittal or coronal sections were collected using SuperFrost® Plus slides (Menzel, Germany). The slides were stored in -80 °C.

For the paraffin sections, the embryonic eyes were cut at a thickness of 8 µm using Microtome

(Leica Microsystems, Germany), floated out on a warm water bath (37-40 °C) and then picked up by SuperFrost® Plus slides. The slides were dried on the warm plate at 37 °C for 1 hour and then stored at -20 °C.

For the plastic sections, the eyes were cut along a sagittal plane with a glass knife on a Microtome (Leica Microsystems, Germany) and the thickness of each section was at 2-3 µm. Then the sections were put into a drop of distilled water on the SuperFrost® Plus slides to remove any folding, followed by drying them on the hot plate (100 °C). The slides were stored at room temperature.

4.2.2 Clinical samples

This study was conducted in cooperation with Dr. Goran Petrovski from Department of Ophthalmology, University of Debrecen, Hungary and Dr. Xhevat Lumi from University Medical Centre Ljubljana, Slovenia. The study was approved by the Medical Ethics Committee of University Medical Centre Ljubljana, Slovenia, and informed consent was obtained from each patient according to the tenets of the Declaration of Helsinki. All the epiretinal membranes (ERM) and inner limiting membranes (ILM) were kindly provided by Dr. Goran Petrovski and Dr. Xhevat Lumi in the University Medical Centre Ljubljana. The ERMs and ILMs samples were collected from 15 patients with retinal gliosis, which were used for studying the expression of four different markers (GFAP, Sox2, Pax2 and Nestin) by whole-mount immunofluorescence. There are 6 patients with secondary retinal gliosis (retinal detachment, PVR, diabetic retinopathy, and uveitis) and 9 patients with idiopathic retinal gliosis. Totally 14 epiretinal membranes and 15 inner limiting membranes were used in the study. All the samples were fixed in 4% PFA for 24 hour to 1 week until further whole-mount immunofluorescence. The protocol details were described in 4.2.3.5. The clinical characteristics is summarized in Table 4.5.

Table 4.5 Clinical characteristics of epiretinal and inner limiting membranes

<i>No</i>	<i>Diagnosis</i>	<i>Types of Membrane</i>
1	Epimacular membrane (fibrotic), Lattice degeneration, retinal detachment	Secondary (Retinal detachment)
2	Epimacular membrane	Idiopathic
3	Epimacular membrane	Idiopathic

4	Rhegmatogenous retinal detachment	Secondary (Retinal detachment)
5	Proliferative diabetic retinopathy	Secondary (Diabetic retinopathy)
6	Epimacular membrane	Idiopathic
7	Epimacular membrane	Idiopathic
8	Epimacular membrane, uveitis	Secondary (uveitis)
9	Retinal detachment after PPV	Secondary (PVR)
10	Epimacular membrane	Idiopathic
11	Epimacular membrane	Idiopathic
12	Proliferative diabetic retinopathy	Secondary (Diabetic retinopathy)
13	Vitreomacular traction (VMT)	Idiopathic/VMT
14	Epimacular membrane	Idiopathic
15	Epimacular membrane	Idiopathic

PPV: Pars Plana Vitrectomy; PVR: Proliferative vitreoretinopathy.

4.2.3 Histology

4.2.3.1 Methylene blue and Basic fuchsin staining

The plastic sections were directly immersed in Methylene blue-Basic fuchsin solution for 25 seconds, followed by washing 4 times in MilliQ water, with each for 2-3 minutes. The slides were dried in the fume hood and mounted using EUKITT quick-hardening mounting medium.

4.2.3.2 Hematoxylin and Eosin staining

The paraffin sections were deparaffinized in xylene, with first change for 15 minutes and second change for 10 minutes. Then the slides were rehydrated in graded ethanol series (100%, 100%, 95%, 80%, 70%, 50%, 30%) with each for 2 minutes. After rinsing in MilliQ water, the slides were stained with Mayer's Hematoxylin for 3-5 minutes and then washed in tap water. The slides were immersed in 0.1% sodium bicarbonate solution for 1 minute. After rinsing in 95% ethanol, the slides were counterstained in Eosin Y solution for 30 seconds. Then the slides were dehydrated through 95% ethanol and 100% ethanol, with each for 5 minutes. The slides were dried in the fume hood and mounted with EUKITT quick-hardening mounting medium.

4.2.3.3 Toluidine blue staining

The cross sections (2-3 μm) of the optic nerve were immersed in Toluidine blue solution and dried on a hot plate for 1 minute, followed by washing them with tap water. The slides were mounted with EUKITT quick-hardening mounting medium after completely dried.

4.2.3.4 *In-situ* hybridization

Paraffin sections were deparaffinized through two changes of xylene with each for 15 minutes and then rehydrated in a graded series of ethanol (100%, 100%, 95%, 90%, 80%, 70%, 50%, 30%) with 2 minutes per change. Then the slides were fixed in 4% PFA for 30 minutes, incubated with proteinase K (2 mg/ml) and re-fixed in 4% PFA. After washing in PBS with two changes for 5 minutes each and in SSC for two times with each 2 minutes, the slides were incubated with hybridization solution for 30 minutes. Then the slides were incubated at 65°C overnight in hybridization solution with the DIG labelled probes.

Unbound probes were removed by washing three times with 20 minutes each, with 5 X SSC at room temperature and 0.5 X SSC with 20% formamide at 65 °C. After that, it cooled down to 37 °C in the same solution for 30 minutes. Then the slides were treated with RNase A (10 $\mu\text{g}/\text{ml}$) for 30 minutes at 37 °C. After washing, the slides were incubated with NTE buffer for 15 minutes at 37 °C.

After washing with 0.5X SSC for three times with each for 30 minutes at 65 °C and 2X SSC for 30 minutes, the slides were incubated in 1% blocking solution for 45 minutes and then overnight with antibody (1: 5000) at 4 °C.

After washing with TBST to remove unbound antibodies for 2 hours and with NTMT for 3 times with each for 15 minutes, and developed in staining solution at 4 °C. The slides were washed with NTMT for two times with each for 15 minutes, fixed in 4% PFA for 5 minutes, dried and mounted with Roti-mount and stored at 4 °C.

The results for *in-situ* hybridization were repeated in a series sections (5 sections per slide, two

slides) from two independent samples in each group at the same stage.

4.2.3.5 Immunofluorescence

Immunofluorescence for cryosections

The cryosections were washed in PBS, and then incubated with primary antibody in PBS/0.25%TritonX-100/3%FBS overnight at 4°C. After washing the slides for 3 times, with each for 5 minutes, the slides were incubated with secondary antibody in PBS/0.25%TritonX-100/3%FBS for 1-1.5 hours at room temperature. Then the slides were stained with DAPI (1:10000) for 10 minutes. After washing in PBS for three times, the slides were dried at room temperature in dark, mounted with Aqua-PolyMount medium and then stored at 4°C.

Immunofluorescence for paraffin sections

For the paraffin sections, the slides were deparaffinized in xylene for two times (15 minutes and 10 minutes, respectively). Then the slides were serially hydrated with 100% ethanol, 100% ethanol, 95% ethanol, 80% ethanol, 60% ethanol and 30% ethanol, with each for 5 minutes. After rinsing in distilled water, the slides were heated with antigen unmask solution (0.1 M sodium citrate buffer, pH 6.0) for antigen retrieval using microwave oven at 600W for 15 minutes, and then cooled down for 15 minutes at room temperature. The following procedure is the same to the immunofluorescence for cryosections.

Whole-mount or Flat-mount immunofluorescence

For the whole-mount immunostaining, E9.5 embryos were fixed in 4%PFA for 20 minutes, and then washed in PBS/0.1%TritonX-100 for two times, and penetrated in 0.1M Glycin/PBS. The embryos were incubated in primary antibodies or blocking solution (Control) for two days. After washing in PBST, the embryos were incubated with secondary antibodies for 24 hours, followed by staining in DAPI (1:10000) for 20 minutes. The embryos were preserved and imaged in 80% glycerol and the Poly-Mount mounting medium (Polysciences, USA). All the procedures were conducted under a microscope.

For the flat-mount immunofluorescence, the whole mouse retina and clinical gliosis samples (epiretinal membrane and inner limiting membrane) were used. The general procedure is the same

as whole-mount immunofluorescence, for the staining of clinical samples, the first antibody was incubated overnight and second antibodies were incubated for 1 hour at room temperature.

Immunofluorescence for staining cells

The cultured cells were washed with PBS for three times, with each for 5 minutes, followed by fixation with 4% PFA for 20 minutes. Then after washing in PBS for three times, the cells were rinsed in PBS/0.25% TritonX-100 for 10 minutes, followed by incubation with first antibody at 4°C overnight. After washing in PBS for three times, the samples were incubated with second antibody for 1 hour at room temperature. Finally, the samples were stained with DAPI for 10 minutes. Then the samples were mounted with Aqua-PolyMount medium.

In all the immunofluorescence methods above, negative control (without primary antibody but the same dilution of secondary antibody) were used to test whether the binding of the primary antibody with the given sample tissue is specific. All these immunohistochemistry mouse experiments were performed using a series of sections (4-10 sections per slide) from at least two independent samples at the same stage. For the whole-mount or flat-mount immunofluorescence mouse experiments, two samples from wild types and two samples from mutants or two samples from wild types and one sample as negative controls were used at one stage. Representative pictures were selected.

Table 4.6 Primary antibodies used in the study

Target protein	Species	Dilution	Catalog number	Company
β -actin-peroxidase (WB)	Mouse	1:2000	A3854	Sigma-Aldrich, Germany
BrdU	Rat	1:500	OBT0030CX	AbD Serotec, Germany
Brn3	Goat	1:100	Sc-6026	Santa Cruz, Germany
Calretinin	Rabbit	1:1000	7699/3H	Swant, Switzerland
Caspase 3	Rabbit	1:200	557035	BD Pharmingen, Germany
Col4A2	Rabbit	1:200	sc-70246	Santa Cruz, Germany
E-cadherin	Rat	1:200	U3254	Sigma-Aldrich, Germany

Foxe3	Rabbit	1:200	sc-134536	Santa Cruz, Germany
GFAP	Rabbit	1:500	G9269	Sigma-Aldrich, Germany
Glutamine Synthetase	Mouse	1:200	BD 610517	BD Biosciences, Germany
N-Cadherin(H-63)	Rabbit	1:250	sc-7939	Santa Cruz, Germany
Neurofilament 2H3	Mouse	1:100	None	Developmental Studies Hybridoma Bank, U.S
Neurofilament 200	Rabbit	1:500	N4142	Santa Cruz, Germany
Nestin	Mouse	1:500	561230	BD Pharmingen, Germany
Otx2	Rabbit	1:200	-----	From Dr. A. Simeone
Pax2	Rabbit	1:200	2549-1	Epitomics, Germany
Pax6	Rabbit	1:400	PRB-278P	Chemicon, Germany
PDE6b	Rabbit	1:500	PA1-722	Thermo Scientific, Germany
PKC- α	Mouse	1:500	Ab1723	Abcam, Germany
Prox1	Rabbit	1:1000	AB 5475	Millipore, Germany
PXDN (MG50)	Goat	1:80	sc-168598	Santa Cruz, Germany
PXDN (Immuno)	Rabbit	1:500	-----	From Dr. G. Bhave
PXDN (WB)	Rabbit	1:1000	-----	From Dr. G. Bhave
Sox2	Goat	1:500	sc-17320	Santa Cruz, Germany
γ -crystallin	Rabbit	1:200	sc-22746	Santa Cruz, Germany
TGF β 1	Rabbit	1:200	NB100-91995	Novus Biologicals, Germany

(BrdU Ab: a gift from Dr. Chichung Lie, IDG, HGMU; GS and CRALBP Ab: gifts from Mrs. Nicole Senninger and Prof. Marius Ueffing, Protein Science Department, HGMU; Neurofilament 200 Ab: a gift from Dr. Andrea Huber-Brösamle, IDG, HGMU; OTX2 Ab: a gift from Dr. Antonio Simeone, Institute of Genetics and Biophysics, CNR, Napoli, Italy; PXDN Ab (one for immunofluorescence and the other one for Western blot): gifts from Dr. Gautam Bhave, Vanderbilt University Medical Center, USA; WB: Western blot)

Table 4.7 Second antibodies used in the study

Name	Species	Dilution	Catalog No.	Company
Alexa Fluor ® 488	Anti-Rabbit	1:250	A21206	Invitrogen, Germany
Alexa Fluor ® 488	Ant-Rat	1:250	A21208	Invitrogen, Germany
Cy3	Anti-Goat	1:250	705-165-147	Dianova, Germany
Cy3	Anti-Rat	1:250	712-165-153	Dianova, Germany
Cy5	Anti-Mouse	1:250	715-175-150	Jackson immuno, Germany
Goat Anti-Rabbit IgG (HRP) (WB)	Anti-rabbit	1:1000	Ab6721	Abcam, Germany

(WB: Western blot)

Confocal microscopy

All the immunofluorescence pictures (single plane images and Z-stacks) were taken by Olympus confocal microscopy (Olympus, Hamburg, Germany). 20X, 40X, and 60X confocal objectives were used. The DAPI, Alex488, Cy3 and Cy5 fluorescence were detected by DAPI, 488, Cy3 and Cy5 (647) channel, respectively. The tissue sections (10-12 µm) were scanned from top to the bottom with 0.5-1 µm thickness of each scan. The colocalisation of two different fluorescence was observed by the scanning of the same thin sections (0.5-1 µm). For the control and mutant samples, the same laser power and the same HDR (High Dynamic Range Imaging) were used to take the pictures. The images were analyzed by a FluoView 1.7 software (Olympus, Japan).

4.2.3.6 Anterograde tracing

E15.5 embryos were fixed in 4% PFA in PBS overnight, and the cornea was incised by a forcep, the lens was removed and the optic cup was packed with DiI or DiO. The lens was sent back into the eyes and the cornea was covered. The embryos were refixed in 4% PFA in PBS for about 5 weeks at room temperature or 3 weeks at 37°C to allow the tracers to diffuse along axons completely. The optic nerve, optic chiasm and optic tract were exposed after removing the heads,

and analyzed under the stereo-fluorescence microscopy.

4.2.3.7 Morphometric analysis

For *KTA48* project, the middle sections of the eyes stained by methylene blue and Basic fuchsin were used to measure eye size, lens size and the depth of anterior chamber at E15.5, E17.5 and P21. The length between the central corneal epithelium and the central point of the optic nerve head was measured as eye size, the length between the anterior central point of anterior lens capsule and posterior lens capsule was measured as lens size. The depth of anterior chamber was measured between the central point of corneal endothelium and the central point of the anterior lens capsule. To measure the number of the secondary fiber cells of the lens in *KTA48* project (E15.5 and P21), the number of these cells with nuclei was calculated at the bilateral lens equator regions using Image J (<http://rsb.info.nih.gov/ij/>) and the average number was calculated and used for statistics. For *Ali030* project, the pictures from the anterograde tracing experiments were used to measure the thickness of the optic nerve at E15.5. The thickness was measured at three points of the optic nerve (proximal, distal and central) where are perpendicular to the optic nerve. The average thickness was calculated for statistical analysis.

4.2.4 Molecular biology technology

4.2.4.1 DNA isolation

The tails were collected and digested in 500 μ l lysis buffer containing protein kinase K and incubated at 55°C overnight (350 rpm shaking speed). Then proteins were precipitated with 5M NaCl and incubated on ice for 10 minutes. The samples were centrifuged at 6500 rpm for 15 minutes, followed by transferring the supernatant to new 1.5 ml tubes. DNA was precipitated with absolute methanol and centrifuged at 13000 rpm for 15 minutes at 4°C. Then the DNA pellet was washed with 70% ethanol to wash out the salts. After drying for 10 minutes, DNA was dissolved in dH₂O and stored at 4°C.

4.2.4.2 PCR reaction

PCR for genotyping

The primers Pxdn-Ex19-L1 and Pxdn-Ex19-R1 were used for *KTA48* genotyping and the primers AliCR, AliCF, AliWtF and AliMtF were used for *Ali030* genotyping. The sequence of the primers

were given in Table 4.1. The PCR reaction mix is given in Table 4.8 and 4.9. For *KTA48* genotyping, PCR initial activation step was at 94 °C for 2 min, followed by 40 three-step cycles (denaturation at 95 °C for 30 seconds, annealing at 55°C for 30 seconds, and extension at 72 °C for 30 seconds). Then PCR product was enzymatically digested with *Alw36I* at 37 °C for 2 hours. The DNA bands size were checked by agarose gel electrophoresis. For *Ali030* genotyping, PCR initial denaturation/enzyme activation step is carried out at 94 °C for 30 seconds, and the PCR cycles (32 cycles) consist of three-step cycling (denaturation at 95 °C for 30 seconds, annealing at 62°C for 30 seconds, and extension at 72 °C for 80 seconds). The PCR products were run on the 1.5% agarose gel to check the band size.

Table 4.8 The components of reaction mix for *KTA48* genotyping

Reagent	Volume per reaction (µl)
DreamTaq Green PCR Master Mix (2X)	5
Pxdn-Ex19-L1 (10 µM)	1
Pxdn-Ex19-R1 (10 µM)	1
Genomic DNA (100ng/µl)	1
MilliQ-H ₂ O	2
Total volume	10

Table 4.9 The components of reaction mix for *Ali030* genotyping

Reagent	Volume per reaction (µl)
DreamTaq Green PCR Master Mix (2X)	5
AliCR (10 µM)	1
AliCF (10 µM)	0.5
AliWtF/AliMtF (10 µM)	0.5
Genomic DNA (100ng/µl)	1
MilliQ-H ₂ O	2
Total volume	10

PCR for cloning *Bmpr1b* cDNA

The primers *Bmpr1b*-cDNA-CACCL1 and *Bmpr1b*-cDNA-R1SC were used for amplifying the whole-length *Bmpr1b* cDNA. The sequence of the primers were given in Table 4.2. The PCR reaction mix is given in Table 4.10. PCR initial denature step was at 98 °C for 30 seconds, followed

by 40 three-step cycles (denaturation at 95 °C for 10 seconds, annealing at 55°C for 30 seconds, and extension at 72 °C for 1 minutes). The target band was checked by running agarose gel electrophoresis.

Table 4.10 The components of reaction mix for amplifying *Bmpr1b* cDNA

Reagent	Volume per reaction (µl)
Phusion HF buffer (5X)	10
10 mM dNTPs (10 µM)	1
Forward primer (10 µM)	2.5
Reverse primer (10 µM)	2.5
Phusion DNA polymerase	0.5
cDNA (100ng/µl)	2
Nuclease-free H ₂ O	31.5
Total volume	50

4.2.4.3 Real time PCR

RNA isolation

RNA was extracted using RNeasy Mini Kit (Qiagen) according to the manufacture's instruction. Briefly, the samples were homogenized in 350 µl RLT containing 1% β-mercaptoethanol and then loaded in Qia-shredder column. After centrifugation, 100 µl DPEC-H₂O and 200 µl absolute ethanol were added into the lysate. After incubation at the RNeasy mini spin columns and centrifugation, the RNA was combined on the column. The column was washed with 350 µl RW1 buffer for 1 minute and centrifuged at maximum speed for 15 seconds. 70 µl RDD buffer containing 10 µl DNase 1 was added on the column to degrade DNA in the samples and incubated for 15 minutes. Then the columns were washed for two times using RW1 buffer. Then the columns were washed for two times with RPE buffer. Then transfer the column into new tubes and centrifuge for 2 minutes and further 5 minutes with open lid. The columns were left with open lids for 10 minutes and the RNA was dissolved in 30-50 µl DEPC-H₂O. RNA yield and purity were measured using NanoDrop ND-1000. The samples with A260/A280 above 2.0 and A260/A230 above 2.0 were used in the study.

cDNA synthesis

cDNA was synthesized using Ready-To-Go T-primed first strand kit (Invitrogen). 1-5 µg total RNA was used in 33 µl DEPC-H₂O and then was heated at 65°C for 5 minutes. Then it was incubated

at 37°C for 5 minutes and meanwhile the first-strand reaction mix was also incubated at 37°C for 5 minutes, followed by transferring the RNA solution to the first-strand reaction mix and incubating at 37°C for 5 minutes. After that, the reaction mix containing RNA was gently vortexed and briefly centrifuged. The mixture solution was incubated 37°C for 1 hour and then the cDNA was diluted 1:10 for PCR experiments. The samples were stored at -20°C.

Standardization of real-time PCR primers

The primers were standardized and the efficiency was tested before performing real-time PCR. Five different concentrations were used with each concentration repeating three times. The components of PCR reaction were described in Table 4.11. PCR reaction was performed with StepOne™ Real-Time PCR System (Applied Biosystem) and the standard curve was generated and analyzed by StepOne software 2.0. The primers with the efficiency above 90 were used in this study.

Table 4.11 The components of reaction mix for standardizing the primers

Reagent	Volume per reaction (µl)
5X HOT FIREPol® Eva Green qPCR mix	4
Primer Forward (10 µM)	0.5
Primer Reverse (10 µM)	0.5
cDNA (1:10)	4
DEPC-H ₂ O	11
Total volume	20

Quantitative real-time PCR

Quantitative real-time PCR was performed with StepOne™ Real-Time PCR System (Applied Biosystem). The components of the reaction mix was described in Table 4.12. In each reaction, 1 µl cDNA, 1 µl reverse and forward primers (1:1), 4 µl EvaGreen mix and 14 µl DEPC-H₂O were mixed in one well in a 96-well plate and centrifuged briefly. After the initial denaturation step at 95°C for 15 minutes, PCR reaction was cycled for 40 times with denature at 95°C for 30 seconds and annealing-extension temperature at 65 for 30 seconds. Relative expression was calculated following 2(-Delta Delta C(T)) method (Livak and Schmittgen, 2001).

Table 4.12 The components of reaction mix for qRT-PCR

Reagent	Volume per reaction (µl)
5X HOT FIREPol® Eva Green qPCR mix	4
Primer Forward (10 µM)	0.5
Primer Reverse (10 µM)	0.5
cDNA (1:10)	1
DEPC-H ₂ O	14
Total volume	20

4.2.4.4 Molecular cloning

DNA extraction from agarose gel

PCR product was amplified by Phusion DNA polymerase (New England Biolabs, Germany) and then run on 1.5% agarose gel. The target PCR band was extracted from the gel under UV illumination and purified using the NucleoSpin Gel kit (Macherey-Nagel, Germany). Briefly, the agarose gel with target band was dissolved in NT buffer (binding buffer) at 55°C for 10 minutes. Then the sample was transferred to a column and centrifuged at 12000 rpm for 1 minute to make DNA bind to the silica membrane, followed by wash with NT3 buffer (wash buffer) and centrifugation. The column was re-centrifuged to dry the silica membrane at 13,000 rpm for 2 minutes. DNA was eluted in 30 µl of elution buffer and stored at -20°C. DNA yield and purity were measured by NanoDrop ND-1000.

Adding 3' A overhang to a PCR product

Taq DNA polymerase (Invitrogen) was used to add 3' A overhang to the purified PCR (amplified by Phusion DNA polymerase). The reaction mix was described in Table 4.13. In each reaction, purified PCR product, dATP, PCR buffer, Taq DNA polymerase and DEPC-H₂O were mixed. Then the reaction mix was incubated at 72°C for 20 minutes to add 3' polyA tail.

Table 4.13 The mix components for A-addition reaction

Reagent	Volume per reaction (μ l)
Purified PCR product (10 ng/ μ l)	20
dATP (10 mM)	10
PCR buffer with Mg (10X)	5
Taq DNA polymerase (5U/ μ l)	0.2
DEPC-H ₂ O	14.8
Total volume	50

TA cloning

The PCR fragments were cloned into pcDNA3.1 vector according to the instruction (pcDNATM3.1/V5-His TOPO TA Expression Kit, Invitrogen). The components of TOPO Cloning reaction was described in Table 4.14. The reagents were mixed gently and incubated for 5 minutes at room temperature.

Table 4.14 The mix components of TOPO Cloning reaction

Reagent	Volume per reaction (μ l)
Fresh PCR product	3
Salt solution	1
TOPO vector	1
DEPC-H ₂ O	1
Total volume	6

Then 3 μ l of the TOPO Cloning reaction was added to a thawed vial of One Shot Chemically Competent *E.coli* and incubated on ice for 20 minutes, followed by incubation at 42°C for 1 minutes to heat-shock the cells. Then transfer the tube on ice. After mixing with 250 μ l S.O.C medium, the cells were incubated at 37°C for 1 hour with a shaking speed of 400 rpm. Then 80 μ l cells were put on the agarose gel with ampicillin and incubated at 37°C overnight. 5 single positive colonies were selected and then incubated in 5 ml LB medium at 37°C overnight, respectively. 4 ml of culture medium was used to isolate plasmid using mini-preparation by Nucleospin plasmid kit (Macherey-Nagel, Germany). *Hind*III and *Xho*I enzymes were used to digest the plasmid to see whether there is a target band. Then the plasmids were confirmed by sequencing in GATC Biotech. For the transfection experiments, the plasmid will be further amplified in 200 ml LB medium and purified by midi preparation.

Mini-preparation

The NucleoSpin Plasmid kit (Macherey-Nagel) was used for mini-preparation. 4 ml of culture medium was spinned down at 13,000 rpm for 30 seconds. After discarding the supernatant, 250 μ l Buffer A1 (resuspension buffer) was added to resuspend the cell pellet by vortex. Then 250 μ l Buffer A2 (lysis buffer) was added and mixed gently by inverting the tube and incubated for 5 minutes at room temperature. 300 μ l Buffer A3 (neutralization buffer) was added and mixed by inverting the tube, followed by centrifugation at 13,000 rpm for 5 minutes. The supernatant was transferred on the column and spinned down to make the plasmids bind to the silica membrane. The column was washed by 600 μ l Buffer A4 (wash buffer) and centrifuged at 13,000 rpm for 1 minute, followed by re-centrifugation for 2 minutes to dry the silica membrane. Then 50 μ l Buffer AE (Elution buffer) was used to elute the plasmid DNA. The DNA yield and purity were measured by NanoDrop ND-1000.

Midi-preparation

The Qiagen Midi Prep Kit was used for isolate large amounts of plasmids. Briefly, a single colony was cultured in 25 ml LB medium with selective antibiotic and then incubated at 37°C with vigorous shaking for 12-16 hours. The cells were centrifuged at 6000 x g for 15 min in a 15 ml falcon tube. Resuspend the bacterial pellet in 4 ml Buffer P1 thoroughly. 4 ml Buffer P2 (lysis buffer) was added and mixed by inverting the sealed tube for 5 times, and then incubate at room temperature for 5 min. 10 ml of Buffer P3 (neutralization buffer) was added and mixed by vigorously inverting for 5 times, and then incubated on ice for 15 min. Then the solution was centrifuged at 20,000 x g for 30 min at 4°C. The supernatant was transferred to a new falcon tube and centrifuged again at 20,000 x g for 15 min at 4°C. Transfer the supernatant to a new falcon tube gently. A QIAGEN-tip 100 was equilibrated by 4 ml Buffer QBT and allow the liquid to pass through the column by gravity flow. Then the QIAGEN-tip was washed by 10 ml Buffer QBT for two times. DNA was eluted with 5 ml Buffer QF (elution buffer). Then 3.5 ml isopropanol was added and mixed gently and centrifuged at 15,000 x g for 30 min at 4°C. The supernatant was discarded carefully.

DNA pellet was washed with 2 ml 70% ethanol and then centrifuged at 15,000 x g for 10 min.

After carefully discarding the supernatant, the pellet was air-dried for 5–10 min and dissolved in 100 µl TE buffer. Then DNA yield and purity were measured by NanoDrop ND-1000. The samples were used in this study with A260/A280 above 2.0 and A260/A230 above 2.0. All the samples were stored at -20°C.

4.2.4.5 Sequencing

PCR product and plasmids were sent to GATC Biotech (Konstanz, Germany) for sequencing using the Sanger method.

4.2.5 Cell culture techniques

4.2.5.1 Cell culture

MIO-MI (Moorfields/Institute of Ophthalmology-Müller 1) cell line, a retinal Müller cell line derived from postmortem adult human neural retina, was kindly provided by Dr. Stefanie Hauck (Research Unit Protein Science, HGMU) which originates from Dr. Astrid Limb (Moorfields Eye Hospital, London) (Limb et al., 2002; Lawrence et al., 2007). The cells were cultured in DMEM (Dulbecco's Modified Eagle's Medium) supplemented with L-glutamine, sodium pyruvate, 10% FBS (Fetal bovine serum) and 100× penicillin/streptomycin. The cells were kept in a humidified 5% CO₂ incubator at 37°C. When the adherent cells reach 80% confluence, they were detached with 1 × Trypsin-EDTA and split 1:6.

4.2.5.2 Cell number counting

The cultured cells were diluted in trypan blue at 1:1 - 1:3, and the cell number was counted in 2-3 big squares of a Neubauer chamber under the microscopy. The cells on the lower and right limits, and the dead cells stained with trypan blue were excluded. The cell number was calculated by the following formula.

$$\text{Cell concentration (number/ml)} = \text{average cell number/large square} \times \text{dilution factor} \times 10^4$$

4.2.5.2 Transient transfection of DNA plasmids into the cells

The day before transfection, 1×10^5 cells were grown in 500 µl of culture medium in 24-well cell culture plate without antibiotics. The next day when the cells grew to 80-90% confluent,

transfection reagents were prepared. Briefly, 2 µg plasmid (pcDNA3.1 *Bmpr1b* wt cDNA or pcDNA *Bmpr1b* mt cDNA or GFP-plasmid) was firstly diluted in 50 µl Opti-MEM medium and mixed gently. Then 1 µl lipofectamine 2000 was diluted in 50 µl Opti-MEM medium for 5 minutes at room temperature. The two solutions were mixed gently and incubated for 20 minutes at room temperature. 100 µl transfection complex were added to the culture medium from each well. The cells were incubated for 48 hours. TOPO2.1-GFP plasmid was used to test the transfection efficiency. Then the culture well was changed by new medium with antibiotics and for some wells, they were treated by BMP-2 (500 ng/ml) or GDF-5 (100 ng/ml; 500 ng/ml). The cells were incubated for 4 days before further processing.

4.2.6 Protein techniques

4.2.6.1 Total protein isolation from tissues

Add 20 µl RIPA buffer with protease inhibitors (Protease inhibitor cocktail, Roche, Germany) per 100 mg tissue to the tube and the sample was homogenized in a 1.5 ml tube, followed by sonication for three times on ice and then centrifugation at 13,000 rpm for 10 minutes at 4°C. The supernatant was removed and saved in a new tube.

4.2.6.2 Protein concentration measurement

Protein concentrations were measured using Roti®-Nanoquant protein quantitation assay (Roth, Germany) which is the modified Bradford method (Bradford, 1976). A series of the dilutions of BSA (Bovine serum albumin) was prepared (0; 2.5; 5; 10; 25; 50; 100; 200; 300; 400; 500 mg/l). 200 µl diluted Roti®-Nanoquant (5x) (1:5) was added into standard BSA and the diluted samples on 96-well plate. Incubate the culture plate for 5 mins at room temperature. OD590 and OD450 were measured and OD590/OD450 was plotted to yield the calibration curve.

4.2.6.3 Western blot analysis

Briefly, protein samples were adjusted to the same amount (20 µg). The loading buffer (4x) was added into the samples and incubated at 95°C for 10 minutes. The samples were loaded on the gel and the proteins were firstly transferred to a PVDF (Polyvinylidene fluoride) membrane in a transfer chamber by electrophoresis. The blotting is performed with plate electrodes in a horizontal direction with sandwiching gel and membrane between sheets of transfer buffer. The

electrophoretic transfer was carried out at a constant flow of 400 mA for 60 minutes at room temperature. The PVDF membranes were blocked in 5% milk powder in TBST for 30 minutes at room temperature. The membranes were washed with PBST on the shaker for two times, with each for 5 minutes. Then the membranes were incubated with primary antibody at 4°C overnight. After washing the membrane for 3 times in PBST, the horseradish peroxidase (HRP)-conjugated secondary antibodies were incubated for 45 minutes at room temperature on the PVDF membrane. After washing the membranes in PBST, the HRP from secondary antibody was detected by adding chemiluminescence detection reagent (ECL Prime Western Blotting Detection Reagent, Cat. No. RPN2232, GE Healthcare, UK) on the membrane. The membrane was visualized and the images were produced using ChemiDoc XRS system (Bio-Rad, Germany). Each Western blot result was repeated for three times.

4.2.7 *In vivo* retinal imaging and electrophysiology

4.2.7.1 Spectral domain optical coherence tomography (SD-OCT) imaging

This experiment was approved by the ethics committee of the upper Bavarian government (No. TVA#55.2-1-54-2531-78-06). SD-OCT was used to acquire retinal images. The mice were anesthetized with intraperitoneal injection of ketamine and xylazine and the pupils were dilated with 1% atropine. Then the mouse eyes were covered with lens glass to neutralize the refractive power of the cornea and make the OCT beam focus on the retina. OCT images were recorded with the equipment set to 30° field of view. Horizontal or vertical consecutive images were made in the center of the optic nerve head. To improve the ratio of the signal-to-noise, the images were averaged using the built-in functions in the system.

4.2.7.2 Electroretinography (ERG)

This experiment was approved by the ethics committee of the upper Bavarian government (No. TVA#55.2-1-54-2531-78-06). Ganzfeld ERG was performed in both eyes of the mice to examine the retinal function as described earlier (Dalke et al., 2004). The mice were kept in dark for at least 12 hours and then anesthetized with intraperitoneal injection of ketamine and xylazine. After the pupils were dilated with 1% atropine, the mice were placed on the sled. The ground electrode was inserted subcutaneously around the tail, the active electrodes were placed on both corneas and the reference electrode was inserted subcutaneously between the two eyes. The mice were introduced

into a handheld Ganzfeld LED stimulator (Espion ColorBurst; Diagnosys LLC, Littleton, MA) on a rail to guide the sled (High-Throughput Mouse ERG setup, Steinbeis-Transfer Centre for Biomedical Optics and Function Testing, Tübingen, Germany). The impedance of electrodes was tested before each measurement using the built-in algorithm (less than 10 k Ω at 50 Hz). ERGs were recorded from both eyes respectively under Ganzfeld stimulation at a frequency of 0.48 Hz in 10 steps at 0.0125, 0.025, 0.125, 0.5, 12.5, 5, 12.5, 50, 125, 500 and 12500 cd-s/m² and analyzed by built-in softwares.

4.2.8 Statistics

The two sample t-test was used to compare the means of two groups. If the variance was not equal and confirmed by F-test, a nonparametric Mann–Whitney test was used for further statistical analysis. If $p < 0.05$, it is reported as statistically difference.

5 Results

5.1 Part I : *Peroxidasin* is essential for eye development

5.1.1 The expression of peroxidasin in the developing and postnatal eye

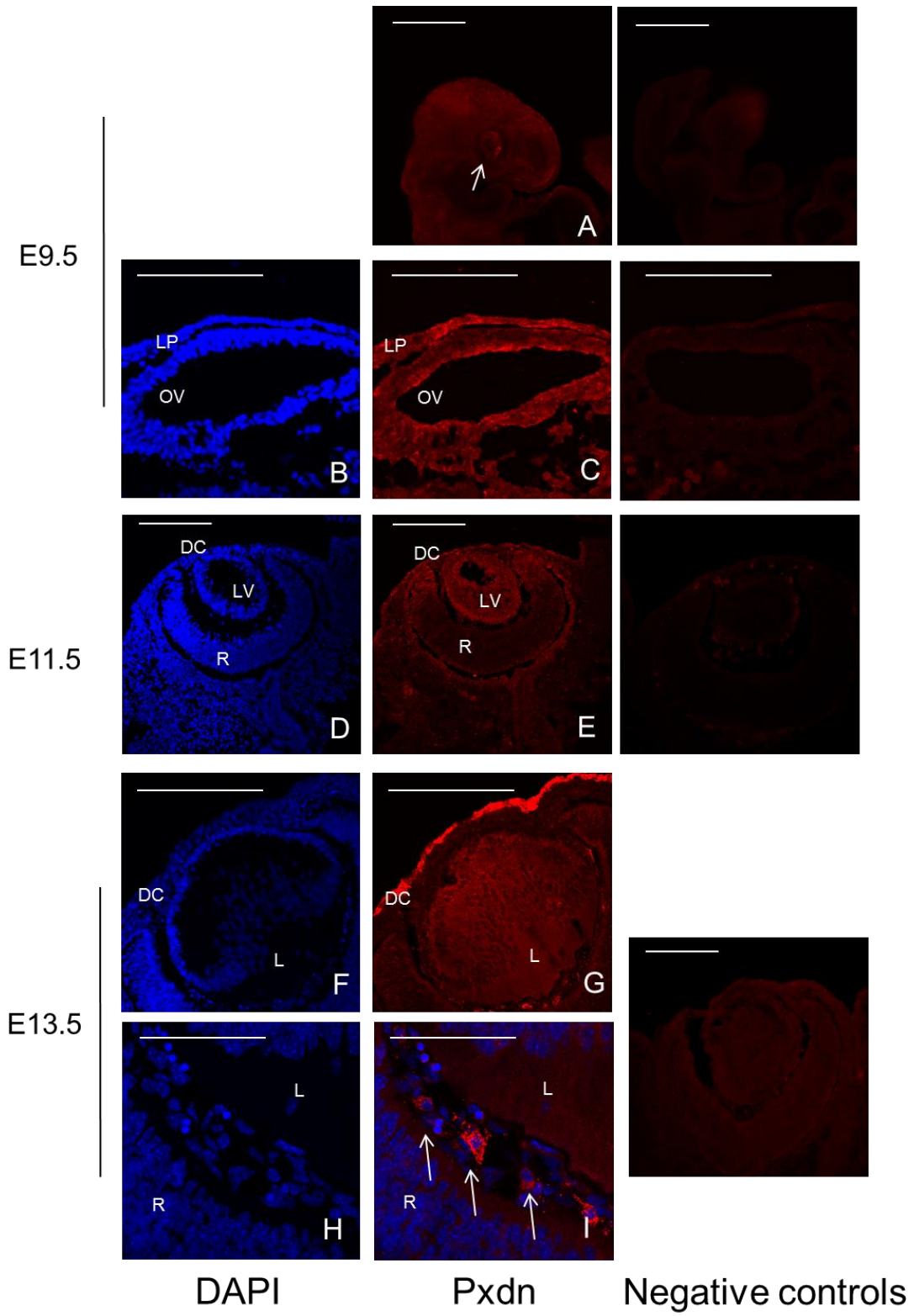
To investigate the expression of peroxidasin in eyes, immunofluorescence staining for Peroxidasin (PXDN) was performed at different stages. The embryonic eyes were analyzed at E9.5, E11.5, E13.5 and E17.5. Postnatally, the peroxidasin expression was analysed at 3 months. At E9.5, the earliest stage of eye development, the expression of peroxidasin is mainly detected in the eyes by whole-mount immunostaining (Figure 5.1, I, A), and further immunostaining for sections demonstrated that peroxidasin is specifically expressed in the lens placode and optical vesicle at E9.5 (Figure 5.1, I, B-C). At E11.5, peroxidasin is mainly expressed in the developing cornea and lens (Figure 5.1, I, D-E). At E13.5, peroxidasin is strongly expressed in the developing cornea and nucleated cells in the vitreous and weakly expressed in the anterior lens (Figure 5.1, I, F-I). Interestingly, these nucleated cells appear to secrete peroxidasin into the vitreous cavity (Figure 5.1, I, I). At E17.5, the expression of peroxidasin is dramatically decreased compared to the previous stages and it is still highly expressed in the corneal epithelium and eye lids, but weakly expressed in the lens and inner limiting membrane (Figure 5.1, I, J-O). Peroxidasin staining is not found in the vitreous at E17.5, because the vitreous cells are almost missing at this stage. Interestingly, similar to the nucleated cells in the vitreous at earlier stage, these cells in the anterior chamber also express peroxidasin but the expression is weaker (Figure 5.1, I, L). In adult mice (3 months), the expression of peroxidasin is only maintained in the corneal epithelium, the lens epithelium and in the outer layer of lens capsule (Figure 5.1, I, P-S). All the negative controls (without primary antibody) showed absent fluorescence or very weak fluorescence compared to wild types (Figure 5.1, I, negative controls).

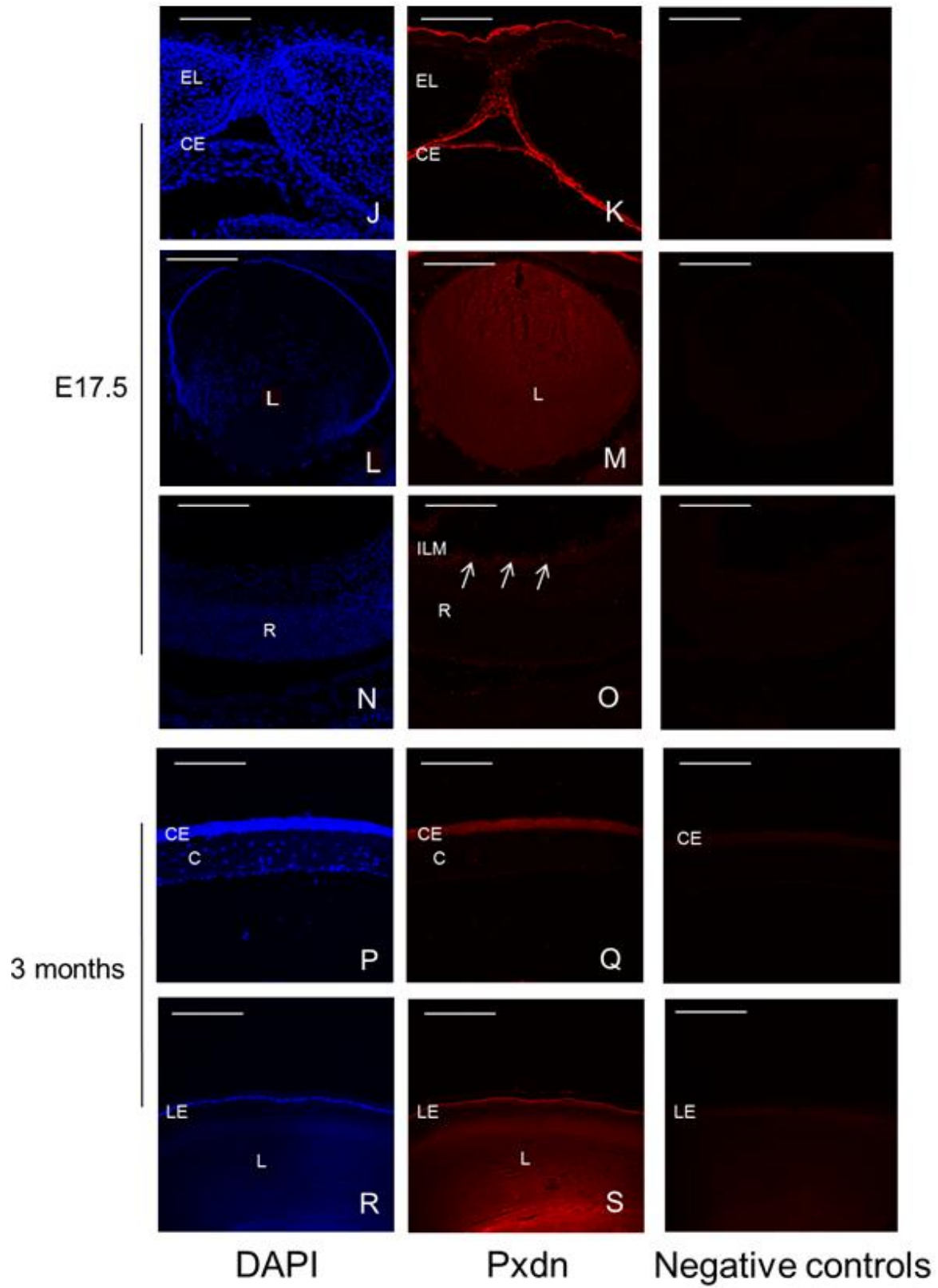
Moreover, I would like to confirm the expression pattern of *Pxdn* in the eyes using a different PXDN antibody. Therefore, I did the expression pattern of peroxidasin during eye development using another PXDN antibody from Dr. Gautam Bhawe (Vanderbilt University Medical Center, USA). At E11.5, *Pxdn* is weakly expressed in the lens vesicle especially the lens epithelium cells

(Figure 5.1, II, A-B). At E13.5, Pxdn is highly expressed in the lens especially the lens epithelium cells and also expressed in the nuclear cells in the vitreous (Figure 5.1, II, C-D). At E17.5, Pxdn is mainly expressed in the lens including the epithelium cells as well as the inner nuclear blast layer (Figure 5.1, II, E-F). All the negative controls (without primary antibody) showed absent fluorescence or very weak fluorescence compared to wild types (Figure 5.1, II, negative controls).

From the results performed by MG50 antibody, peroxidase is strongly expressed in developing cornea especially corneal epithelium, and vitreous nucleated cells, but weakly expressed in the lens and inner limiting membrane during eye development. Later the expression is reduced during postnatal period and in adult it is only expressed in the corneal epithelium and the lens epithelium. These peroxidase-positive nucleated cells in the vitreous could be some of the component cells of vitreous hyaloid vascular system during eye development. From the results performed by another PXDN antibody (Dr. G. Bhave), peroxidase is mainly expressed in the lens especially lens epithelium cells, vitreous nucleated cells and inner part of the retina, but weakly expressed in the developing cornea during eye development. The differences between both antibodies may be due to a different sensitivity of the antibodies and different antigen epitopes. For MG50 antibody, an internal region of MG50 of human origin was used to raise the antibody. However, the exact amino acid sequence of this internal region is lacking due to the Santa Cruz company proprietary information. For PXDN antibody from Dr. G. Bhave, the peptide (sequence: IREKLRLYGSTLNI) from human PXDN was used to raise the antibody and antigen affinity purification was used to purify the antibody. The mouse sequence differs only by the sixth amino acid of this peptide (K in humans and Q in mouse).

I.





II.

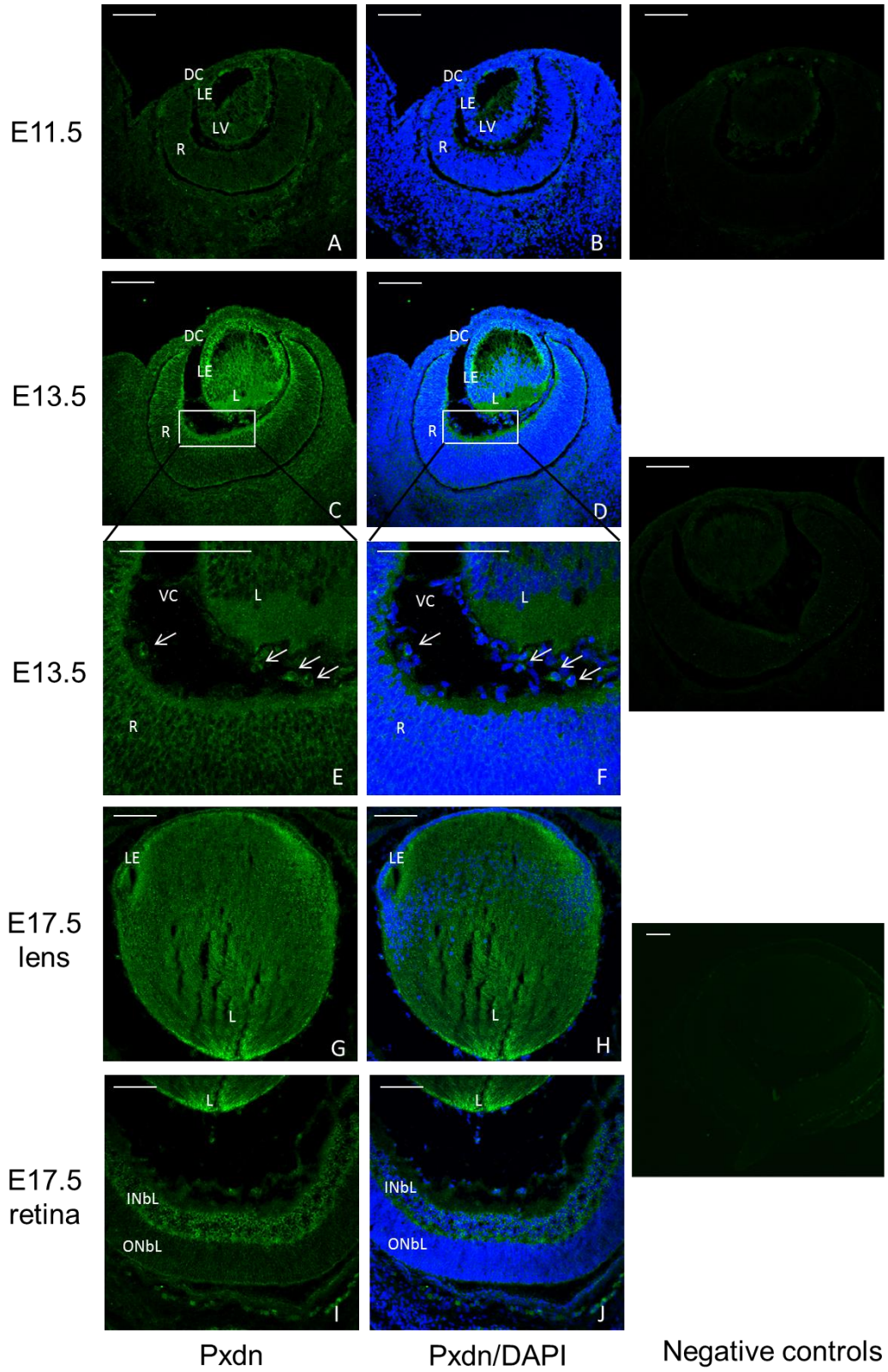


Figure 5.1 The expression pattern of peroxidasin from eye development to adult.

I. The expression pattern of peroxidasin in the eyes using MG50 antibody. (A-E) Whole-mount immunostaining showed that peroxidasin is expressed in the eye at E9.5 (A, arrow) and there is no staining in the eyes of the negative control. Further sectional immunostaining showed that it is expressed in the lens placode and optic vesicle at E9.5 (C) and it is still expressed in the developing cornea and lens vesicle at E11.5 (E). (F-I) By E13.5, it is still highly expressed in the developing cornea but weakly expressed in the anterior lens (G). In addition, it is highly expressed in the vitreous nucleated cells and it appears to be secreted by these cells (I, arrow). (J-O) At E17.5, the expression level of peroxidasin is reduced and it is mainly expressed in the developing corneal epithelium and eye lid (K) and the lens (M). It appears that it is weakly expressed in the inner limiting membrane at this stage (O, arrow). (P-S) At adult (3 months), it is only expressed in the cornea epithelium (Q), lens epithelium and outer layer of the lens capsule (S). C: cornea; CE: corneal epithelium; DC: developing cornea; EL: eye lid; ILM: inner limiting membrane; L: lens; R: retina; LC: lens capsule; LE: lens epithelium; LP: lens placode; LV: lens vesicle; OV: optic vesicle. Red: peroxidasin; Blue: DAPI. Scale bar: 100 μ m.

II. The expression pattern of peroxidasin in the eyes using PXDN antibody (from Dr. G. Bhawe). (A-B) At E11.5, Pxdn is weakly expressed in the lens vesicle. (C-F) At E13.5, Pxdn is expressed in the lens especially in the lens epithelial cells, the nuclear cells in the vitreous (arrow) and inner part of the retina. (E-H) At E17.5, Pxdn is mainly expressed in the lens (E-F) and inner nuclear blast layer (G-H). There is very weak or absent staining in the eyes of the negative control on the most right side of each column. DC: developing cornea; L: lens; R: retina; LE: lens epithelium; LV: lens vesicle; INBL: inner neuroblast layer; ONBL: outer neuroblast layer. VC: vitreous cavity. Green: peroxidasin; Blue: DAPI. Scale bar: 50 μ m.

5.1.2 The point mutation in *peroxidasin* causes loss of function of peroxidasin

In the ENU-induced *peroxidasin* mutant mice (*KTA48* mutants), a point mutation (T3816A in the *peroxidasin* mRNA coding sequence) was found in the peroxidase domain. It is predicted that it causes a premature stop codon, resulting in a partial loss of function of peroxidasin. Whether this mutation affects the expression level of peroxidasin is unclear. Peroxidasin is predicted to have two isoforms, one is full-length protein (X1 isoform, 1475 aa) and the molecular weight is 167 kDa (NCBI Reference Sequence: XP_006515268.1), and the other one is X2 isoform (784 aa) and the molecular weight is 88 kDa (NCBI Reference Sequence: XP_006515269.1). The total amino acid sequence of the X2 isoform is the sequence from 720 aa to 1503 aa of the X1 isoform. This PXDN antibody was made against the peptide (sequence: IREKLRLYGSLNI) from human PXDN. The mouse sequence differs only by the sixth amino acid (K in humans and Q in mouse). Western blot showed that peroxidasin is expressed in E15.5 eyes (target band 167 kDa, the first band, Figure 5.2, A), whereas it is absent in the mutant eyes at E15.5 (Figure 5.2, A). This result showed that peroxidasin is expressed in a relatively low level compared to β -actin in wild types (Figure 5.2, A) and loss of function of peroxidasin occurs in the eyes of *KTA48* mutants during embryonic eye development. This may be due to instability of N-terminal structure of the protein (a stop codon is formed in the peroxidase domain at the N-terminal of this protein) which could further lead to protein degradation. Interestingly, there is a 150 kDa band in E15.5 wild-type eyes.

This band could be a proteolytic processing product or alternative splicing of Pxdn. However, nonspecific band cannot be ruled out completely. At 1 month, the target band (167 kDa) was not found in wild-type eyes at 1 month (Figure 5.2, B). However, there is only one band (around 100 kDa) found in wild-type and mutant eyes, and there are no obvious differences in the level of protein expression between wild-type and mutant eyes (Figure 5.2, B). Thus, whole-length peroxidasin could not be expressed or very weakly expressed in the mouse eyes at 1 month. Moreover, this 100 kDa band was also found in both wild types and mutants at E15.5. The 100 kDa band could be an alternative splicing product of Pxdn (Figure 5.2, B). However, nonspecific band cannot completely be ruled out. Mass spectrometry could be helpful to identify them in the future.

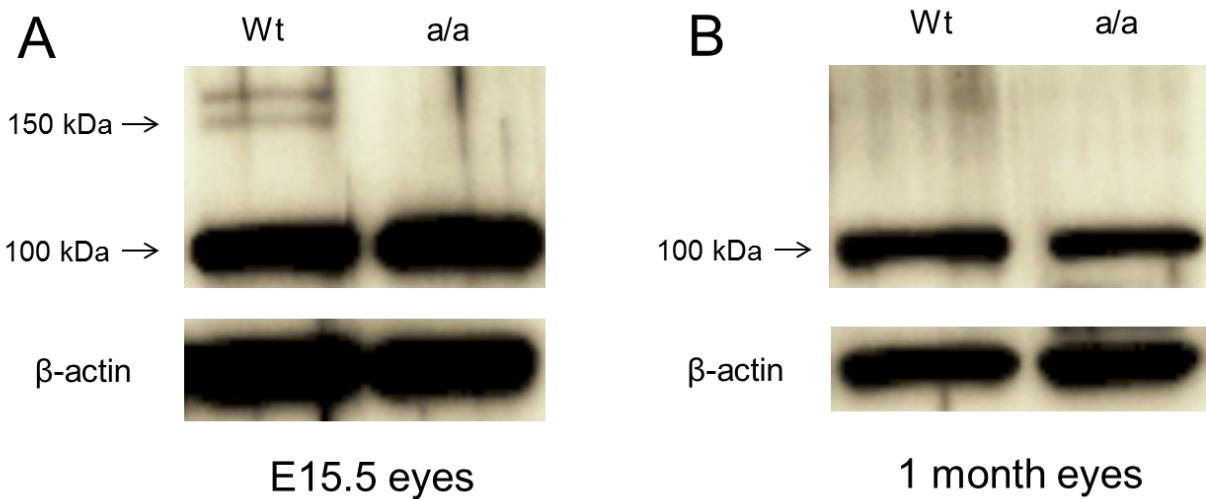


Figure 5.2 The expression of peroxidasin is reduced in *KTA48* mutants. (A) The comparison of peroxidasin expression from whole eyes protein between wild types and mutants at E15.5 by western blot. There are three bands (target band 164 kDa, 150 kDa and 100 kDa) detected in wild-type eyes at E15.5 by Western blot. However, in mutants, there are one band (100 kDa) detected, whereas two bands (164 kDa and 150 kDa) are absent. β -actin was used as positive controls and there are no obvious differences in the protein expression between wild types and mutants at E15.5. Compared to the expression of β -actin, peroxidasin expresses in very low level. (B) The comparison of peroxidasin expression from whole eyes protein between wild types and mutants at 1 month by western blot. There is one band (around 100 kDa) in both wild-type eyes and mutant eyes at 1 month. β -actin was used as positive controls and there are no obvious differences in the protein expression level between wild types and mutants at 1 month. The band marker (Precision Plus Protein™ Dual Colour Standards (BIO-RAD, Germany)) was used.

5.1.3 Anterior segment and eye size are severely affected in *KTA48* mutant embryos during eye development

Based on the expression pattern of peroxidasin in the embryonic eyes, the role of peroxidasin in

eye development was investigated using *peroxidasin*-mutant mice (also called *KTA48* mutants). Here I compared wild types and *KTA48* homozygous mutants. Firstly, I performed and analysed eye histology in different embryonic stages. At E9.5 and E11.5, there is no obvious difference between wild types and mutants (Figure 5.3, A-D). At E13.5, there are no obvious differences in the lens and eye size between wild types and mutants, but retroental cell mass is found in the vitreous in mutants (Figure 5.3, E-F). At E15.5, the ocular phenotype is the most obvious in *KTA48* mutants compared to previous periods (Figure 5.3 G-H and 5.5 A-H). Specifically, the lens size is significantly reduced in mutants compared to wild types ($p < 0.05$) but there is no statistical difference in eye size between wild types and mutants at this stage (Figure 5.4). Moreover, the anterior segment is severely impaired in mutants compared to the wild types. All the mutants showed that the lens epithelia and capsule are ruptured which causes abnormal migration of the lens fiber cells into the anterior and posterior chamber and vitreous (Figure 5.3, H; Figure 5.5, D, F; Table 5.1). The anterior and posterior chamber including iridocorneal angle are filled by lens fiber cells. In some cases (12/28, 42.9%), the lens vesicle remains attached to the cornea by a persistent connecting lens stalk (Figure 5.5, B; Table 5.1). In 75% mutant mice (21/28), retroental tissue in the vitreous (Figure 5.3, H, J; Table 5.1). The corneal stroma thickens, the number of keratocytes is increased, their parallel arrangement is distorted and the keratocytes are more densely distributed (Figure 5.5, B). This corneal phenotype was found in those mutants with lens stalk, which could be due to the differentiation of mesenchymal cells into corneal stromal cells affected by the lens stalk. At E17.5, the mutant eyes present more severe ocular phenotypes (Figure 5.3, J; Figure 5.5, J, K-M), both the eye and lens size were significantly smaller than those in wild types ($p < 0.05$) (Figure 5.4) and the anterior segment was further developmentally delayed in mutants and the anterior chamber angle is filled by lens fibers depending on the range which lens fibers invade (Figure 5.3, J; Figure 5.5, J). At E15.5, a part of the anterior chamber (Fig. 5.3, H) was filled by the lens fibers, whereas at later stage the anterior chamber is further filled by more lens fibers (Fig. 5.3, J). The lens epithelium was severely disorganized with some cells missing and the lens capsule was more severely ruptured, and the anterior and posterior chamber were filled with more lens fibers (Figure 5.3, J). The retina in a few mutants (9/28, 32.1%) showed ruptures of the inner limiting membrane which were accompanied by the inner retinal cells migrating out of the inner limiting membrane, and retinal folds are also found (Figure 5.5, L-M; Table 5.1). All the mutant eyes and lens analysed were smaller than wild types from E17.5 to adult

($p < 0.05$, Figure 5.4) and the depth of anterior chamber is progressively reduced from E17.5 to adult ($p < 0.05$, Figure 5.4), suggesting that the development of normal eye growth is affected in these mutant mice and the anterior segment development is progressively affected.

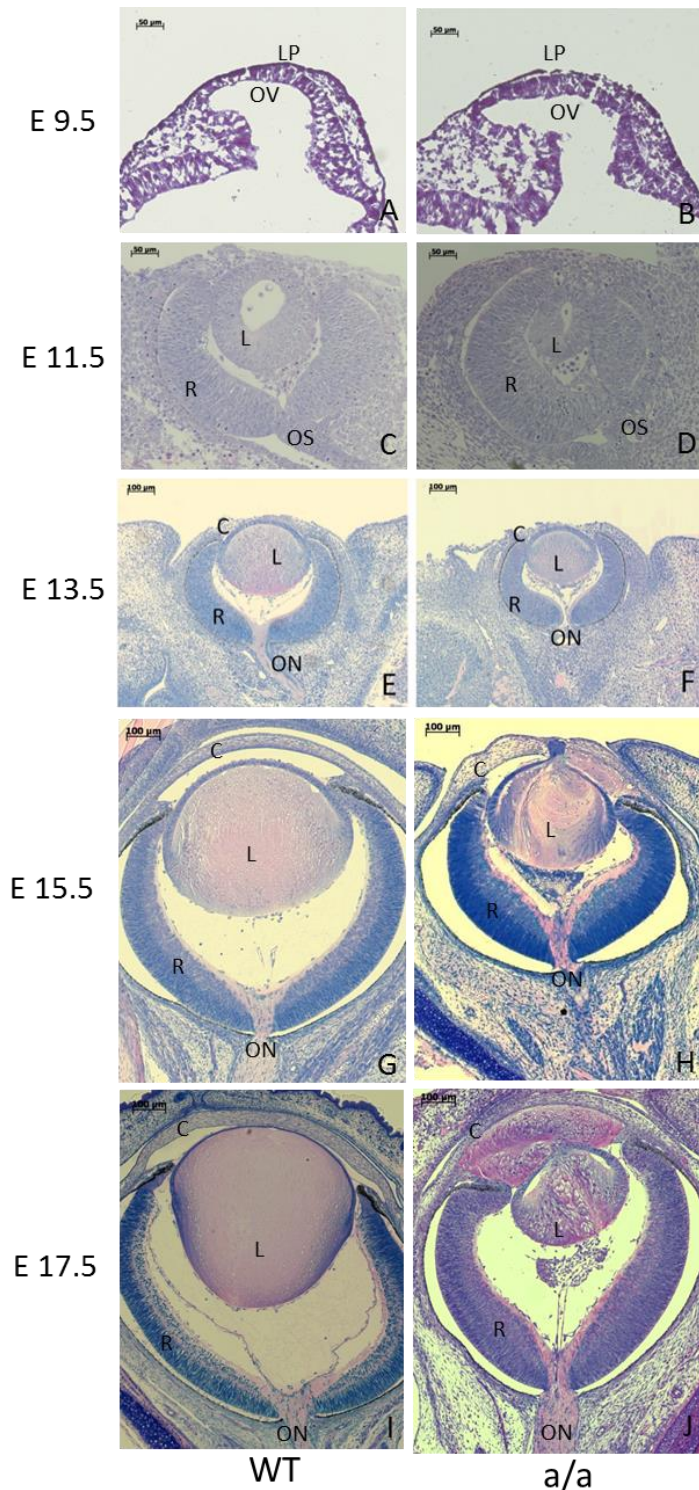


Figure 5.3 Anterior segment is severely affected during eye development in *KTA48* mutants. (A-D) At E9.5 and E11.5, there is no obvious difference between wild types and mutants. (E-F) At E13.5, there are not dramatic difference in the lens between wild types and mutants, but there is abundant retrolental cells in the vitreous in mutants. (G-H, O-P) At E15.5, when the eye phenotype is the most obvious, the lens size is smaller in mutants compared to wild types. The lens epithelium and capsule are ruptured and lens fibers migrate into the anterior chamber and posterior chamber. The lens matrix is disorganized and in some cases the lens is attached to the cornea by a persistent lens stalk and the retrolental tissue in the vitreous. (I-J) At E17.5, the eye phenotype is more severe in mutants. The anterior chamber is further filled by the lens fibers and the lens matrix is obviously disorganized. There are still retrolental tissues in the vitreous in mutants. (K-L). The ocular phenotypes in mutants are variable. In most cases, the cornea is detached from the lens, but in some cases the corneal-lens adhesion are persistent. All the cases have a rupture in the lens epithelium and capsule. C: cornea; L: lens; R: retina; LP: lens placode; OV: optic vesicle; ON: optic nerve. Scale bar: A-D, 50 μm; E-J, 100 μm.

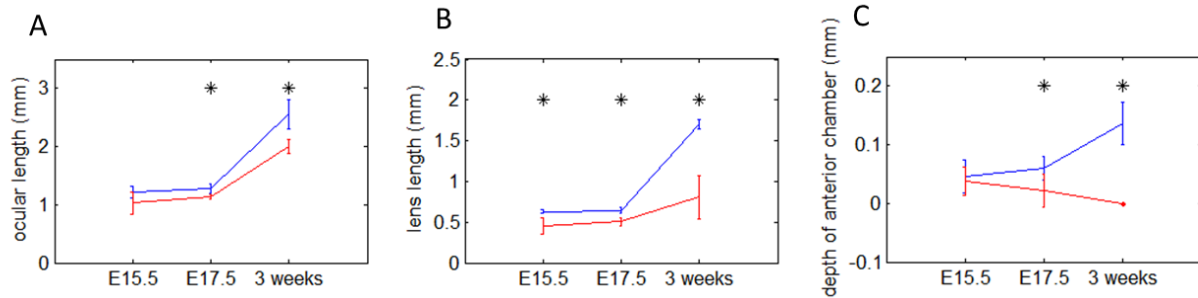
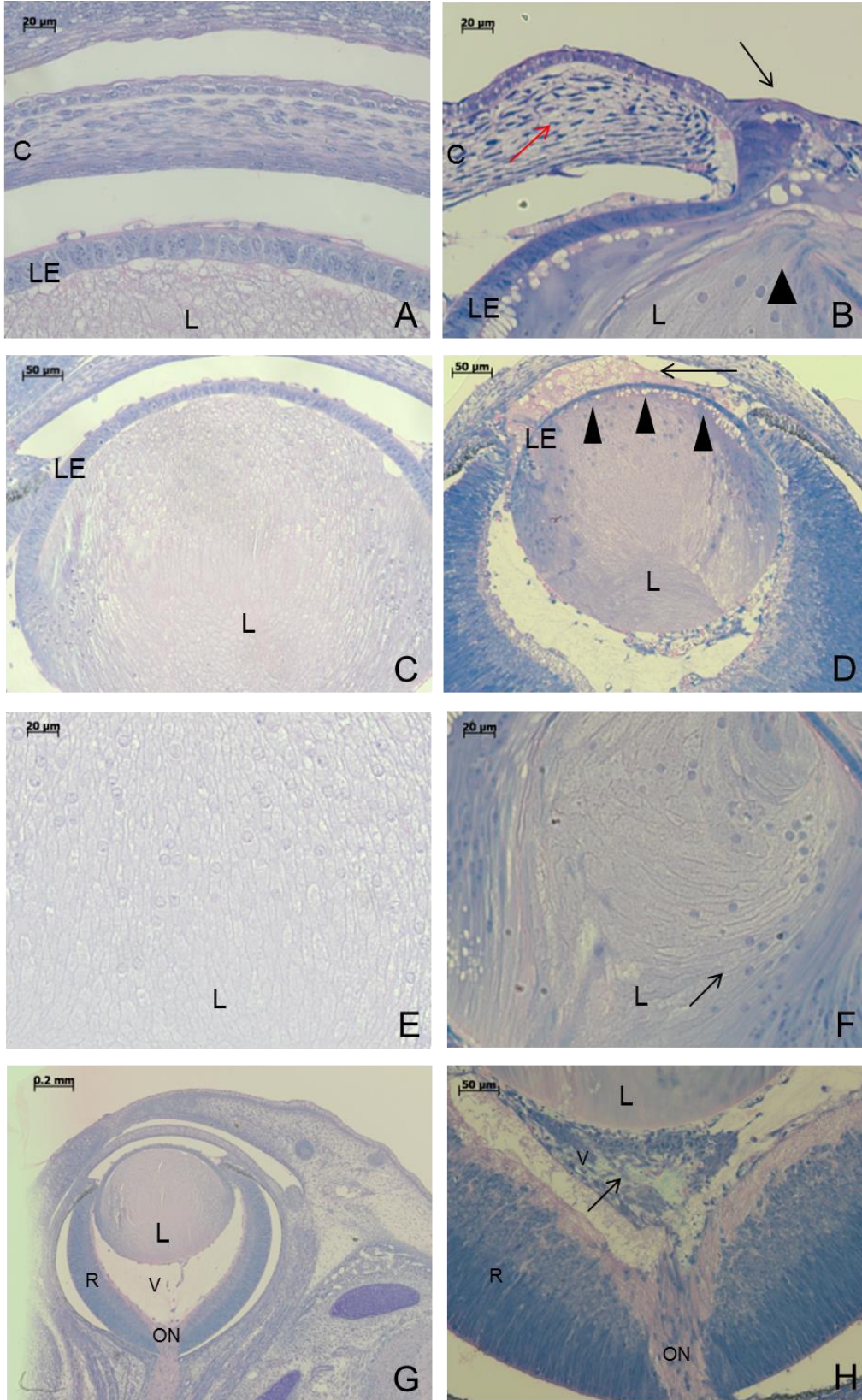


Figure 5.4 Reduced eye and lens size, and the depth of anterior chamber in *KTA48* mutants during eye development. (A) At E15.5, there is no differences in ocular length between wild types (blue line) and mutants (red line) ($p>0.05$), but the ocular length is significantly reduced at E17.5 and further decreased at P21 (red line) compared to wild types (blue line) ($p<0.05$). (B) Then lens size is slightly reduced at E15.5 and E17.5 and obviously decreased in mutants (red line) compared to wild types (blue line) at P21 ($p<0.05$). (C) There is no significant difference in the depth of anterior chamber between wild types (blue line) and mutants (red line) at E15.5 ($p>0.05$). But from E17.5, the depth of the anterior chamber is obviously reduced in mutants (red line) compared to wild types (blue line) ($p<0.05$) due to the lens fibers moving outside, especially at P21, the anterior chamber is almost missing because the anterior chamber is filled by the lens fibers and the lens is attached to the cornea. Blue line: wildtype; Red line: homozygous mutants; asterisk (*): $p<0.05$. The number of the sample eyes was used: E15.5 (Wt 4, Mt 4); E17.5 (Wt 6, Mt 7); P21 (Wt 6, Mt 6).

Table 5.1 Summary of eye phenotypes in *KTA48* homozygous mutants at E15.5-E17.5

Phenotype	Smaller lens	Disorganized lens matrix	Lens rupture	Lens tissue in AC	Lens tissue out of the eye	Lens stalk	Retrolental tissue in the vitreous	Retinal folds and rosset
Number (28 eyes)	25/28	27/28	28/28	26/28	2/28	12/28	21/28	9/28
Percentage	89.3%	96.4%	100%	92.9%	7.1%	42.9%	75%	32.1%

This data is based on the histological observation of 28 eyes. AC: anterior chamber



WT

a/a

E15.5

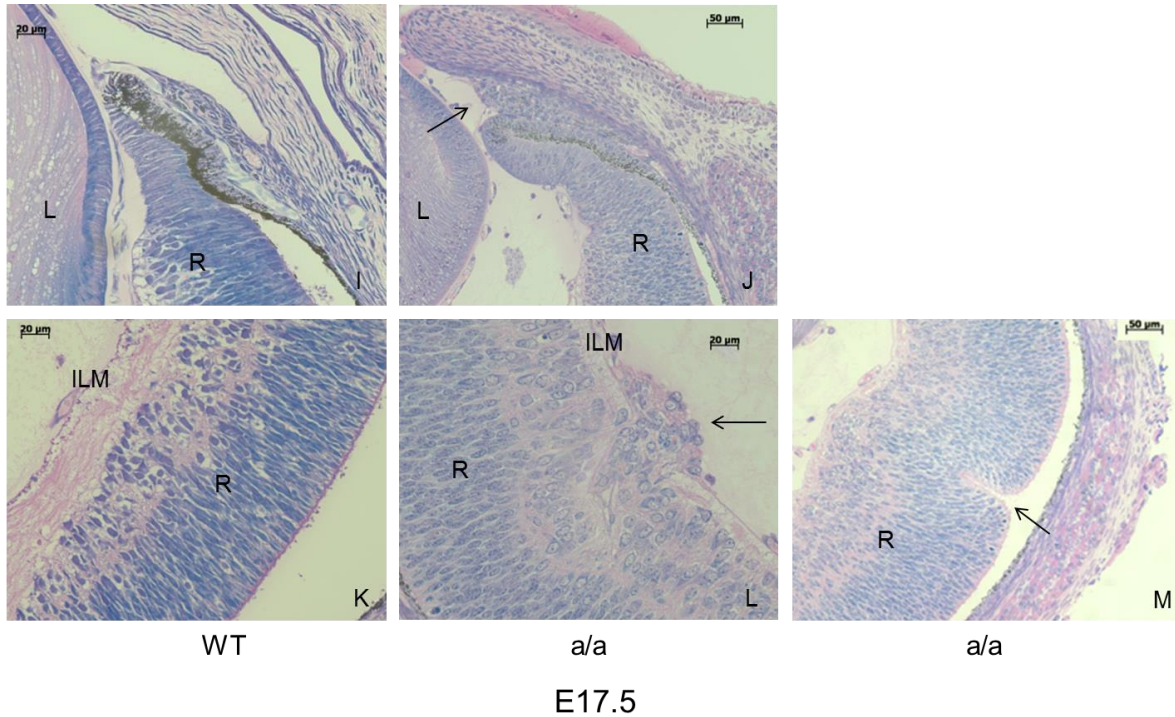


Figure 5.5 The most obvious ocular phenotype in *KT448* mutants at E15.5 and E17.5. (A-H) At E15.5, there are persistent corneal-lens adhesion (B, black arrow), disorganized corneal stroma (B, red arrow), rupture in lens capsule and lens epithelia (B, arrowhead), lens matrix in the anterior chamber (B), thinner lens epithelium (D, arrowheads), disorganized lens matrix (F), abnormal fiber cell migration (F, arrow) and more vitreous mesenchymal tissues (H, arrow) in *KT448* mutants. (I-M) At later stage E17.5, the anterior chamber angle is developmentally delayed (J) in mutants and there are more mesenchymal cells in the anterior chamber angle (J) compared to wild types (I). In very few cases, the rupture in retinal limiting membrane was found (L) and retinal rosette structure is formed (M). C: cornea; L: lens; R: retina; V: vitreous cavity; LE: lens epithelium; ON: optic nerve; ICA: corneal-iris angle; ILM: inner limiting membrane. Scale bar: A-B, E-F, I-M, 20 μm ; C-D, H, 50 μm ; G, 200 μm .

5.1.4 Reduced proliferation and aberrant differentiation of the lens during eye development in *KT448* mutants

E14.5, E15.5 and E17.5 pregnant mice were injected with BrdU and sacrificed two hours after injection. At E14.5, BrdU labelling showed an intense cell proliferation of lens epithelium and cornea in wild types (N=2), but a sparse distribution of BrdU positive cells in the anterior lens epithelium of the mutants (N=2) (Figure 5.6, A-B). At E15.5, there are a number of lens epithelial cells which were incorporated with BrdU in wild types (N=5), whereas in mutants BrdU incorporated cells were obviously reduced in the lens epithelial cells (N=5) (Figure 5.6, C-D). At E17.5, there is a number of BrdU positive cells in the anterior lens epithelium of wild types (N=2), whereas very few positive cells are found in mutants, but the proliferation of the epithelial cells in

the transition zone is not affected (N=2) (Figure 5.6, E-G). These results demonstrated that the lens proliferation of *KTA48* mutant embryonic eyes is reduced but the proliferation of the epithelial cells in the transition zone is not severely affected.

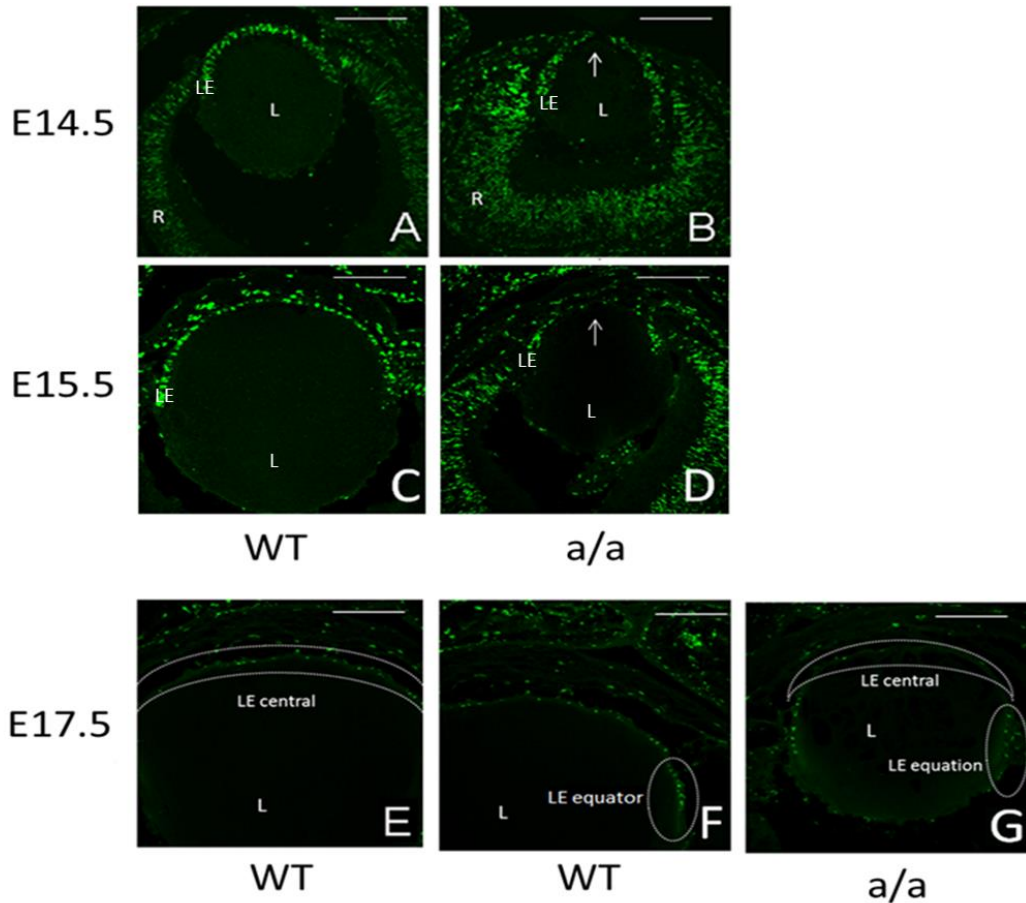
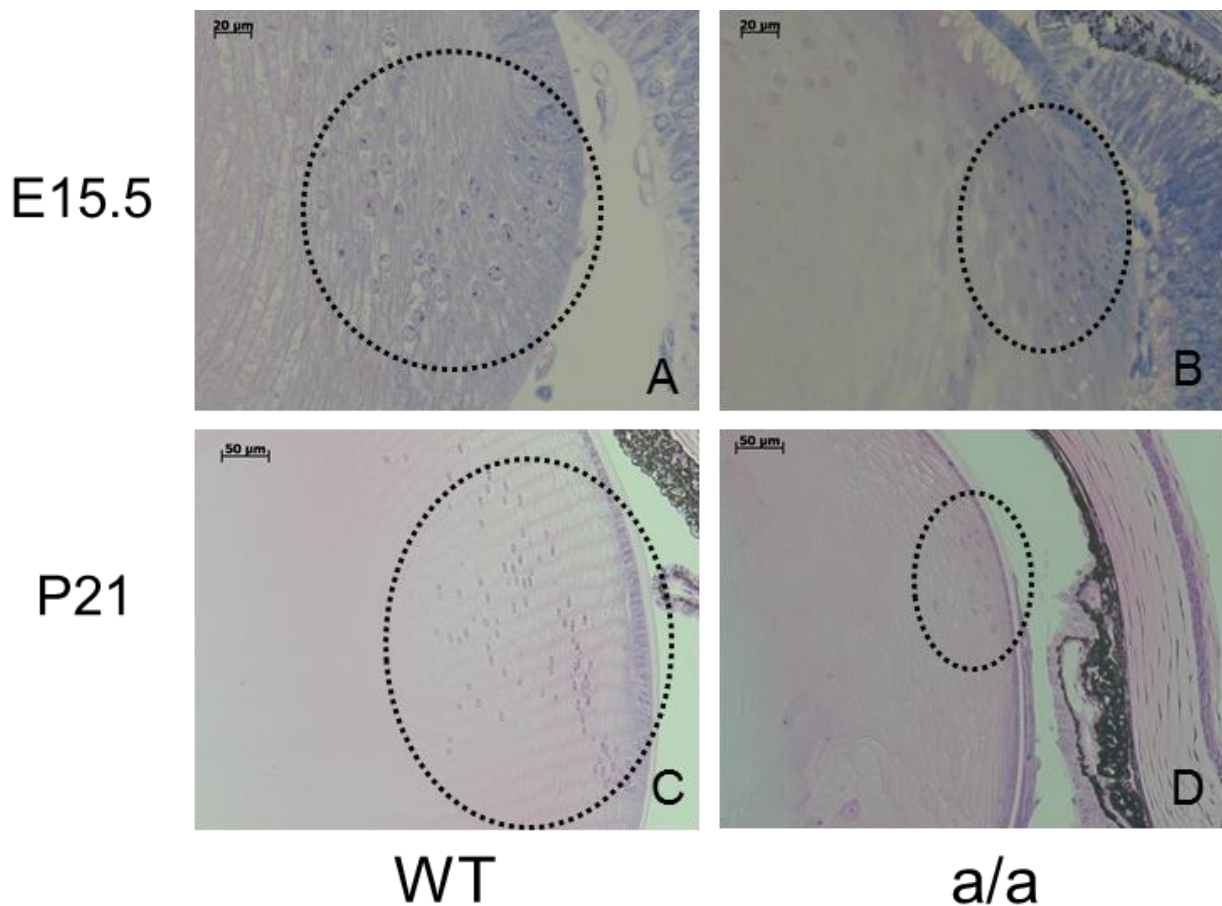


Figure 5.6 Reduced proliferation in *KTA48* mutant embryos. (A-B) At E14.5, the lens epithelial cells were incorporated with a number of BrdU in wild types (N=2) (A), while the mutant lens showed that there are a reduced number of BrdU incorporated cells in the central part of lens epithelium (N=2) (B). (C-D) At E15.5, there are a number of lens epithelial cells which were incorporated with BrdU in wild types (N=5), whereas in mutants BrdU incorporated cells were obvious reduced in the lens epithelial cells (N=5). (E-G) At E17.5, in wild-type lenses, there are a number of lens epithelial cells labelled with BrdU (N=2) but in mutants (N=2) there is greatly decreased numbers of lens epithelial cells in the central part of the mutant lenses (G) compared to wild-type lenses (E). However, the proliferation of the epithelial cells (BrdU labelled) in the transition zone of the lenses is not severely affected in mutants. L: lens; R: retina; LE: lens epithelium. Scale bar: 50 μ m.

In addition to proliferation, the lens differentiation is also affected in *KTA48* mutant embryonic and postnatal eyes. The transition zone is a region necessary for lens differentiation where the lens epithelial cells differentiate into the secondary lens fiber cells (Wride, 2011). By E15.5, the nuclei of the transition zone are organized well as a bow-like pattern in wild-type lenses, whereas the

cells in the transition zone were disorganized and the number of secondary fiber cells is less in mutant lens than wild types (Figure 5.7, A-B, E). At P21, the defect of the transition zone is more severe: the number of secondary fibers in the transition zone is greatly reduced and they are disorganized (Figure 5.7, C-D, E). In consistency with the histology showing that the lens is broken (Figure 5.3, H, J, L; Figure 5.5, B, D), γ -crystallin was found in the anterior chamber of the mutants by immunostaining at E15.5 (Figure 5.8, E-H) and E17.5 (Figure 5.8, I-L), which could trigger an eye inflammation response. In addition, the expression of γ -crystallin appears normal compared to the wild types at E13.5 but is reduced in the secondary fibers at E17.5 in mutants compared to the wild types (Figure 5.8, A-H), indicating that lens fiber cell differentiation is defect during embryonic eye development. These results suggest that the lens epithelial cells in the transition zone fail to differentiate into the secondary fiber cells in *KTA48* mutants.



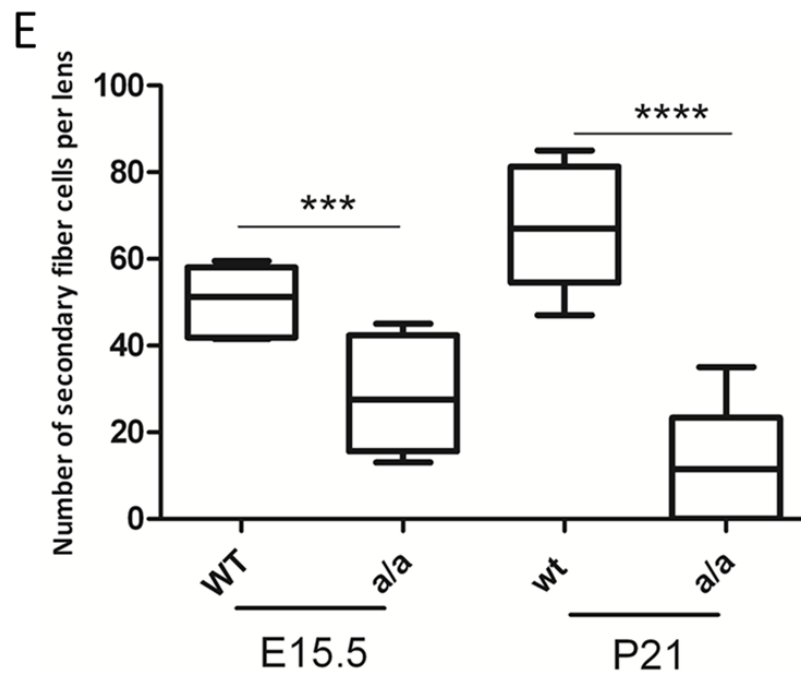


Figure 5.7 Lens differentiation is affected in *KTA48* mutant embryos. (A-B) The transition zone is disorganized and the number of secondary fiber cells is significantly reduced in mutants (B) at E15.5 (N=5) compared to wild types (A) (N=6) ($***p < 0.001$, E). (C-D) At P21, the epithelial cells in the transition zone is thinner and correspondingly the number of secondary fiber cells is also greatly reduced in mutants (N=6) (C) compared to wild types (N=6) (D) ($****p < 0.0001$, E). Scale bar: A-B, 20 μm ; C-D, 50 μm .

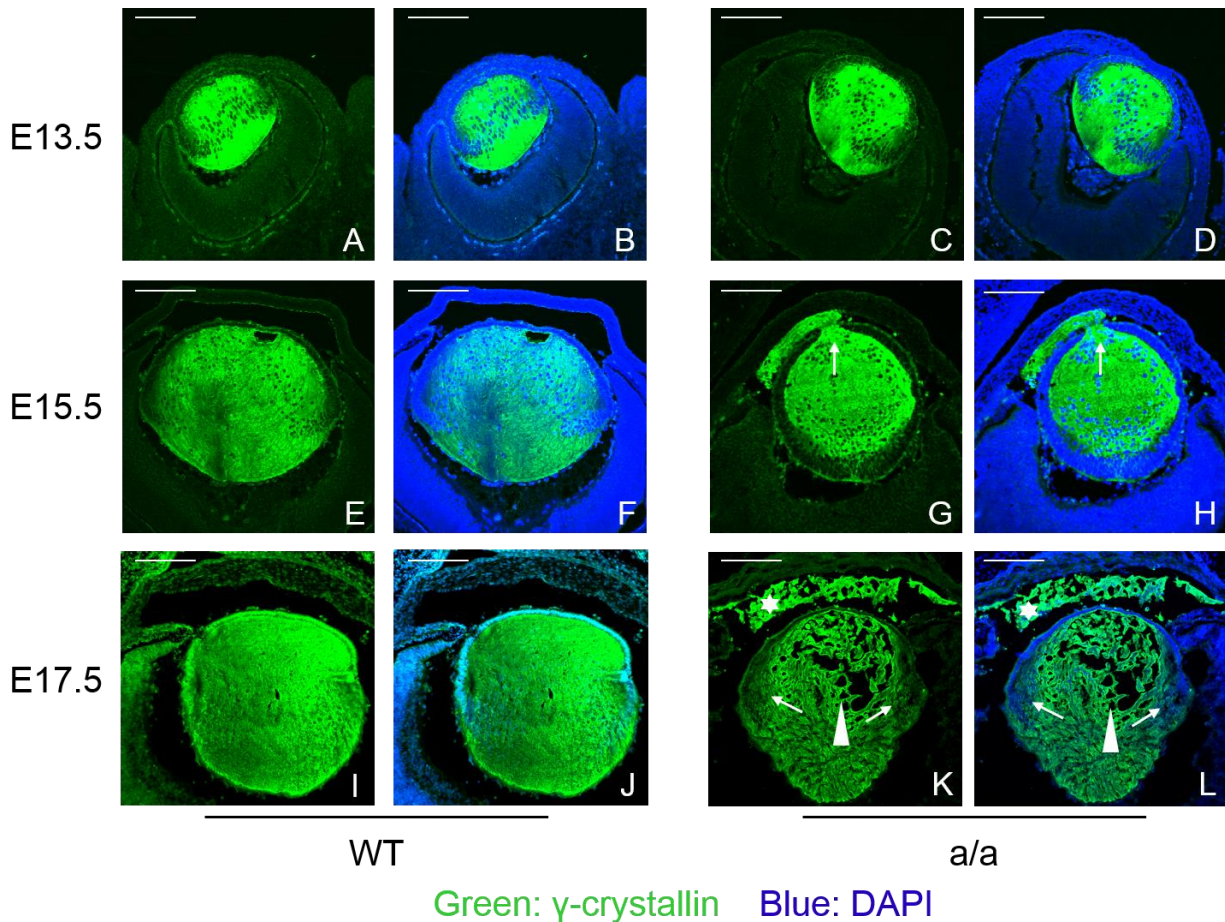


Figure 5.8 γ -crystallin in the anterior chamber and disrupted lens differentiation in *KTA48* mutant embryonic eyes. (A-L) γ -crystallin is a marker for differentiated lens fiber cells. At E13.5, γ -crystallin is expressed in the whole lenses but not in the nuclei of the wild types (A and B) and there are no differences in the lenses between wild types (A and B) and mutants (C and D). At E15.5, γ -crystallin is still expressed in the whole lenses but not in the nuclei of the wild types (E and F) but the mutants exhibited a rupture of the anterior lens which causes γ -crystallin extruding in the local anterior chamber (G and H, arrow). At E17.5, the expression of γ -crystallin was found more broadly in the anterior chamber of the mutants (K and L, white asterisk) accompanied by loss of lens fibers in the lens (K and L, arrowhead) due to a rupture in the lens capsule and epithelium. Moreover, the mutants showed reduced expression of γ -crystallin in the transition zone at E17.5 (K and L, arrow) compared to wild types (I and J) which suggests that the fiber cells differentiation is affected. Scale bar: 150 μ m.

Then I analyzed the expression of several genes which control and regulate lens proliferation and differentiation by immunostaining. Foxe3 is necessary for lens proliferation and differentiation (Blixt et al., 2000, 2007; Medina-Martinez, 2005). Staining for Foxe3 was performed in the eyes at E14.5, E17.5 and P11. In the wild-type lenses, Foxe3 is robustly expressed in the lens epithelial cells in different stages (Figure 5.9, A, C and E). In the mutant lens, at E14.5 and E17.5, there is reduced expression of Foxe3 in the central part of the lens epithelial cells, which are also

incorporated with less BrdU (Figure 5.9, B and D). At P11, the expression of Foxe3 is greatly reduced and some lens epithelial cells do not express Foxe3, and Foxe3 expression can be ectopically found the cells outside of the lens, suggesting the lens epithelial cells may migrate out of the lens (Figure 5.9, F). TGF β signalling is crucial for lens fiber cell differentiation (de Jongh et al., 2001; Lovicu et al., 2004). At P11, TGF β 1 is expressed in the lens epithelium and secondary fiber cells in the transition zone in the wild-type lens (Figure 5.10, A-F), whereas the mutants showed reduced expression of TGF β 1 in the lens epithelium and secondary fiber cells in the lens, but it is expressed in the ectopical lens cells in the vitreous (Figure 5.10, G-L). These results suggested that the expression of some key genes controlling and regulating lens proliferation and differentiation is affected in *KTA48* mutants during lens development and in the early postnatal periods.

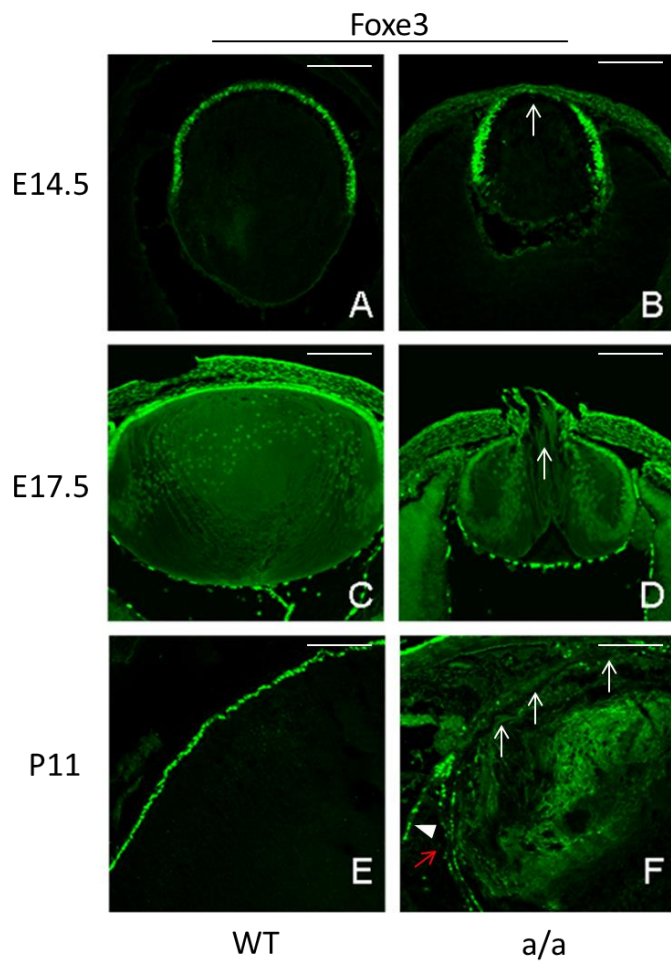


Figure 5.9 Aberrant expression of Foxe3 in mutants. (A-F) At E14.5, there is robust expression of Foxe3 in lens epithelia cells in wild types (A), while in the anterior lens epithelium in mutants the expression of Foxe3 is decreased (B, arrow). At E17.5, there is still strong expression of Foxe3 in lens epithelia cells in wild types (C), but decreased expression of Foxe3 in mutants due to persistent cornea-lens adhesion (D, arrow). At the later stage, P11, Foxe3 is only expressed in lens epithelial cells (E) while in mutants Foxe3 expression is completely absent in most lens epithelial cells (F, white arrow) and decreased expression of the other lens epithelial cells (F, red arrow) and it is ectopically expressed in some lens epithelium cells outside of the lens (F, arrowhead). Scale bar: 50 μ m.

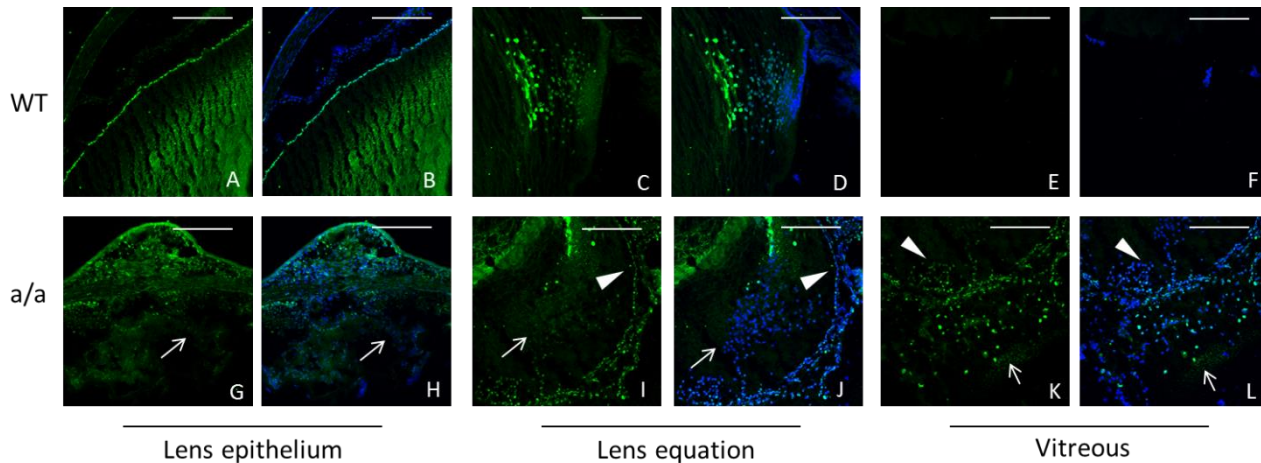


Figure 5.10 Aberrant expression of TGF β 1 in mutant lens at P11. (A-F) TGF β 1 is expressed in the lens epithelium (A-B) and lens secondary fibers (C-D) in wild types. (G-L) In mutants, the expression of TGF β 1 is reduced in the lens epithelium (G-H; I-J, arrowhead) and lens secondary fiber cells (I-J, arrow) and it is ectopically expressed in the lens cells in the vitreous (K-L). There are a number of cells in the posterior lens of mutants which express TGF β 1 (K-L, arrowhead), whereas there are only a few cells in the posterior lens of wild types which do not express TGF β 1 (E-F). Scale bar: 50 μ m.

On the other hand, peroxidasin was found to be cross-linked with Collagen IV in the basement membrane *in vitro* and the Collagen IV network is disorganized in *peroxidasin*-mutant *Drosophila* (Bhave et al., 2012). Then I investigated whether the expression pattern of Collagen IV is changed in *KTA48* mutants. At E12.5, Col4a2 (Collagen IV a2) is mainly expressed in the lens epithelium and inner limiting membrane in the wild-type eyes, and no obvious differences in the expression pattern were found between wild types and mutants (Figure 5.11, A-B). At E17.5, Col4a2 is still expressed in the lens epithelium (Figure 5.11, C) in wild types, but a disrupted local cell adhesion of lens epithelium was found in mutants (Figure 5.11, D-E). E-cadherin is one of the main cell adhesion molecules in the epithelial cells (van Roy and Berx, 2008). It is also a marker for epithelium-mesenchymal cell transition (EMT) and the expression of E-cadherin is decreased during EMT and loss of E-cadherin also promotes EMT (Zeisberg and Neilson et al., 2009). Detailed analysis of this disrupted region with staining against E-cadherin showed that the expression of E-cadherin is decreased, and some lens epithelial cells are missing and a small hole is formed in this region (Figure 5.11, E-G). Interestingly, there are a mass of cells nearby expressing E-cadherin in the anterior chamber, which cover the lens epithelial cells (Figure 5.11, E-G). These cells are likely to be mesenchymal transmitted from epithelial cells and they express E-cadherin. These data suggest that the cell adhesion of the lens epithelium is disrupted in *KTA48*

mutants which may be an early event for lens rupture and the lens fiber cells migrating into the anterior chamber.

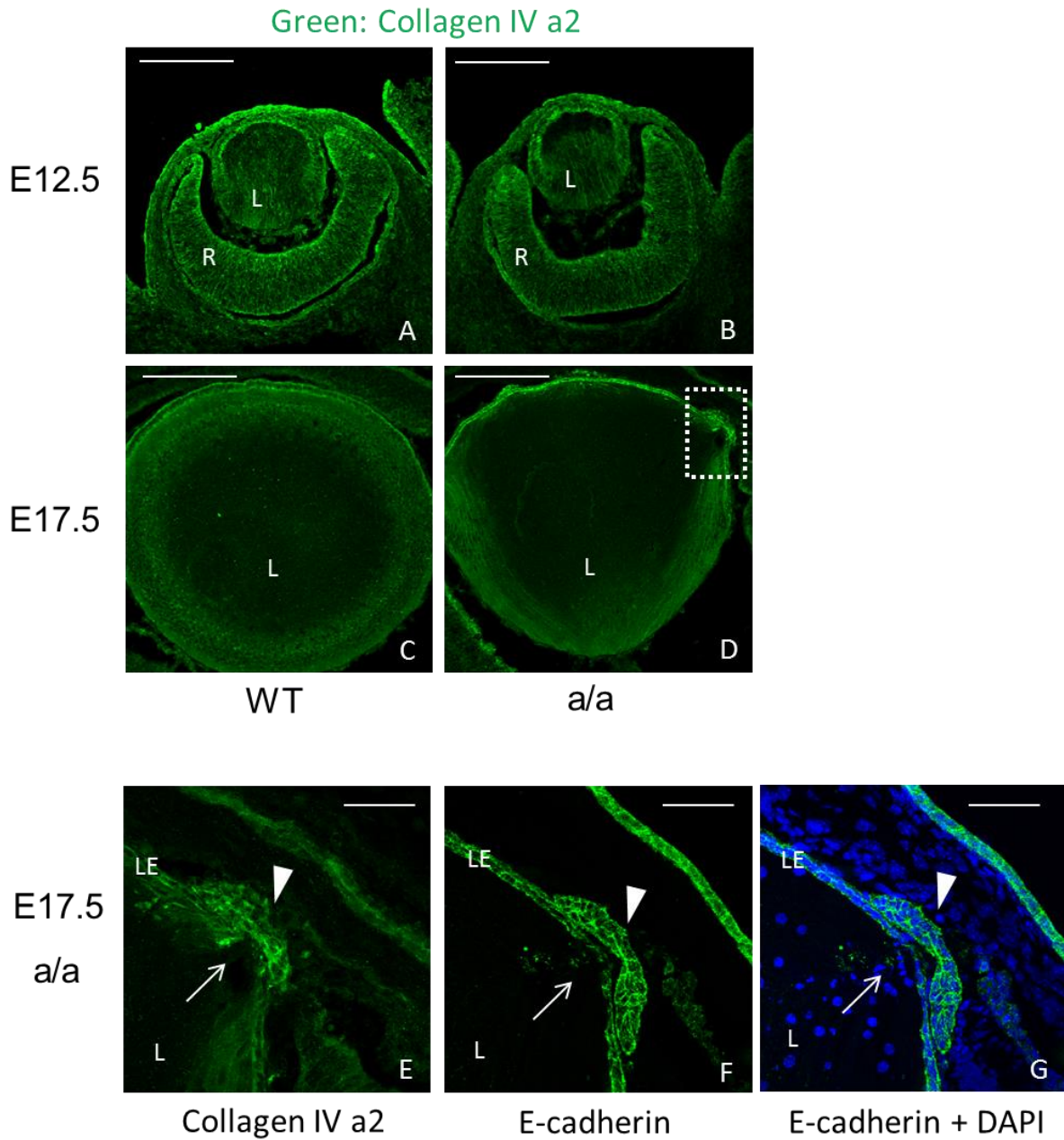


Figure 5.11 The cell adhesion of lens epithelium is locally disrupted in mutants during eye development. (A-B) At E12.5, collagen IV (a2) (Col4a2) is highly expressed in the lens epithelium and inner limiting membrane in wild types (A). No obvious differences in the expression pattern of Col4a2 were found between wild types (A) and mutants (B). (C-D) However, at E17.5, the mutant lens exhibits a local disruption of lens epithelium (D, marked). (E-G) The lens epithelium is severely disrupted in this local region of the mutants by Col4a2 staining (E, arrow) and E-cadherin staining (F-G, arrow). Interestingly, there is a mass of cells expressing epithelial cell adhesion molecule E-cadherin near the lens epithelial cells (F-G, arrowhead). L: lens; R: retina; LE: lens epithelium. Scale bar: A-D, 50 μ m; E-G, 20 μ m.

5.1.5 The defects in peroxidase may affect eye development through regulation of Pax6 and Tgf β 1 expression and increased inflammation

To further investigate the possible signalling pathways of peroxidase, I firstly compared quantitatively and spatiotemporal expression of different genes which are critical for eye development in *KTA48* mutants and wild-type mice. RNA was isolated from the whole eyes and quantitative real-time PCR (qRT-PCR) was performed at E12.5, E15.5 and P10. The genes which are critical for eye development and inflammation were selected, including *Pax6*, *Tgf- β 1*, *TNF- α* and *IL-1 β* . *Pax6*, a master control gene of eye development, is up-regulated at E15.5 and then down-regulated to normal level at P10 in *KTA48* mutants (Figure 5.12, A-C). Then *in-situ* hybridization and immunofluorescence were performed to confirm the qRT-PCR results. At E12.5, *Pax6* is highly expressed in lens epithelium and retina in wild-type eyes (Figure 5.15, A-B), whereas *Pax6* is not only expressed in the lens epithelium, but also in the lens fiber cells, and the expression of *Pax6* seems to be decreased in the retinal ciliary margin in mutants (Figure 5.15, C-D). *Pax6* mRNA is also expressed in the lens fiber cells (Figure 5.14, B) compared to wild types (Figure 5.14, A), but mRNA expression of *Pax6* was not changed in mutants compared to wild types by qRT-PCR. At E17.5, *KTA48* mutants also showed strong expression of *Pax6* in the eye, especially in retina (Figure 5.15, E-J), which was consistent with *in-situ* hybridization data at E15.5 (Figure 5.14, C-E). *Tgf- β 1* is another key gene for eye development and overexpression of *Tgf- β 1* causes anterior segment dysgenesis in mice (Flügel-Koch et al., 2002) and the ocular phenotype is similar to *KTA48* mutants. *Tgf- β 1* has an increasing trend in expression at E12.5, and its expression is up-regulated at E15.5 and then down-regulated to normal level at P10 in *KTA48* mutants (Figure 5.12, D-F). These data showed that peroxidase may affect eye development through regulation of *Pax6* and *Tgf- β 1* expression.

On the other hand, considering the point mutation in *peroxidase* may cause a reduced activity of peroxidase and increase the level of inflammation, the inflammation-associated genes including *TNF- α* and *IL-1 β* were selected to measure inflammation. The expression of *TNF- α* and *IL-1 β* are up-regulated in E15.5 in mutants and continued to be up-regulated at P10, which is around 4 days before eye open in mice (Figure 5.13, A-D). These data suggest that congenital ocular inflammation occurs in the *KTA48* mutants.

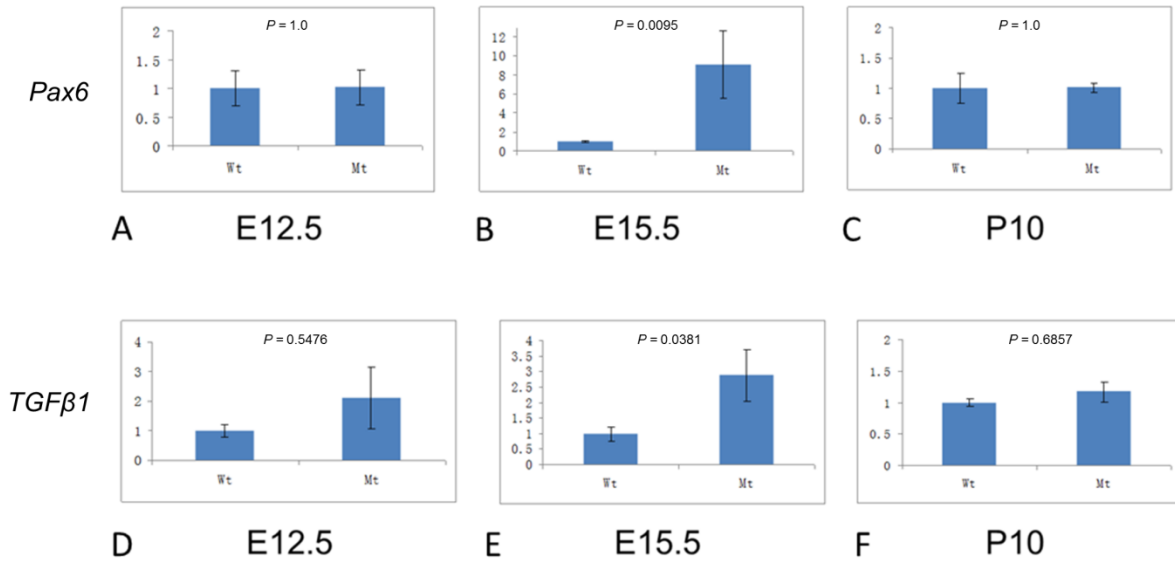


Figure 5.12 Up-regulation of *Pax6* and *Tgf-β1* in the embryonic eyes at E15.5. (A-C) Real-time PCR showed that the expression of *Pax6* is not altered at E12.5 in mutant eyes compared to wild types ($p > 0.05$), but up-regulated at E15.5 ($p < 0.01$) and then reduced to the level comparable to the wild types ($p > 0.05$). (D-F) The expression of *Tgf-β1* has a trend to be up-regulated at E12.5 ($p > 0.05$) and up-regulated at E15.5 in mutant eyes ($p < 0.05$), and then decreased to the expression level comparable to wild-type eyes at P10 ($p > 0.05$). Mt: a/a; E12.5 (N: Wt 5 Mt 5); E15.5 (N: Wt 4 Mt 6); P10 (N: Wt 4 Mt 4).

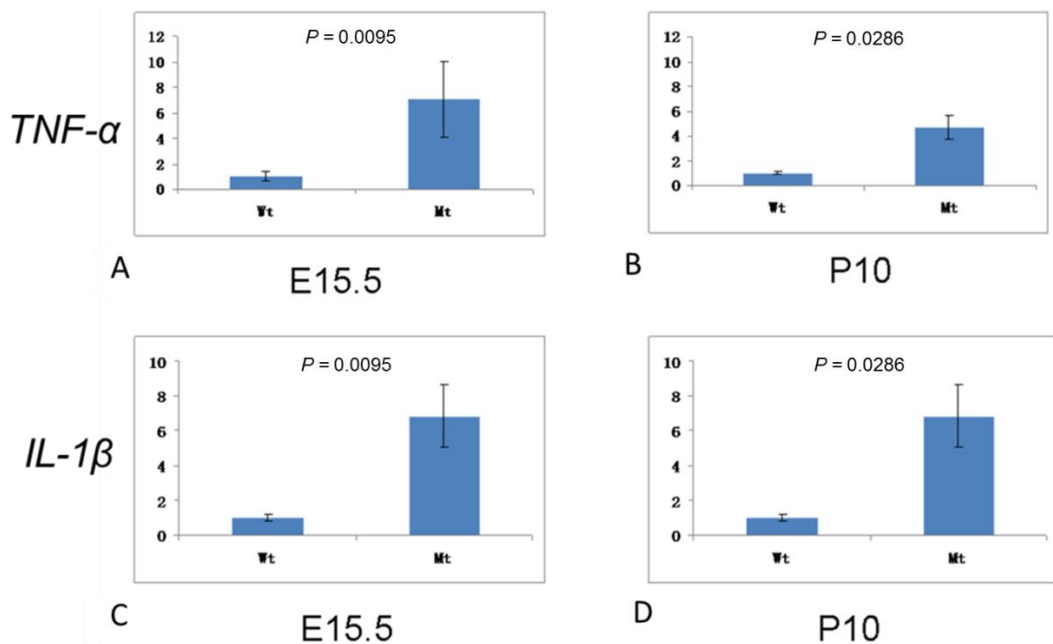


Figure 5.13 Up-regulated mRNA expressions of inflammation marker genes at E15.5 mutant eyes. (A-D) Real-time PCR showed that the expression of inflammation marker genes (*TNF-α* and *IL-1β*) is up-regulated in

mutant eyes at E15.5 ($p < 0.01$) and P10 ($p < 0.05$), which suggests that ocular inflammation occurs in mutant eyes during eye development. Mt: a/a; E15.5 (N: Wt 4 Mt 6); P10 (N: Wt 4 Mt 4).

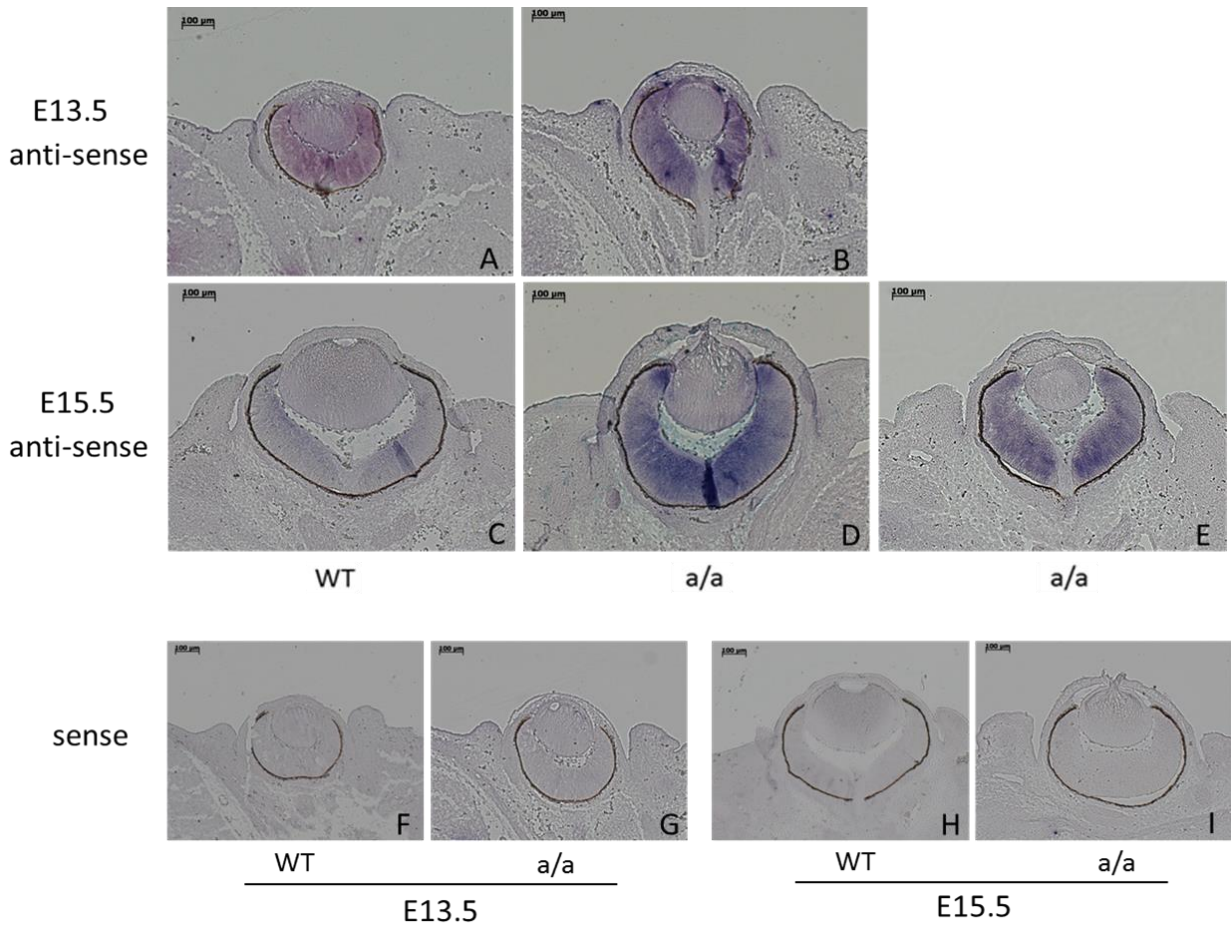


Figure 5.14 The mRNA expression of *Pax6* is still intensively expressed in the retina of *KTA48* mutants by *in-situ* hybridization. (A-E) *In-situ* hybridization of the sections with *Pax6* anti-sense RNA probes showed positive staining in the wild types and mutants. (A-B) At E13.5, *Pax6* mRNA is mainly expressed in the retina and weakly expressed in the lens of the wild types (A). In mutants, *Pax6* mRNA is not only expressed in the retina, but also expressed in the lens (B). (C-E) At E15.5, *Pax6* mRNA is expressed in the lens epithelium and retina in wild types (C) and *Pax6* mRNA is still intensively expressed in the retina of *KTA48* mutants compared to wild types (D, E). (F-I) *In-situ* hybridization of the sections with *Pax6* sense RNA probes showed no positive staining in the negative controls. Scale bar: 100 μm.

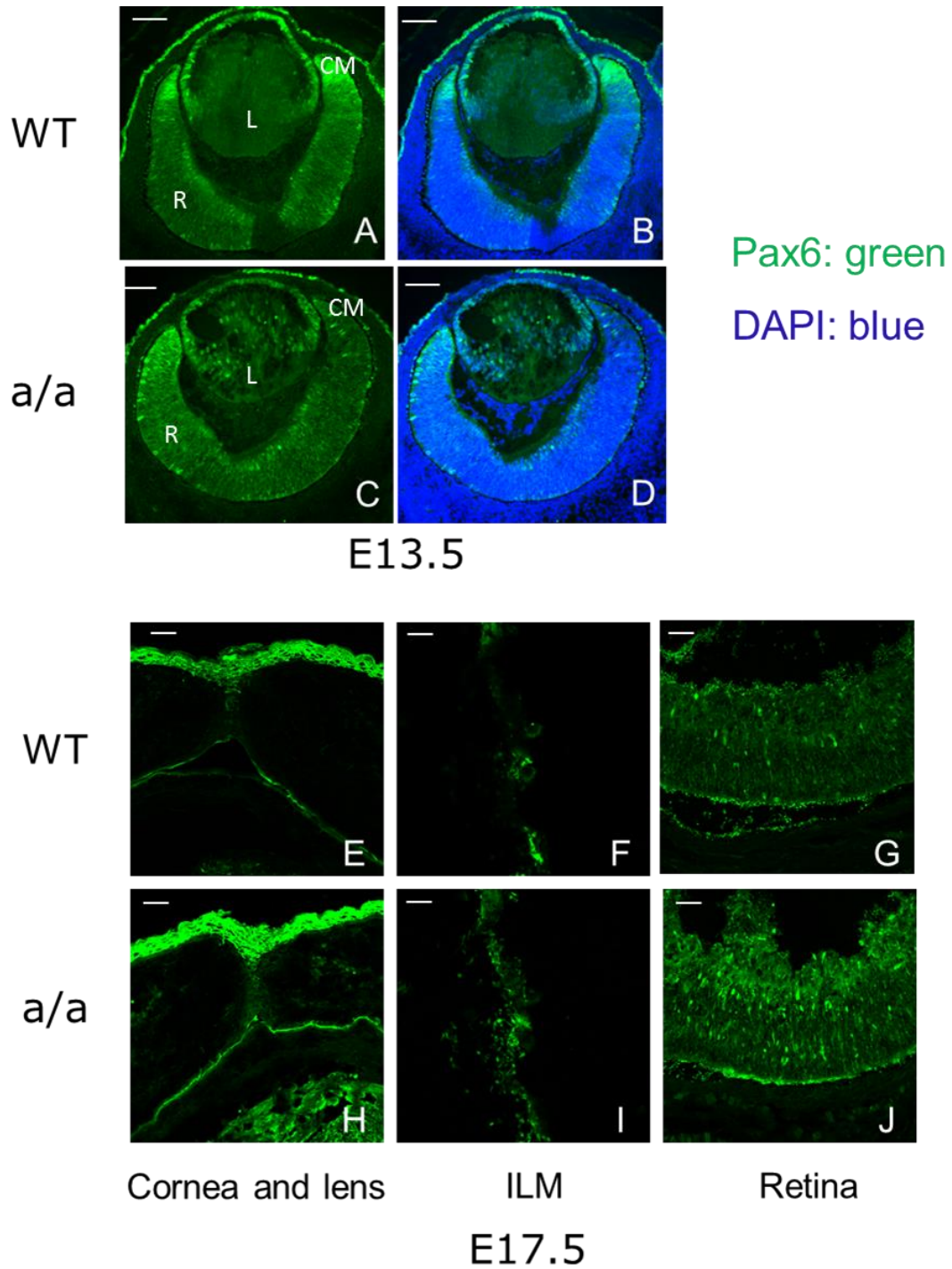


Figure 5.15 The localisation of Pax6 expression is changed in *KTA48* mutant embryonic eyes by immunofluorescence. (A-D) At E13.5, Pax6 is highly expressed in the lens epithelium and retina in wild-type eyes (A-B), but it appears that Pax6 is not only expressed in the lens epithelium, but also in the lens fiber cells, and the expression of Pax6 seems to be decreased in the retinal ciliary margin in mutants (C-D). (E-J) At E17.5, Pax6 is expressed in the eye lids, corneal epithelium, lens, inner limiting membrane and retina in wild-type eyes (E-G). However, the expression of Pax6 is up-regulated in retina at E17.5 and it appears that there are more Pax6-positive cells in the outer layer of the retina (J) compared to wild types (G). Scale bar: A-D, 50 μ m; E-J, 20 μ m.

5.1.6 Axon guidance from optic disc to optic tract is not affected in *KTA48* mutant embryos at E15.5

Axon guidance is also a very important event in visual system development, and PXN-2 (one of two types of peroxidase in *C. elegans*) plays a role in axon guidance in *C. elegans* (Gotenstein et al., 2010). Therefore, I performed anterograde tracing to see whether there are morphological differences in the optic chiasm and optic nerve between wild types (N=5), heterozygous (N=3) and homozygous mutants (N=5) at E15.5, a stage when the optic chiasm has formed. No difference in the crossing and fasciculation of the optic chiasm and optic nerve was found between wild types and *KTA48* mutants at E15.5 (Figure 5.16), suggesting that peroxidase may not play a role in axon guidance during visual system development.

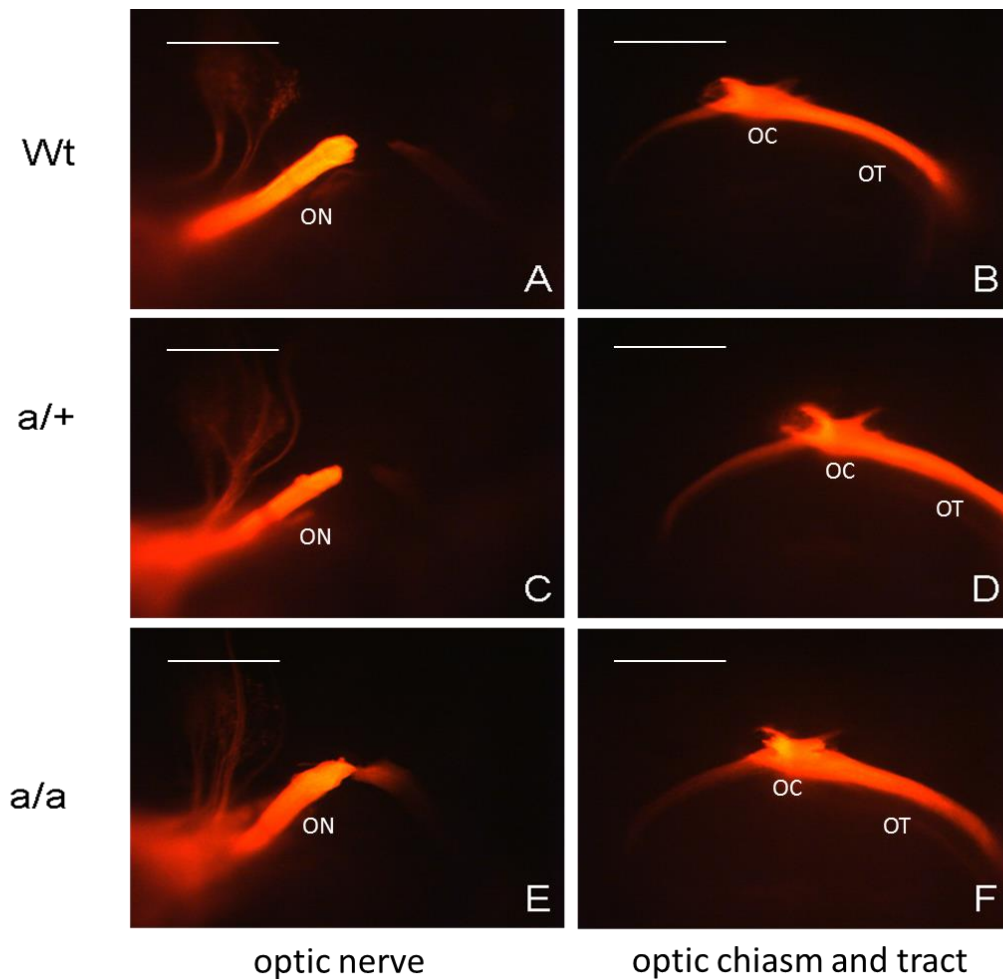


Figure 5.16 No difference in the crossing and fasciculation of the optic chiasm and optic nerve was found between wild types and mutants at E15.5. Anterograde tracing showed that there is no difference in the crossing and fasciculation of the optic nerve (A, C, E), optic chiasm and optic tract (B, D, F) between wild types (A, B), heterozygous (C, D) and homozygous mutants (E, F). ON, optic nerve; OC, optic chiasm; OT, optic tract. Scale bar: 100 μ m.

5.1.7 *KTA48* is a new mouse model of anterior segment dysgenesis particularly Peters anomaly associated with microphthalmia and early-onset glaucoma

To further investigate the eye phenotype of *KTA48* mutants during postnatal periods, I observed the ocular structure by light microscopy and histology from early postnatal period to adult. Apparently, all the mutants presented microphthalmia, corneal opacity and shallow/missing anterior chamber. Most of the mutants showed broad corneal opacity, but in very few cases (less than 5%) the opacity is located at the central area of the cornea. At P21, when major eye morphogenesis is completed, more severe phenotypes are found in *KTA48* mutants compared to the embryonic stages, including smaller eyes and lenses, the lens-cornea adhesion, thinner corneal epithelium and disorganized corneal stroma, missing or very shallow anterior chamber, lens matrix disorganization and disorganized lens epithelium, and iris and ciliary body hypoplasia (Figure 5.17). All these phenotypes were found in all mutants at P17-P21 (Table 5.2). Although the lens stalk was found in 42.9% mutants at E15.5-E17.5 (Table 5.1), the corneal-lens adhesion was found in all mutants (Table 5.2). This data suggests that the corneal-lens adhesion can be formed at later stages. Since corneal-lens adhesion and corneal opacity, two typical hallmarks of Peter's anomaly, are obvious in mutants, *KTA48* homozygous mutant mice are also a new mouse model of Peters anomaly. Moreover, lens matrix was also found in the vitreous cavity as well as in the anterior chamber, whereas the lens matrix was only found in the anterior chamber and the area around the lens capsule. This data indicates that lens rupture is more severe and more lens fibers leak out of the lens into the vitreous cavity at the postnatal period. These phenotypes of the anterior segment dysgenesis are also a high risk for glaucoma and retinal damage.

In addition, the retinal phenotypes occur more frequently at postnatal periods (Figure 5.17, F; Table 5.2) compared to embryonic stages (Table 5.1). Not only retinal folds and rosette-like structure but also retinal retraction and retinal dysgenesis occur in 88.9% mutants (8/9, Table 5.2), whereas only retinal folds and rosette-like structure were found in 32.1% mutants (9/28, Table 5.1). This data indicates that retinal damage is progressively severe from embryonic stages to the postnatal periods. There are two possible reasons for retinal phenotypes in the mutants. One is that high ocular pressure caused by the anterior segment dysgenesis and ocular inflammation during embryonic stages, which could damage the retina. The second possibility is that vitreous scar is formed due to vitreous inflammation induced by the lens fibers in the vitreous cavity, which could cause

vitreous-retinal traction.

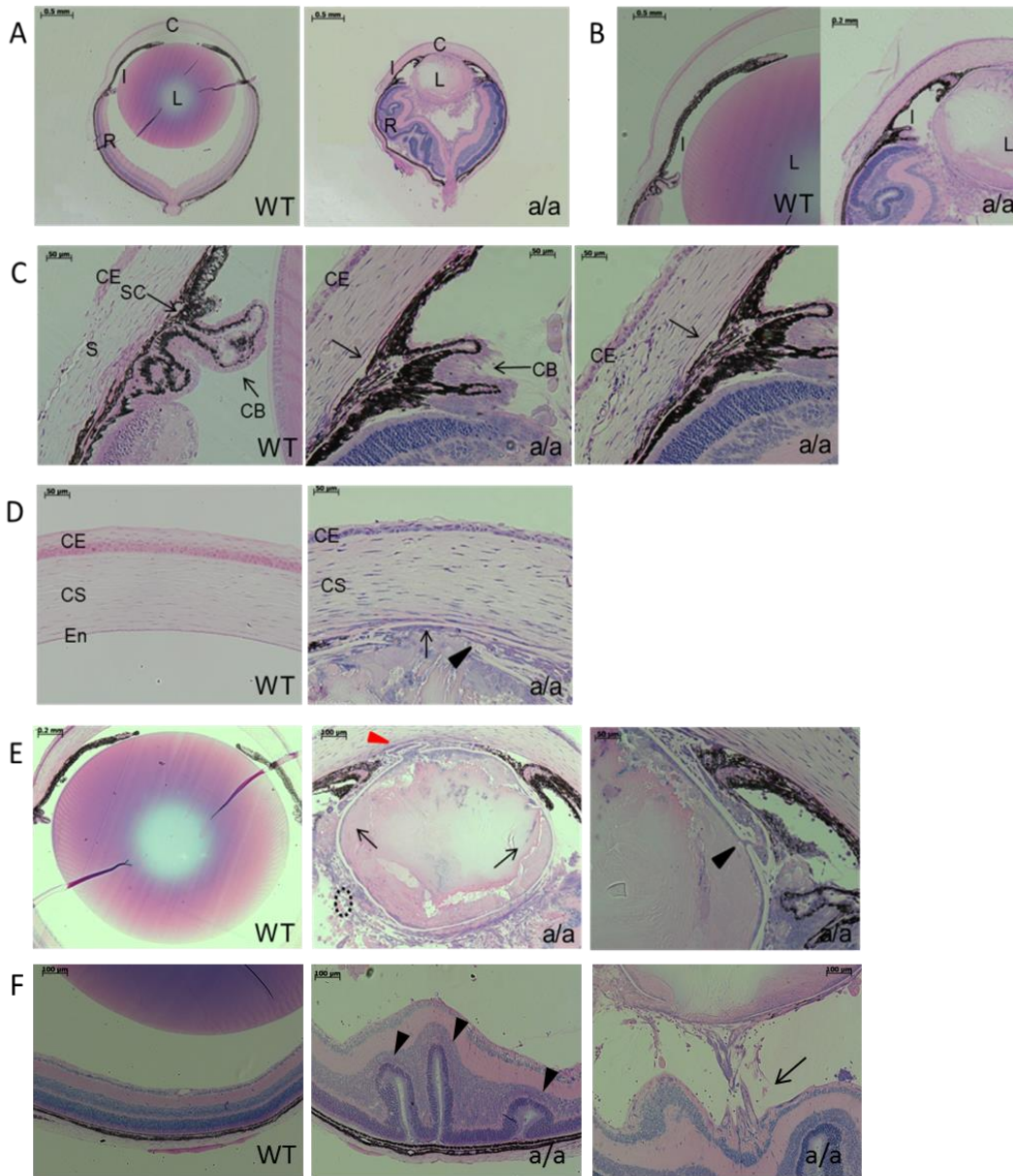


Figure 5.17 Anterior segment dysgenesis in postnatal eye development in *KTA48* mutants at three weeks.

At P21, the stage that major eye morphogenesis is completed, the mutant eyes and lens displayed remarkable smaller eyes compared to wild types (A) and severely anterior segment dysgenesis including iris hypoplasia and underdevelopment of ciliary body (B and C), lens-corneal adhesion (D, E), thinner corneal epithelium and disorganized corneal stroma (D), disorganized lens matrix which leads to congenital cataract (E). The iris is attached to the cornea and lens (A, B and E), resulting in the block of aqueous humor flow into trabecular meshwork which is high risk for high ocular pressure and glaucoma. Ruptured lens capsule is also found in mutants (black arrowhead, E) and the lens matrix is found around the lens in the vitreous cavity (black arrow, E). The lens equator in mutants is also totally destroyed and there are very few secondary fiber cells near the lens equator (black broken circle, E). In wild types, the Schlemm's canal develops well and ciliary body is located between cornea and sclera (arrow, C, WT), whereas in mutants the Schlemm's canal is not obviously

found and cornea extends to retina regions (C). (F) Retinal rosette-like structure (arrowhead) and retinal traction (arrow) occur in mutants compared to wild types. C: cornea; I: iris; L: lens; R: retina; CE: corneal epithelium; CS: corneal stroma; En: endothelium; CB: ciliary body. Scale bar: A-B, 500 μm ; C-D, 50 μm ; E (WT), 200 μm ; E (a/a, left), 100 μm ; E (a/a, right), 50 μm .

Table 5.2 Summary of eye phenotypes in *KTA48* homozygous mutants at P17-P21

Phenotype	Disorganized corneal stromal cells	Smaller eyes and lenses	Disorganized lens matrix and lens rupture	Lens tissue in AC and VC	Lens-corneal adhesion	Iris-corneal adhesion	Iris and ciliary body hypoplasia	Vitreous tissue	Retinal folds and rosette	Retinal tract
Number (9 eyes)	9/9	9/9	9/9	9/9	9/9	9/9	9/9	2/9	8/9	8/9
Percentage	100%	100%	100%	100%	100%	100%	100%	22.2%	88.9%	88.9%

This data is based on the histological observation of eyes. AC: anterior chamber; VC: vitreous cavity.

To determine whether loss of function of peroxidase induces glaucoma, I further analyzed the phenotypes of optic nerve head and retina in *KTA48* mutants at P21 and 3 months. 3 wild-type eyes and 3 mutants were performed for immunofluorescence and the results were similar at each stage, respectively. At P21, retinal rosette-like structures were also found in the optic nerve head region in mutants (Figure 5.18, F) compared to wild types (Figure 5.18, A). GFAP is ectopically expressed in the inner plexiform layer in mutants (Figure 5.18, H, L-M, arrow), indicating that activated glial cells occur in this region. In some local regions, GFAP is expressed all through the retina and it appears that retinal Müller cells are activated in these regions (Figure 5.18, O). Neurofilament, a type of neuronal intermediate filament proteins, is a major component of the neuronal cytoskeleton and it is abundant in axons (Yuan et al., 2012). Therefore, the antibody against neurofilament can be used to stain the neuronal axons. Neurofilament staining showed that there are robust retinal ganglion cell axons stained in the optic nerve (Figure 5.18, E-F) and in the retinal nerve fiber layer and it is also expressed in the axons of the horizontal cells in wild types (Figure 5.19, F-G), whereas in mutants the optic nerve (axons of the retinal ganglion cells) is thinner (Figure 5.18, I-J) and disrupted axons of the retinal ganglion cells and horizontal cells (Figure 5.19, M-N) were found. Moreover, the cell number in the retinal ganglion cell layer is increased but interestingly the number of Brn3-positive retinal ganglion cells is almost absent in mutants. Although the retina appears thicker in mutants, the other retinal layers (except retinal ganglion cells) are well-

developed compared to wild types (Figure 5.19, A-E and H-L). These data indicate that the retinal ganglion cells and the axons of the retinal ganglion cells (nerve fibers) are damaged in mutants at the early postnatal period (3 weeks). At 5 months, there is considerable loss of retinal ganglion cells and reduced thickness of the inner and outer nuclear layer in *KTA48* mutants (Figure 5.20, I), suggesting that progressive damage of retinal ganglion cells occur in the mutants. Together, these data suggest that peroxidasin plays a role in the onset and development of early glaucoma.

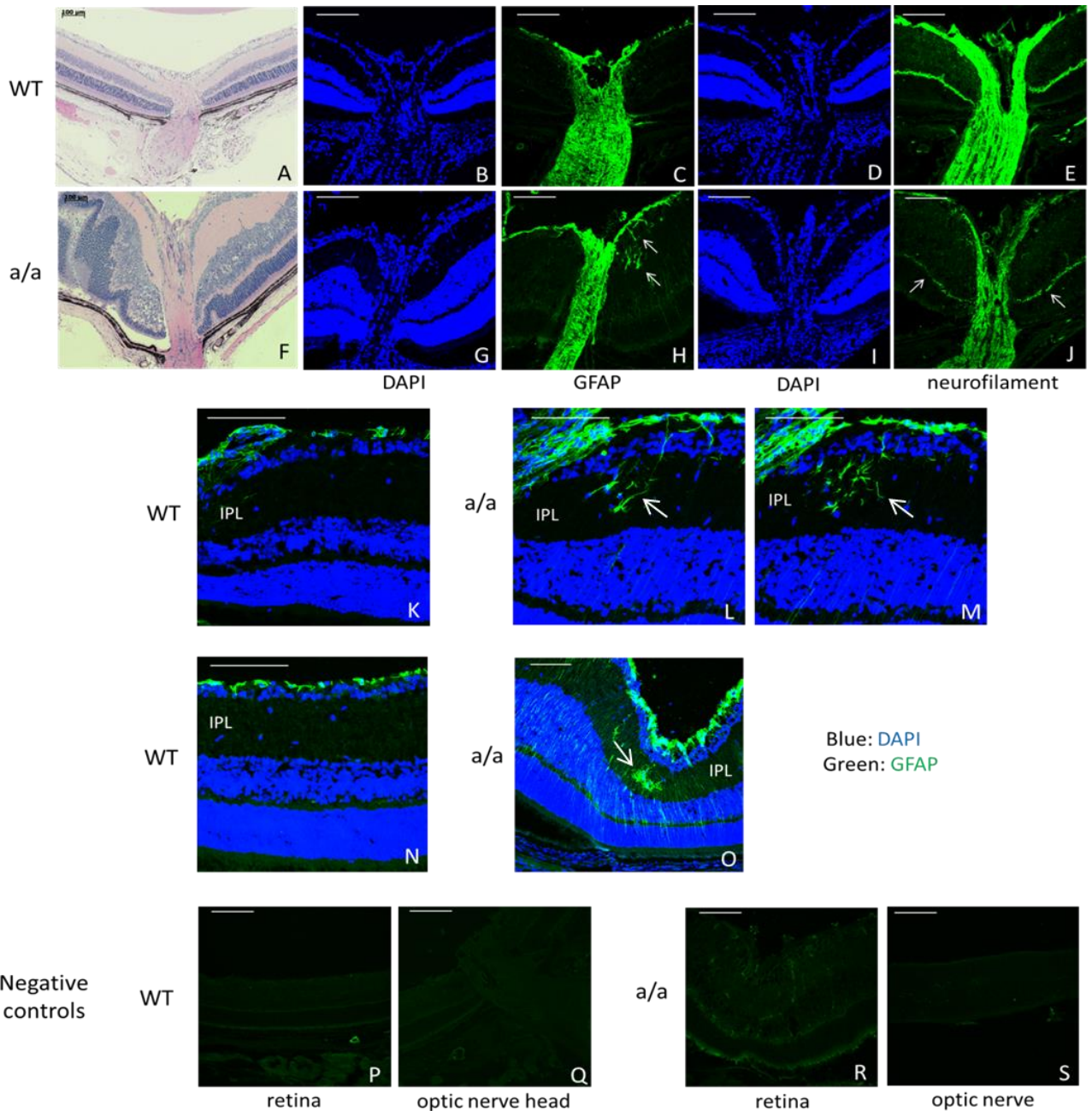


Figure 5.18 Phenotypes of the retina and optic nerve in *KTA48* mutants at P21. (A-J) Apparently the optic nerve is thinner in *KTA48* mutants than in the wild types. There are local retinal folds and rosettes and retinal detachment (F) in the mutant retina. There is less staining for neurofilament in the neural fiber layer and optic nerve in mutants (J, arrow) compared to the wild-type controls (E), suggesting defects in the axons of retinal ganglion cells in the mutants. Some retinal glial cells are activated in the local inner plexiform layers of the mutants (arrow, H; L-M; L-M; O) and GFAP expression is increased in some regions of the mutant retina (O) compared to wild types (C, H, K and N). (P-S) Negative controls for the immunostaining in wild types and mutants. The fluorescence is absent or very weak non-specific fluorescence in the negative controls compared to wild-type positive staining. Scale bar: 100 μ m. IPL: inner plexiform layer.

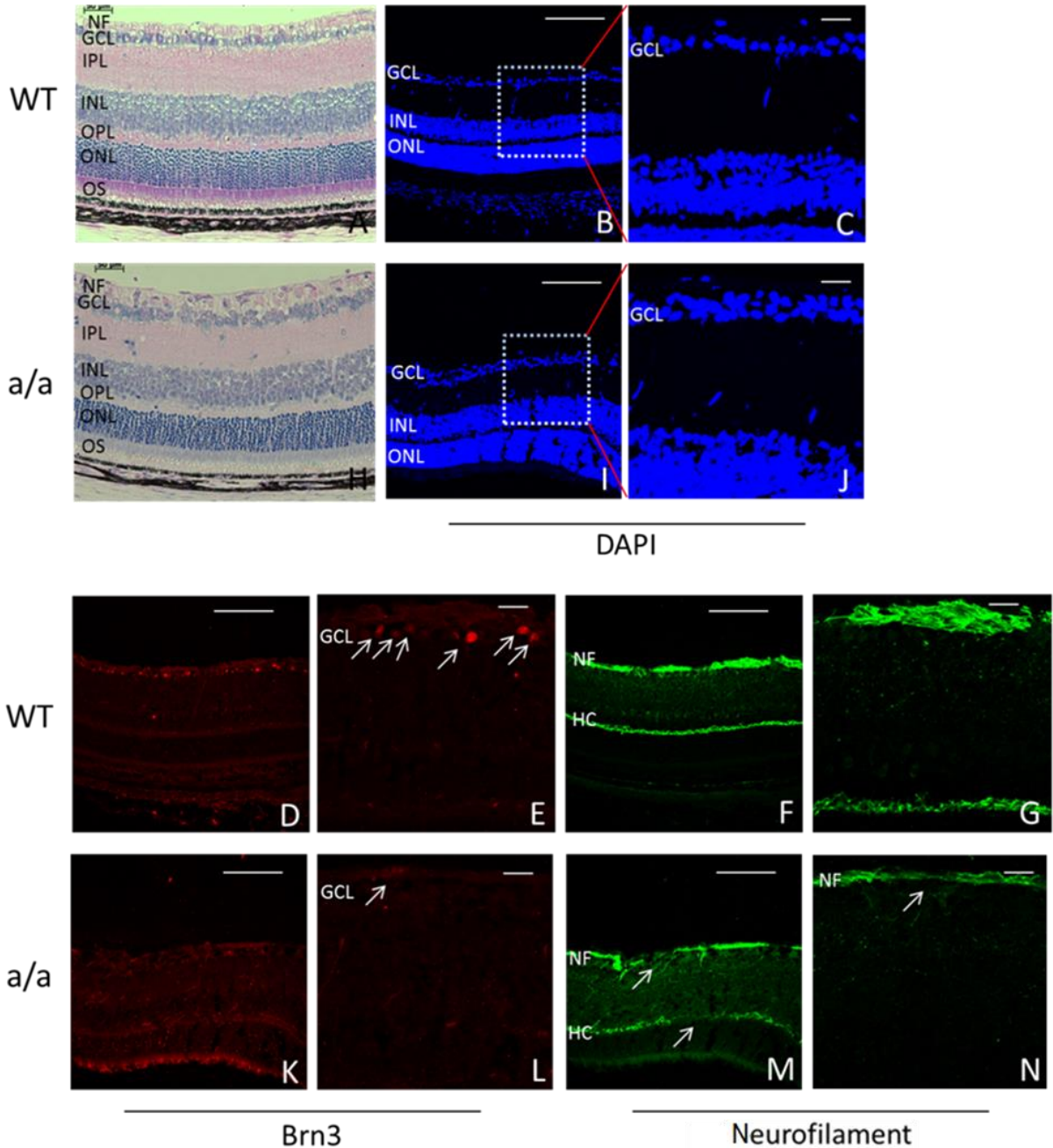


Figure 5.19 The number of retinal ganglion cells is increased but loss of Brn3 expression in *KT448* mutants at 5 months. (A-C, H-J) The number of retinal ganglion cells is increased in mutants (H, I, J) compared to wild types (A, B, C) but interestingly the expression of Brn3 is obviously decreased in mutants (K and L, arrow) compared to wild types (D and E, arrow). Correspondingly, the RGC axons in mutants are thinner (M; N, arrow) and both neural fiber layer and horizontal cells are disrupted in mutants compared to wild types (F and G). Negative controls showed no staining or very weak staining. NF: nerve fiber layer; GCL: retinal ganglion cell layer; IPL: inner plexiform layer; INL: inner nuclear layer; OPL: outer plexiform layer; ONL: outer nuclear layer; PL: out segments of photoreceptor; HC: horizontal cells. Scale bar: A-B, H-I, D, F, K, M, 50 μm ; C, E, G, J, L, N, 20 μm .

In adults, the mutants displayed more severe phenotypes and eye lids appeared to be nearly closed. The eye phenotypes in this stage are similar due to severe destruction of the eyes during development. 5 independent samples were used for histology. Histology demonstrated more anterior segment phenotype compared to P21 including lens-cornea adhesion, cornea matrix disorganization and disarranged keratocytes, ruptures in lens epithelium and capsule, and lens matrix disorganization in mutants (performed in 5 independent mutant eyes). In addition, sclera uveolma, missing anterior chamber and the anterior segments attached together can also be found in mutants (Figure 5.20). The iris is attached to the corneal endothelium and the anterior chamber is very shallow or even missing, suggesting that high ocular pressure or glaucoma occurs in the mutants. These eye phenotypes of the anterior segment and microphthalmia are similar to clinical manifestation of patients with anterior segment dysgenesis, particularly with Peters anomaly. In addition, the extracellular matrix of the eyes is severely disrupted in adult mutant mice, which was revealed by Col4a2, E-cadherin and N-cadherin immunostaining (Figure 5.21). In wild types, Col4a2 is highly expressed in corneal epithelium, the outer layer of lens capsule and lens epithelium (Figure 5.21, A-C), whereas in mutants the expression of Col4a2 is significantly reduced in the corneal epithelium and lens capsule (Figure 5.21, D-E). E-cadherin is also expressed in the corneal epithelium and lens epithelium (Figure 5.21, F-G), and N-cadherin is expressed in the lens epithelium (Figure 5.21, H) in adult wild types. In mutants, the expression of E-cadherin is also obviously decreased in the corneal epithelial cells and lens epithelial cells (Figure 5.21, I-J), and N-cadherin expression is reduced in the lens epithelial cells (Figure 5.21, K). Compared to the embryonic stage (Figure 5.11), the extracellular matrix and cell adhesion were progressively and severely damaged in adult mutant (Figure 5.21).

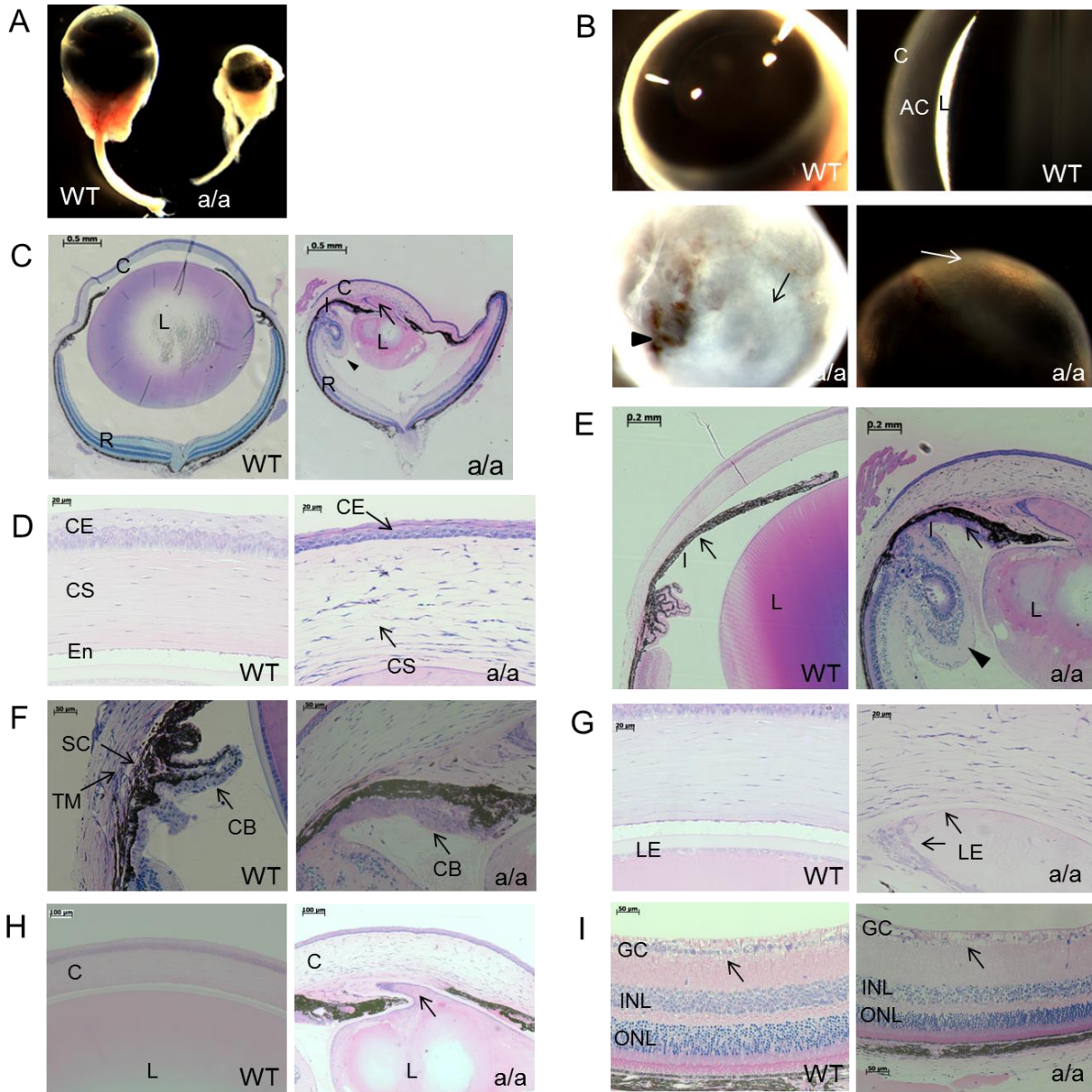


Figure 5.20 Microphthalmia, corneal opacity, cataract, iris and ciliary body hypoplasia, anterior chamber angle abnormalities, retinal dysplasia and ganglion cell loss in *KTA48* adult mutants at 5 months. (A and C) Microphthalmia, smaller lens and local retinal dysplasia in *KTA48* adult mutants. (B) Corneal opacity (black arrow), very shallow anterior chamber (white arrow) and scleral staphyloma (black arrowhead) in *KTA48* mutants. (D) Thinner corneal epithelium, disorganized stromal keratocytes and fibrosis-like changes in the region of corneal opacity of *KTA48* mutants compared to wild types. (E) Iris hypoplasia, iris-corneal adhesion and iris-lens adhesion were found in *KTA48* mutants compared to wild types. (F) Ciliary body and Schlemm's canal develop well in wild types, whereas the ciliary body is poorly developed and not formed as triangular structure in the cross-sections and the Schlemm's canal is not seen and the anterior chamber angle is fully filled and the cornea extends to the scleral region in *KTA48* mutants compared to wild types. (G-H) Severely disrupted lens epithelium, disorganized lens matrix and thinner lens capsule in *KTA48* mutants compared to wild types. (I) Loss of ganglion cells, and the inner and outer nuclear layer become thinner in *KTA48* mutants compared to wild types at 3 months. Scale bar: C, 500 μm ; E, 200 μm ; H, 100 μm ; F and I, 50 μm ; D and G, 20 μm .

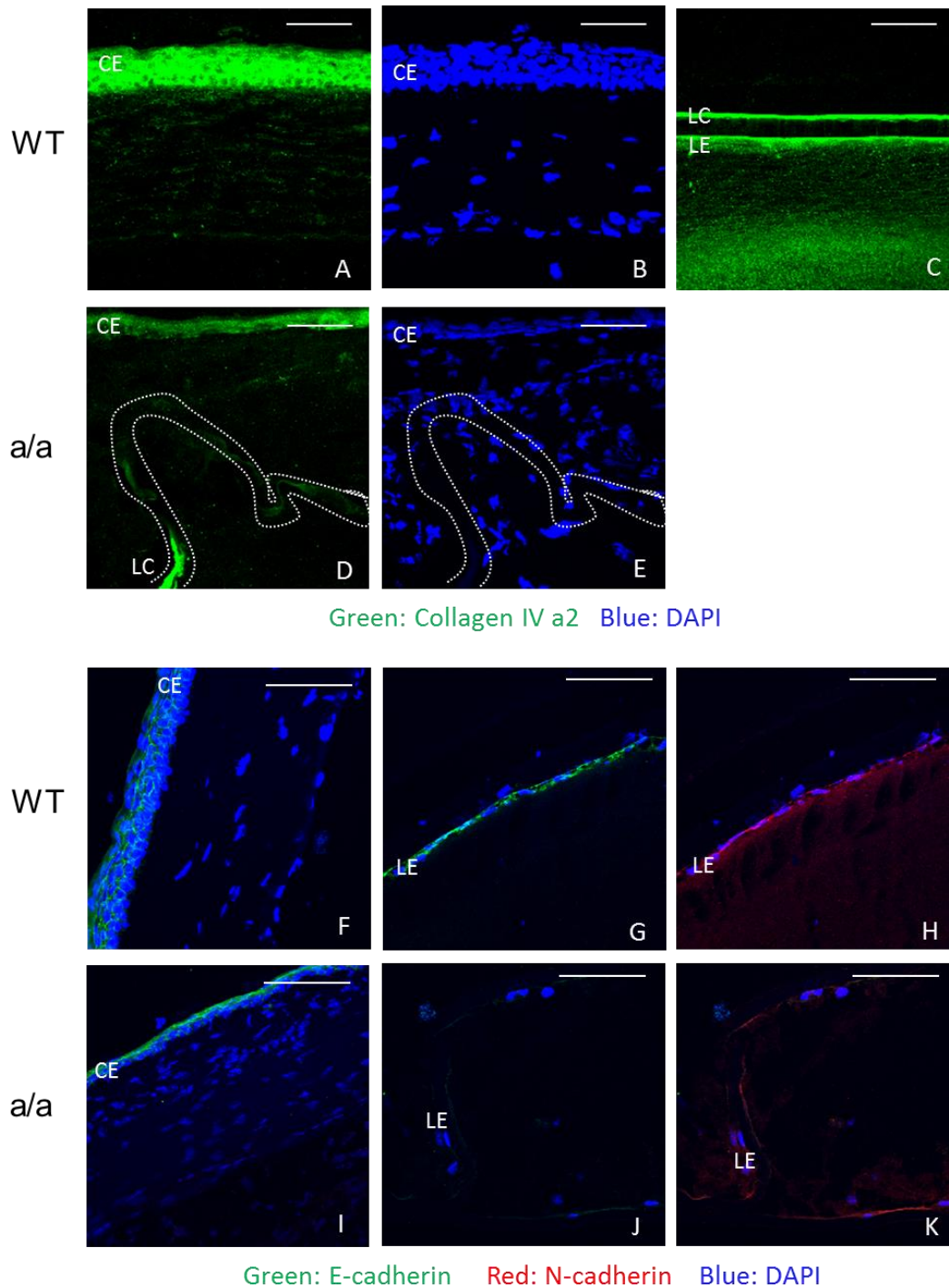


Figure 5.21 Decreased expression of extracellular matrix molecule (Col4a2) and cell adhesion molecules (E-cadherin and N-cadherin) in *KT448* mutants. (A-E) Col4a2 is expressed in the corneal epithelium (A-B), lens epithelium and the outer layer of the lens capsule (C) in wild types. The expression of Col4a2 is decreased in the corneal epithelium and lens capsule in mutants (D-E). (F-K) E-cadherin is expressed in the corneal epithelium (F) and lens epithelium (G), and N-cadherin is expressed in the lens epithelium (H) in wild types. The expression of E-cadherin and N-cadherin is greatly decreased and disrupted in the corneal epithelium and lens epithelium in mutants (I-K). Negative controls showed very weak non-specific staining in the corneal epithelium but absent staining in the lens epithelium cells. Double stained: G and H; J and K. Scale bar: A-E, 20 μ m; F-K, 50 μ m.

5.2 Part II : *Bmpr1b* is essential for optic nerve and ventral retinal development

5.2.1 Mis-splicing of exon 10 in *Ali030* homozygous mutants

The genetic analysis showed that the point mutation (T->G transversion) was found at the second base pair of intron 10 of the *Bmpr1b* gene in *Ali030* mutant mice (Figure 1.8, A), which suggests that it probably affects the splicing pattern of exon 10 or intron 10. To analyze the RNA splicing product of *Bmpr1b* gene in *Ali030* mutants, RT-PCR was performed on retinal and whole eye preparations from the wild-type and mutant mice, respectively. The difference in *Bmpr1b* cDNA length between wild types and mutants was not obvious from the gel (Figure 5.22, A). Then full-length *Bmpr1b* cDNA PCR product was purified from the gel and sent to GATC company for sequencing, but unfortunately most part of the cDNA can not be sequenced by the Sanger method, which may be due to the large size and low amount of cDNA, and the sensitivity of the sequencing method. Therefore I cloned *Bmpr1b* cDNA from mutant and wild-type eyes into the pcDNA3.1 vector and sent it for sequencing. The sequencing results were shown as below (Figure 5.22, B). In wild types, exon 10 is located between exon 9 and exon 11, whereas in mutants, the exon 10 is missing between exon 9 and exon 11. This data suggests that exon 10 is mis-splicing by a mutation in the splicing donor site although it is located in the intron. There was no difference in splicing pattern between eyes and retina in mutants (the sequences are the same to Figure 5.22, B). The mis-splicing of exon 10 (1614-1744 bp, *Bmpr1b* mRNA NCBI reference sequence: NM_007560.4) in mutant *Bmpr1b* cDNA causes a translational frameshift from 1600 bp and a premature stop codon in 1822-1824bp (TAA), which is predicted to affect the cytoplasm domain including the conserved serine/threonine kinase (Figure 5.22, C).

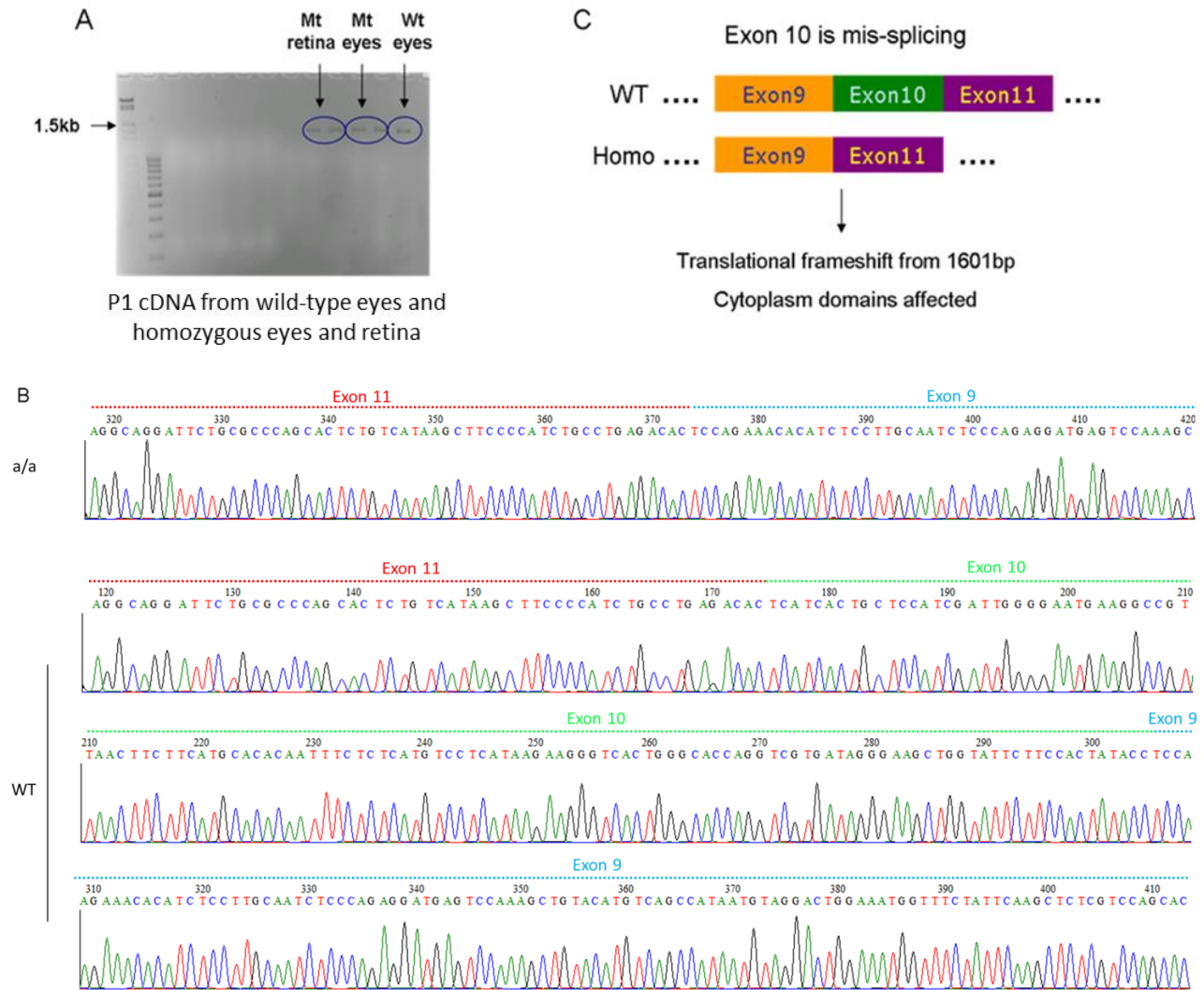


Figure 5.22 Mis-splicing of exon 10 of *Bmpr1b* mRNA in *Ali030* homozygous mutants. (A) Purified *Bmpr1b* cDNA product (wild types and mutant eye tissues) on the agarose gel and there is no obvious difference in the size of band between wild types and mutants. (B) The exon 10 is mis-spliced (skipped) in mutant *Bmpr1b* mRNA. *Bmpr1b* cDNA from P1 wild-type and mutant retina was cloned and sequenced, respectively. In homozygous mutants, there is a missing exon 10 between exon 9 and exon 11 compared to wild types. (C) Mis-splicing of exon is predicted to cause a translational frameshift after 1601 bp and affect the cytoplasm domain including the conserved serine/threonine kinase.

5.2.2 Optic nerve head hypoplasia and ventral retinal gliosis without lens phenotypes in *Ali030* mutants

Previous studies showed that *Bmpr1b* affects optic nerve axon guidance (Liu et al., 2003) and BMP signaling is required for lens induction and development (Furuta and Hogan, 1998; Faber et al., 2002). The eye phenotypes of *Ali030* mutant mice were initially screened using funduscopy and

AC Master (a special equipment used to measure the depth of anterior chamber, lens thickness and eye size (Puk et al., 2006)), respectively. Funduscopy examination showed enlarged optic disc, and AC Master examination revealed that the axial length in mutant eyes is slightly longer than wild types which may be due to enlarged optic disc, but lens transparency are not affected in mutants by slit-lamp analysis (GMC report for *Ali030*, unpublished).

Next, I analyzed the phenotype of optic nerve head (ONH), optic nerve, retina and lens by *in-vivo* retinal imaging (Spectral Domain Optic Coherence Tomography, SD-OCT) and histology. SD-OCT revealed an enlarged and a very thin optic disc in the optic nerve head but a thicker inner plexiform layer in the ventral retina of the mutants (N=12 eyes, 6 mice) compared to wild types (N=10 eyes, 5 mice) (Figure 5.23, A-C). In addition, the remnant of the hyaloid vessel was found to be dislocated at the rim of the optic nerve head compared to the central location of the ONH in wild types (Figure 5.23, B). Moreover, a long retinal glial scar occurred in the ventral retina (Figure 5.23, D), which was confirmed by further flat-mount immunostaining. Up-regulation of GFAP expression was found in the ventral retina of the mutants compared to wild types (Figure 5.24, A-J). The activated glial cells were both found in the optic nerve head and ventral retina in mutants and they formed a glial scar in the ventral retina which is connected to the optic nerve head (Figure 5.24, F-G). From the OCT section, there are distinct retinal layers in wild types (Figure 5.23, A and B, WT). However, in mutants, the distinct layers in most areas of the ventral retina disappear but form a dark zone from retinal ganglion cell layer to outer plexiform layer and some retinal defects showing small dark zone similar to rosette structure found in or between the photoreceptor layer and the RPE or choroid layer (Figure 5.23, B).

Histology demonstrated that enlarged optic disc, especially in the central part, is found in the optic nerve head from early postnatal periods to adult, which suggests that it is optic nerve head hypoplasia (Figure 5.25, G-L). Moreover, a number of cells were aggregated in the inner plexiform layer and some cells seem to migrate from the inner nuclear layer to the inner plexiform layer (Figure 5.25, D and F). In addition, the inner limiting membrane and the retinal ganglion cell layer in the ventral retina are broken and the cells proliferate and migrate out of the retina (Figure 5.25, A-F). In consistency with OCT results, there are similar findings revealed by histology. Firstly, there is also a retinal delamination in the ventral gliosis retina and retinal rosette structure is clearly

found in this region. Secondly, the photoreceptor layer is thinner in mutants than wild types and rosette-like structure is formed. Thirdly, the remnant of the hyaloid vessels is located at the peripheral part of the ONH in mutants compared with wild-type controls where it is located in the central part (Figure 5.25, A-F). These data showed that *Bmpr1b* is essential for ventral retinal development in mice. However, no difference was found between mutant and wild-type lenses by histology, which suggests that *Bmpr1b* may be not critical for lens development.

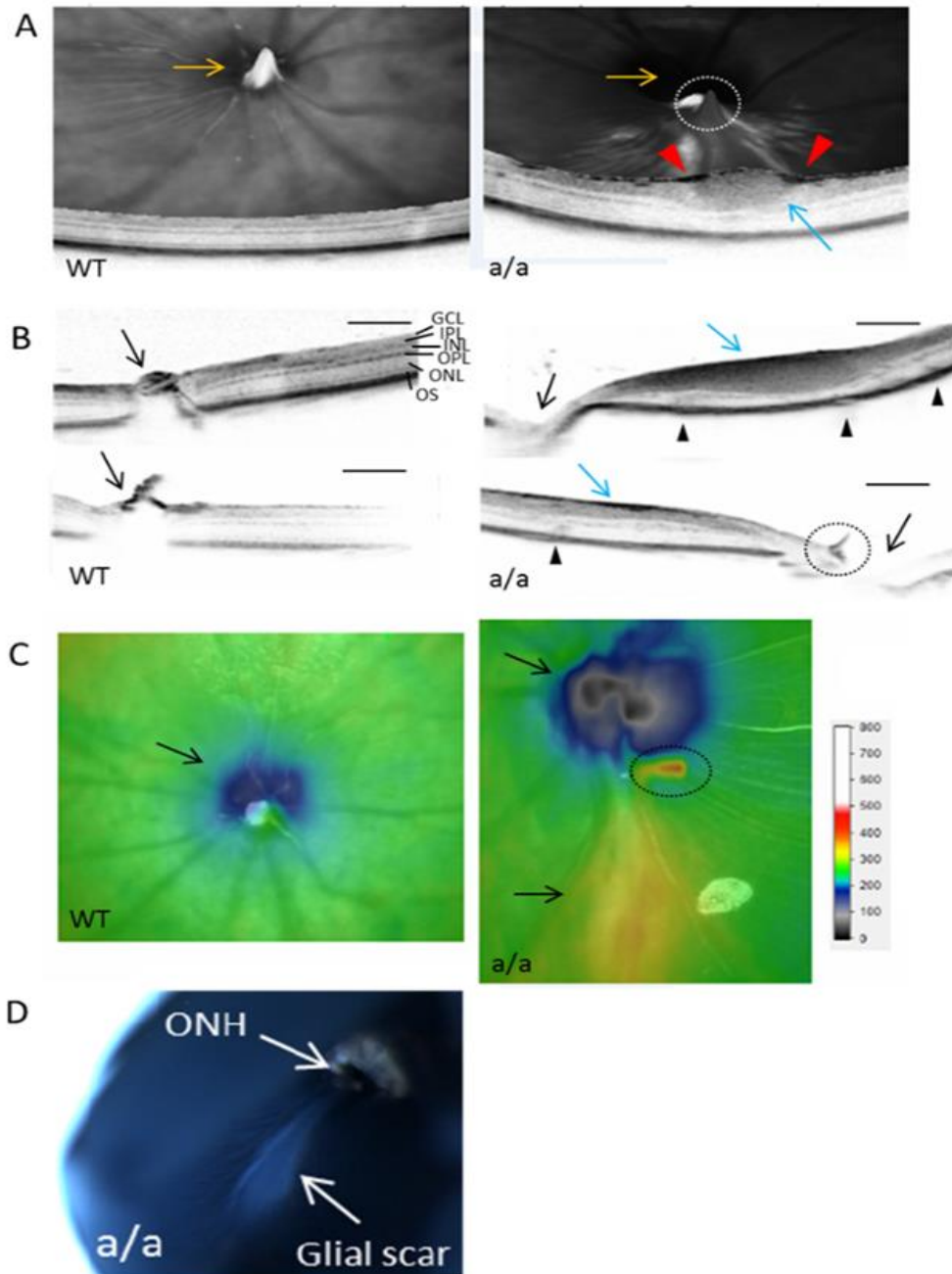


Figure 5.23 Excavation of the optic nerve head, ventral retinal gliosis scar and epiretinal membrane in ventral retina in *Ali030* mutants at 3 months. (A-C) OCT showed that the optic nerve is fully filled and there is a remnant of the hyaloid artery on the center of the optic nerve head in wild types (A-C, WT, yellow and black arrow), whereas in mutants the excavation of the optic nerve head was found, the central thickness is remarkably reduced and the remnant of the hyaloid artery was found in the rim of the optic nerve head in *Ali030* mutants (A-C, yellow and black arrow and broken circle). There are several retinal defect regions showing small dark zone similar to rosette structure found in the photoreceptor layer or between the photoreceptor layer and the RPE (B, arrowheads). (D) A long retinal glial scar was found in the ventral retina in the mutants (white arrow) which was confirmed by later GFAP immunostaining (Figure 5.24) and the thickness of the ventral retina is increased (C, arrow, yellow area). (A-C) The ventral retinal gliosis is connected to the optic nerve head and it is involved in multiple layers in ventral retina (A-C, a/a, blue arrow), and there is a thick black layer on the surface of peripheral retinal region of the gliosis scar in mutants which is similar to epiretinal membrane (A, a/a, red arrowheads; B, a/a, blue arrow).

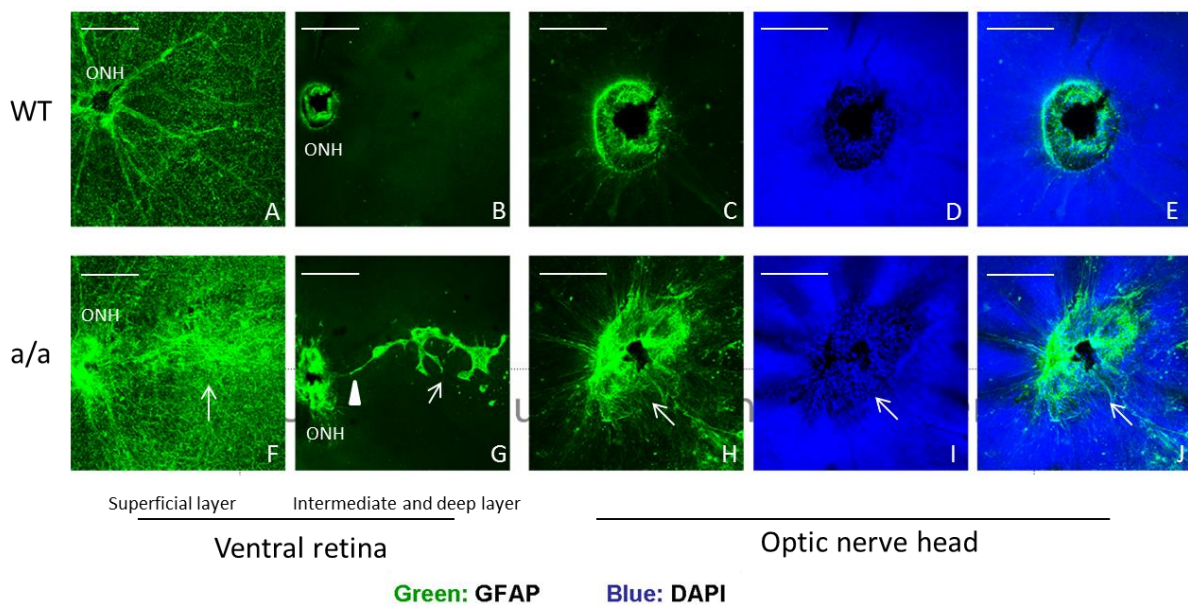


Figure 5.24 Activated glial cells in optic nerve head and ventral retina at 1 month. (A-J) Flat-mount immunostaining showed that there are much more ONH cells (I, arrow) in the optic nerve of the mutants compared to wild-type controls (D). GFAP expression is up-regulated in the optic nerve head (H, J, arrow) and ventral retina (F, G, arrow) in mutants compared to wild-type controls (A-C, E), suggesting that glial cells are activated in these regions. These activated glial cells form a long aggregate (glial scar) in the ventral retina (G, arrow) and the glial scar is connected to the optic nerve head (G, arrowhead). Scale bar: A-B, 300 μ m; C-E, H-J, 200 μ m.

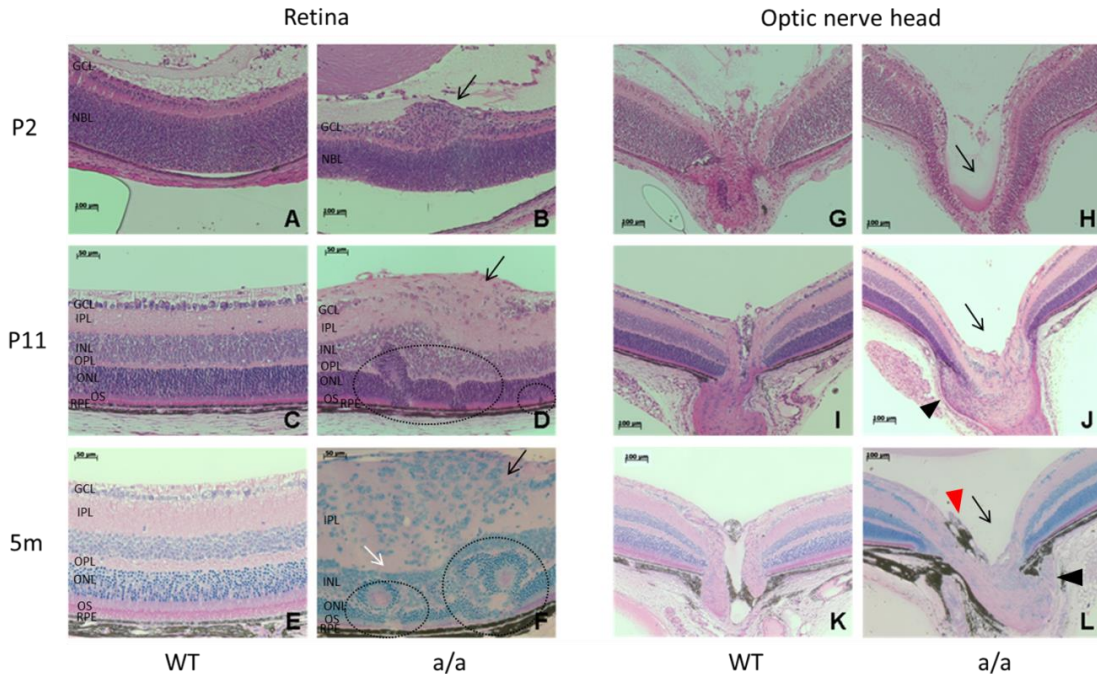


Figure 5.25 Ventral retinal gliosis and optic nerve head hypoplasia in *Ali030* mutants. (A-F) Retinal gliosis and retinal dysplasia are found in ventral retina in mutants. (A-B) At P2, there are some more cells in the retinal ganglion cell layer in mutants (B, arrow), but it seems that there is no difference in the neural blast layer between wild types and mutants. (C-D) At P11, there are distinct retinal layers in the wild-type retina (C), but in mutants there are much more cells in the inner plexiform layer and it appears that the retinal ganglion cell layer is broken and the neural fibers from inner plexiform layer grow out of the retina through the broken GCL through cell migration (D, arrow). In addition, some cells appear to be from inner nuclear layer and retinal rosettes are found (D, broken circles). (E-F) At adult (5 months), the cell number in the inner plexiform layer is significantly increased compared to early postnatal periods (F, arrow), and there are thinner inner and outer nuclear layer and photoreceptor layer (F) compared to the wild-type controls (E). It is obvious that some cells in the inner plexiform are from inner nuclear layer (F, white arrow) and more severe retinal rosettes are found and the photoreceptor layer is disrupted (F, broken circles). (G-L) Enlarged optic nerve head holes were found in mutants at P2 (H, arrow), P11 (J, arrow) and adult (5 months) (L, arrow) compared to the wild-type controls (G, I, K). It appears that there are some more cells in the verge of the optic nerve head at P11 (J, arrowhead) and adult (L, black arrowhead) in mutants. The remnant of the hyaloid artery was found in the rim of the optic nerve head (L, red arrowhead) in mutants which was consistent with the OCT finding. Scale bar: A-B, G-L, 100 μ m; C-F, 50 μ m.

5.2.3 Activated glial cells in the optic nerve head and in the ventral retina, and hypodevelopment of the optic nerve in *Ali030* mutants

Immunofluorescence for sections also showed up-regulation and robust expression of GFAP in the optic nerve head and in the ventral retina compared to the wild-type controls, which demonstrated that the retinal gliosis occurs in the ventral retina of the mutants. Further analysis was performed to observe the distribution and morphology of activated glial cells in mutants. At different stages

in wild-type mice from P5 to adult, GFAP-positive cells are only found in the nerve fiber layer and retinal ganglion cell layer (Figure 5.26, A-D). However, in the mutants, the number of activated glial cells is significantly increased from P5 to adult (Figure 5.26, E-H). In the early postnatal period, the number of activated glial cells is mainly located at the inner plexiform layer and outer plexiform layer, and retinal rosettes were not found, whereas at later stages, such as P21 and adult, the range of retinal gliosis is more broad and the inner nuclear layer and outer plexiform layer are also involved as well as the inner plexiform layer. It appears that the activated glial cells with long processes invade different layers of the retina in mutants (Figure 5.26, G, H) compared to wild types (Figure 5.26, C, D). There is an increased area of the ventral gliosis retina at later stages. In addition, there are more activated glial cells above the retinal ganglion cell layer compared to the early period, indicating that these glial cells are proliferating and produce more glial cells.

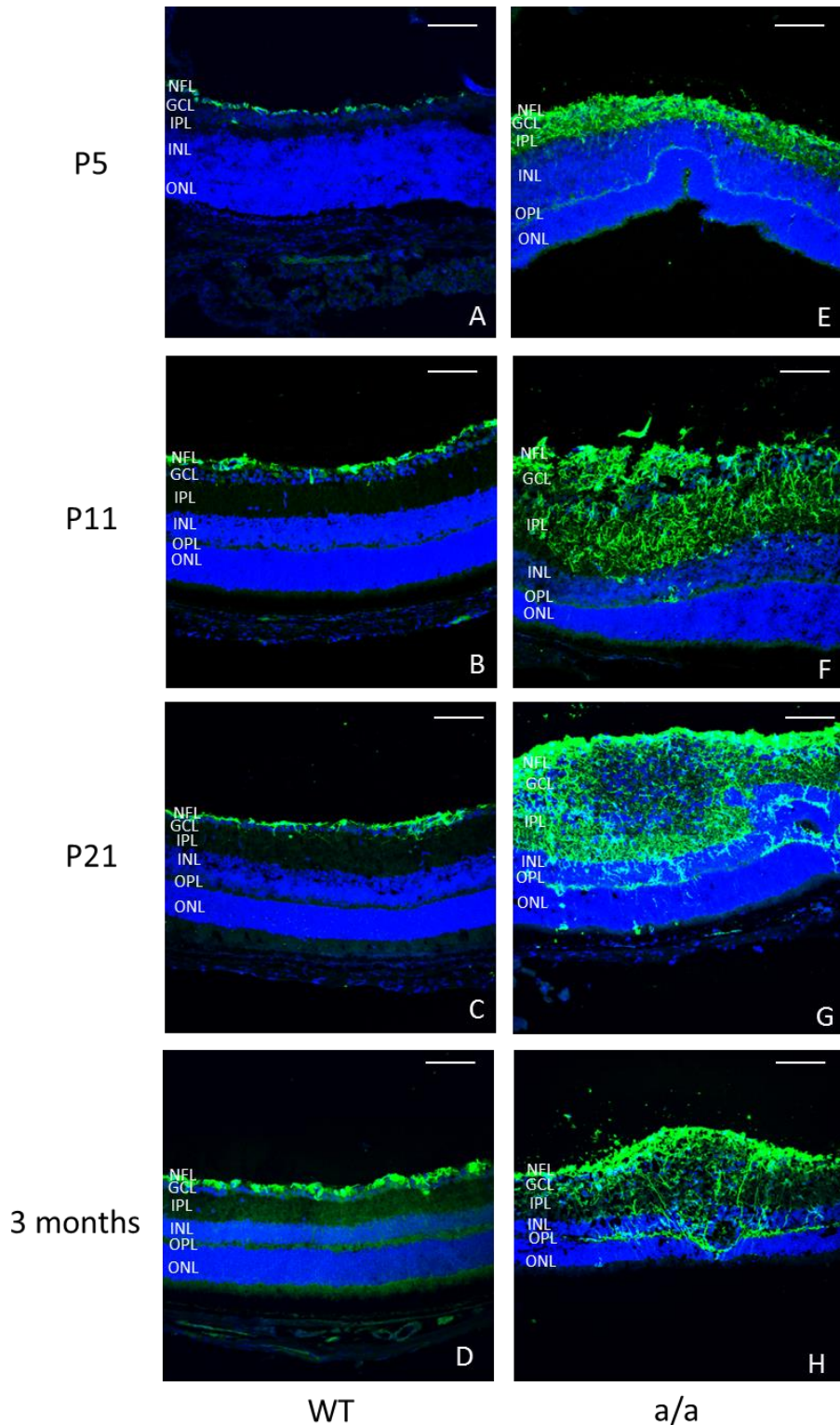


Figure 5.26 Retinal gliosis in *Ali030* mutants. (A-H) Ventral retinal gliosis was detected from early postnatal periods (P5) to adult (3 months) in *Ali030* mutants. (A-D) In wild-type retina from P5 to 3 months, GFAP is only expressed in the retinal ganglion cell and nerve fiber layer. (E-H) Robust up-regulation of GFAP expression was found in nerve fiber layer, retinal ganglion cell layer, inner plexiform layer and outer plexiform layer, especially in the inner plexiform layer where there are a significantly increased number of activated glial cells. At P5, the

outer plexiform is not clearly formed in wild types (A) and is also not clear from DAPI picture in mutants (E). However, the expression of GFAP is significantly up-regulated in the outer plexiform in mutants (E) compared to wild types (A). The retinal gliosis occur more broadly with strong up-regulation of GFAP in the outer plexiform layer in the adult mutant retina compared to the early periods. The retinal fold is formed in the early period (P5, E) and at the later stage (P21, G; 3 months, H) retinal rosettes are formed. NFL: nerve fiber layer; GCL: ganglion cell layer; IPL: inner plexiform layer; INL: inner nuclear layer; OPL: outer plexiform layer; ONL: outer nuclear layer. Scale bar: 50 μ m.

In the optic nerve head, GFAP-positive cells are only found in the retinal ganglion cell layer and in the optic nerve in wild-type mice, while GFAP-positive cells with long branches are found in homozygous mutants (Figure 5.27, A-B and D-E), which suggests that the glial cells are activated in the optic nerve. In the optic nerve head, the astrocytes are also disorganized and GFAP-positive fibers are intercrossed in homozygous mutants compared to wild types (Figure 5.27, C and F).

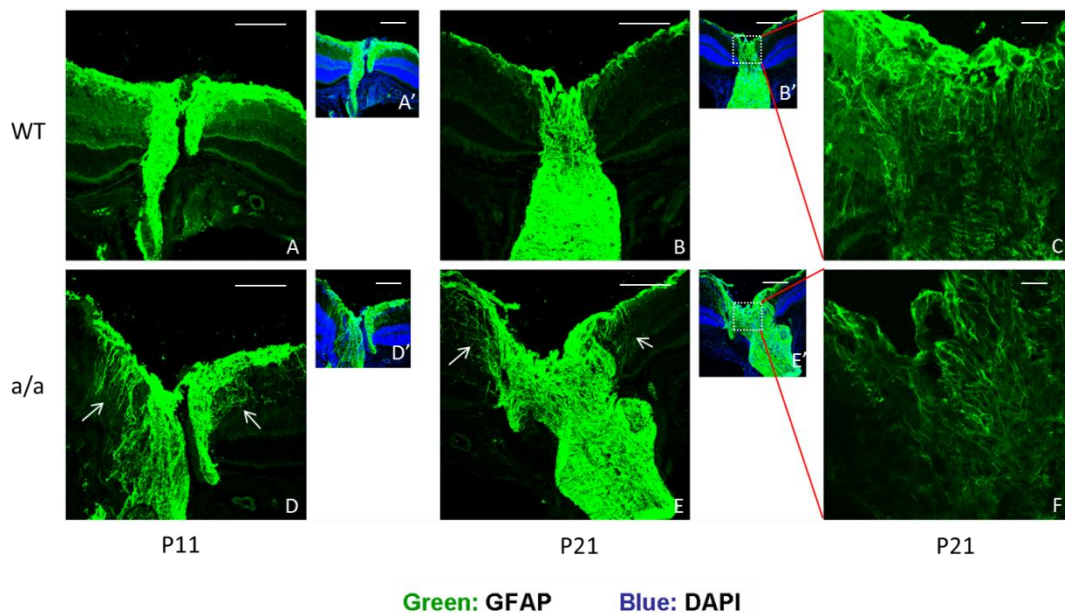


Figure 5.27 Activated and disorganized astrocytes in optic nerve head. (A-C) The wild-type retina showed GFAP-positive staining in the retinal ganglion cell layer and the optic nerve. (D-F) In mutants activated astrocytes with long processes were found in optic nerve head (arrow). In the optic nerve head, the astrocytes were disorganized in mutants (F) compared to the wild-type controls (C). Scale bar: A-B, A'-B', D-E, D'-E', 50 μ m; C and F, 20 μ m.

Further, we analyzed the optic nerve in the cross and longitudinal sections. The glial cells in the optic nerve is also activated compared to the wild-type controls (Figure 5.28, C, G), which is consistent with the findings in the optic nerve head (Figure 5.27). Moreover, the optic nerve is covered by three meningeal layers in the wild-type mice (Figure 5.28, A), whereas these meningeal layers are absent in the local area of the optic nerve but some cells of the optic nerve instead (Figure

5.28, E). The disrupted meningeal layers were located at the proximal and local area of the optic nerve in mutants. Interestingly, the number of Sox2-positive cells is obviously decreased in the optic nerve in mutants compared to the wild-type controls (Figure 5.28, B, F, I, K). Together with the histological findings, it suggests that the development of optic nerve is disrupted and this could be a hypodevelopmental process.

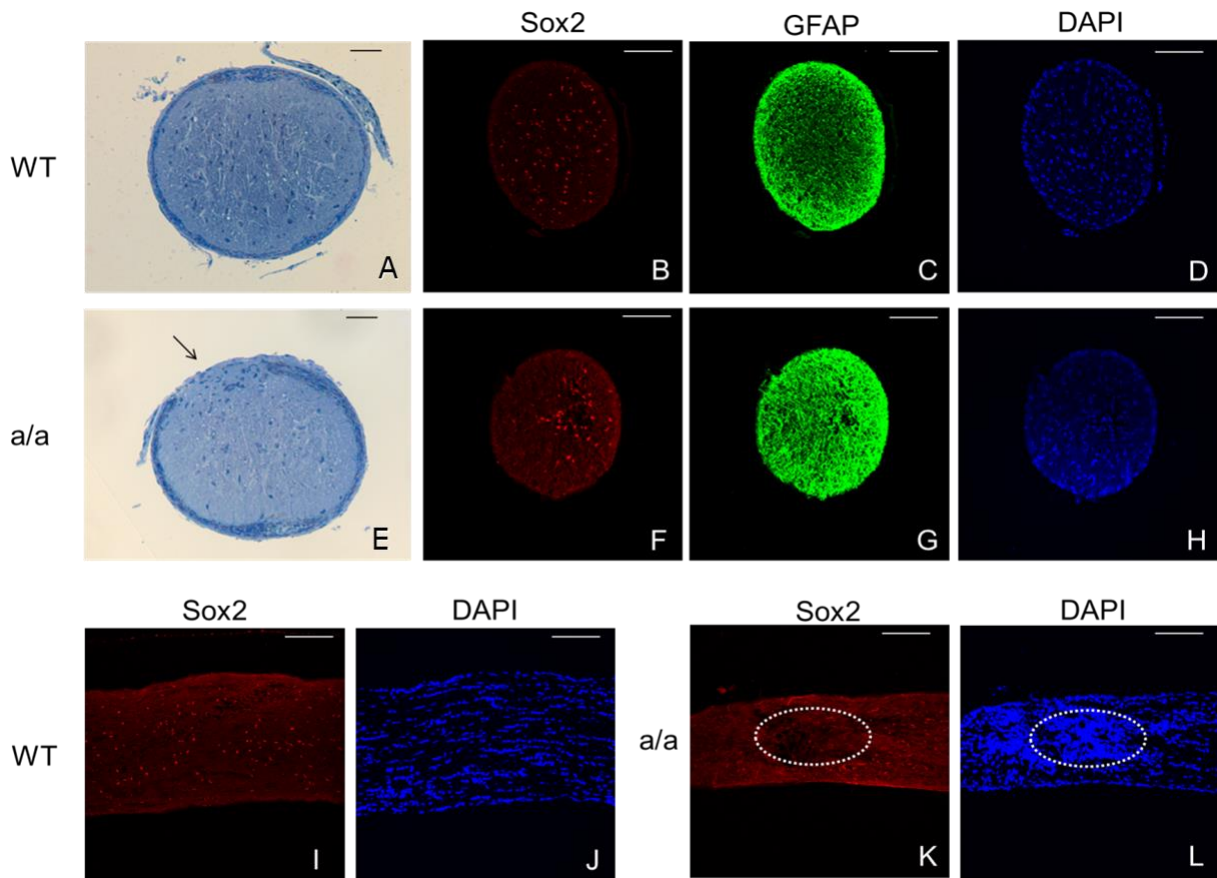


Figure 5.28 Disrupted optic nerve of *Ali030* mutants at P21. (A-H) Cross sections of the optic nerve. In wild types the optic nerve is covered by intact meningeal layers (A), but in the mutants the meningeal layers of the optic nerve are disrupted (E, arrow). (B-C) A number of Sox2-positive cells are in the optic nerve (B) and the glial cells are mainly located at the peripheral region of the optic nerve (C) in wild types. In contrast, in mutants the number of Sox2-positive cells is decreased in the optic nerve (F) and the glial cells are more activated in the whole optic nerve (G). (I-L) Longitudinal sections of the optic nerve. Obviously, there are very few Sox2-positive cells in some areas with the dense cells of the optic nerve in mutants (K and L, broken circles) compared to the broad Sox2-positive cells in the wild-type controls (K). (B-D, F-H, I-L) Red: Sox2; Green: GFAP; Blue: DAPI. Scale bar: A, E, 20 μ m; B-D, F-H, I-L, 50 μ m.

5.2.4 Loss of ventral retinal ganglion cells, axon misguidance in ventral retina and defective axons in the optic nerve in *Ali030* mutants

To investigate whether retinal ganglion cells and axons are affected by retinal gliosis, I did flat-mount immunostaining to label retinal ganglion cells using Brn3, a marker for retinal ganglion cells (Soto et al., 2008; de Melo et al., 2011). Interestingly, I found only a few Brn3-positive cells in the ventral retina in mutants, whereas there are a number of Brn3-positive cells in any area of the retina in the wild-type controls (Figure 5.29, A-F). This result suggests that the number of retinal ganglion cells is greatly decreased in the ventral retina in mutants compared to wild types. This result indicates that increased number of activated glial cells in ventral retina could destroy retinal ganglion cells. The axons from retinal ganglion cells need to pass through the retina and enter the optic nerve head during eye development. I further observed the retinal ganglion cell axons by flat-mount immunostaining using the antibody against axons marker neurofilament. In consistency with the decreased number of retinal ganglion cells in the ventral retina, there are indeed a greatly decreased number of axons in the central ventral retina (Figure 5.29, I and L) compared to the wild-type controls (Figure 5.29, G and J). In wild-type mice, all the axons pass through the retina and enter the optic nerve head (Figure 5.29, I). Surprisingly, there are two bundles of axons in both sides near the central ventral retina, and almost all the axons in ventral retina do not enter the optic nerve head but go into both two bundles instead (Figure 5.29, I), which is not found in dorsal retina in mutants (Figure 5.29, H). In addition, there are several mislocalised axons found in the peripheral ventral retina and only a few found in the dorsal retina in mutants (Figure 5.29, K-L). These results suggest that axon guidance is severely affected in ventral retina in mutants. Furthermore, sectional immunostaining against neurofilament found that neurofilament is strongly expressed in the retinal nerve fiber layer, the optic nerve and horizontal cells in wild types at P11 and P21 (Figure 5.30, A-B and E-F). The strong axons bundles exist in the optic nerve of the wild-type mice at P11 and P21 (Figure 5.30, A and E). However, in mutants, the expression of neurofilament is both disrupted in the horizontal cells and is absent in some areas of the optic nerve at P11 and P21 (Figure 5.30, C-D and G-H). These results suggest that the axons of the optic nerve are defective and the horizontal cells are disrupted in the mutants at P11 and P21.

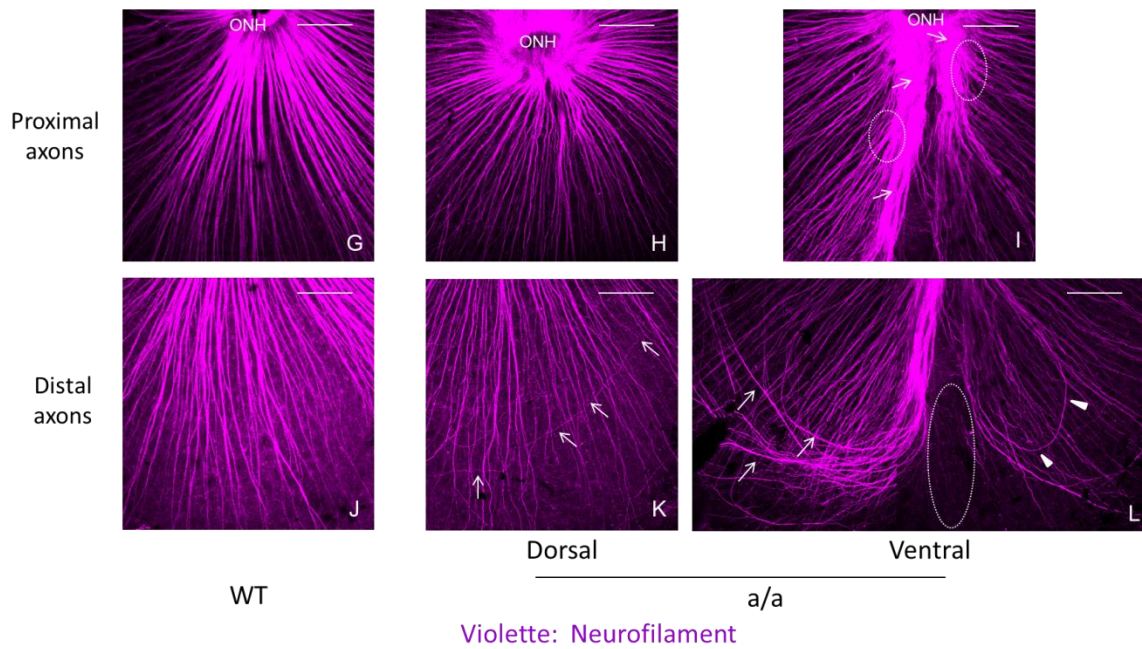
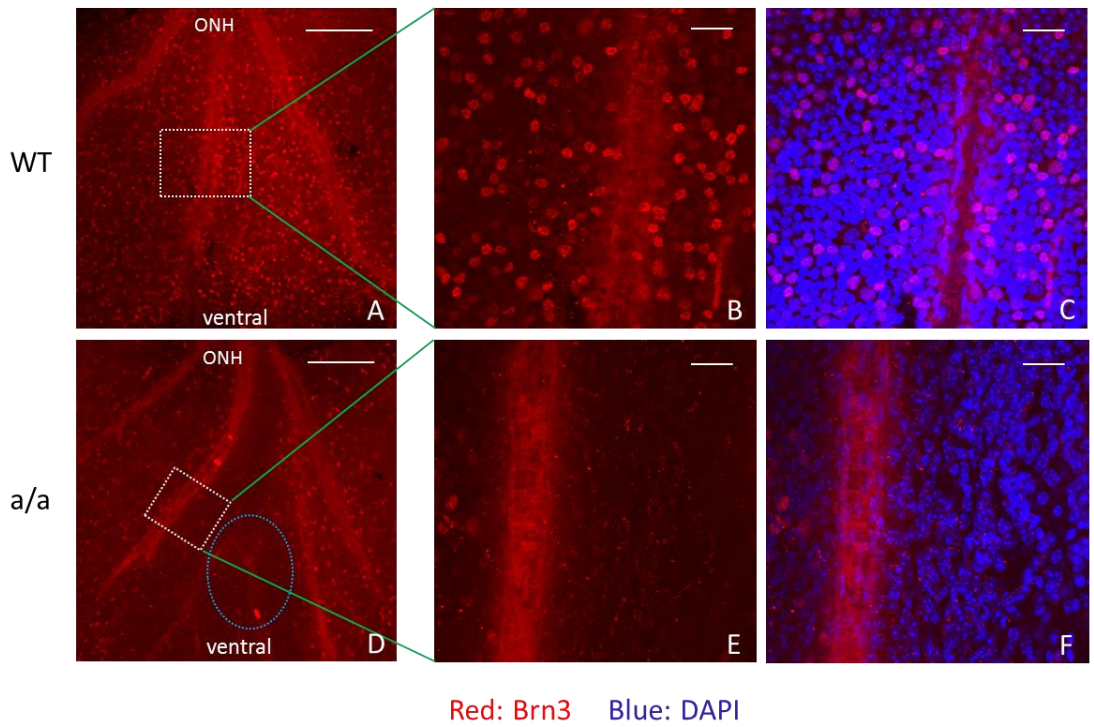


Figure 5.29 Loss of retinal ganglion cells and axon misguidance in gliosis retina in mutants. (A-F) Flat-mount immunostaining against Brn3 showed that the number of retinal ganglion cells is greatly reduced and only a few retinal ganglion cells are found in the ventral retina in mutants (D-F) compared to wild types (A-C) at 3 months. (G-L) In consistency with the loss of retinal ganglion cells, the number of retinal nerve fibers is also decreased in the center of the ventral retina, especially in the distal area in mutants (L, broken circle), but the

proximal retina exhibits two separate accumulation of axons to form the bundles (I, arrow) and nearly all the retinal axons project from peripheral to the two bundle, instead of the optic nerve head (I, broken circle). In addition, there are still a few mislocalised axons in the dorsal retina (K, arrow) in mutants although the global pattern is similar to wild types. Mislocalised axons are found in the distal ventral retina in mutants (L, arrow and arrowhead) (About L, to see the picture of ventral retina clearly in a global manner, L is composed of two pictures overlapped by manually). Scale bar: A, D, 300 μ m; B-C, E-F, 50 μ m; G-L: 300 μ m.

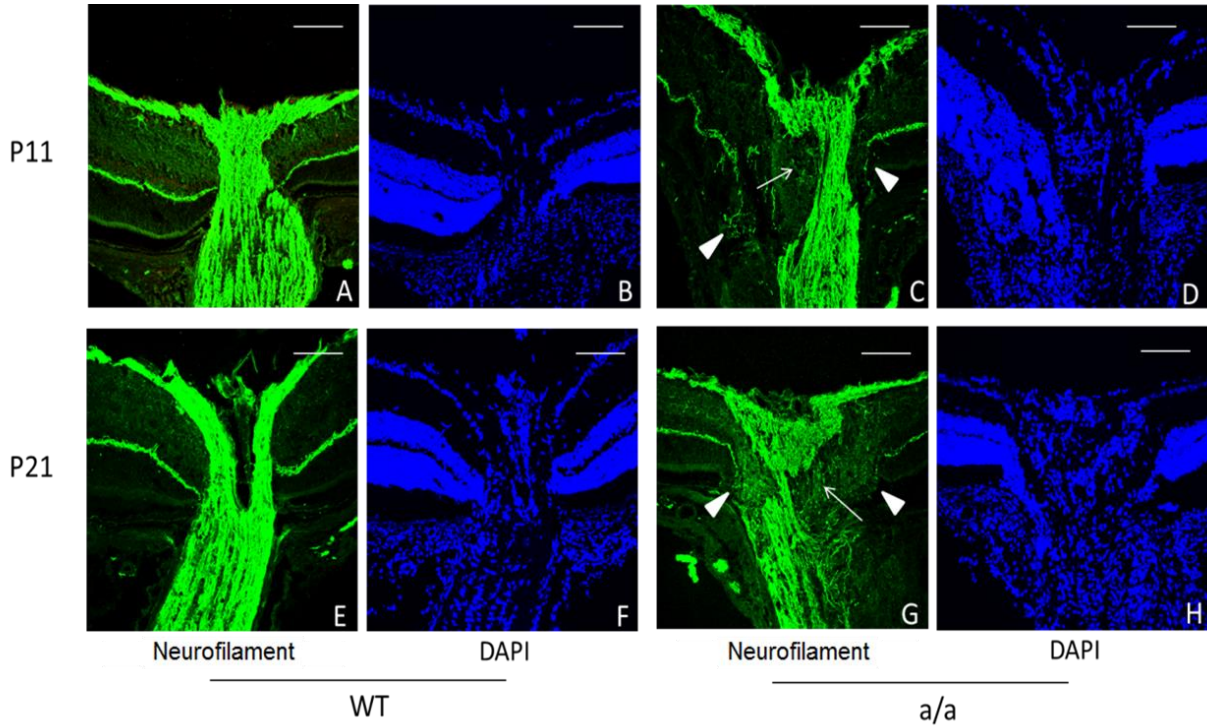


Figure 5.30 Axon defects of the optic nerve in *Ali030* mutants. (A-B, E-F) Neurofilament is expressed in retinal axons in the nerve fiber layer and optic nerve and also expressed in the axons of the horizontal cells in the outer plexiform layer in wild types at P11 and P21. (C-D, G-H) The retinal ganglion cell axons are similar to wild types but seem thinner in mutants. However, disorganized axons are found in the optic nerve head at P11 (C, arrow) and P21 (G, arrow). In addition, the axons of the retinal horizontal cells are also disorganized around the optic nerve head at P11 (C, arrowhead) and P21 (G, arrowhead). Scale bar: 50 μ m.

5.2.5 Retinal dysgenesis is associated with reactive gliosis in *Ali030* mutants

Another hallmark of ventral retinal gliosis in *Ali030* mutants is retinal dysplasia. As we can see from the histology picture, retinal rosette and delamination are formed in *Ali030* mutants (Figure 5.25, D and F). The photoreceptor layer was thinner and a clump of inner nuclear layer abuts directly onto the retinal pigmental epithelium in mutants compared to wild types (Figure 5.23, B; Figure 5.25, D-E), which suggests that retina dysplasia occurs in the ventral gliosis retina in *Ali030* mutants. Then I further analyzed the dysplasia retina in greater details using different antibodies

to specific retinal cell markers. PDE6b is a marker for rod photoreceptor in retina (Pittler et al., 2004; Mali et al., 2007). PDE6b immunostaining demonstrated a disruption and delamination in photoreceptor layers in the mutant ventral retina compared to wild types (Figure 5.31, A and E). Protein kinase C- α (PKC- α) is a specific marker for retinal bipolar cells (Greferath et al., 1990), through which visual information can be transmitted from photoreceptor to retinal ganglion cells. The lamination of retinal bipolar cells is disrupted in the ventral retinal gliosis region and some ectopic bipolar cells were found in the outer nuclear layer of the mutants (Figure 5.31, B and F). Otx2 can control the fate of photoreceptors and the specification of RPE cells, and it is expressed in the inner nuclear layer and RPEs in the retina (Beby and Lamonerie, 2013). Otx2 immunostaining showed that the inner nuclear layer is disrupted and splits into two layers in retina (Figure 5.31, G) in mutants. The retinal pigmental epithelium is also disrupted and less RPE cells are in the ventral gliosis retina in *Ali030* mutants compared to wild-type controls (Figure 5.31, C and G). Calretinin can be used to mark all amacrine cells and retinal ganglion cells (Haverkamp and Wässle, 2000). In wild types, calretinin is expressed in the retinal ganglion cells, amacrine cells and inner plexiform layer (Figure 5.31, D), whereas in mutants, missing retinal ganglion cells are found in the inner plexiform layer and the retinal ganglion cell layer is thinner or missing in the gliosis retina (Figure 5.31, H). The amacrine cells are located at the inner nuclear layer in the wild types (Figure 5.31, D), whereas in mutants the inner nuclear layer is totally disrupted in the ventral gliosis retina and interestingly there are some mislocalized amacrine cells in the inner plexiform layer (Figure 5.31, H). In contrast, the lamination and genesis of dorsal retina is not affected in mutants (data not shown). These results demonstrate that the retinal dysplasia occurs in the ventral gliosis retina of the mutants.

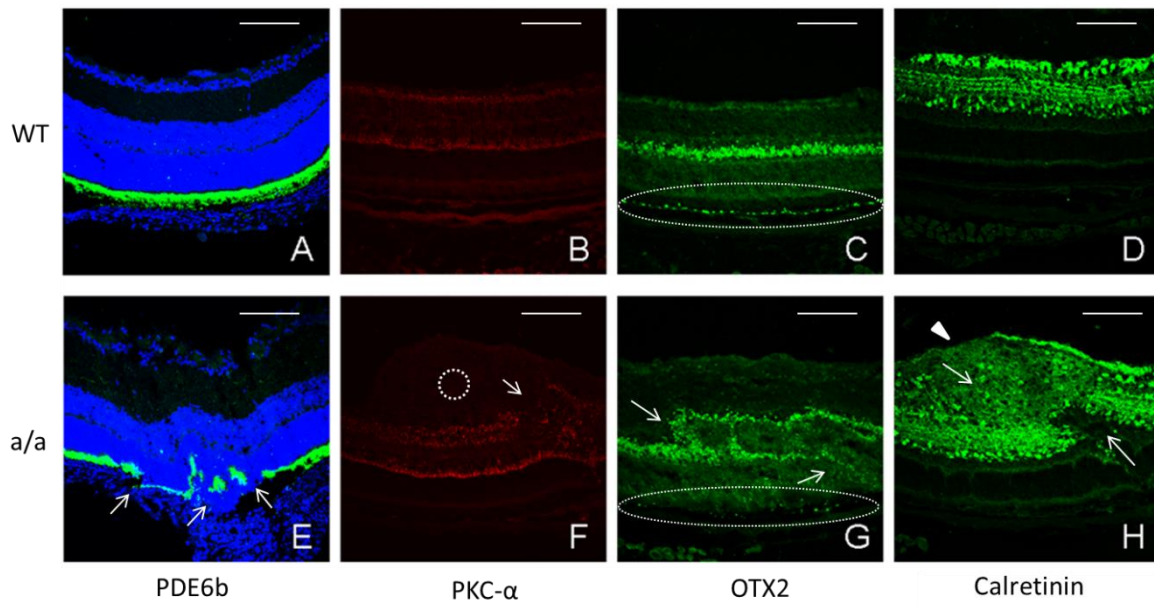


Figure 5.31 Retinal dysgenesis is found in the ventral gliosis region in *Ali030* mutants at P21. (A-D) There is regular retinal lamination, and different types of retinal cells develop well in the wild-type retina. PDE6b is expressed in the photoreceptor layer (A); PKC- α is expressed in the bipolar cells (B); OTX2 is expressed in the inner nuclear layer and retinal pigmental epithelium (C); Calretinin is expressed in the ER lumen and is also a marker for immature neurons: it is expressed in the retinal ganglion cells, inner plexiform layer and inner nuclear layer (D). (E-F) The retina displayed delamination and rosettes of the photoreceptor in mutants. (E) The photoreceptor layer is discontinuous and some parts are thinner in mutants compared to wild types. (F) The bipolar cells are disrupted and their connections and axons are destroyed in mutants (arrow); a proliferative retinal gliosis region is above the axon terminals of the bipolar cells (circle), which is not found in wild types (B). (G) The inner nuclear layer is disrupted and it splits into two layers in retina (arrow) and there are remarkably decreased number of RPE cells compared to the wild-type controls (circles). (H) In the mutants, the number of retinal ganglion cells (arrowhead) is significantly reduced, the inner nuclear layer is disrupted and the connection of the inner nuclear layer is destroyed (arrow, below) in mutants. There is a retinal gliosis region with a number of ectopic calretinin-positive amacrine neurons (arrow, above). Scale bar: 50 μ m.

5.2.6 Regular ERG response in *Ali030* aged mutants

Electroretinogram (ERG) can be used to test the retinal function in mice as a screen method (Dalke et al., 2004). At 10 weeks, *Ali030* homozygous mutants showed regular electrical response in retina compared to wild types by ERG (Figure 1.8, E, performed by Susanne Weber, HGMU). I further performed the ERG measurements in older mice (12 months) to investigate whether the ventral retina gliosis affects the retinal function in aged mutant mice. At 12 months, *Ali030* mutants still showed regular electricity response to light flashes (500 and 12,500 cd/m^2) (Figure 5.32). This data suggests that ventral retinal gliosis and local retinal dysplasia do not severely affect global retinal function. Further multi-focal ERG may be helpful to test and analyze local retinal functions. In

addition, due to the limitation of the small sample size (N=3 per group) used in this study, large samples could be needed to find the subtle changes.

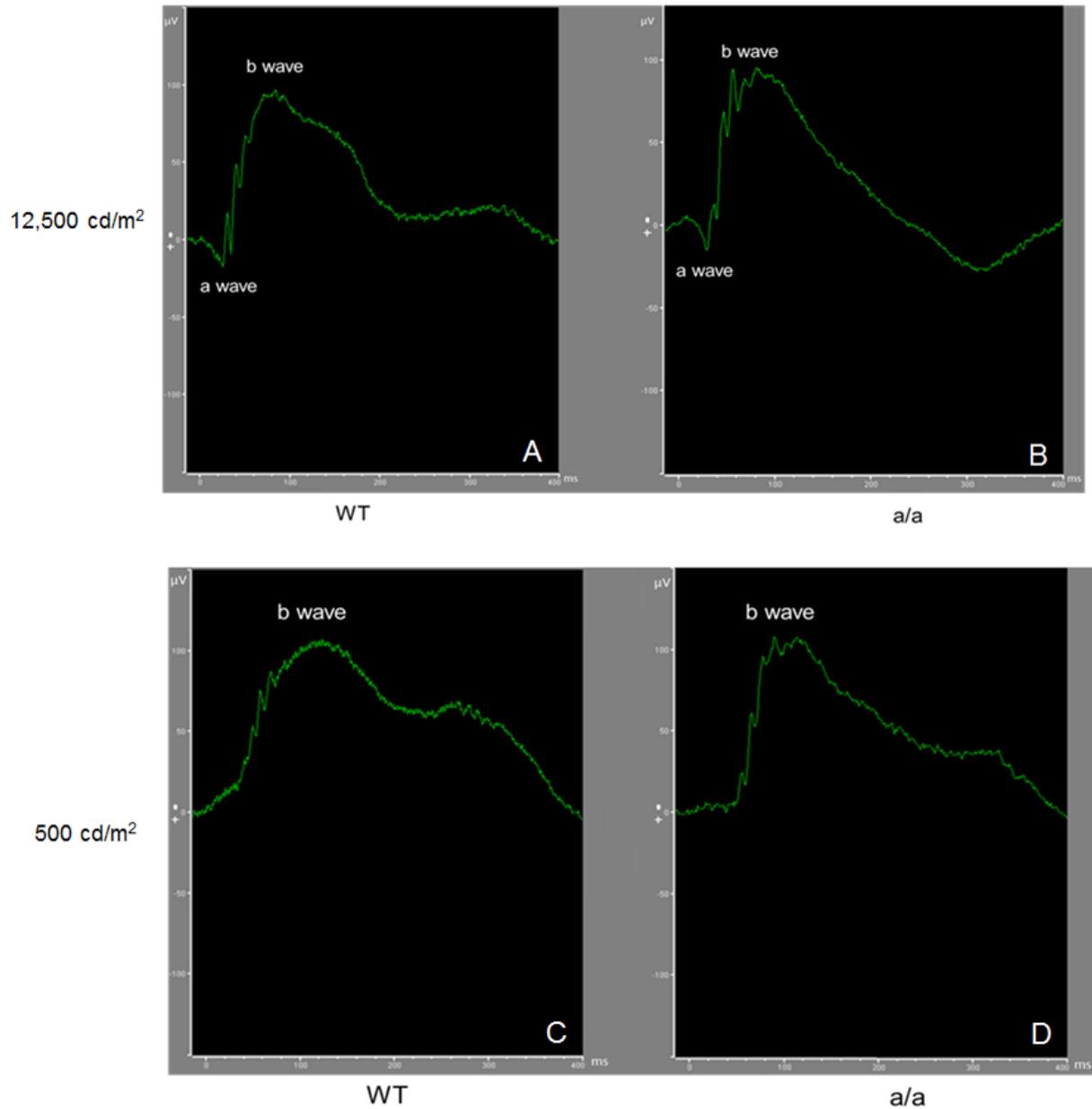


Figure 5.32 Regular global ERG responses in *Ali030* mutants at 12 months. (A-B) At 12 months, *Ali030* mutants exhibit regular electrical response to the high light flashed ($12,500 \text{ cd/m}^2$) in retina revealed by ERG (B) compared to wild types (A). (C-D) At 12 months, *Ali030* mutants exhibit regular electrical response to the low light flashed (500 cd/m^2) revealed by ERG (D) compared to wild types (C). The number of mice was used in this study (WT: N = 3; Mt: N = 3). This figure here is one example of the three independent results.

5.2.7 Glial-like cells expressing Sox2, Pax2 and Nestin but not Pax6 are found in the ventral retinal gliosis and they are proliferating in Ali030 mutants

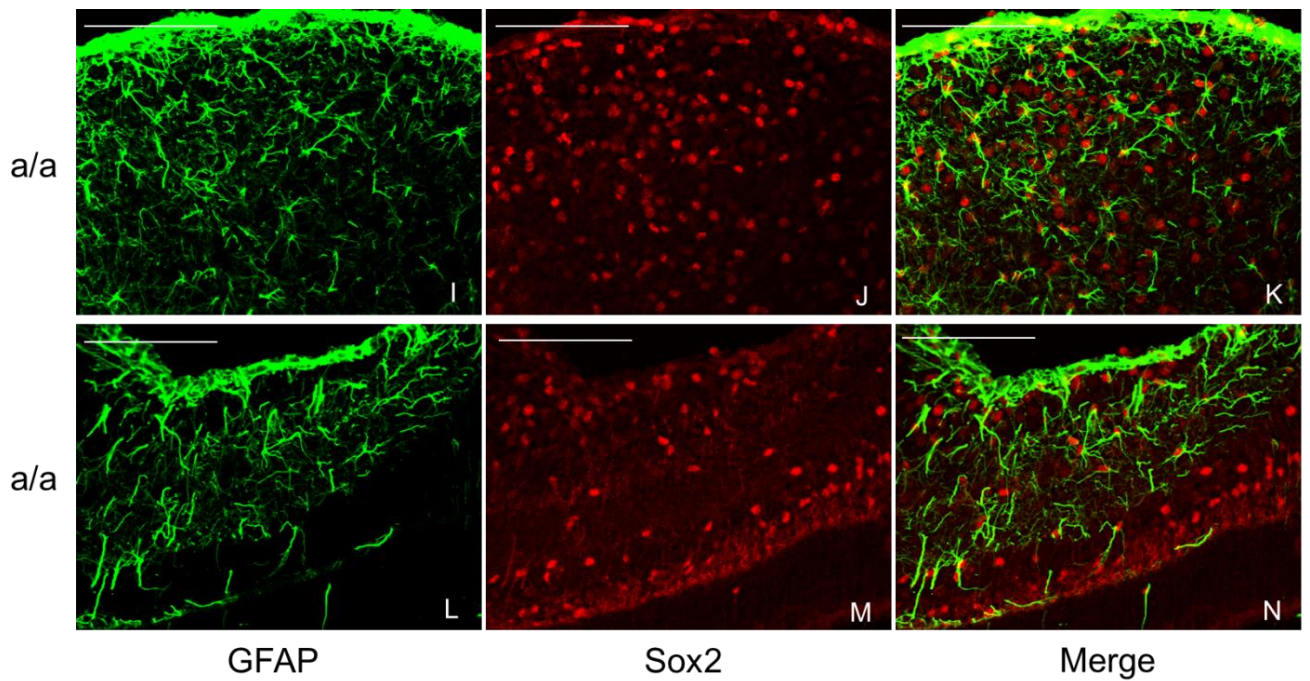
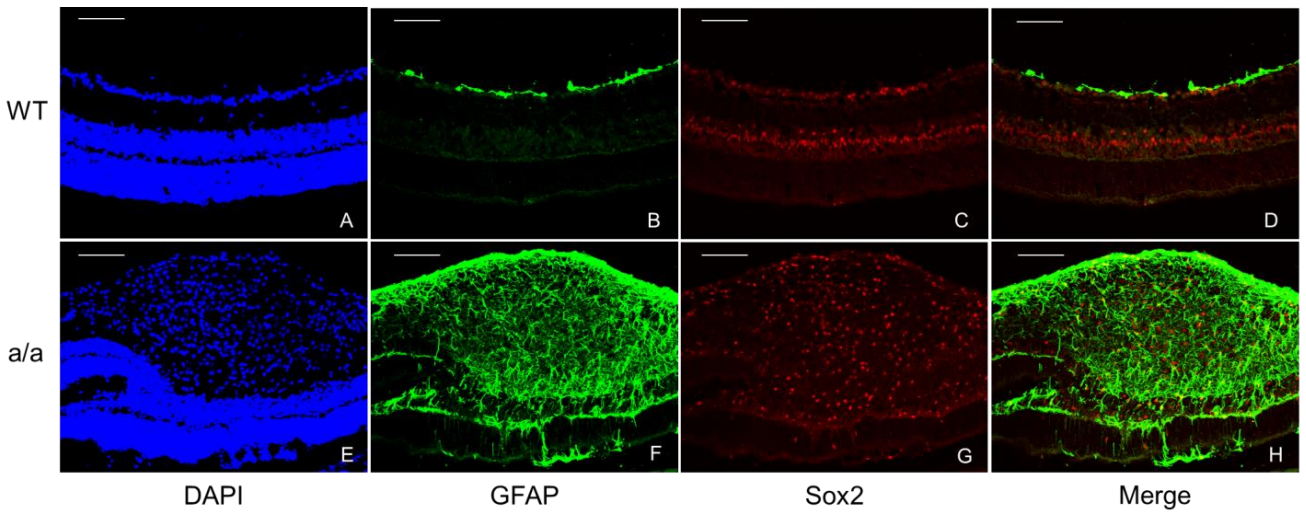
Next, I analyzed the properties of these activated astrocytes in gliosis ventral retina. I chose four different stem cell/progenitor cell markers, Sox2, Pax2, Pax6 and Nestin. Sox2 (SRY (sex determining region Y)-box 2) is a transcription factor that is essential for stem cells pluripotency (Sarkar and Hochedlinger, 2013). Pax2 (Paired box gene 2) is a transcription factor which can control the fate choice of neuron and glia (Soukkaieh et al., 2007). *Pax6* is a master control gene for eye development (Shaham et al., 2012) and it is essential for neuronal fate differentiation and determination in the retina (Philips et al., 2005) and also required for neurogenesis (Sansom et al., 2009). I performed double immunofluorescence staining using two different antibodies on the retina and found that in wild-type retina some retinal ganglion cells express Sox2 (Figure 5.33, A and C), and GFAP-positive cells are only observed in the nerve fiber layer and retinal ganglion cell layer (Figure 5.33, A-B). However, in mutants there are a number of activated glial cells in all different retinal layers including inner plexiform layer and inner nuclear layer (Figure 5.33, E-F), and these activated glial cells express Sox2 (Figure 5.33, H, I-Q). Interestingly, in the vitreal side of the retinal glial region, as OCT demonstrated it is a thick epiretinal membrane (Fig. 5.23, A, red arrow; B, blue arrow), GFAP is also highly and densely expressed in the epiretinal membrane (Figure 5.33, F, I and L). In the epiretinal membrane, GFAP is overlapped with Sox2 which suggests that GFAP is not only expressed in the cytoplasm but also in the nuclei in this region. Interestingly, in the inner plexiform layer and inner nuclear layer, it appears that GFAP is mainly expressed in the cytoplasm and Sox2 is expressed in the nucleus of the same cells (Figure 5.33, H, I-K). Similar finding also occurs in the peripheral part of the ventral gliosis (Figure 5.33, L-N). These results suggest that the activated glial cells may undergo dynamic changes from inside to the outside of the retina. Nestin is not obviously expressed in the wild-type retina at P21 (Figure 5.33, R-T), but Nestin can be detected in the ventral retinal gliosis region and it is co-expressed with GFAP in mutants (Figure 5.33, U-W), suggesting that activated glial cells also express Nestin. Pax2 is expressed in the retinal ganglion cell layer and some Pax2-positive cells also express Sox2 in wild types (Figure 5.35, E-H), but Pax2 is highly expressed in the ventral retinal gliosis region of the mutants. It is localized in the nucleus and it co-expressed with Sox2 in the ventral retina gliosis region (E-H). Pax6 is expressed in the retinal ganglion cell layer and inner nuclear layer in

wild-type retina (Figure 5.35, I-J), whereas in mutants Pax6 is almost absent the ventral retina gliosis region (Figure 5.35, K-L). These data suggest that these ventral activated glial cells may have properties of retinal progenitor cells, especially which have the capacity to be driven to the glial cell fate.

To further investigate whether these activated glial cells in the ventral retina are proliferating during the gliosis process, BrdU was injected intraperitoneally to label the proliferating cells at P21 and I found that the glial cells in the inner plexiform layer of the ventral gliosis retina are proliferating at P21 (Figure 5.33, A-F). The number of these BrdU-positive cells are obviously increased in mutants compared to wild types (Figure 5.34, A-F). Interestingly, these BrdU-positive cells also co-express with Sox2 but very few cells do not express Sox2 (Figure 5.34, J-O). Therefore, proliferative retinal gliosis occurs in the mutants. This proliferative ability could be due to the property of the progenitor cells.

Interestingly, these GFAP/Sox2 positive cells in mutants display a remarkable heterogeneity in their morphology. Some GFAP/Sox2 positive cells have the star-like appearance (Figure 5.33, E-N) and others have the morphology of bipolar cells (Figure 5.33, O-Q). Glutamate synthase (GS) is a marker for retinal Müller cells (the main type of glial cells in retina) which can be used to test whether activated glial cells are retinal Müller cells (Chen and Weber, 2002). Most of the activated glial cells do not express GS (5.36, H-S), suggesting that these cells are not retinal Müller cells, but astrocytes. Some cells in the inner plexiform layer are not retinal Müller cells because of their smaller size and different morphology although they co-express GS (Figure 5.36, H-K). The other activated glial cells in the outer plexiform layer which co-express GS, indicating that these cells are retinal Müller cells (Figure 5.36, P-S). Interestingly, up-regulation of GFAP expression can be found in some bipolar cells of the inner nuclear layer (Figure 5.33, O-Q). From the morphology and location and Sox2-positive expression, this type of the cells could be due to the changed fate of bipolar cells. In addition, Brn3 is normally expressed in the retinal ganglion cell layer and it does not co-express GFAP in wild types (Figure 5.37, A-C), whereas in mutants retinal ganglion cell layer was disrupted and ectopical Brn3-positive retinal ganglion cells were found in the inner plexiform layer (Figure 5.37, E). However, some Brn3-positive retinal ganglion cells in mutants showed up-regulation of GFAP (Figure 5.37, D-I), which indicates that these retinal neurons may

acquire the fate of glial cells. In addition, there are also some other astrocytes which are activated in the outer side of the photoreceptor layer which do not co-express with GS (Figure 5.36, P-S). These results showed that the activated glial cells are heterogeneous and at least three types of activated glial cells (retinal astrocytes, retinal Müller cells and the glial cells transdifferentiated from some retinal neurons) are involved in the ventral gliosis in mutants.



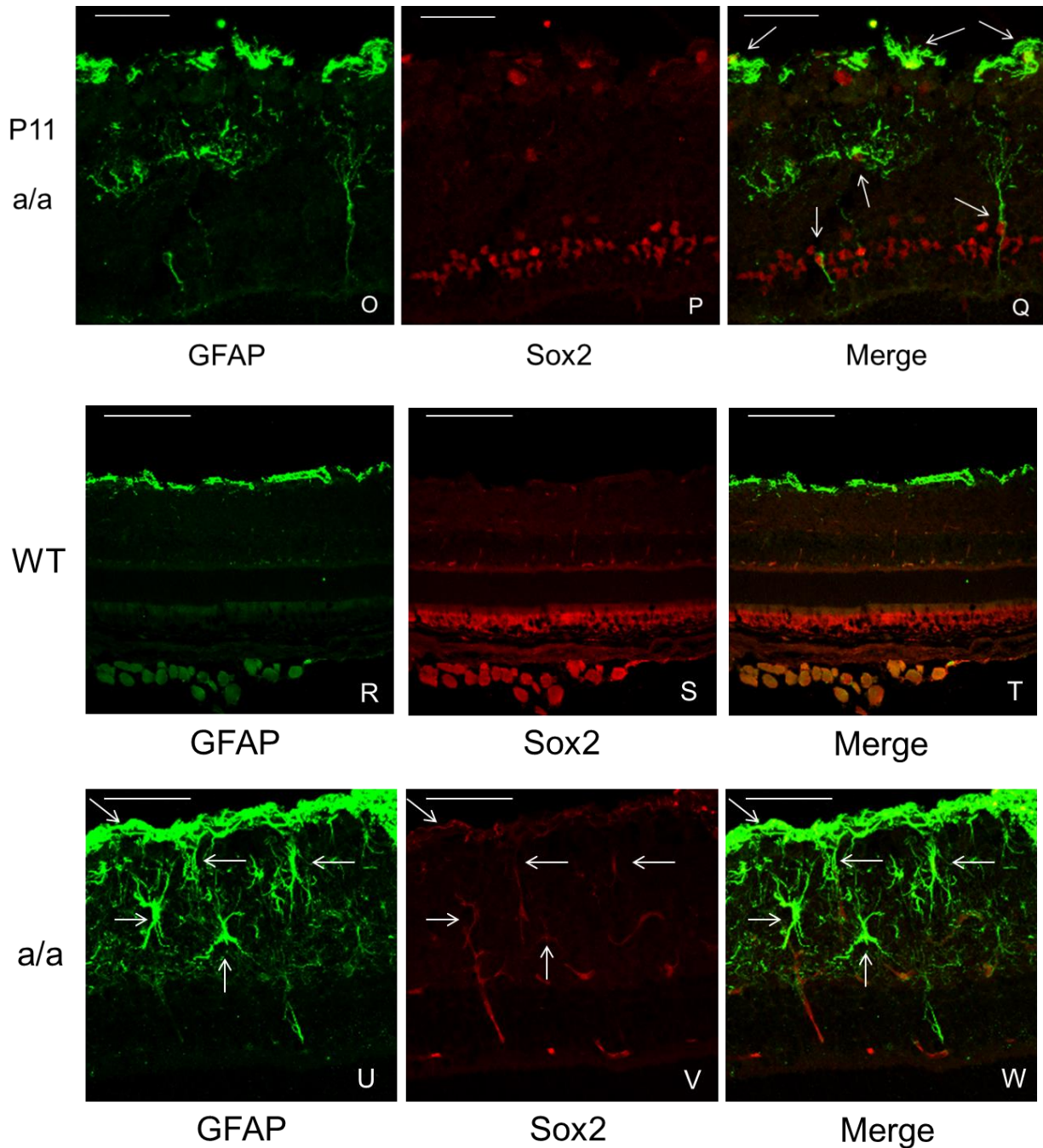
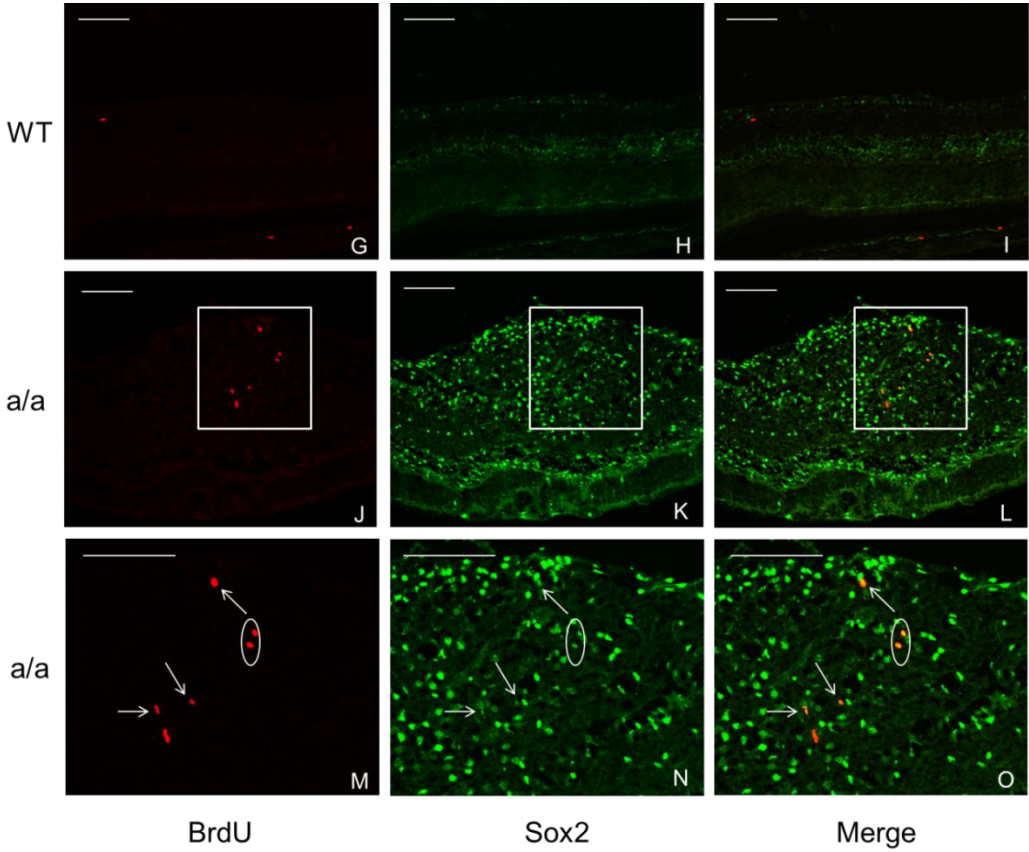
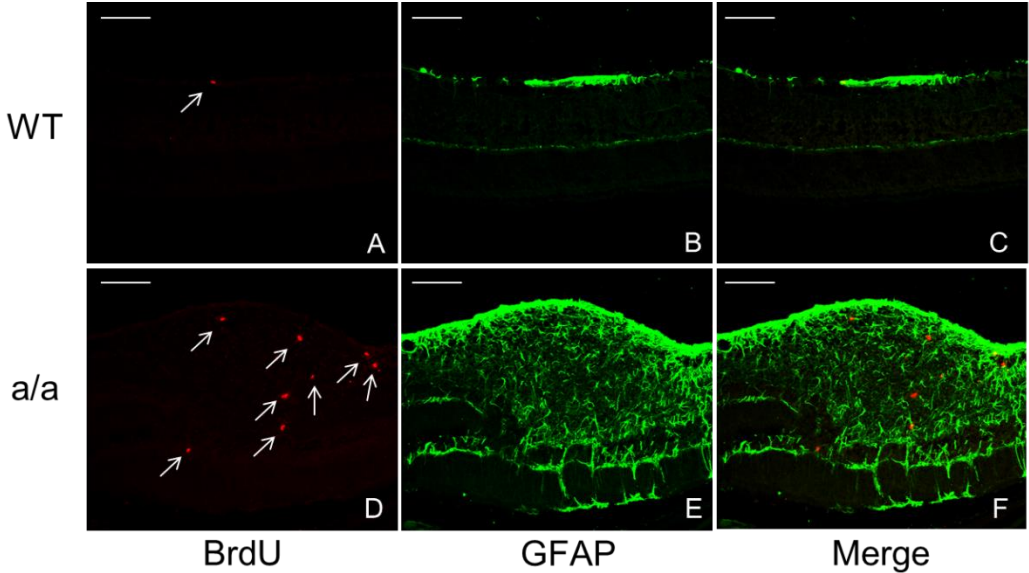


Figure 5.33 The activated glial cells in ventral retina express stem cell markers Sox2 and Nestin, and the heterogeneity of activated glial cells in *Ali030* mutants at P21. (A-C) In wild types, Sox2 is expressed in the retinal ganglion cell layer and inner nuclear layer (A and C) and GFAP is only expressed in the nerve fiber layer and retinal ganglion cell layer (A and B). (E-H) However, in the gliosis ventral retina there are an increased number of activated glial cells in all different retinal layers (E and F) and Sox2 is abundantly expressed in the cell nuclei of the ventral gliosis retina (E and G). Moreover, Sox2 is expressed in the activated glial cells in the ventral gliosis retina. Interestingly, GFAP is overlapped with Sox2 in the vitreal side of the central part of the mutant retina (K, yellow), whereas in the inner nuclear layer and inner plexiform layer of the central retina (I-K) and the peripheral gliosis region (L-N), GFAP is mainly expressed in the cytoplasm and Sox2 is expressed in the nucleus of the same cells (I-Q). In addition, GFAP can be found in the cytoplasm of the bipolar cells (with

bipolar structure) from the inner nuclear layer (**O-Q**, the right most cells). From the morphology, activated glial cells displayed different types of cell patterns, some with star structure and some with single process and some with bipolar appearance (**K, N and Q**). (**R-W**) In wild types, Nestin is not expressed in the retina (**R-T**), whereas in mutants Nestin is expressed and it can co-express with activated glial cells (**U-W**), which is a marker of stem cells. Scale bar: A-N, R-T, 100 μm ; O-Q, U-W, 50 μm .



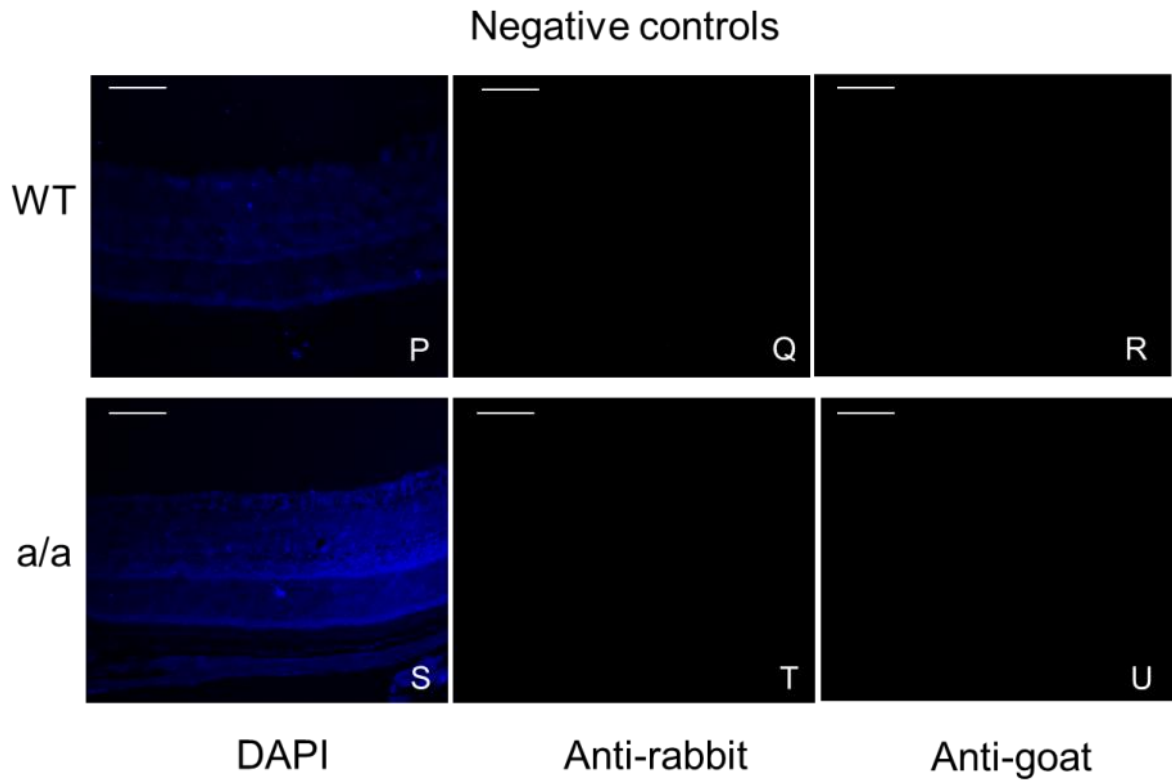


Figure 5.34 Proliferative ventral retinal gliosis in *Ali030* mutant mice at P21. (A-F) In wild types, there are very few BrdU-positive cells in the retina (A-C, G). Compared to wild types, there are remarkably increased BrdU-positive cells in the ventral retinal gliosis region (D-F). (G-O) In wild types, very few BrdU-positive cells do not express Sox2. Interestingly, most of these BrdU-positive cells also express Sox2 in mutants (J-L, M-O). (P-U) For the negative controls, there is absent staining in the sections labeled with BrdU from wild types and mutants. The number of the samples was used in this study (WT: N=3; Mt: N=3). Scale bar: 100 μ m.

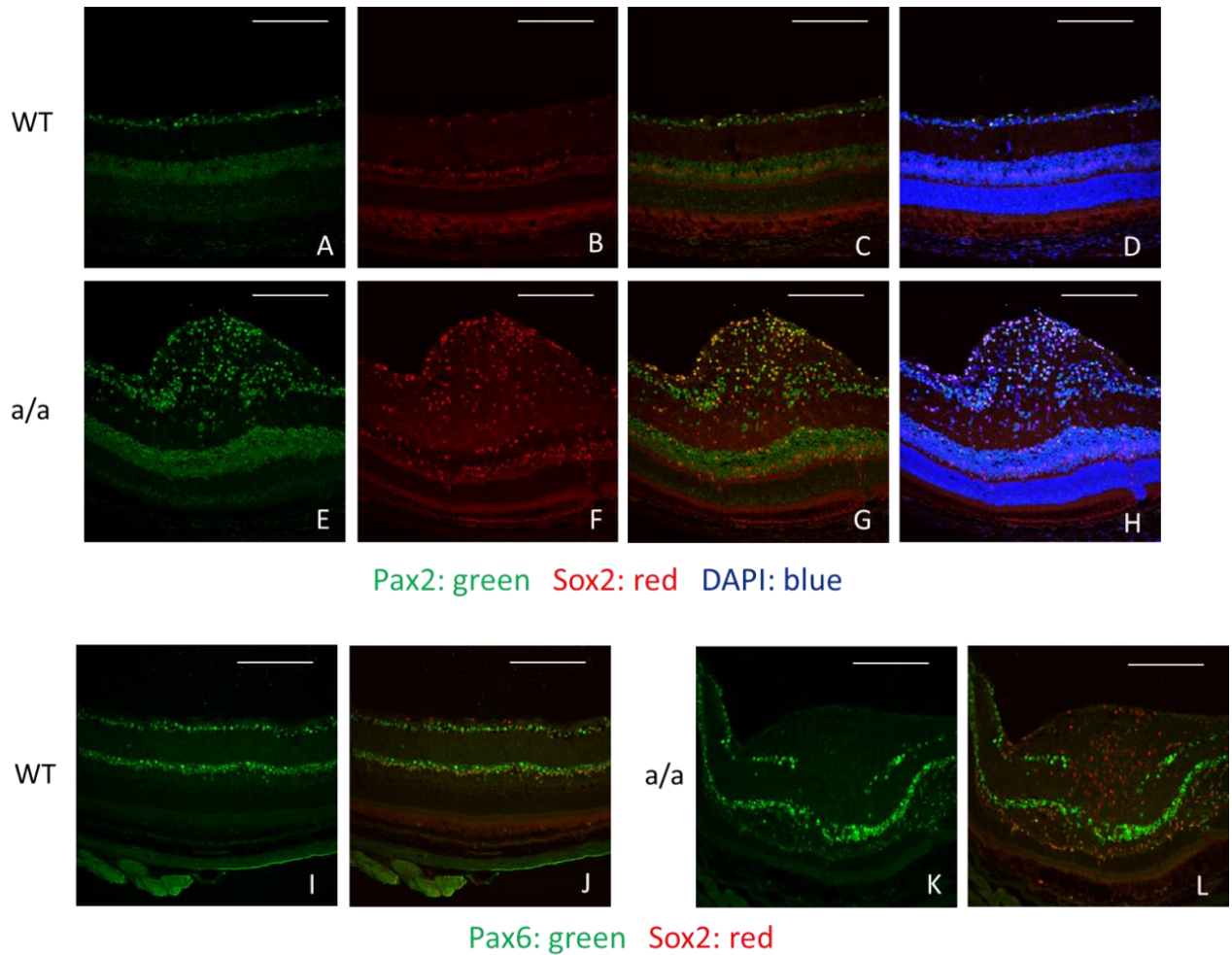


Figure 5.35 Increased numbers of activated glia cells co-expressing Pax2 and Sox2, but not pax6 in the ventral gliosis retina in *Ali030* mutants at 3 months. (A-D) In wild types, Pax2 is mainly expressed in the retinal ganglion cell layer and weakly expressed in inner nuclear layer, and there are a few Sox2-positive retinal ganglion cells highly-expressing Pax2 in the RGC layer. (I-J) Pax6 is normally expressed in the retinal ganglion cell layer and inner nuclear layer and some cells can be co-expressed with Sox2 in the outer region of inner nuclear layer in wild types. (E-H) However, in mutants, there are an increased number of cells expressing Pax2 in the inner plexiform layer, ganglion cell layer and epiretinal membrane. In the epiretinal membrane there are a number of cells co-expressing Pax2 and Sox2, especially in the most inner layer of the epiretinal membrane, nearly all the cells co-express Pax2 and Sox2. (K-L) There are some disruption in the inner nuclear revealed by Pax6 immunostaining in mutants. Some Pax6-positive retinal ganglion cells are missing and form a discontinuous and disrupted RGC layer and all the cells in the epiretinal membrane don't express Pax6 in mutants. Scale bar: 50 μ m.

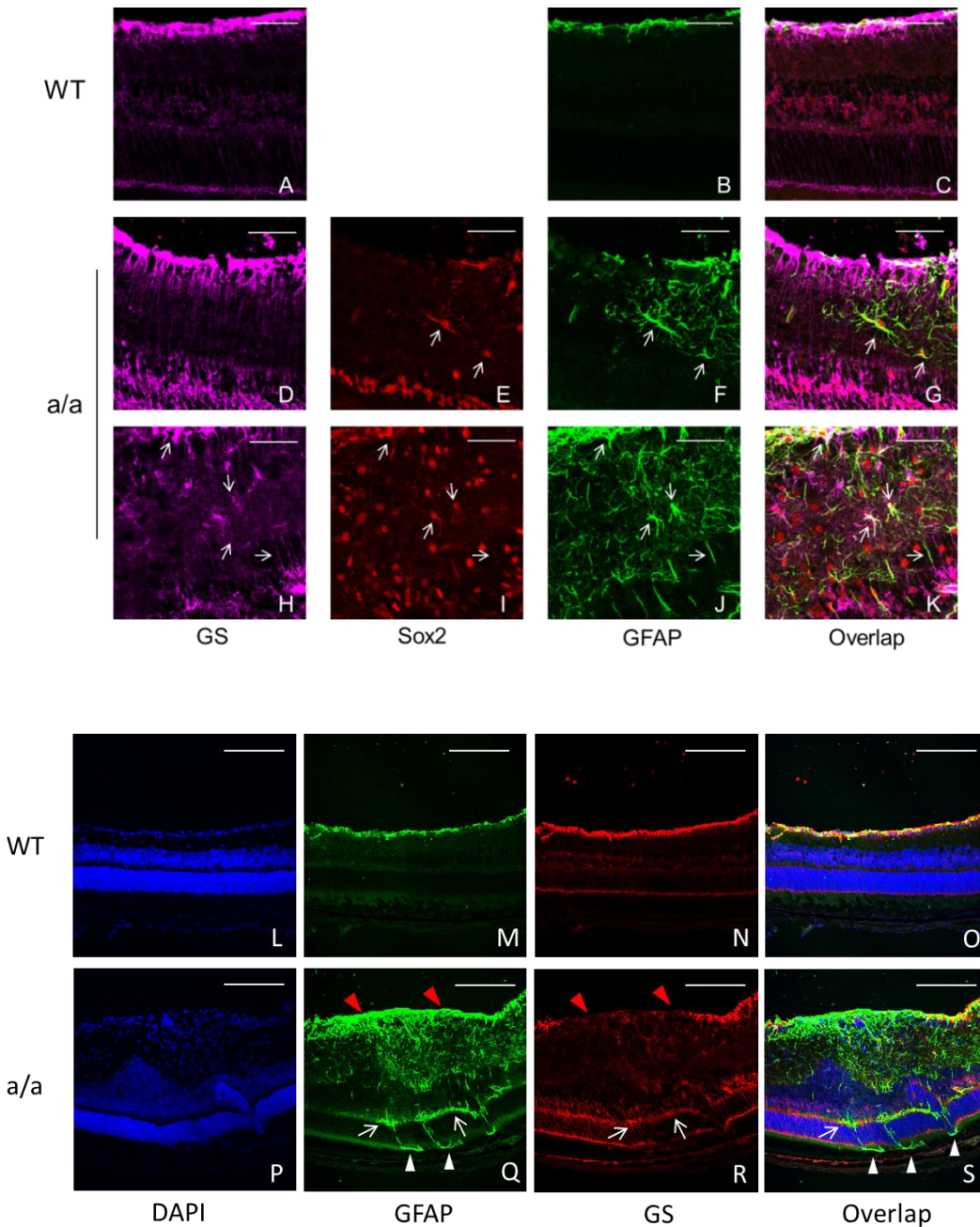


Figure 5.36 Mixed types of activated glial cells in the ventral gliosis retina in *Ali030* mutants. (A-C) Glutamate synthase (GS), a marker for retinal Müller cells, is expressed in the nerve fiber and retinal ganglion cell layer. (D-G) In mutants, some activated glial cells do not co-express GS in the inner plexiform layer indicating that they are activated astrocytes although retinal Müller cells are activated and they can express Sox2 in the nuclear layer. (H-K) But there are still some activated glial cells co-express GS in the inner plexiform layer, but they do not seem to be retinal Müller cells because of the smaller size and different morphology of these cells. (L-S) Double immunostaining of GS and GFAP was used to test whether activated glial cells are retinal Müller cells in ventral gliosis retina in mutants. In the inner plexiform layer and epiretinal membrane the main cells are activated astrocytes (Q-S, red arrowheads) and also some retinal Müller cells are activated in the outer plexiform layer due to up-regulated expression of GFAP (Q-S, arrow). There are still a few activated glial cells, which do not express GS (Q-S, white arrowheads). Scale bar: A-K, 20 μ m; L-S, 50 μ m.

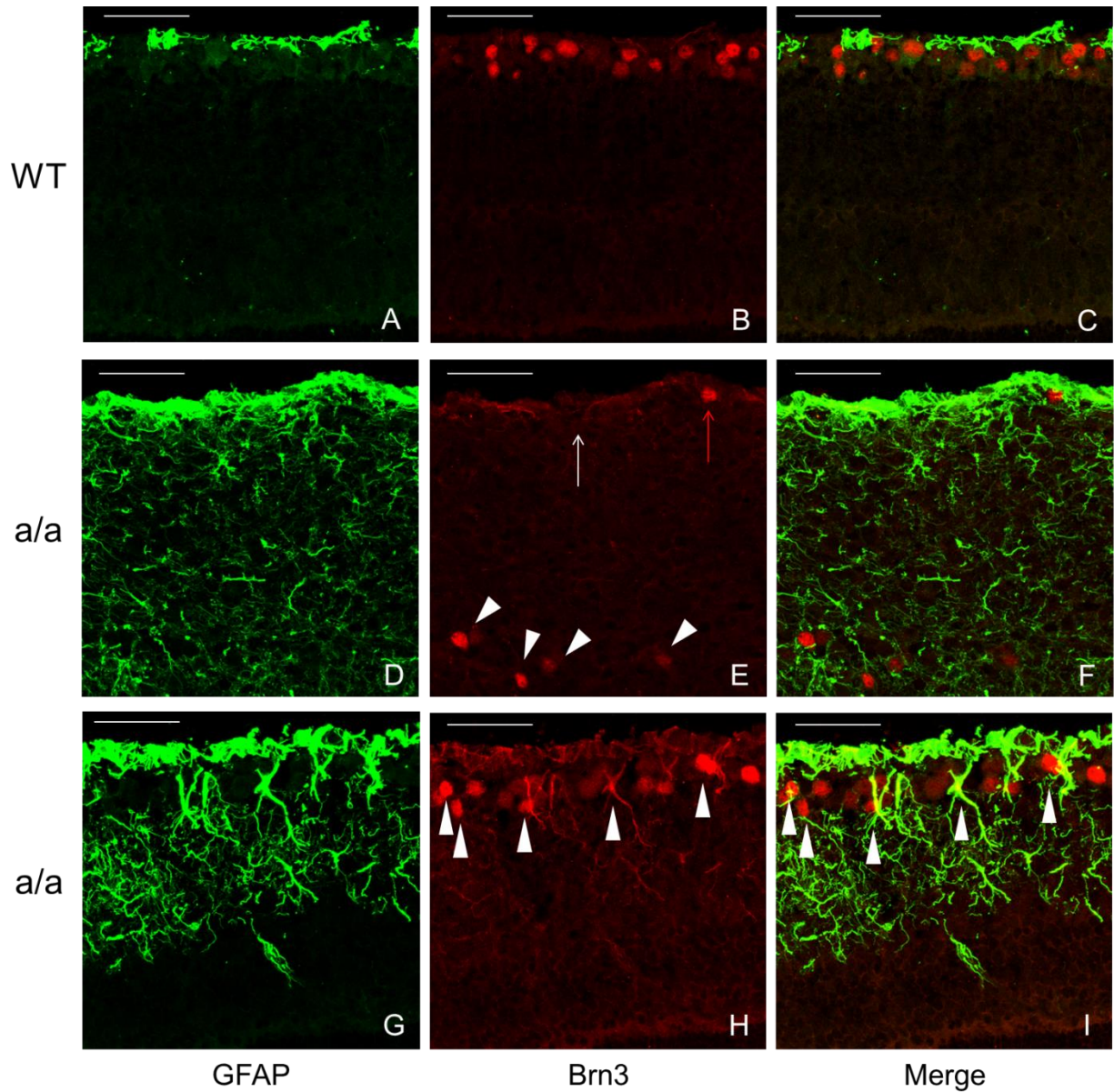


Figure 5.37 Retinal ganglion cells could acquire the fate of glial cells in *Ali030* mutants at P21. (A-C) In wild types, Brn3 is expressed in the retinal ganglion cell layer and GFAP is expressed in the nerve fiber layer and retinal ganglion cell layer; (D-E) In the central part of the ventral retinal gliosis in mutants, only a few Brn3-positive cells are detected in the retinal ganglion cell layer (E, red arrow) but there are a number of activated astrocytes in the retinal ganglion cell layer (E, white arrow) and inner plexiform layer instead. There are some ectopical Brn3-positive retinal ganglion cells in the inner plexiform layer (E, white arrowhead). (G-I) In the peripheral region of the ventral retinal gliosis in mutants, there are still some Brn3-positive retinal ganglion cells and some of them showed up-regulation of GFAP (G-I, white arrowhead). In the negative controls, fluorescence was absent on the retina. Scale bar: 100 μ m.

5.2.8 Mis-splicing of *Bmpr1b* may not play a role in the activation of retinal Müller cells *in vitro*

MIO-MI cells, a retinal Müller cell line derived from postmortem adult human neural retina, retains the characteristics of primary retinal Müller cells in culture (Limb et al., 2002) and exhibited the characteristics of neural stem cells (Lawrence et al., 2007). In the mouse study, I found that only a few retinal Müller cells are activated in the ventral retina. Therefore, I further investigated whether *Bmpr1b* plays a direct role in the activation of retinal Müller cells using this cell line *in vitro*. Without any treatments, very few MIO-MI cells express GFAP (Figure 5.38, A), which is consistent with another study showing that occasional MIO-MI cells express GFAP (Limb et al., 2002). Interestingly, I found that the MIO-MI cells exhibited strongly enhanced expression of GFAP under the stimulation of GDF-5 (100 ng/ml and 500 ng/ml) (5.38, B-C) and BMP-2 (500 ng/ml) (5.38, D) for 4 days. These indicate that GDF-5 and BMP2 may promote the activation of retinal Müller cells. After overexpression of *Bmpr1b* cDNA (wildtype and mutant, respectively), a few MIO-MI cells showed up-regulated expression of GFAP (5.38, E-F). However, these transfected MIO-MI cells were treated with BMP-2 for 4 days, there is still strongly up-regulated expression of GFAP in the cells, but there is no obvious difference between *Bmpr1b* wild-type cells and mutant cells (5.38, G-H). This data suggests that BMP-2 can activate retinal Müller cell line but may not signal through *Bmpr1b*. In contrast, a treatment of the transfected cells with GDF-5 (500 ng/ml; 1500 ng/ml) for 4 days, fewer cells express GFAP compared to BMP-2 treatment group, and no obvious differences in GFAP expression were found between those cells overexpressing *Bmpr1b* wild-type cDNA and the cells overexpressing mutant cDNA (5.38, I-L). From my mouse study, only a few of activated retinal Müller cells were detected compared to a high number of activated astrocytes in ventral retina in *Bmpr1b*-mutant mice. Together, I found that two proteins, GDF-5 and BMP-2, induces the activation of MIO-MI cells, and BMP-2 functions independently of *Bmpr1b*. Overexpression of *Bmpr1b* may play a role in the inhibition of MIO-MI cells activation, and it seems that the mis-splicing of *Bmpr1b* does not affect this process.

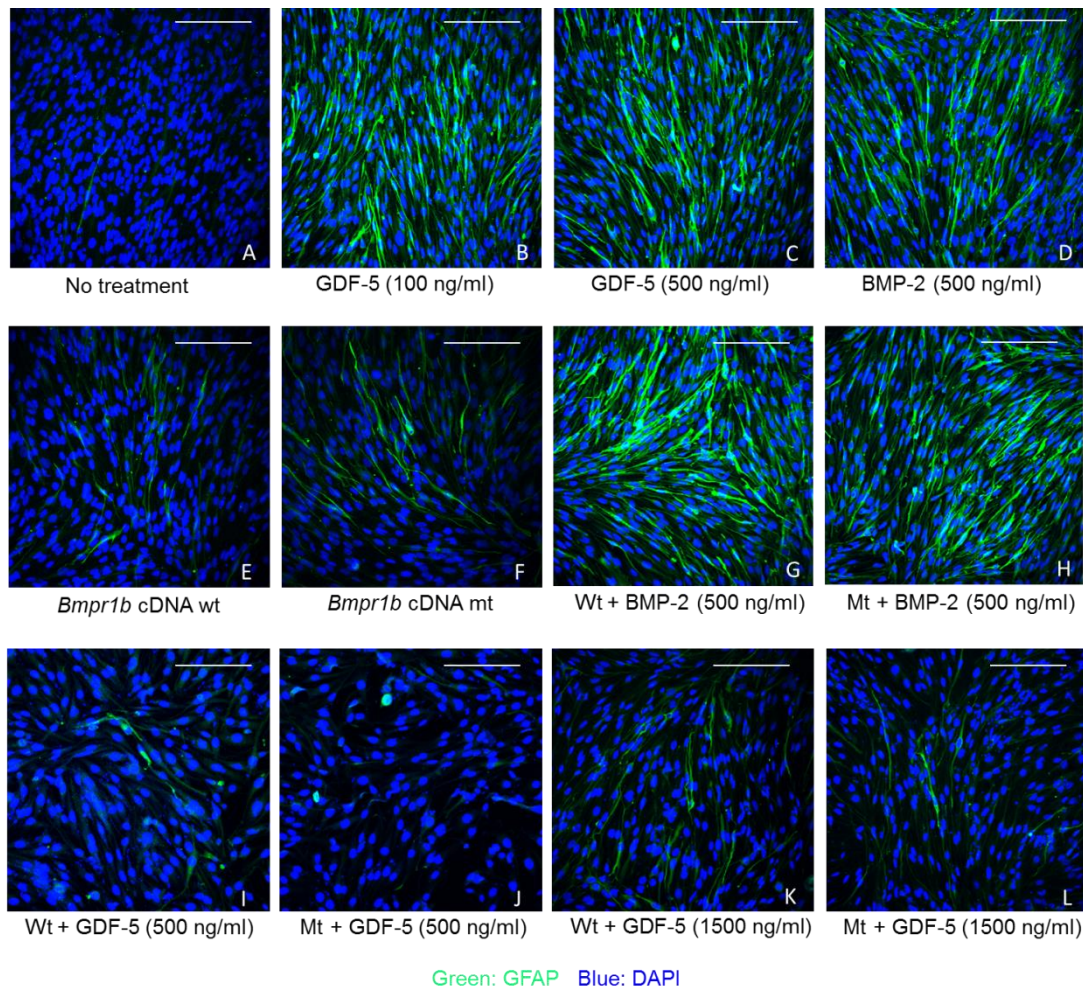


Figure 5.38 Mis-splicing of *Bmpr1b* may not play a role in the activation of retinal Müller cells *in vitro*. (A-D) (A) Occasional MIO-MI cells express GFAP without any treatments. (B-D) Up-regulated expression of GFAP was found in MIO-MI cells when they are treated by GDF-5 (100 ng/ml and 500 ng/ml) and BMP-2 (500 ng/ml) for 96 hours, suggesting that GDF-5 and BMP-2 may promote MIO-MI cells to become activated glial cells. (E-F) There are a few cells expressing GFAP when transfected with *Bmpr1b* wild-type and mutant cDNA, respectively. (G-L) The cells transfected with *Bmpr1b* wild-type (G, I, K) and mutant cDNA (H, J, L) were treated with BMP-2 (500 ng/ml, G, H) or GDF-5 (500 ng/ml, I, J; 1500 ng/ml, K, L). GFAP is still strongly up-regulated in those transfected cells with BMP-2 (G-H), whereas a few cells treated with GDF-5 showed up-regulated expression of GFAP (I-L). Scale bar: 50 μ m.

5.2.9 A delayed retinal development, ectopic expression of Pax2 and congenital ventral retina gliosis in *Ali030* mutants during eye development

As retinal gliosis was found in early postnatal retinal development, the question is that when and how the retinal gliosis happened in mutants. Therefore, I firstly performed ocular histology to see whether there are retinal phenotypes in mutants during embryonic stages. At E10.5, it appears that no obvious difference between mutants and the wild-type controls regarding the eye pattern was

found, but it seems that eye size is bigger in wild types compared to mutants (Figure 5.39). Interestingly, I found that optic fissure fails to close in some mutants (3/10 eyes), but not in all the cases at E17.5 (Figure 5.39). However, the optic fissures are closed at P5, P11, P21 and adult. These results indicate that this is the delayed closure of the optic fissure. Therefore, ventral retina development may be delayed in *Ali030* mutants compared to the wild-type controls.

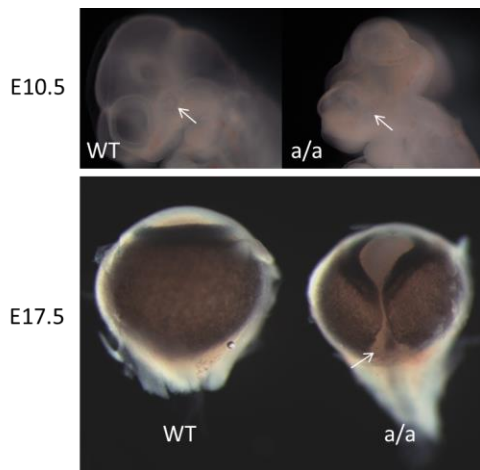


Figure 5.39 Delayed closure of optic fissure at E17.5 in *Ali030* mutants. At E10.5, a clear eye-forming region was formed in the wild types, but in mutants it appears that this eye-forming region is not affected. At E17.5, the optic fissure in the ventral retina is completely closed in wild types, whereas there is a failure in closing the optic fissure in some mutants (3/10 eyes) (arrow).

In consistency with this finding, the expression of Pax2, a transcription factor essential for optic nerve head development and the closure of optic fissure, is also changed in *Ali030* mutants. Pax2 is expressed in the optic stalk and ventral retina in early retinal development and then reduced to be limited to a junction between optic nerve and retina during late retinal development (Figure 5.40, A-F). The expression pattern of Pax2 is dynamically changed in mutants in embryonic retinal development (Figure 5.40, G-L). At E10.5, Pax2 is expressed in the ventral retina and optic stalk in wild types, and the expression of Pax2 is not affected in mutants compared to wild types (Figure 5.40, A-B, G-H). At E15.5, Pax2 is over-expressed in the ventral retina and the expression of the optic nerve head including dorsal junction is reduced in mutants, whereas it is only expressed in the retina-optic nerve junction in wild types (Figure 5.40, C-D, I-J). In addition, Brn3 immunostaining showed that the neurogenesis of retinal ganglion cells is decreased (Figure 5.41, A-C) in mutants at E15.5. Anterograde tracing showed that there are no obvious differences in the crossing and fasciculation of the optic nerve and optic chiasm between wild types, heterozygous and homozygous mutants (5.41, D-F). However, the optic nerve tends to be thinner in mutants () compared to the wild-type controls () at E15.5 ($p=0.0524$) (Figure 5.41, D-F). At E17.5, the expression of Pax2 is still reduced in retinal-optic nerve junction but ectopically expressed in retinal pigment epithelium at the dorsal retina, whereas Pax2 begin to disappear compared to E15.5,

but still up-regulated expression in mutants compared to wild types in the ventral retina (Figure 5.40, E-F, K-L). These results demonstrated that loss of function of *Bmpr1b* affects the closure of optic fissure and expression of Pax2 during embryonic retinal development.

At E17.5, GFAP is strongly expressed in the optic nerve (Figure 5.42, A-B) and weakly expressed in the nerve fiber layer and inner plexiform layer (Figure 5.42, E-F) in wild types, whereas in mutants, the retinal folding are formed and GFAP is strongly expressed in different retinal layers in the retinal folding area (Figure 5.42, G-H). In the optic nerve, retinal folds are also found and interestingly GFAP is ectopically expressed in the RPE layer in mutants (Figure 5.33, C-D) compared to wild types (Figure 5.33, A-B), suggesting that the glial cells is ectopically activated in the optic nerve head during development. These results demonstrated that ventral retinal gliosis and ectopical glial cells in the optic nerve head are congenital in *Ali030* mutants.

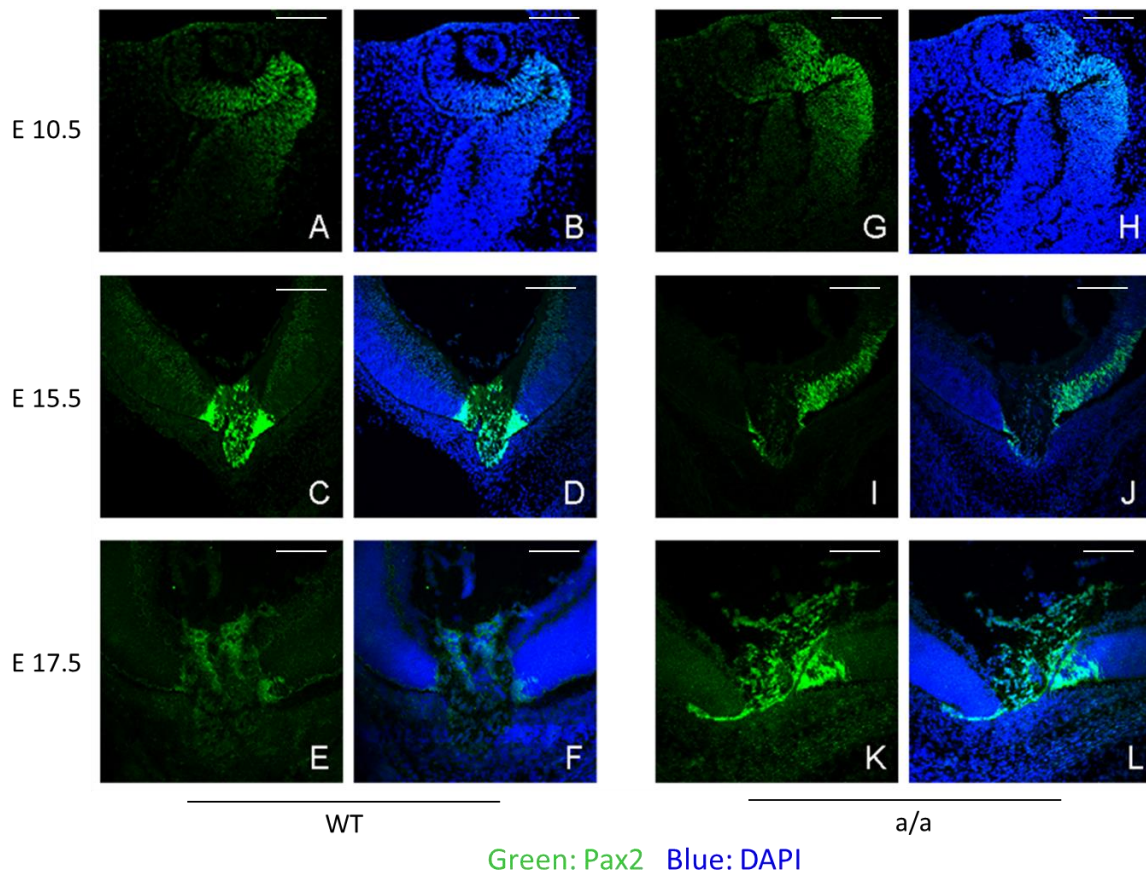


Figure 5.40 Ectopic expression of Pax2 during eye development in *Ali030* mutants. (A-F) At E10.5, Pax2 is mainly expressed in the ventral retina and in the optic stalk in wild-type embryos (A, B). At later stages, such as E15.5 and E17.5, Pax2 is limited to be expressed in optic nerve-retina junction and some cells in the optic nerve

head (C, D, E, F). (G-L) In mutants, at E10.5, Pax2 is mainly expressed at ventral retina, which seems similar expression to the wild-type controls (G, H). However, Pax2 is ectopically up-regulated expression in ventral retina and decreased expression in the dorsal junction between optic nerve and retina in mutants at E15.5 (I, J). At E17.5, Pax2 is also ectopically up-regulated expression in ventral retina but begin to disappear compared to E15.5 in mutants, and in the dorsal retina Pax2 is decreased to be expressed in RPE layer like a line structure mutants. Scale bar: 50 μ m.

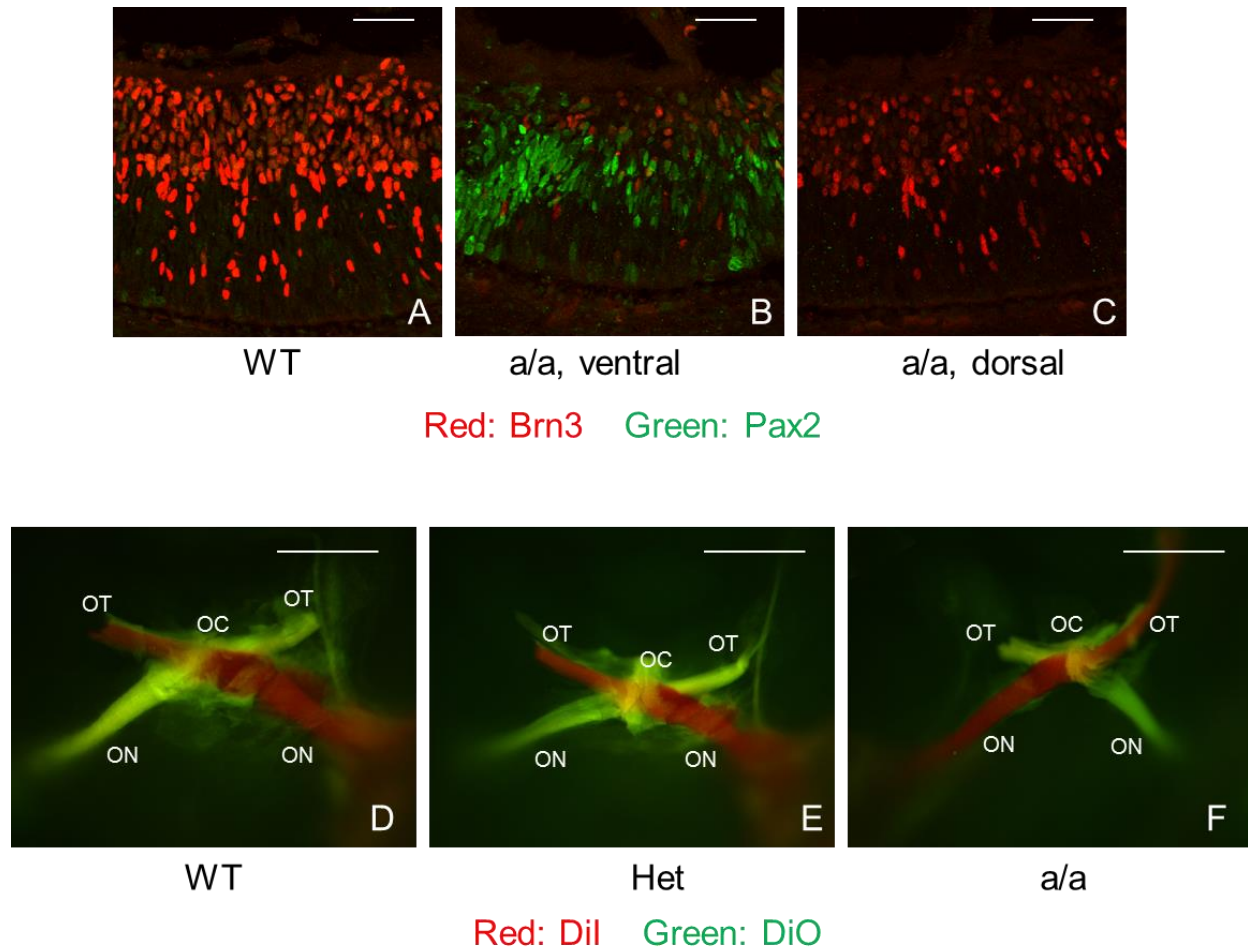


Figure 5.41 Decreased neurogenesis of retinal ganglion cells and thinner optic nerve in *Ali030* mutant at E15.5. (A-C) In wild-type retina, there is a number of retinal ganglion cells and very few cells express Pax2 (A), whereas in mutant retina there is still a number of cells expressing Pax2 in ventral retina and the retinal ganglion cells production is decreased in ventral retina during retinal neurogenesis at E15.5 (B, C). (D-F) Decreased number of retinal ganglion cells leads to decreased optic nerve thickness at E15.5. Anterograde tracing demonstrated normal crossing and fasciculation of the optic nerve and optic chiasm between wild types, heterozygous and homozygous mutants, but there is a trend that the optic nerve is thinner in homozygous mutants than that in the wild-type controls ($p=0.0524$), which is due to decreased number of retinal ganglion cells during retinal neurogenesis at E15.5 (D, F). OC: optic chiasm; ON: optic nerve; OT: optic tract. Scale bar: A-C, 20 μ m; D-F, 100 μ m.

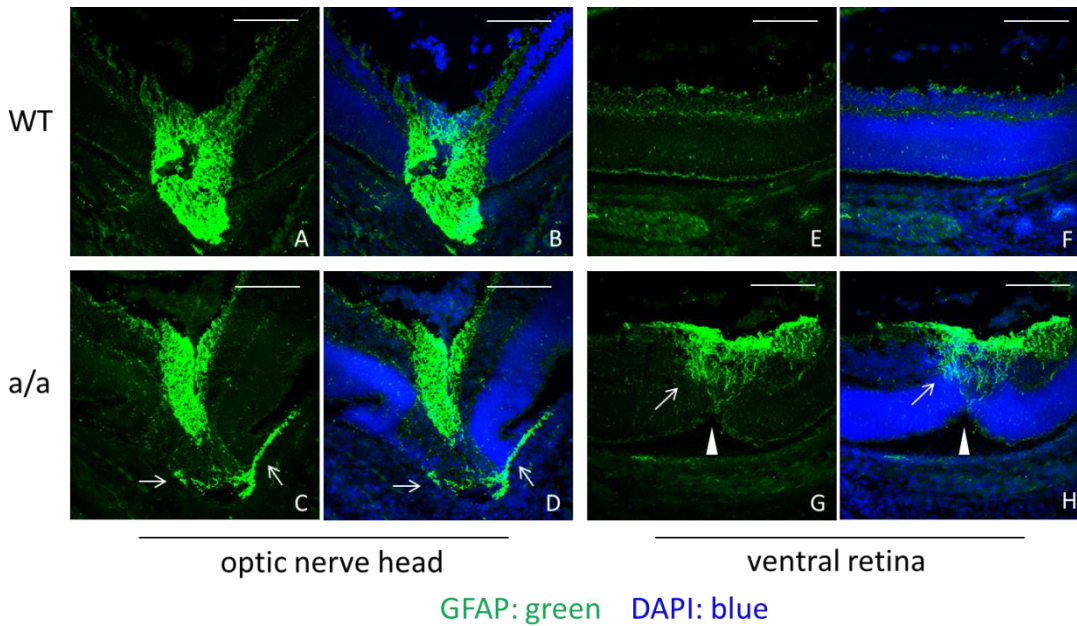


Figure 5.42 Congenital ventral retinal gliosis and ectopic expression of GFAP in the optic nerve head of the *Ali030* mutants at E17.5. (A-D) Strong GFAP is expressed in the optic nerve at E17.5 in wild types (A-B), whereas in mutants the GFAP is ectopically expressed in the RPE layer except the optic nerve (C-D). (E-H) GFAP is weakly expressed in the nerve fiber layer and inner plexiform layer of the wild-type retina at E17.5, whereas it strongly ectopically expressed in the retinal folding area in ventral retina (G-H). Scale bar: 50 μ m.

5.2.10 Glial-like cells expressing Sox2, Pax2 and Nestin are found in the epiretinal membranes and in the inner limiting membranes in patients with retinal gliosis

In the mouse study, I found that the progenitor cell markers Sox2 and Nestin are co-expressed in the activated glial cells of the ventral gliosis retina in mutants. In another study, in the injury-induced mouse brain gliosis, the astrocytes are activated and can be proliferative, which have the multiple-potent properties for self-renewal *in vitro* (Buffo et al., 2008). Then I put forward a hypothesis that these glial cells in retinal gliosis may have stem cell properties in order to maintain self-renewal and produce more glial cells. Therefore, I extend our mouse study to the analysis of clinical retinal gliosis samples to see whether similar cells expressing stem cell markers can be found. Firstly, I tested whether Sox2 and Nestin are also expressed in the glial cells in the epiretinal membrane (ERM) and inner limiting membrane (ILM) in the two different types of retinal gliosis samples, one is idiopathic retinal gliosis without other disease causes, and the other one is the retinal gliosis caused by specific reasons, such as diabetes, proliferative vitreous-retina diseases (PVR) and uveitis (an inflammation of uveal tract in the eye). Here, I referred to the latter with

specific reasons as secondary retinal gliosis. All the clinical samples were kindly provided by Dr. Petrovski and Dr. Lumi (Ljubljana, Slovenia). In general, the cell density in ERMs is much higher than those in ILMs, and correspondingly GFAP is highly expressed in ERMs (Figure 5.43; Figure 5.44; Figure 5.45), suggesting that these cells are activated glial cells. GFAP is also highly expressed in some cells or even more from ILMs, but in a limited number (Figure 5.44; Figure 5.47). Interestingly, the activated glial cells with long processes are both found in ILMs and ERMs and they seem to form a local network by their processes, and some cells form a multi-branch structure or form an aggregate in ERMs or ILMs (Figure 5.43-5.47). The glial cells expressing stem cell markers Sox2 and Nestin were found in all clinical samples (14 ERMs and 15 ILMs) (Figure 5.43-5.47). These cells in ERMs and ILMs also express Pax2 (Figure 5.48). These results suggest that activated glial cells are the dominant cells in ERMs and some cells or even more in ILMs seem to be GFAP-positive glial cells. Furthermore, some of these activated glial cells are not pure glial cells but glial-like cells due to the co-expression of progenitor cell markers Sox2, Pax2 and Nestin. These glial-like cells may have the properties of stem cells and they can keep them self-renewal and differentiate into more glial cells in the retina. Whether these glial-like cells initiate and produce a number of activated glial cells in ERMs remains to be investigated.

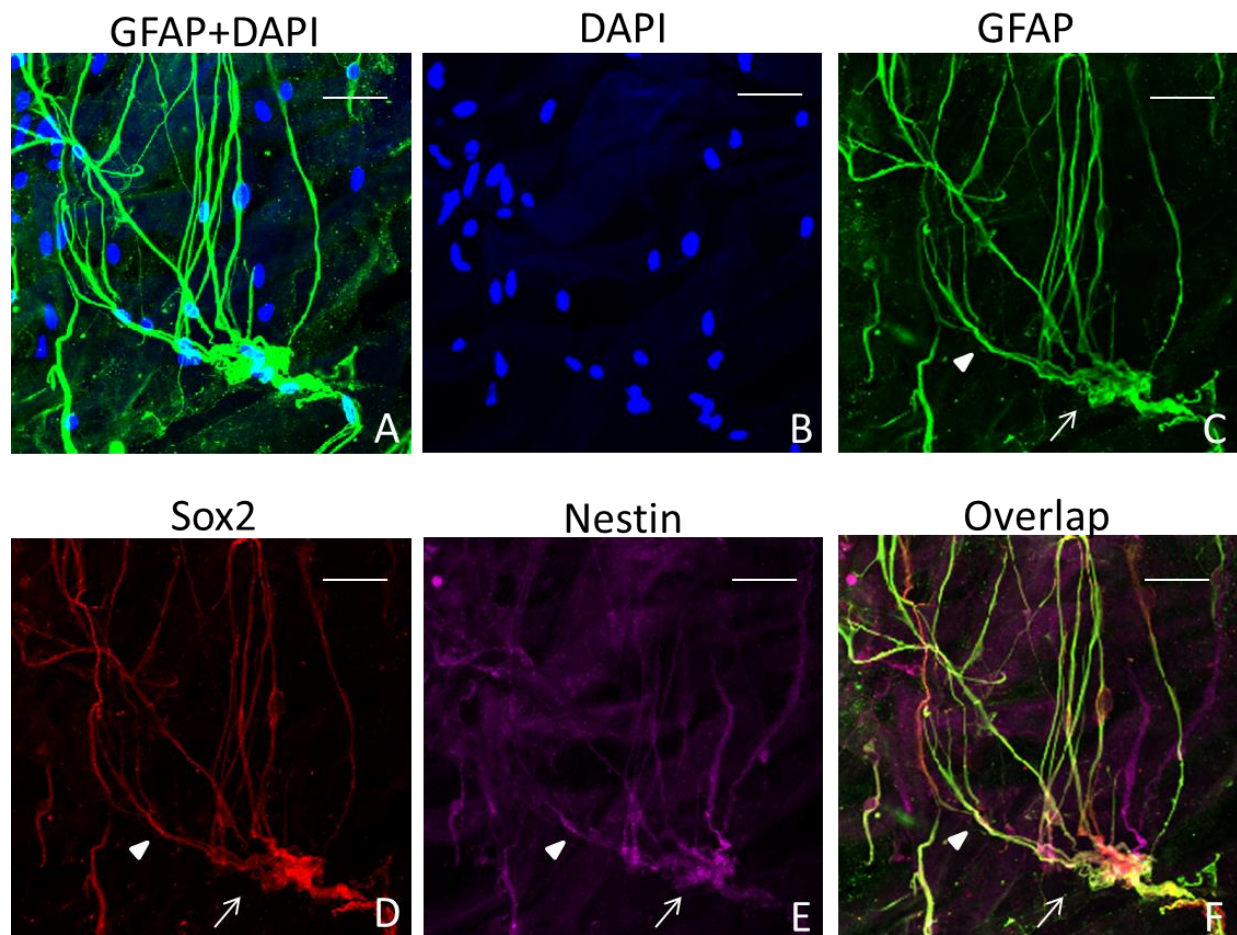


Figure 5.43 The glial-like cells in the epiretinal membranes from patients with idiopathic retinal gliosis. (A-C) There are a number of activated glial cells with long axons from cell bodies and they seem to form a local network in the epiretinal membranes from patients with idiopathic retinal gliosis. (C-F) These activated glial cells co-express stem cell markers Sox2 and Nestin (arrow and arrowhead). In these cells, there are some axons co-express Sox2, but not nestin and some processes only express nestin, but not sox2 and GFAP. Scale bar: 20 μ m.

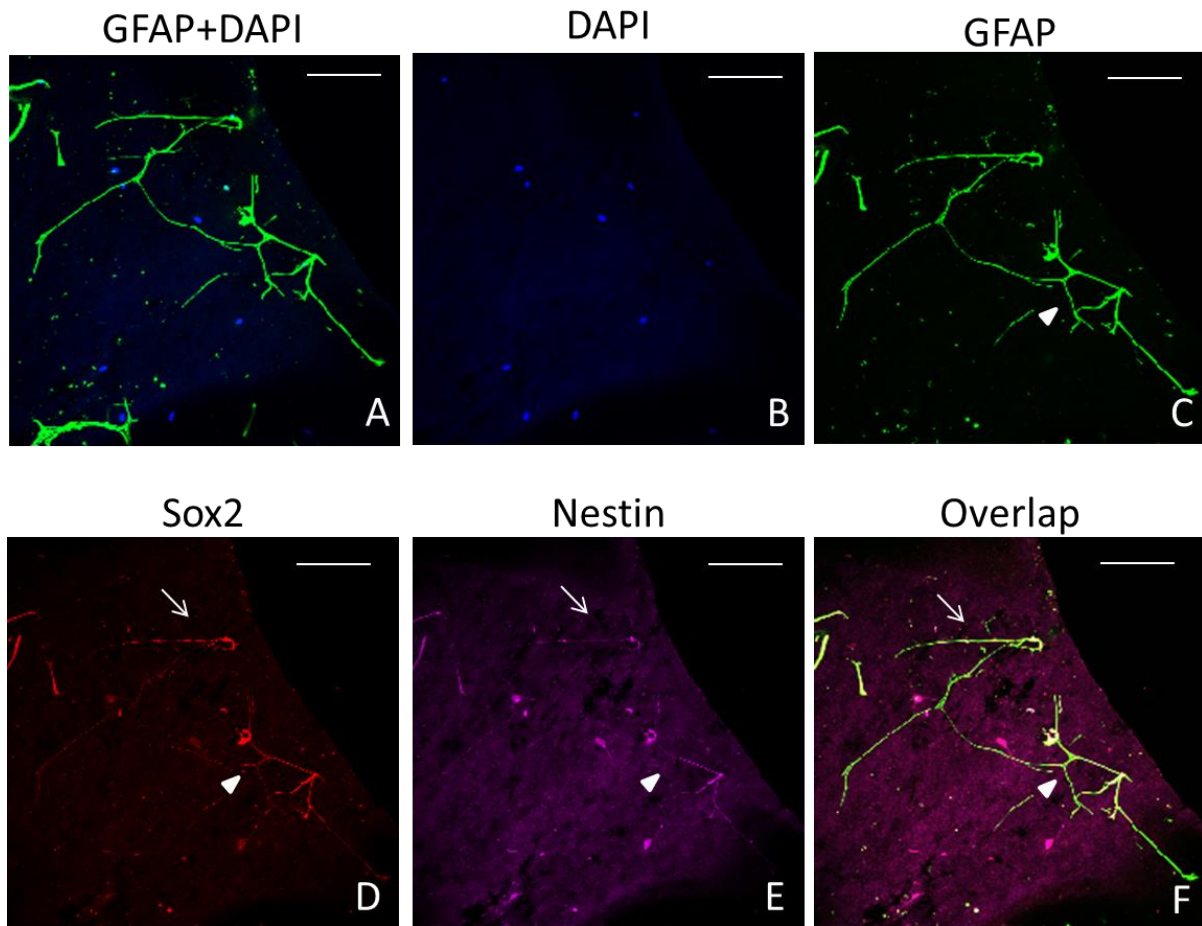


Figure 5.44 The glial-like cells in the inner limiting membrane from patients with idiopathic retinal gliosis. In most cases, there are much less cells in the inner limiting membrane compared to the epiretinal membrane and correspondingly there are much fewer glial cells in the ILMs. These glial cells have long axons and exhibit multi-branch structure. It appears that these cells interact with each other by their processes. These glial cells also co-express stem cell markers Sox2 and Nestin. In very few cases, the ILM have the cells as many as ERMs, and these cells exhibit strong expression of GFAP, especially the area near macula. Scale bar: 50 μ m.

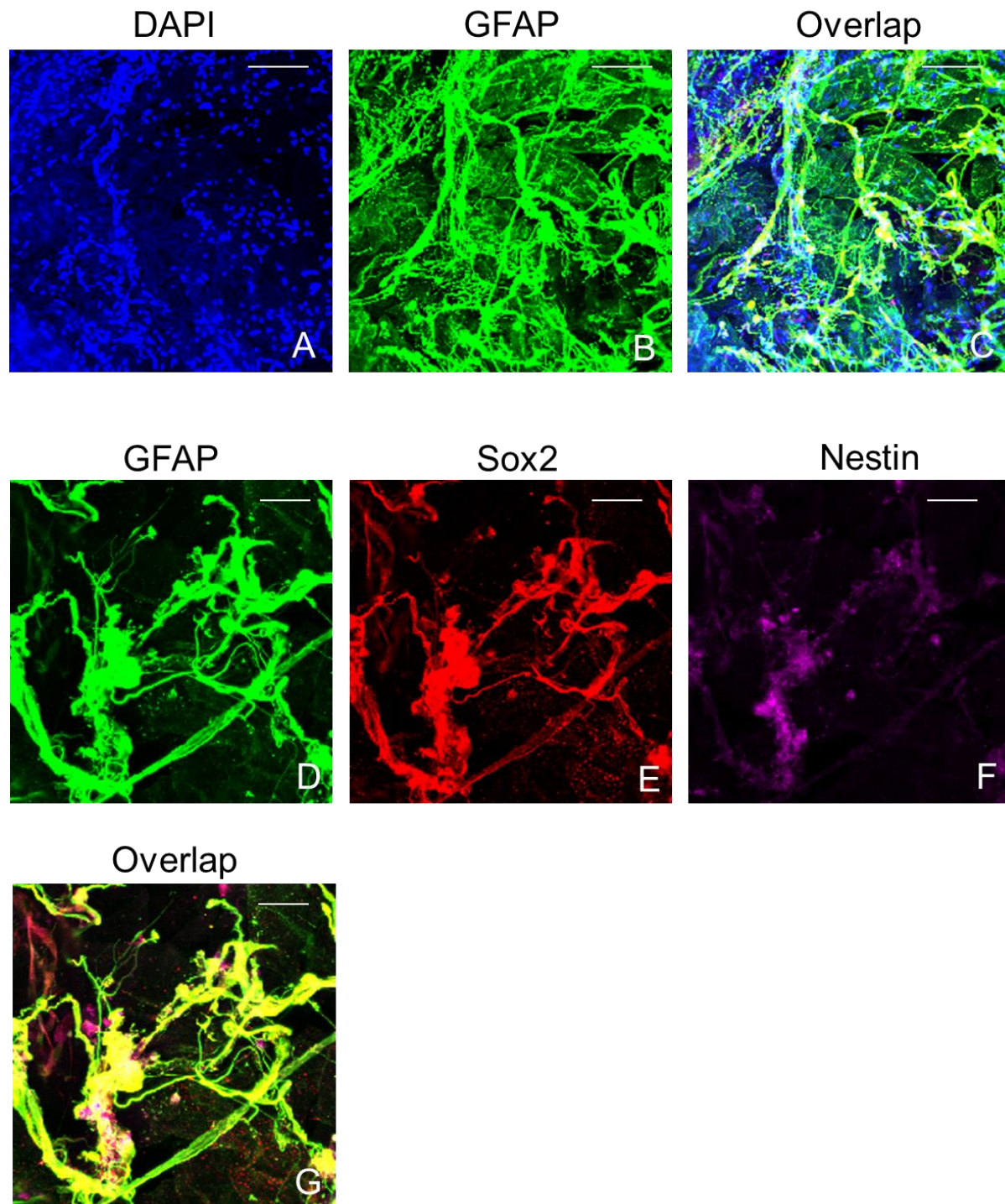


Figure 5.45 The glial-like cells in the epiretinal membranes from patients with secondary retinal gliosis. (A-C) There are a number of cells in the epiretinal membranes and GFAP is highly expressed in these cells. These activated glial cells also have long processes. (D-G) These activated glial cells also co-express Sox2 and Nestin (E-G). Scale bar: A-C, 50 μ m; D-G, 20 μ m.

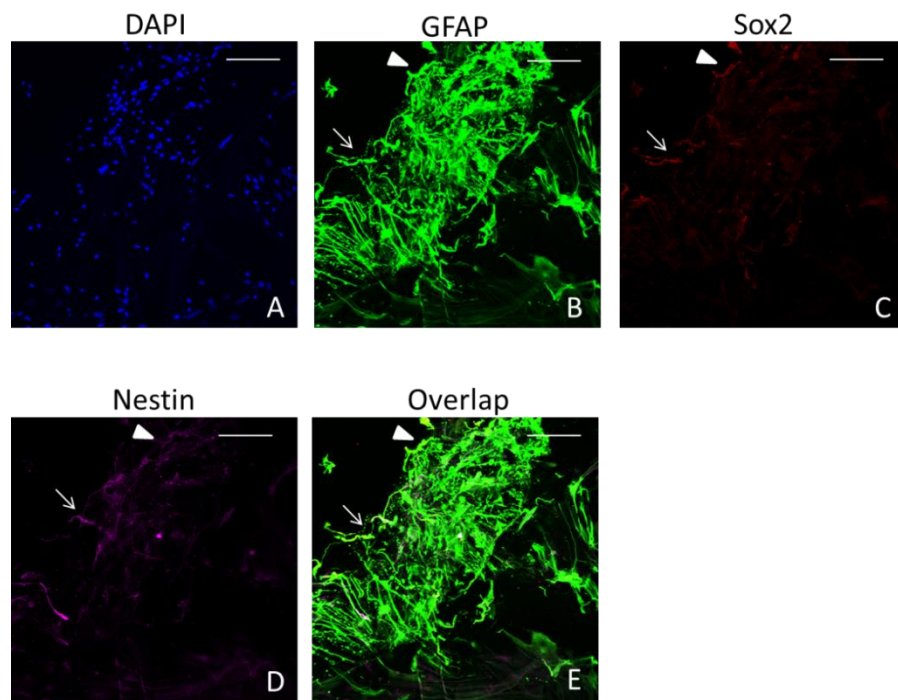


Figure 5.46 The glial-like cells in the epiretinal membrane from a patient with VMT. (A-E) There are a number of activated glial cells in the epiretinal membranes (B), in which a few cells co-express with stem cell markers Sox2 and Nestin (B-E, arrow) and most cells are the activated glial cells which do not express Sox2 and Nestin (B-E). Scale bar: 20 μ m.

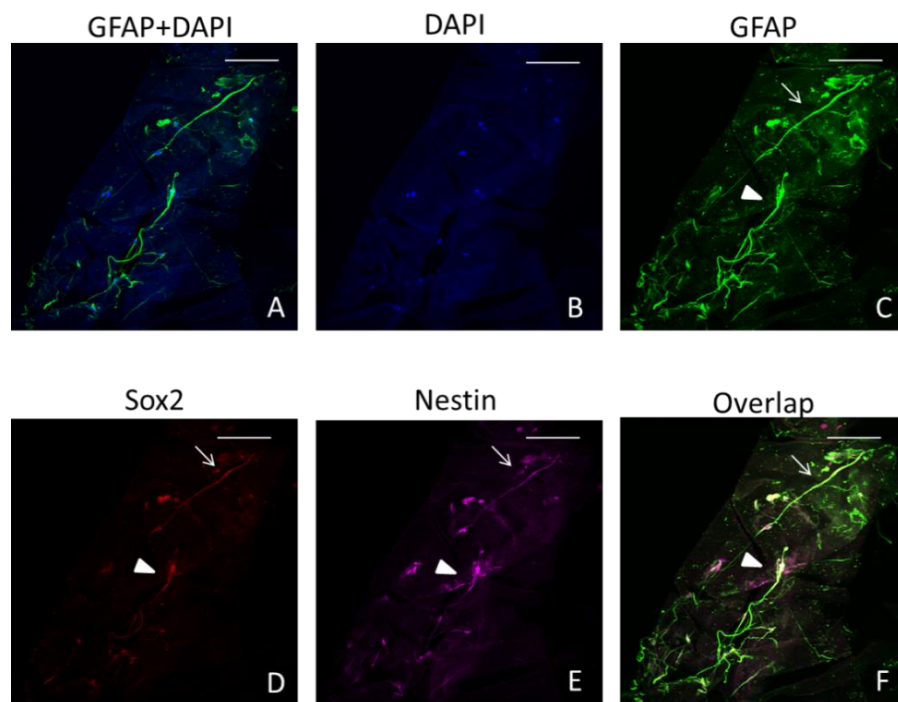


Figure 5.47 The glial-like cells in the inner limiting membrane from a patient with VMT. (A-F) There are a few activated glial cells on the ILMs and the cells have long processes which co-express with stem cell markers Sox2 and Nestin. Scale bar: 20 μ m.

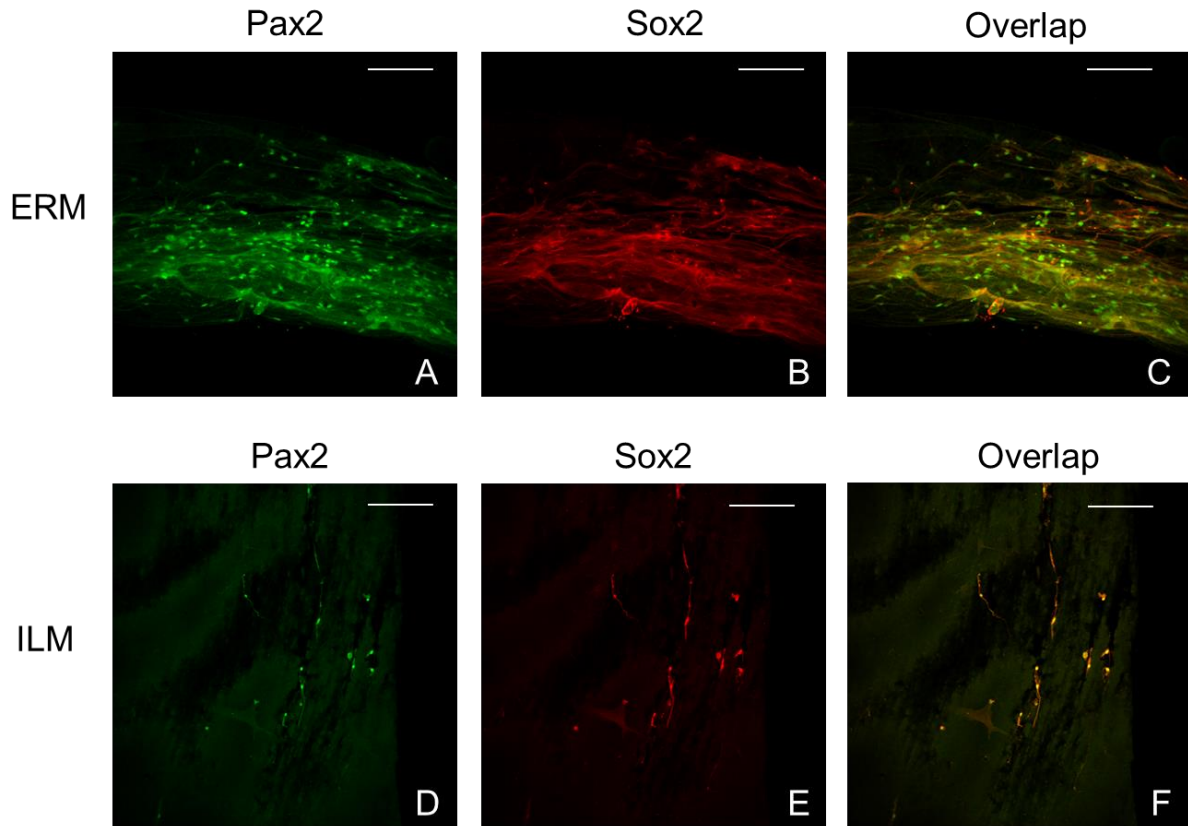


Figure 5.48 The glial-like cells co-express Pax2 and Sox2 in ERMs and ILMs. (A-C) In ERMs, there are a number of Pax2-positive cells and some of them co-express with Sox2. (D-F) There are fewer cells in ILMs than in ERMs, and they also express Pax2 and Sox2. Scale bar: 50 μ m.

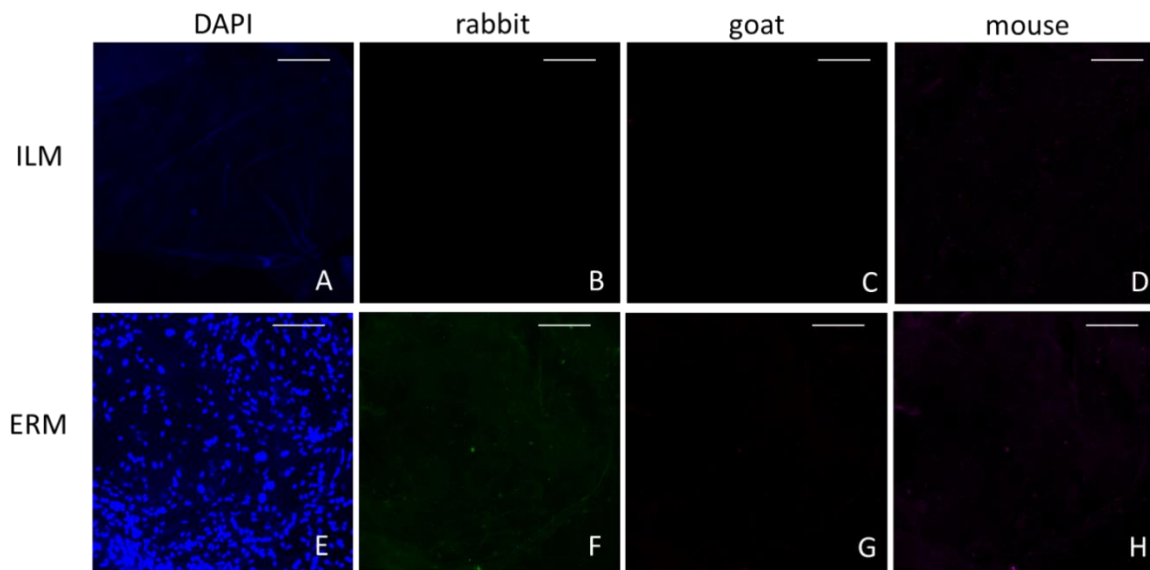


Figure 5.49 Negative control of the epiretinal and inner limiting membrane. (A-H) Staining for these ERMs and ILMs using secondary antibodies (anti-rabbit, anti-goat, anti-mouse) without primary antibody. The cells in ERMs and ILMs are not stained with secondary antibodies. Scale bar: 50 μ m.

6 Discussion

6.1 *Peroxidasin* is essential for eye development

The purpose of this study was to characterize the first rodent model suffering from a mutation within the *peroxidasin* gene. The main findings in this study is that the mutation within *peroxidasin* results in abnormal proliferation and differentiation of the lens, leading to anterior segment dysgenesis and microphthalmia, and this process could be mediated by up-regulation of *Pax6* and *Tgf- β 1*, two conserved and key genes for eye development. In addition, peroxidasin is involved in the consolidation of basement membrane (lens capsule) in the eyes and the deficiency in peroxidasin causes a rupture in the lens capsule together with lens epithelium, resulting in abnormal lens fibers extruding into the anterior and posterior chamber from the lens, which is another factor affecting anterior segment development and inflammation. Moreover, the mutant eyes at E15.5 and in the early postnatal period showed a condition of inflammation. Based on the data obtained from this study, we propose a series of events initiated by deficiency of peroxidasin.

In *KTA48* mutants (ENU-induced *peroxidasin* mutant mice), a nonsense mutation in the peroxidase domain within *peroxidasin* was identified, and it is predicted to form a premature stop codon within the peroxidase domain causing a loss of function including peroxidase enzyme activity. The microarray data showed that the expression of peroxidasin is reduced in mutant eyes (2.21 times) compared to the wild-type eyes at E12.5 (From Dr. Marion Horsch, Institute of Experimental Genetics, Helmholtz Center Munich). Moreover, western blot showed that peroxidasin is not expressed in E15.5 mutant eyes compared to wild types. These results suggest that loss of function of peroxidasin occurs in *KTA48* mutants. Our mutant mice display an autosomal recessive pattern of inheritance with complete penetrance, which is also in accordance to the condition in human patients with ASD (Reis and Semina, 2011). Compared to the manifestation in the patients with *peroxidasin* mutations presenting congenital cataract, corneal opacity and developmental glaucoma (Khan et al., 2011), our *peroxidasin*-deficient mice exhibit very similar but more severe eye defects, including severe anterior segment dysgenesis and microphthalmia (particularly Peters' anomaly mainly due to corneal-lens adhesion and corneal opacity) and some mutant mice present retinal dysplasia including retinal rosette-like structures.

During embryonic eye development, the mutant mice exhibit obvious eye phenotypes, suggesting that peroxidasin plays an important role in eye development. Especially at E15.5, histology showed smaller eyes, corneal epithelial dysplasia, disorganized keratocytes and corneal stroma, smaller lenses with ruptures in the lens epithelium and in the capsule, disorganized lens fibers and abundant retrolental cells in the vitreous and anterior chamber angle in mutants; in some cases (nearly 50%) of the mutant embryos, persistent corneal-lens adhesion was found. These observations on pathological morphology provide a general pathogenesis process by which mutations in *peroxidasin* leads to delayed and abnormal eye development.

Interestingly, the ocular abnormalities of the mutant mice are little variable both within and between eyes, and most mutants exhibit broad corneal opacity with corneal-lens adhesion while a few mutants present central corneal opacity with or without congenital corneal-lens adhesion and even the severity of the lens ruptures. This is in accordance to the studies showing that specific gene mutations in human patients cause a range of anterior segment dysgenesis phenotypes including Peters anomaly, Axenfeld-Rieger anomaly and iridogoniodysgenesis (Gould and John, 2002). Also, in Khan's study the patients with the mutation in *PXDN* showed a different pattern of corneal opacity, including broad and central opacity (Khan et al., 2011). I detected the eye morphology of the mutant mice based on C3H and C57BL/6 background by histology and found that there is no obvious difference in these mice with different genetic background. These indicated that the variability of eye phenotypes may be dependent on the complexity in the function of peroxidasin during eye development as well as the complex molecular process of the anterior segment development but not on the genetic background. Moreover, the corneal phenotypes in *KTA48* mutants are similar to the histological findings from the cornea with Peters anomaly, including disrupted endothelial, immature cells with a fibroblastic configuration, higher cell density and abnormal extracellular matrix in the central cornea (Ohkawa et al., 2003).

Peroxidasin does not strongly affect early eye development, because *peroxidasin*-mutants do not exhibit gross morphological changes at E9.5-E12.5. At E13.5, the lens vesicle is filled by the lens fibers and the expression of γ -crystallin is not changed, suggesting that the primary lens differentiation is not affected at this stage. However, more retrolental cells in the vitreous were found in the mutant eyes, suggesting it may be involved in the aberrant development of the ocular

hyaloid vascular system during the early eye development. Later at E15.5, the anterior segment dysgenesis and smaller eye size are obvious and similar to the adult in mutants. The ocular mesenchymal cells in the anterior chamber angle form abnormal aggregate population. Anterior segment development depends on the interaction between mesenchymal cells and other eye tissues; abnormal development of mesenchymal cells could cause a failure of proper interaction resulting in anterior segment dysgenesis (Cvekl et al., 2004).

Considering smaller eye and lens size and abnormal anterior segment development in *peroxidasin*-mutant eyes during embryonic stages, I propose that the mutant eyes underwent abnormal proliferation and differentiation. *In-vivo* BrdU labeling demonstrated a decreased number of proliferating cells in the lens epithelium compared to the wild types at E14.5, E15.5 and E17.5. Correspondingly, *Foxe3*, a molecule which is necessary for lens cell proliferation (Medina-Martinez and Jamrich, 2007; Tholozan et al., 2007), is expressed at a lower level in the lens epithelium in the mutant eyes during eye development at E15.5, E17.5 and P11; it is also ectopically expressed in the posterior chamber and vitreous at P11. In addition, caspase-3 positive cells was not detected in the mutant embryonic eyes. Therefore, I conclude that smaller eye size is not mediated by apoptosis, but by a decreased cell proliferation during development. On the other hand, I further propose that the anterior epithelial cells failed to differentiate into secondary fiber cells so that the lens cannot grow to the normal size. The primary fiber cells, which are differentiated from posterior lens epithelial cells and elongate to fill the lens vesicle, do not seem to be affected during early eye development before E14.5. But subsequently, the secondary fiber cells which are differentiated from the lens epithelial cells in the lens equator are greatly affected after E14.5. In the mutants, less secondary fiber cells with their dramatic changes in cell shape are present. The lens epithelial cells in the equator are thinner in the mutants compared to the wild-type controls. *Prox1*, a molecule necessary for lens differentiation (Wigle et al., 1999; Cui et al., 2004), is ectopically expressed in the vitreous, posterior lens and central lens; its expression is decreased in the lens epithelium at P11. Together, these results demonstrate that *peroxidasin* is required for regulation of cell proliferation and differentiation in the lens during development.

Mutations in most genes coding for transcription factors can lead to anterior segment dysgenesis, such as *PAX6*, *FOXC1*, *PITX2*, *PITX3*, *Foxe3*, *Ap2a* (Reis and Semina, 2011). My study

demonstrated that a type of secreted molecule combining extracellular matrix motifs and extracellular peroxidase which is different from transcription factors, is also necessary for anterior segment development. Considering several different domains in peroxidasin, I proposed that peroxidasin may play different roles during eye development. In one aspect, I detected the expression of different conserved genes including transcription factors for eye development and found that *Pax6* and *Tgf-β1* undergo dynamic expression changes during eye development in *peroxidasin*-mutant eyes, which is slightly up-regulated at E12.5 but strongly up-regulated at E15.5 ($p < 0.05$), the stage when most obvious phenotypes occur. However, the expression of *Pax6* and *Tgf-β1* in mutant eyes recovers to the normal level at P10. These results indicate that peroxidasin may regulate eye development through the regulation of *Pax6* and *Tgf-β1* expression. Overexpression of *Pax6* in the mouse eye can also affect the normal development of anterior segment, resulting in corneal opacity (Schedl et al., 1996; Dorà et al., 2008; Davis and Piatigorsky, 2011), iris hypoplasia (Schedl et al., 1996), abnormal lens fiber cell differentiation (Dorà et al., 2008), microphthalmia (Schedl et al., 1996; Manuel et al., 2008) and retinal dysplasia (Manuel et al., 2008). Also, transgenic *Pax6* mice also exhibit a variable phenotype ranging from almost normal eyes to severely microphthalmia (Schedl et al., 1996). These eye malformations are similar to the eye phenotypes in our mutants. The expression of *Tgf-β1* is up-regulated in mutant embryonic eyes, suggesting that Bmp signaling is affected by the deficiency in peroxidasin. A study also showed that overexpression of *Tgf-β1* causes anterior subcapsular cataract and corneal opacity (Srinivasan et al., 1998), and microphthalmia and anterior segment dysgenesis (Flügel-Koch et al., 2002), which are also similar to the eye phenotypes of the *KTA48* mutants. The detailed mechanisms by which peroxidasin regulates the expression of *Pax6* and *Tgf-β1* are still unclear. I propose that peroxidasin may affect *Pax6* and *Tgf-β1* expression through membrane receptors. Thus it could alter downstream signaling and dysregulate the expression of *Pax6* and *Tgf-β1*.

Consistent with an important role of peroxidasin in the formation and consolidation of the extracellular matrix in *Drosophila* and *C. elegans* (Nelson et al., 1994; Gotenstein et al., 2010), I observed that there are dramatic changes in basement membrane in *peroxidasin*-mutant embryonic eyes. Firstly, ruptures of the lens capsule and lens epithelium adhesion occur, and thinner lens capsule was found in embryonic and postnatal eyes of the mutants at E15.5. Secondly, the inner limiting membrane is also disrupted in mutants at E17.5. These also suggest the basement

membrane is aberrant and the amount of ECM is reduced by the deficiency of peroxidase. In our study, peroxidase is also detected in vitreous nucleated cells and can be secreted into the vitreous during embryonic eye development. On the basis of our basement membrane findings and the changes in the anterior segment, I propose that peroxidase-expressing nucleated cells migrate into the vitreous and anterior chamber angle, and then peroxidase is secreted to be involved in the lens capsule and anterior chamber angle to consolidate the extracellular matrix in the eyes, respectively. Moreover, lens epithelial cells also express peroxidase, which can also contribute to the lens epithelium adhesion and could be involved in the consolidation of the lens capsule. Collagen IV, the main component of basement membrane, is mainly expressed in the lens capsule (Kelley et al., 2002) and highly expressed in the inner limiting membrane (Sarthy, 1993; Bradshaw et al., 1995; Halfter et al., 2005) during eye development. A recent study demonstrated that peroxidase crosslinks with Collagen IV in the basement membrane (Bhave et al., 2012). Thus, peroxidase may consolidate the basement membrane of the lens and retina by crossing with Collagen IV during eye development, and a loss of function of peroxidase may probably fail to crosslink collagen IV and thereby destabilize the ocular basement membrane and lens epithelial cell adhesion, resulting in ruptures of the lens capsule and inner limiting membrane and disruptions in the adhesion between the lens epithelial cells. Taken together, these observations confirmed that peroxidase is involved in ECM consolidation in a higher organism and also showed that peroxidase is essential for basement membrane and cell adhesion during embryonic eye development.

In addition, primary lens fiber cells need to grow and elongate; in the mutants, they migrate out of the lens into the anterior chamber and vitreous cavity through the rupture of lens capsule and the lens epithelium. The lens fibers in the anterior chamber can worsen the development of the anterior segment, and lens matrix in the anterior chamber including corneal-iris angle could severely affect the contribution of the mesenchymal cells to differentiate into the different cell types during anterior segment development. Moreover, the lens crystallin in the anterior chamber can induce ocular inflammation and glaucoma (Chang et al., 1989; Xiao et al., 1992; Sowka et al., 2004). During the embryonic stage (E15.5) and the early postnatal period before eye opening (P11), some key cytokines for promoting inflammation such as *IL-1 β* and *TNF- α* are also up-regulated suggesting that congenital ocular inflammation occurs. There are two possible factors contributing

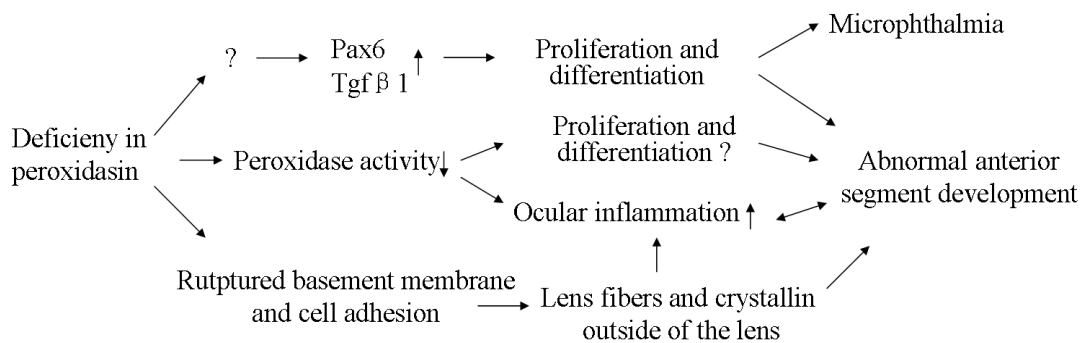
to the ocular inflammation, one is a reduced peroxidase activity which can produce more active oxygen species. The other one is lens crystallin in the anterior chamber.

Many risk factors for glaucoma were found in *KTA48* mutants including smaller eyes, and iris-corneal adhesion, lens-corneal adhesion and lens crystallin in the anterior chamber. Therefore, *KTA48* mutants could have glaucoma although it is very difficult to measure ocular pressure in these mice due to nearly closed eye lids. The hallmark of glaucoma is the damage of optic nerve head and retina including loss of retinal ganglion cells and their axons (Quigley, 2011). I examined the retina and optic nerve head during early postnatal periods and adult by immunostaining. I found that the expression of Brn3 in the retinal ganglion cell layer at 3-week is significantly decreased in the retina, suggesting that RGCs are damaged. Moreover, the nerve fibers, consisting of retinal ganglion cell axons, are much thinner in the retina and optic nerve head in mutants than in normal controls, suggesting that the retinal ganglion cells are degenerative and the axons are damaged in mutants. Together, these indicate that glaucoma occurs in the *KTA48* mice in early periods after births and it could be congenital glaucoma due to congenital anterior segment dysgenesis. Compared to retinal changes at 3 weeks, in adult mutant mice loss of retinal ganglion cells, thinner inner and outer nuclear layers were found, suggesting that progressive retinal degeneration occurs. Taken together, these indicate that congenital glaucoma occurs in the early postnatal period and develops progressively. Therefore, peroxidase could play a role in the onset of congenital glaucoma. Our study also provides possible reasons and mechanisms for the developmental glaucoma found in the patients with *PXDN* (Khan et al., 2011).

A missense mutation in the peroxidase domain of *PXN* causes abnormal axon guidance in *C.elegans*, specifically left-right guidance of commissural guidance (Gotenstein et al., 2010). Axon guidance also plays an important role during visual system development (Petros, et al., 2008; Haupt C et al., 2008). However, there are no obvious differences in the morphology of the optic nerve, optic tract and optic chiasm when the optic chiasm is mature at E15.5. This indicates that peroxidase may not play a general role in axon guidance but a specific function in *C.elegans*.

In summary, our ENU-induced *peroxidase* mutant mice mimic most features of patients with corneal opacity, congenital cataract and developmental glaucoma due to *PXDN* mutations. Our

study suggests that peroxidasin is essential for eye development including proliferation and differentiation, which is most probably mediated by regulation of *Pax6* and *Tgf-β1*. In addition, peroxidasin is also essential for basement membrane integrity and cell adhesion during lens and retinal development. Our studies provide insights for the eye defects found in the patients with *PXDN* mutations and we propose a series of events initiated by the deficiency of peroxidasin, which may not only help to understand the role of peroxidasin in eye development, but also aid in the development of novel strategies to treat congenital anterior segment dysgenesis including corneal opacity, cataract and glaucoma.



Perspective

1. Due to up-regulated expression of *Pax6* and *Tgf-β1* was found in mutant eyes at E15.5, peroxidasin may regulate the expression of *Pax6* and *Tgf-β1*. To confirm this point, one can use *pax6* or *Tgf-β1*, *peroxidasin* double mutant mice to investigate whether the eye phenotypes can be partially rescued compared to the eye phenotypes in *peroxidasin* mutants. Another question is that how peroxidasin regulates the expression of *Pax6* and *Tgf-β1*. *In vitro* study by treatment with peroxidasin or transfection with peroxidasin cDNA in cell lines could help to solve this question.
2. Peroxidasin can be secreted by vitreous nucleated cells in the embryonic stages. It appears that there are different cell types in the vitreous during eye development based on different morphologies. The immunostaining for some cell markers are helpful to indentify the

properties of these cells. It appears that extraocular mesenchymal cells can enter into the eye through the space of the optic nerve head. This work will help to understand brain-eye interactions during embryonic development.

3. There are multiple domains in the peroxidasin including leucine-rich repeats, peroxidase domain and von Willebrand factor domain. These different domains should have different roles during eye development. What's the special role of its different domains during the eye development? Are there any alternative protein products? Is it also a transmembrane receptor? What is the possible existing ligands/receptors and the signaling pathways of peroxidasin? Does peroxidasin have protective effect on anterior segment dysgenesis?
4. Peroxidasin is a secreted molecule and recent study showed that it can be fastly secreted and circulates in the plasma. Whether peroxidasin can enter into the eye through circulating blood during eye development is unclear. Another question is that whether peroxidasin also functions within the cell cytoplasm or cell nuclear is also unclear.

6.2 *Bmpr1b* is essential for ventral retinal development

In the present study, I characterized a mouse cells and disorganized axons in the optic nerve head and optic nerve in mutants, model of optic nerve hypoplasia and retinal gliosis caused by a splice donor site mutation in *Bmpr1b*. This splice donor site mutation in intron 10 of *Bmpr1b* results in skipping of exon 10, thereby introducing a translational frameshift and a premature stop codon, which is predicted to affect the cytoplasm domain including conserved serine/threonine kinase. Then I demonstrated that this event has dysregulated the expression of ocular Pax2 in embryonic development leading to optic nerve hypoplasia and ventral retinal gliosis associated with retinal dysplasia in mice. Subsequently, the ventral retina gliosis is associated with decreased neurogenesis of retinal ganglion cells. Moreover, the astrocytes are also more activated and they are associated with a decreased number of Sox2-positive precursor and disorganized axons in the optic nerve head and optic nerve in mutants, suggesting a hypodevelopmental event. The activated astrocytes in ventral gliosis retina are proliferating and likely to be gliogenic precursors. In addition, these precursor-like glial cells may play a general role in the pathogenesis of retinal gliosis in mice and humans.

The most important finding of the study is that *Bmpr1b* mutant mice exhibit ventral retinal gliosis caused by a genetic defect, which is different from most other studies on reactive gliosis by chemical toxicity or injury. Although Bmp signalling pathway is shown to be necessary for the oligodendrocyte development (Feigenson et al., 2011), there remains the debate between the relationship between *Bmpr1b* and gliosis. *Bmpr1b*-null mice develop hyperactive reactive astrocytes and have attenuated glial scar following injury in the spinal cord (Sahni et al., 2010), whereas another study showed that the number of activated astrocytes in *Bmpr1b*-null mice is less than in wild types which was due to the defect of glia cell maturation (See et al., 2007). In consistency with Sahni et al (2010), our mutant mice showed ventral retinal gliosis that increased numbers of strong activated astroglia cells are found in the ventral retina, optic nerve head and optic nerve from early postnatal period to adult. These activated glial cells form a long aggregate with branches in the ventral retina which are involved in different retinal layers and this long glial cell aggregate is also connected to the optic nerve head. These demonstrate that *Bmpr1b* is essential for ventral retinal glial cells development. *In-vivo* BrdU labelling revealed that the activated glial cells are proliferating in the postnatal eye development and these glial cells can express Pax2, Sox2

and Nestin, but not Pax6. Pax2 can inhibit the fate of neuron but promotes the differentiation of glial cells (Soukkaieh et al., 2007) and Pax6 is required for neuronal differentiation (Hsieh and Yang, 2009). Together, these suggest that the activated glial cells in the ventral retina probably have properties of precursors with the gliogenic population (Pax2) but not neurogenic populations (Pax6). Here the deficiency in *Bmpr1b* causes more gliogenic precursor population in the retina, which is also consistent with the work by Lee et al (2008) demonstrating that inhibition of *BMPR1B* expression in primary glioblastomas can expand the clonogenic stem population. In addition, astrocytes can acquire the properties of stem cells and become multi-potent cells in the reactive gliosis induced by brain injury (Buffo et al., 2008). Furthermore, a few activated cells in the outer plexiform layer of the ventral gliosis retina express GS, the markers for retinal Müller cells (Das et al., 2006; Del Debbio et al., 2010), suggesting that the glial cells are from retinal Müller cells. This finding is consistent with the study showing that activated retinal Müller cells express progenitor markers such as Nestin in the retinal gliosis induced by toxic substances (Chang et al., 2007). A small population of the other activated glia cells do not express GS but they show a star-like morphology which indicates that they are probably from retinal astrocytes. These suggest that different types of glial cells including retinal Müller cells and astrocytes are involved in the ventral retinal gliosis. Interestingly, I found that a few BrdU-positive cells co-express PKC α , a marker for bipolar cells, in the gliosis retina in mutants after injection of BrdU in adult mice. It suggests that these GFAP and Pax2-positive/Pax6-negative precursor cells may still have the ability to differentiate into interneurons. This finding is consistent with another study that reduced expression of Pax6 in retinal progenitors decreases the neurogenesis of retinal ganglion cells but enhances the amacrine interneuron production (Hsieh and Yang, 2009).

Together with other studies showing that the reactive cells (Müller cells) in the retinal gliosis may also have properties of stem cells (Das et al., 2006), I put forward the hypothesis that activated glial cells having a characteristic of precursors may play a general role in the pathogenesis of retinal gliosis, which keeps them to differentiate into more glia cells under the specific conditions. Clinically, there are only a few studies showing that those cells expressing Nestin were found in the epiretinal membranes (Mayer et al., 2003) and that the proliferating cells expressing neural stem cell markers (Nestin, Sox2 and Pax6) were around the ora seratta region in human PVR (Proliferative vitreoretinopathy) eyes (Johnsen et al., 2012). Then we further analyzed clinical

retinal gliosis samples including idiopathic retinal gliosis and secondary retinal gliosis using similar progenitor markers in the mouse study. Similar to our mouse data, we found that there are a number of activated glia cells (strong GFAP expression) in the epiretinal membrane and inner limiting membrane, which also express Pax2, Sox2 and Nestin. These data supports our hypothesis that GFAP-positive precursors play a general role in the pathogenesis of retinal gliosis. Interestingly, the morphology of these glia cells is variable, some exhibit long branches and the others display star-like morphology and they form networks with their long branches in the epiretinal membrane and inner limiting membrane, which is similar to the activated glial cells aggregate in our mouse models. Together, these demonstrated that these astrocytes expressing markers of progenitors in the retinal gliosis are similar between mouse and human, indicating similar intrinsic mechanism in the formation and development of retinal gliosis.

Another striking finding is the finding of optic nerve head coloboma in the mutants. The optic nerve head coloboma was found in the very early postnatal period such as P5, suggesting that this is the change of optic nerve head hypoplasia arising from hypodevelopment of the optic nerve head. Similar to the gliosis in the ventral retina, the glial cells in the optic nerve head and optic nerve are also activated. The axons and the glia cells in the optic nerve also showed disorganized arrangements and decreased numbers of Sox2-expressing cells, indicating a hypodevelopmental/degenerating change in the optic nerve. We further found that Pax2 is ectopically expressed in the optic disk and ventral retina during embryonic retinal development, suggesting that these events may be initiated by the mutation in *Bmpr1b*. Meanwhile, aberrant expression of Pax2 in the retina causes decreased neurogenesis of retinal ganglion cells resulting in a reduced number of axons from RGC which is also another factor for the optic nerve hypoplasia. Therefore, we showed that *Bmpr1b* is necessary for optic nerve development and it can lead to optic nerve head coloboma through regulation of Pax2.

Furthermore, we examined ventral embryonic retina and optic nerve in mutants compared to the wild-type controls during embryonic eye development. Consistent with our data from postnatal periods, there are also dramatic changes in ventral retina and optic nerve head during the embryonic retinal development. We found that Pax2 is ectopically over-expressed in the ventral retina and asymmetrically expressed in the optic nerve head, whereas it is only symmetrically

expressed in the optic nerve head region in wild types at E15.5 and E17.5. Several studies showed that mutations in *PAX2/Pax2* gene are associated with or even causes optic nerve coloboma in humans (Tagami et al., 2010; Alur et al., 2010) and mice (Alur et al., 2010). The number of axons is also reduced in mice with *Pax2* mutations (Alur et al., 2008). Previous studies showed that the retinal astrocytes are immigrants from the optic nerve through retinal vessel (Watanabe and Raff, 1988), whereas others showed that they derive from retinal Müller cells (Reichenbach and Wohlrab, 1986). In my study, I did not find abnormal migration of activated astrocytes from optic nerve head to retina, but found ectopically activated glial cells across the different layers of the ventral retina in the mutants, suggesting that these activated glial cells may occur after migration or they originate from retinal progenitors. Together, *Bmpr1b* may control the expression of *Pax2* in ventral retina during retinal development and play an important role in the differentiation and maturation of retinal glial cells. The ectopical expression of *Pax2* and abnormal activation of glial cells may be the initial events for optic nerve hypoplasia and later ventral retinal gliosis. The relationship between *Bmp* signalling and *Pax2* remains unclear. Another study showed that *BMP7* interacts with *SHH* to regulate *Pax2* expression in astrocytes (Sehgal et al., 2009), which also supports that *Bmp* signalling regulated the expression of *Pax2*. Meanwhile, the number of retinal ganglion cells is reduced in the ventral retina where ectopical *Pax2* is expressed, suggesting that decreased neurogenesis of RGC by overexpression of *Pax2*. In addition, the optic nerve in mutants tends to be thinner than wild types at E15.5 revealed by anterograde tracing, which may be due to reduced number of retinal ganglion cells I found. In addition, *Bmpr1b* is also necessary for the fate determination of commissural neurons and axon guidance in the spinal cord (Yamauchi et al., 2008). In *Bmpr1b*-knockout mice, abnormal axon guidance was found in the ventral retina in during embryonic eye development (Liu et al., 2003). We further analyzed the morphology of the optic nerve and optic chiasm at E15.5, when the optic chiasm is already mature. However, axon guidance in the optic nerve and optic chiasm are not affected in mutants. Interestingly, there are a number of retinal ganglion cell axons entering into the axon bundles instead of optic nerve head in the ventral retina, and there are also a few axons mislocalised in the dorsal retina in mutants, indicating that retinal axon misguidance occurs *Bmpr1b*-mutant mice. Together, these results indicate that *Bmpr1b* may play a role of axon guidance in the retina, but not in the higher visual pathway. Meanwhile, on the basis of our results, axon guidance may be a secondary event or affected by abnormal ventral retinal gliosis in *Bmpr1b*-mutant mice.

In addition, retinal dysgenesis is associated with the ventral retinal gliosis in the mutants. The ventral gliosis retina exhibits dysplasia conditions in mutants, including retinal delamination and retinal rosettes. More interestingly, the cells from the inner nuclear layer migrate into the inner plexiform layer in mutants. The synapses of the bipolar cells are disrupted and ectopical retinal ganglion cells are found in the inner plexiform layer. These retina changes may be partly due to abnormal retinal development and partly due to the gliosis. Interestingly, ERG showed regular retinal electricity transmission in the mutant retina although retinal gliosis and retinal dysplasia occurs in the ventral retina. Considering that global ERG was performed in our study, local retina dysfunction may not be detected because of less sensitivity. To find some more details of ERG in *Ali030* mutants, ERG and visually evoked potential (VEP, it is a tool to be used to test electricity transmission from optic nerve head to visual cortex) were performed and analyzed in Prof. Jan Kremers' lab (Department of Ophthalmology, University of Erlangen-Nürnberg). The amplitudes of the a- and b-wave are reduced in the *Ali030* mutants by scotopic and photopic flash ERG, which suggest that the function of outer retina is impaired. This result is consistent with the histology and immunostaining results showed that disrupted photoreceptor layer and outer nuclear layer. Currently, the data of visually evoked potential (VEP) is being analysed. The decreased visual acuity revealed by optokinetic drum in *Ali030* mutants may due to the abnormal electrical transmission in retina and the optic nerve.

Although a few studies demonstrated that lens development is mediated by *Bmpr1* (Rajagopal et al., 2008; 2009) and the downstream signalling molecule *Smad4* (Liu et al., 2010). These results suggest that *Bmp* signalling pathway is important for lens development. However, lens is not affected in *Ali030* mutant mice, indicating that *Bmpr1b* is not important for lens development, and the deficiency effect of *Bmpr1b* can be compensated by *Bmpr1a* during lens development.

In summary, we characterized a mouse model of optic nerve head hypoplasia and retinal gliosis induced by a splicing donor site mutation in *Bmpr1b*. Our work demonstrated that this mutation causes optic nerve head coloboma and ventral retinal gliosis by overexpression of *Pax2* in the ventral retina and ectopic expression of *Pax2* in the optic nerve head region during embryonic retinal development. This also helps to significantly advance the understanding of intrinsic mechanisms of the retinal gliosis and optic nerve hypoplasia.

Perspective

Our study demonstrated that *Bmpr1b* is key for optic nerve head and ventral retina development through regulation of *Pax2* expression. How Bmp signalling regulates *Pax2* and what the downstream signalling is remains unclear. Further *in vitro* study using cell culture combined with knockdown of *Bmpr1b*, transfection with mutant *Bmpr1b* cDNA and other biochemical methods may elucidate the mechanism. In the other aspect, our work showed that the activated astrocytes are proliferating and express precursor markers such as *Pax2*, *Sox2* and *Nestin*. We are still lacking of direct evidence showing that they are stem cells. Lineage tracing (for example, electroporation transfection of GFP-*Sox2* plasmid in the retina *in vivo*) combined with BrdU labelling can solve this question. Also, similar methods can be used in the cultured human retinal gliosis samples, such as epiretinal membrane and internal limiting membrane, which will not only help us to understand the mechanism of retinal gliosis, but also may develop a novel strategy for treatment. Some *Sox2*-positive cells in the inner nuclear layer (showing neuron-like morphology) and some retinal ganglion cells (expressing *Brn3*) can express GFAP, a glial cell marker. Whether *Bmpr1b* can be used for cell reprogramming (for example, glial cell to neuron) is to be investigated. In addition, retinal gliosis can be induced by gene defects. Whether the idiopathic retinal gliosis is caused by the gene mutations in humans is to be investigated. In my study, I realized that there is a number of *Sox2* positive and/or *Pax6* positive cells in the inner nuclear layer in the adult retina. These cells have a very small population co-expressing *Sox2* and *Pax6*. The question is that what the role of these cells in adult retina is and whether these cells keep the properties of stem cells and also differentiate into postmitotic cells in adult retina. Understanding of these questions may help to find novel treatments for retinal degenerative diseases.

7. References

Abdollahi MR, Morrison E, Sirey T, Molnar Z, Hayward BE, Carr IM, Springell K, Woods CG, Ahmed M, Hattingh L, Corry P, Pilz DT, Stoodley N, Crow Y, Taylor GR, Bonthron DT, Sheridan E. Mutation of the variant alpha-tubulin TUBA8 results in polymicrogyria with optic nerve hypoplasia. *Am J Hum Genet.* 2009; 85:737-44.

Abrous DN, Koehl M, Le Moal M. Adult neurogenesis: from precursors to network and physiology. *Physiol Rev.* 2005; 85:523-69.

Agathocleous M, Harris WA. From progenitors to differentiated cells in the vertebrate retina. *Annu Rev Cell Dev Biol.* 2009; 25:45-69.

Akagi, T., Inoue, T., Miyoshi, G., Bessho, Y., Takahashi, M., Lee, J. E., Guillemot, F. and Kageyama, R. Requirement of multiple basic helix-loop-helix genes for retinal neuronal subtype specification. *J. Biol. Chem.* 2004; 279:28492-28498.

Aldahmesh MA, Mohammed JY, Al-Hazzaa S, Alkuraya FS. Homozygous null mutation in ODZ3 causes microphthalmia in humans. *Genet Med.* 2012; 14:900-4.

Ali M, Buentello-Volante B, McKibbin M, Rocha-Medina JA, Fernandez-Fuentes N, Koga-Nakamura W, Ashiq A, Khan K, Booth AP, Williams G, Raashid Y, Jafri H, Rice A, Inglehearn CF, Zenteno JC. Homozygous FOXE3 mutations cause non-syndromic, bilateral, total sclerocornea, aphakia, microphthalmia and optic disc coloboma. *Mol Vis.* 2010; 16:1162-8.

Alur RP, Cox TA, Crawford MA, Gong X, Brooks BP. Optic nerve axon number in mouse is regulated by PAX2. *J AAPOS.* 2008; 12:117-21.

Alur RP, Vijayasarathy C, Brown JD, Mehtani M, Onojafe IF, Sergeev YV, Boobalan E, Jones M, Tang K, Liu H, Xia CH, Gong X, Brooks BP. Papillorenal syndrome-causing missense mutations in *PAX2/Pax2* result in hypomorphic alleles in mouse and human. *PLoS Genet.* 2010; 6:e1000870.

Anjum I, Eiberg H, Baig SM, Tommerup N, Hansen L. A mutation in the FOXE3 gene causes congenital primary aphakia in an autosomal recessive consanguineous Pakistani family. *Mol Vis*. 2010; 16:549-55.

Azuma N, Yamada M. Missense mutation at the C terminus of the PAX6 gene in ocular anterior segment anomalies. *Invest Ophthalmol Vis Sci*. 1998; 39:828-30.

Bai YP, Hu CP, Yuan Q, Peng J, Shi RZ, Yang TL, Cao ZH, Li YJ, Cheng G, Zhang GG. Role of VPO1, a newly identified heme-containing peroxidase, in ox-LDL induced endothelial cell apoptosis. *Free Radic Biol Med*. 2011; 51:1492-500.

Banh A, Deschamps PA, Gauldie J, Overbeek PA, Sivak JG, West-Mays JA. Lens-specific expression of TGF-beta induces anterior subcapsular cataract formation in the absence of Smad3. *Invest Ophthalmol Vis Sci*. 2006; 47:3450-60.

Bardakjian TM, Schneider A. The genetics of anophthalmia and microphthalmia. *Curr Opin Ophthalmol*. 2011; 22:309-13.

Barna M, Pandolfi PP, Niswander L. Gli3 and Plzf cooperate in proximal limb patterning at early stages of limb development. *Nature*. 2005; 436:277-81.

Baulmann DC, Ohlmann A, Flügel-Koch C, Goswami S, Cvekl A, Tamm ER. Pax6 heterozygous eyes show defects in chamber angle differentiation that are associated with a wide spectrum of other anterior eye segment abnormalities. *Mech Dev*. 2002; 118:3-17.

Baur ST, Mai JJ, Dymecki SM. Combinatorial signaling through BMP receptor IB and GDF5: shaping of the distal mouse limb and the genetics of distal limb diversity. *Development*. 2000; 127:605-19.

Bebby F, Lamonerie T. The homeobox gene Otx2 in development and disease. *Exp Eye Res*. 2013; 111C:9-16.

Bernardos RL, Lentz SI, Wolfe MS, Raymond PA. Notch-Delta signaling is required for spatial patterning and Müller glia differentiation in the zebrafish retina. *Dev Biol.* 2005; 278:381-95.

Bhave G, Cummings CF, Vanacore RM, Kumagai-Cresse C, Ero-Tolliver IA, Rafi M, Kang JS, Pedchenko V, Fessler LI, Fessler JH, Hudson BG. Peroxidase forms sulfilimine chemical bonds using hypohalous acids in tissue genesis. *Nat Chem Biol.* 2012; 8:784-90.

Blixt A, Landgren H, Johansson BR, Carlsson P. Foxe3 is required for morphogenesis and differentiation of the anterior segment of the eye and is sensitive to Pax6 gene dosage. *Dev Biol.* 2007; 302:218-29.

Blixt A, Mahlapuu M, Aitola M, Pelto-Huikko M, Enerbäck S, Carlsson P. A forkhead gene, FoxE3, is essential for lens epithelial proliferation and closure of the lens vesicle. *Genes Dev.* 2000; 14:245-54.

Bohnsack BL, Kasprick DS, Kish PE, Goldman D, Kahana A. A zebrafish model of axenfeld-riege syndrome reveals that pitx2 regulation by retinoic acid is essential for ocular and craniofacial development. *Invest Ophthalmol Vis Sci.* 2012; 53:7-22.

Bradford MM. A rapid and sensitive method for the quantitation of microgram quantities of protein utilizing the principle of protein-dye binding. *Anal Biochem.* 1976; 72:248-54.

Bradshaw AD, McNagny KM, Gervin DB, Cann GM, Graf T, Clegg DO. Integrin alpha 2 beta 1 mediates interactions between developing embryonic retinal cells and collagen. *Development.* 1995; 121:3593-602.

Brederlau A, Faigle R, Elmi M, Zarebski A, Sjöberg S, Fujii M, Miyazono K, Funa K. The bone morphogenetic protein type Ib receptor is a major mediator of glial differentiation and cell survival in adult hippocampal progenitor cell culture. *Mol Biol Cell.* 2004; 15:3863-75.

Bringmann A, Iandiev I, Pannicke T, Wurm A, Hollborn M, Wiedemann P, Osborne NN,

Reichenbach A. Cellular signaling and factors involved in Müller cell gliosis: neuroprotective and detrimental effects. *Prog Retin Eye Res.* 2009; 28:423-51.

Bringmann A, Wiedemann P. Müller glial cells in retinal disease. *Ophthalmologica.* 2012; 227:1-19.

Brown NL, Patel S, Brzezinski J, Glaser T. Math5 is required for retinal ganglion cell and optic nerve formation. *Development.* 2001; 128:2497-508.

Buffo A, Rite I, Tripathi P, Lepier A, Colak D, Horn AP, Mori T, Götz M. Origin and progeny of reactive gliosis: A source of multipotent cells in the injured brain. *Proc Natl Acad Sci U S A.* 2008; 105:3581-6.

Cai F, Zhu J, Chen W, Ke T, Wang F, Tu X, Zhang Y, Jin R, Wu X. A novel PAX6 mutation in a large Chinese family with aniridia and congenital cataract. *Mol Vis.* 2010; 16:1141-5.

Cai Y, Brophy PD, Levitan I, Stifani S, Dressler GR. Groucho suppresses Pax2 transactivation by inhibition of JNK-mediated phosphorylation. *EMBO J.* 2003; 22:5522-9.

Chang B, Smith RS, Peters M, Savinova OV, Hawes NL, Zabaleta A, Nusinowitz S, Martin JE, Davisson ML, Cepko CL, Hogan BL, John SW. Haploinsufficient Bmp4 ocular phenotypes include anterior segment dysgenesis with elevated intraocular pressure. *BMC Genet.* 2001; 2:18.

Chang ML, Wu CH, Jiang-Shieh YF, Shieh JY, Wen CY. Reactive changes of retinal astrocytes and Müller glial cells in kainate-induced neuroexcitotoxicity. *J Anat.* 2007; 210:54-65.

Chang MS, Chiou GC. Prevention of lens protein-induced ocular inflammation with cyclooxygenase and lipoxygenase inhibitors. *J Ocul Pharmacol.* 1989; 5:353-60.

Chen D, Ji X, Harris MA, Feng JQ, Karsenty G, Celeste AJ, Rosen V, Mundy GR, Harris SE. Differential roles for bone morphogenetic protein (BMP) receptor type IB and IA in differentiation

and specification of mesenchymal precursor cells to osteoblast and adipocyte lineages. *J Cell Biol.* 1998; 142:295-305.

Chen H and Weber AJ. Expression of glial fibrillary acidic protein and glutamine synthetase by Müller cells after optic nerve damage and intravitreal application of brain-derived neurotrophic factor. *Glia.* 2002; 38:115–125.

Chen H, Weber AJ. Expression of glial fibrillary acidic protein and glutamine synthetase by Müller cells after optic nerve damage and intravitreal application of brain-derived neurotrophic factor. *Glia.* 2002; 38:115-25.

Cheng G, Salerno JC, Cao Z, Pagano PJ, Lambeth JD. Identification and characterization of VPO1, a new animal heme-containing peroxidase. *Free Radic Biol Med.* 2008; 45:1682-94.

Churchill AJ, Booth AP, Anwar R, Markham AF. PAX 6 is normal in most cases of Peters' anomaly. *Eye (Lond).* 1998; 12:299-303.

Cui W, Tomarev SI, Piatigorsky J, Chepelinsky AB, Duncan MK. Mafk, Prox1, and Pax6 can regulate chicken betaB1-crystallin gene expression. *J Biol Chem.* 2004; 279:11088-95.

Cvekl A, Tamm ER. Anterior eye development and ocular mesenchyme: new insights from mouse models and human diseases. *Bioessays.* 2004; 26:374-86.

Dalke C, Löster J, Fuchs H, Gailus-Durner V, Soewarto D, Favor J, Neuhäuser-Klaus A, Pretsch W, Gekeler F, Shinoda K, Zrenner E, Meitinger T, Hrabé de Angelis M, Graw J. Electroretinography as a screening method for mutations causing retinal dysfunction in mice. *Invest Ophthalmol Vis Sci.* 2004; 45:601-9.

Danesh SM, Villasenor A, Chong D, Soukup C, Cleaver O. BMP and BMP receptor expression during murine organogenesis. *Gene Expr Patterns.* 2009; 9:255-65.

Danysh BP, Duncan MK. The lens capsule. *Exp Eye Res.* 2009; 88:151-64.

Das AV, Mallya KB, Zhao X, Ahmad F, Bhattacharya S, Thoreson WB, Hegde GV, Ahmad I. Neural stem cell properties of Müller glia in the mammalian retina: regulation by Notch and Wnt signaling. *Dev Biol.* 2006; 299:283-302.

Davis J, Piatigorsky J. Overexpression of Pax6 in mouse cornea directly alters corneal epithelial cells: changes in immune function, vascularization, and differentiation. *Invest Ophthalmol Vis Sci.* 2011; 52:4158-68.

de Jongh RU, Lovicu FJ, Overbeek PA, Schneider MD, Joya J, Hardeman ED, McAvoy JW. Requirement for TGFbeta receptor signaling during terminal lens fiber differentiation. *Development.* 2001; 128:3995-4010.

de Melo J, Miki K, Rattner A, Smallwood P, Zibetti C, Hirokawa K, Monuki ES, Campochiaro PA, Blackshaw S. Injury-independent induction of reactive gliosis in retina by loss of function of the LIM homeodomain transcription factor Lhx2. *Proc Natl Acad Sci U S A.* 2012; 109:4657-62.

de Melo J, Peng GH, Chen S, Blackshaw S. The Spalt family transcription factor Sall3 regulates the development of cone photoreceptors and retinal horizontal interneurons. *Development.* 2011; 138:2325-36.

Del Debbio CB, Balasubramanian S, Parameswaran S, Chaudhuri A, Qiu F, Ahmad I. Notch and Wnt signaling mediated rod photoreceptor regeneration by Müller cells in adult mammalian retina. *PLoS One.* 2010; 5:e12425.

Demirhan O, Türkmen S, Schwabe GC, Soyupak S, Akgül E, Tastemir D, Karahan D, Mundlos S, Lehmann K. A homozygous BMPR1B mutation causes a new subtype of acromesomelic chondrodysplasia with genital anomalies. *J Med Genet.* 2005; 42:314-7.

Diehl AG, Zarepari S, Qian M, Khanna R, Angeles R, Gage PJ. Extraocular muscle

morphogenesis and gene expression are regulated by *Pitx2* gene dose. *Invest Ophthalmol Vis Sci*. 2006; 47:1785-93.

Ding Q, Chen H, Xie X, Libby RT, Tian N, Gan L. *BARHL2* differentially regulates the development of retinal amacrine and ganglion neurons. *J Neurosci*. 2009; 29:3992-4003.

Dorà N, Ou J, Kucerova R, Parisi I, West JD, Collinson JM. *PAX6* dosage effects on corneal development, growth, and wound healing. *Dev Dyn*. 2008; 237:1295-306.

Doucette L, Green J, Fernandez B, Johnson GJ, Parfrey P, Young TL. A novel, non-stop mutation in *FOXE3* causes an autosomal dominant form of variable anterior segment dysgenesis including Peters anomaly. *Eur J Hum Genet*. 2011; 19:293-9.

Du Y, Xiao Q, Yip HK. Regulation of retinal progenitor cell differentiation by bone morphogenetic protein 4 is mediated by the smad/id cascade. *Invest Ophthalmol Vis Sci*. 2010; 51:3764-73.

Dutta S, Dietrich JE, Aspöck G, Burdine RD, Schier A, Westerfield M, Varga ZM. *Pitx3* defines an equivalence domain for lens and anterior pituitary placode. *Development*. 2005; 132:1579-90.

Dutton GN. Congenital disorders of the optic nerve: excavations and hypoplasia. *Eye (Lond)*. 2004; 18:1038-48.

Dyer MA, Cepko CL. Control of Müller glial cell proliferation and activation following retinal injury. *Nat Neurosci*. 2000; 3:873-80.

Erkman L, McEvelly RJ, Luo L, Ryan AK, Hooshmand F, O'Connell SM, Keithley EM, Rapaport DH, Ryan AF, Rosenfeld MG. Role of transcription factors *Brn-3.1* and *Brn-3.2* in auditory and visual system development. *Nature*. 1996; 381:603-6.

Evans AL, Gage PJ. Expression of the homeobox gene *Pitx2* in neural crest is required for optic stalk and ocular anterior segment development. *Hum Mol Genet*. 2005; 14:3347-59.

Faber SC, Robinson ML, Makarenkova HP, Lang RA. Bmp signaling is required for development of primary lens fiber cells. *Development*. 2002; 129:3727-37.

Favor J, Sandulache R, Neuhäuser-Klaus A, Pretsch W, Chatterjee B, Senft E, Wurst W, Blanquet V, Grimes P, Spörle R, Schughart K. The mouse Pax2 (1Neu) mutation is identical to a human PAX2 mutation in a family with renal-coloboma syndrome and results in developmental defects of the brain, ear, eye, and kidney. *Proc Natl Acad Sci U S A*. 1996; 93:13870-5.

Feigenson K, Reid M, See J, Crenshaw III EB, Grinspan JB. Canonical Wnt signalling requires the BMP pathway to inhibit oligodendrocyte maturation. *ASN Neuro*. 2011; 3:e00061.

Flügel-Koch C, Ohlmann A, Piatigorsky J, Tamm ER. Disruption of anterior segment development by TGF-beta1 overexpression in the eyes of transgenic mice. *Dev Dyn*. 2002; 225:111-25.

Foos RY. Vitreoretinal juncture--simple epiretinal membranes. *Albrecht Von Graefes Arch Klin Exp Ophthalmol*. 1974; 189:231-50.

Footz T, Idrees F, Acharya M, Kozlowski K, Walter MA. Analysis of mutations of the PITX2 transcription factor found in patients with Axenfeld-Rieger syndrome. *Invest Ophthalmol Vis Sci*. 2009; 50:2599-606.

Furuta, Y. and Hogan, B. L. M. BMP4 is essential for lens induction in the mouse embryo. *Genes Dev*. 1998; 12:3764-75.

Gage PJ, Zacharias AL. Signaling "cross-talk" is integrated by transcription factors in the development of the anterior segment in the eye. *Dev Dyn*. 2009; 238:2149-62.

Gan L, Xiang M, Zhou L, Wagner DS, Klein WH, Nathans J. POU domain factor Brn-3b is required for the development of a large set of retinal ganglion cells. *Proc Natl Acad Sci U S A*. 1996; 93:3920-5.

Gandorfer A, Rohleder M, Charteris D, Kampik A, Luthert P. Ultrastructure of vitreomacular traction syndrome associated with persistent hyaloid artery. *Eye (Lond)*. 2005; 19:333-6.

Gandorfer A, Rohleder M, Grosselfinger S, Haritoglou C, Ulbig M, Kampik A. Epiretinal pathology of diffuse diabetic macular edema associated with vitreomacular traction. *Am J Ophthalmol*. 2005; 139:638-52.

Gandorfer A, Rohleder M, Kampik A. Epiretinal pathology of vitreomacular traction syndrome. *Br J Ophthalmol*. 2002; 86:902-9.

Giannelli SG, Demontis GC, Pertile G, Rama P, Broccoli V. Adult human Müller glia cells are a highly efficient source of rod photoreceptors. *Stem Cells*. 2011; 29:344-56.

Gilboa L, Nohe A, Geissendörfer T, Sebald W, Henis YI, Knaus P. Bone morphogenetic protein receptor complexes on the surface of live cells: a new oligomerization mode for serine/threonine kinase receptors. *Mol Biol Cell*. 2000; 11:1023-35.

Gotenstein JR, Swale RE, Fukuda T, Wu Z, Giurumescu CA, Goncharov A, Jin Y, Chisholm AD. The *C. elegans* peroxidase PXN-2 is essential for embryonic morphogenesis and inhibits adult axon regeneration. *Development*. 2010; 137:3603-13.

Gould DB, John SW. Anterior segment dysgenesis and the developmental glaucomas are complex traits. *Hum Mol Genet*. 2002; 11:1185-93.

Graw J. Eye development. *Curr Top Dev Biol*. 2010; 90:343-86.

Greferath U, Grünert U, Wässle H. Rod bipolar cells in the mammalian retina show protein kinase C-like immunoreactivity. *J Comp Neurol*. 1990; 301:433-42.

Halfter W, Dong S, Schurer B, Ring C, Cole GJ, Eller A. Embryonic synthesis of the inner limiting membrane and vitreous body. *Invest Ophthalmol Vis Sci*. 2005; 46:2202-9.

Hanson IM, Fletcher JM, Jordan T, Brown A, Taylor D, Adams RJ, Punnett HH, van Heyningen V. Mutations at the PAX6 locus are found in heterogeneous anterior segment malformations including Peters' anomaly. *Nat Genet.* 1994; 6:168-73.

Harshman LA, Brophy PD. PAX2 in human kidney malformations and disease. *Pediatr Nephrol.* 2012; 27:1265-75.

Haupt C, Huber AB. How axons see their way--axonal guidance in the visual system. *Front Biosci.* 2008; 13:3136-49.

Haverkamp S, Wässle H. Immunocytochemical analysis of the mouse retina. *J Comp Neurol.* 2000; 424:1-23.

Haÿ E, Lemonnier J, Fromigué O, Guénou H, Marie PJ. Bone morphogenetic protein receptor IB signaling mediates apoptosis independently of differentiation in osteoblastic cells. *J Biol Chem.* 2004; 279:1650-8.

Hill RE, Favor J, Hogan BL, Ton CC, Saunders GF, Hanson IM, Prosser J, Jordan T, Hastie ND, van Heyningen V. Nature. Mouse small eye results from mutations in a paired-like homeobox-containing gene. *Nature.* 1991; 354:522-5.

Homma S, Shimada T, Hikake T, Yaginuma H. Expression pattern of LRR and Ig domain-containing protein (LRRIG protein) in the early mouse embryo. *Gene Expr Patterns.* 2009; 9:1-26.

Honkanen RA, Nishimura DY, Swiderski RE, Bennett SR, Hong S, Kwon YH, Stone EM, Sheffield VC, Alward WL. A family with Axenfeld-Rieger syndrome and Peters Anomaly caused by a point mutation (Phe112Ser) in the FOXC1 gene. *Am J Ophthalmol.* 2003; 135:368-75.

Hooker L, Smoczer C, KhosrowShahian F, Wolanski M, Crawford MJ. Microarray-based identification of Pitx3 targets during *Xenopus* embryogenesis. *Dev Dyn.* 2012; 241:1487-505.

Hopfer U, Fukai N, Hopfer H, Wolf G, Joyce N, Li E, Olsen BR. Targeted disruption of Col8a1 and Col8a2 genes in mice leads to anterior segment abnormalities in the eye. *FASEB J.* 2005; 19:1232-44.

Horikoshi N, Cong J, Kley N, Shenk T. Isolation of differentially expressed cDNAs from p53-dependent apoptotic cells: activation of the human homologue of the *Drosophila* peroxidase gene. *Biochem Biophys Res Commun.* 1999; 261:864-9.

Hsieh YW, Yang XJ. Dynamic Pax6 expression during the neurogenic cell cycle influences proliferation and cell fate choices of retinal progenitors. *Neural Dev.* 2009; 4:32.

Iannetti L, Accorinti M, Malagola R, Bozzoni-Pantaleoni F, Da Dalt S, Nicoletti F, Gradini R, Traficante A, Campanella M, Pivetti-Pezzi P. Role of the intravitreal growth factors in the pathogenesis of idiopathic epiretinal membrane. *Invest Ophthalmol Vis Sci.* 2011; 52:5786-9.

Ide H, Katoh M, Sasaki H, Yoshida T, Aoki K, Nawa Y, Osada Y, Sugimura T, Terada M. Cloning of human bone morphogenetic protein type IB receptor (BMPRII) and its expression in prostate cancer in comparison with other BMPRIIs. *Oncogene.* 1997; 14:1377-82.

Idrees F, Bloch-Zupan A, Free SL, Vaideanu D, Thompson PJ, Ashley P, Brice G, Rutland P, Bitner-Glindzicz M, Khaw PT, Fraser S, Sisodiya SM, Sowden JC. A novel homeobox mutation in the PITX2 gene in a family with Axenfeld-Rieger syndrome associated with brain, ocular, and dental phenotypes. *Am J Med Genet B Neuropsychiatr Genet.* 2006; 141B:184-91.

Iwao K, Inatani M, Matsumoto Y, Ogata-Iwao M, Takihara Y, Irie F, Yamaguchi Y, Okinami S, Tanihara H. Heparan sulfate deficiency leads to Peters anomaly in mice by disturbing neural crest TGF-beta2 signaling. *J Clin Invest.* 2009; 119:1997-2008.

Jia X, Guo X, Jia X, Xiao X, Li S, Zhang Q. A novel mutation of PAX6 in Chinese patients with new clinical features of Peters' anomaly. *Mol Vis.* 2010; 16:676-81.

Johnsen EO, Frøen RC, Albert R, Omdal BK, Sarang Z, Berta A, Nicolaissen B, Petrovski G, Moe MC. Activation of neural progenitor cells in human eyes with proliferative vitreoretinopathy. *Exp Eye Res.* 2012; 98:28-36.

Justice MJ, Noveroske JK, Weber JS, Zheng B, Bradley A. Mouse ENU mutagenesis. *Hum Mol Genet.* 1999; 8:1955-63.

Kampik A, Kenyon KR, Michels RG, Green WR, de la Cruz ZC. Epiretinal and vitreous membranes. Comparative study of 56 cases. *Arch Ophthalmol.* 1981; 99:1445-54.

Kay JN, Finger-Baier KC, Roeser T, Staub W, Baier H. Retinal ganglion cell genesis requires *lakritz*, a Zebrafish atonal Homolog. *Neuron.* 2001; 30:725-36.

Kelley PB, Sado Y, Duncan MK. Collagen IV in the developing lens capsule. *Matrix Biol.* 2002; 21:415-23.

Khan K, Rudkin A, Parry DA, Burdon KP, McKibbin M, Logan CV, Abdelhamed ZI, Muecke JS, Fernandez-Fuentes N, Laurie KJ, Shires M, Fogarty R, Carr IM, Poulter JA, Morgan JE, Mohamed MD, Jafri H, Raashid Y, Meng N, Piseth H, Toomes C, Casson RJ, Taylor GR, Hammerton M, Sheridan E, Johnson CA, Inglehearn CF, Craig JE, Ali M. Homozygous mutations in *PXDN* cause congenital cataract, corneal opacity, and developmental glaucoma. *Am J Hum Genet.* 2011; 89:464-73.

Kim IY, Lee DH, Ahn HJ, Tokunaga H, Song W, Devereaux LM, Jin D, Sampath TK, Morton RA. Expression of bone morphogenetic protein receptors type-IA, -IB and -II correlates with tumor grade in human prostate cancer tissues. *Cancer Res.* 2000; 60:2840-4.

Kim JE, Han MS, Bae YC, Kim HK, Kim TI, Kim EK, Kim IS. Anterior segment dysgenesis after overexpression of transforming growth factor-beta-induced gene, *beta igh3*, in the mouse eye. *Mol Vis.* 2007; 13:1942-52.

Kitamura K, Miura H, Miyagawa-Tomita S, Yanazawa M, Katoh-Fukui Y, Suzuki R, Ohuchi H, Suehiro A, Motegi Y, Nakahara Y, Kondo S, Yokoyama M. Mouse Pitx2 deficiency leads to anomalies of the ventral body wall, heart, extra- and periocular mesoderm and right pulmonary isomerism. *Development*. 1999; 126:5749-58.

Kjaer KW, Eiberg H, Hansen L, van der Hagen CB, Rosendahl K, Tommerup N, Mundlos S. A mutation in the receptor binding site of GDF5 causes Mohr-Wriedt brachydactyly type A2. *J Med Genet*. 2006; 43:225-31.

Kobayashi T, Lyons KM, McMahon AP, Kronenberg HM. BMP signaling stimulates cellular differentiation at multiple steps during cartilage development. *Proc Natl Acad Sci U S A*. 2005; 102:18023-7.

Korotkova TM, Ponomarenko AA, Haas HL, Sergeeva OA. Differential expression of the homeobox gene Pitx3 in midbrain dopaminergic neurons. *Eur J Neurosci*. 2005; 22:1287-93.

Landgren H, Blixt A, Carlsson P. Persistent FoxE3 expression blocks cytoskeletal remodeling and organelle degradation during lens fiber differentiation. *Invest Ophthalmol Vis Sci*. 2008; 49:4269-77.

Lawrence JM, Singhal S, Bhatia B, Keegan DJ, Reh TA, Luthert PJ, Khaw PT, Limb GA. MIO-M1 cells and similar muller glial cell lines derived from adult human retina exhibit neural stem cell characteristics. *Stem Cells*. 2007; 25:2033-43.

Lehmann K, Seemann P, Stricker S, Sammar M, Meyer B, Süring K, Majewski F, Tinschert S, Grzeschik KH, Müller D, Knaus P, Nürnberg P, Mundlos S. Mutations in bone morphogenetic protein receptor 1B cause brachydactyly type A2. *Proc Natl Acad Sci U S A*. 2003; 100:12277-82.

Li D, Zhu Q, Lin H, Zhou N, Qi Y. A novel PITX2 mutation in a Chinese family with Axenfeld-Rieger syndrome. *Mol Vis*. 2008; 14:2205-10.

Li H, Cao Z, Moore DR, Jackson PL, Barnes S, Lambeth JD, Thannickal VJ, Cheng G. Microbicidal activity of vascular peroxidase 1 in human plasma via generation of hypochlorous acid. *Infect Immun*. 2012; 80:2528-37.

Li J, Dani JA, Le W. The role of transcription factor Pitx3 in dopamine neuron development and Parkinson's disease. *Curr Top Med Chem*. 2009; 9:855-9.

Li S, Mo Z, Yang X, Price SM, Shen MM, Xiang M. Foxn4 controls the genesis of amacrine and horizontal cells by retinal progenitors. *Neuron*. 2004; 43:795-807.

Limb GA, Salt TE, Munro PM, Moss SE, Khaw PT. In vitro characterization of a spontaneously immortalized human Müller cell line (MIO-M1). *Invest Ophthalmol Vis Sci*. 2002; 43:864-9.

Lin Y, Liu X, Liang X, Li B, Jiang S, Ye S, Yang H, Lou B, Liu Y. PAX6 analysis of one family and one sporadic patient from southern China with classic aniridia. *Mol Vis*. 2011; 17:3116-20.

Ling TL, Stone J. The development of astrocytes in the cat retina: evidence of migration from the optic nerve. *Brain Res Dev Brain Res*. 1988; 44:73-85.

Liu J, Wilson S, Reh T. BMP receptor 1b is required for axon guidance and cell survival in the developing retina. *Dev Biol*. 2003; 256:34-48.

Liu W, Mo Z, Xiang M. The Ath5 proneural genes function upstream of Brn3 POU domain transcription factor genes to promote retinal ganglion cell development. *Proc Natl Acad Sci U S A*. 2001; 98:1649-54.

Liu Y, Kawai K, Khashabi S, Deng C, Liu YH, Yiu S. Inactivation of Smad4 leads to impaired ocular development and cataract formation. *Biochem Biophys Res Commun*. 2010; 400:476-82.

Livak KJ, Schmittgen TD. Analysis of relative gene expression data using real-time quantitative PCR and the 2(-Delta Delta C(T)) Method. *Methods*. 2001; 25:402-8.

Lovicu FJ, Ang S, Chorazyczewska M, McAvoy JW. Deregulation of lens epithelial cell proliferation and differentiation during the development of TGFbeta-induced anterior subcapsular cataract. *Dev Neurosci.* 2004; 26:446-55.

Ma QL, Zhang GG, Peng J. Vascular peroxidase 1: a novel enzyme in promoting oxidative stress in cardiovascular system. *Trends Cardiovasc Med.* 2013; 23:179-83.

Ma Y, Ma L, Guo Q, Zhang S. Expression of bone morphogenetic protein-2 and its receptors in epithelial ovarian cancer and their influence on the prognosis of ovarian cancer patients. *J Exp Clin Cancer Res.* 2010; 29:85.

Mali RS, Zhang X, Hoerauf W, Doyle D, Devitt J, Loffreda-Wren J, Mitton KP. FIZ1 is expressed during photoreceptor maturation, and synergizes with NRL and CRX at rod-specific promoters in vitro. *Exp Eye Res.* 2007; 84:349-60.

Manuel M, Pratt T, Liu M, Jeffery G, Price DJ. Overexpression of Pax6 results in microphthalmia, retinal dysplasia and defective retinal ganglion cell axon guidance. *BMC Dev Biol.* 2008; 8:59.

Matt N, Ghyselinck NB, Pellerin I, Dupé V. Impairing retinoic acid signalling in the neural crest cells is sufficient to alter entire eye morphogenesis. *Dev Biol.* 2008; 320:140-8.

Mayer EJ, Hughes EH, Carter DA, Dick AD. Nestin positive cells in adult human retina and in epiretinal membranes. *Br J Ophthalmol.* 2003; 87:1154-8.

Medina-Martinez O, Brownell I, Amaya-Manzanares F, Hu Q, Behringer RR, Jamrich M. Severe defects in proliferation and differentiation of lens cells in Foxe3 null mice. *Mol Cell Biol.* 2005; 25:8854-63.

Medina-Martinez O, Jamrich M. Foxe view of lens development and disease. *Development.* 2007; 134:1455-63.

Medina-Martinez O, Shah R, Jamrich M. Pitx3 controls multiple aspects of lens development. *Dev Dyn*. 2009; 238:2193-201.

Meyer E, Michaelides M, Tee LJ, Robson AG, Rahman F, Pasha S, Luxon LM, Moore AT, Maher ER. Nonsense mutation in TMEM126A causing autosomal recessive optic atrophy and auditory neuropathy. *Mol Vis*. 2010; 16:650-64.

Mirzayans F, Pearce WG, MacDonald IM, Walter MA. Mutation of the PAX6 gene in patients with autosomal dominant keratitis. *Am J Hum Genet*. 1995; 57:539-48.

Mitchell MS, Kan-Mitchell J, Minev B, Edman C, Deans RJ. A novel melanoma gene (MG50) encoding the interleukin 1 receptor antagonist and six epitopes recognized by human cytolytic T lymphocytes. *Cancer Res*. 2000; 60:6448-56.

Miyagi M, Mikawa S, Sato T, Hasegawa T, Kobayashi S, Matsuyama Y, Sato K. BMP2, BMP4, noggin, BMPRIA, BMPRIIB, and BMPRII are differentially expressed in the adult rat spinal cord. *Neuroscience*. 2012; 203:12-26.

Murali D, Yoshikawa S, Corrigan RR, Plas DJ, Crair MC, Oliver G, Lyons KM, Mishina Y, Furuta Y. Distinct developmental programs require different levels of Bmp signaling during mouse retinal development. *Development*. 2005; 132: 913-23.

Nanjo Y, Kawasaki S, Mori K, Sotozono C, Inatomi T, Kinoshita S. A novel mutation in the alternative splice region of the PAX6 gene in a patient with Peters' anomaly. *Br J Ophthalmol*. 2004; 88:720-1.

Nelson RE, Fessler LI, Takagi Y, Blumberg B, Keene DR, Olson PF, Parker CG, Fessler JH. Peroxidasin: a novel enzyme-matrix protein of Drosophila development. *EMBO J*. 1994; 13:3438-47.

Nickel J, Kotzsch A, Sebald W, Mueller TD. A single residue of GDF-5 defines binding specificity

to BMP receptor IB. *J Mol Biol.* 2005; 349:933-47.

Nishitoh H, Ichijo H, Kimura M, Matsumoto T, Makishima F, Yamaguchi A, Yamashita H, Enomoto S, Miyazono K. Identification of type I and type II serine/threonine kinase receptors for growth/differentiation factor-5. *J Biol Chem.* 1996; 271:21345-52.

Ohkawa K, Saika S, Hayashi Y, Tawara A, Ohnishi Y. Cornea with Peters' anomaly: perturbed differentiation of corneal cells and abnormal extracellular matrix in the corneal stroma. *Jpn J Ophthalmol.* 2003; 47:327-31.

Ohnuma S, Philpott A, Wang K, Holt CE, Harris WA. p27^{Xic1}, a Cdk inhibitor, promotes the determination of glial cells in *Xenopus* retina. *Cell.* 1999; 99:499-510.

Ohsawa R, Kageyama R. Regulation of retinal cell fate specification by multiple transcription factors. *Brain Res.* 2008; 1192:90-8.

Ordóñez NG. Value of PAX2 immunostaining in tumor diagnosis: a review and update. *Adv Anat Pathol.* 2012; 19:401-9.

Ormestad M, Blixt A, Churchill A, Martinsson T, Enerbäck S, Carlsson P. Foxe3 haploinsufficiency in mice: a model for Peters' anomaly. *Invest Ophthalmol Vis Sci.* 2002 May; 43:1350-7.

Otteson DC, Sheldon E, Jones JM, Kameoka J, Hitchcock PF. Pax2 expression and retinal morphogenesis in the normal and *Krd* mouse. *Dev Biol.* 1998; 193:209-24.

Panchision DM, Pickel JM, Studer L, Lee SH, Turner PA, Hazel TG, McKay RD. Sequential actions of BMP receptors control neural precursor cell production and fate. *Genes Dev.* 2001; 15:2094-110.

Panicker SG, Sampath S, Mandal AK, Reddy AB, Ahmed N, Hasnain SE. Novel mutation in

FOXC1 wing region causing Axenfeld-Rieger anomaly. *Invest Ophthalmol Vis Sci.* 2002; 43:3613-6.

Péterfi Z, Donkó A, Orient A, Sum A, Prókai A, Molnár B, Veréb Z, Rajnavölgyi E, Kovács KJ, Müller V, Szabó AJ, Geiszt M. Peroxidasin is secreted and incorporated into the extracellular matrix of myofibroblasts and fibrotic kidney. *Am J Pathol.* 2009; 175:725-35.

Petros TJ, Rebsam A, Mason CA. Retinal axon growth at the optic chiasm: to cross or not to cross. *Annu Rev Neurosci.* 2008; 31:295-315.

Philips GT, Stair CN, Young Lee H, Wroblewski E, Berberoglu MA, Brown NL, Mastick GS. Precocious retinal neurons: Pax6 controls timing of differentiation and determination of cell type. *Dev Biol.* 2005; 279:308-21.

Pittler SJ, Zhang Y, Chen S, Mears AJ, Zack DJ, Ren Z, Swain PK, Yao S, Swaroop A, White JB. Functional analysis of the rod photoreceptor cGMP phosphodiesterase alpha-subunit gene promoter: Nrl and Crx are required for full transcriptional activity. *J Biol Chem.* 2004; 279:19800-7.

Puk O, Dalke C, Calzada-Wack J, Ahmad N, Klaften M, Wagner S, de Angelis MH, Graw J. Reduced corneal thickness and enlarged anterior chamber in a novel ColVIIIa2G257D mutant mouse. *Invest Ophthalmol Vis Sci.* 2009; 50:5653-61.

Puk O, Dalke C, Favor J, de Angelis MH, Graw J. Variations of eye size parameters among different strains of mice. *Mamm Genome.* 2006;17:851-7.

Puk O, Yan X, Sabrautzki S, Fuchs H, Gailus-Durner V, Hrabě de Angelis M, Graw J. Novel small-eye allele in paired box gene 6 (Pax6) is caused by a point mutation in intron 7 and creates a new exon. *Mol Vis.* 2013; 19:877-84.

Pulkki MM, Mottershead DG, Pasternack AH, Muggalla P, Ludlow H, van Dinther M, Myllymaa

S, Koli K, ten Dijke P, Laitinen M, Ritvos O. A covalently dimerized recombinant human bone morphogenetic protein-15 variant identifies bone morphogenetic protein receptor type 1B as a key cell surface receptor on ovarian granulosa cells. *Endocrinology*. 2012; 153:1509-18.

Qin L, Wine-Lee L, Ahn KJ, Crenshaw EB 3rd. Genetic analyses demonstrate that bone morphogenetic protein signaling is required for embryonic cerebellar development. *J Neurosci*. 2006; 26:1896-905.

Quigley HA. Glaucoma. *Lancet*. 2011; 377:1367-77.

Rajagopal R, Dattilo LK, Kaartinen V, Deng CX, Umans L, Zwijsen A, Roberts AB, Bottinger EP, Beebe DC. Functions of the type 1 BMP receptor *Acvr1* (*Alk2*) in lens development: cell proliferation, terminal differentiation, and survival. *Invest Ophthalmol Vis Sci*. 2008; 49:4953-60.

Rajagopal R, Huang J, Dattilo LK, Kaartinen V, Mishina Y, Deng CX, Umans L, Zwijsen A, Roberts AB, Beebe DC. The type I BMP receptors, *Bmpr1a* and *Acvr1*, activate multiple signaling pathways to regulate lens formation. *Dev Biol*. 2009; 335:305-16.

Ramaesh T, Collinson JM, Ramaesh K, Kaufman MH, West JD, Dhillon B. Corneal abnormalities in *Pax6*^{+/-} small eye mice mimic human aniridia-related keratopathy. *Invest Ophthalmol Vis Sci*. 2003; 44:1871-8.

Reader KL, Haydon LJ, Littlejohn RP, Juengel JL, McNatty KP. Booroola *BMPR1B* mutation alters early follicular development and oocyte ultrastructure in sheep. *Reprod Fertil Dev*. 2012; 24:353-61.

Reese BE. Development of the retina and optic pathway. *Vision Res*. 2011; 51:613-32.

Reichenbach A, Wohlrab F. Morphometric parameters of Müller (glial) cells dependent on their topographic localization in the nonmyelinated part of the rabbit retina. A consideration of functional aspects of radial glia. *J Neurocytol*. 1986; 15:451-9.

Reis LM, Semina EV. Genetics of anterior segment dysgenesis disorders. *Curr Opin Ophthalmol*. 2011; 22:314-24.

Reis LM, Tyler RC, Schneider A, Bardakjian T, Stoler JM, Melancon SB, Semina EV. FOXE3 plays a significant role in autosomal recessive microphthalmia. *Am J Med Genet A*. 2010; 152A:582-90.

Rieger DK, Reichenberger E, McLean W, Sidow A, Olsen BR. A double-deletion mutation in the Pitx3 gene causes arrested lens development in aphakia mice. *Genomics*. 2001; 72:61-72.

Riise R, Storhaug K, Brøndum-Nielsen K. Rieger syndrome is associated with PAX6 deletion. *Acta Ophthalmol Scand*. 2001; 79:201-3.

Robinson ML. An essential role for FGF receptor signaling in lens development. *Semin Cell Dev Biol*. 2006; 17:726-40.

Rødahl E, Knappskog PM, Majewski J, Johansson S, Telstad W, Kråkenes J, Boman H. Variants of Anterior Segment Dysgenesis and Cerebral Involvement in a Large Family With a Novel COL4A1 Mutation. *Am J Ophthalmol*. 2013; 155:946-953.

Roelen BA, Goumans MJ, van Rooijen MA, Mummery CL. Differential expression of BMP receptors in early mouse development. *Int J Dev Biol*. 1997; 41:541-9.

Rosemann M, Ivashkevich A, Favor J, Dalke C, Hölter SM, Becker L, RácZ I, Bolle I, Klempt M, Rathkolb B, Kalaydjiev S, Adler T, Aguilar A, Hans W, Horsch M, Rozman J, Calzada-Wack J, Kunder S, Naton B, Gailus-Durner V, Fuchs H, Schulz H, Beckers J, Busch DH, Burbach JP, Smidt MP, Quintanilla-Martinez L, Esposito I, Klopstock T, Klingenspor M, Ollert M, Wolf E, Wurst W, Zimmer A, de Angelis MH, Atkinson M, Heinzmann U, Graw J. Microphthalmia, parkinsonism, and enhanced nociception in Pitx3 (416insG) mice. *Mamm Genome*. 2010; 21:13-27.

Sahni V, Mukhopadhyay A, Tysseling V, Hebert A, Birch D, Mcguire TL, Stupp SI, Kessler JA. BMPR1a and BMPR1b signaling exert opposing effects on gliosis after spinal cord injury. *J Neurosci.* 2010; 30:1839-55.

Sansom SN, Griffiths DS, Faedo A, Kleinjan DJ, Ruan Y, Smith J, van Heyningen V, Rubenstein JL, Livesey FJ. The level of the transcription factor Pax6 is essential for controlling the balance between neural stem cell self-renewal and neurogenesis. *PLoS Genet.* 2009; 5:e1000511.

Sanyanusin P, Schimmenti LA, McNoe LA, Ward TA, Pierpont ME, Sullivan MJ, Dobyns WB, Eccles MR. Mutation of the PAX2 gene in a family with optic nerve colobomas, renal anomalies and vesicoureteral reflux. *Nat Genet.* 1995; 9:358-64.

Sarkar A, Hochedlinger K. The sox family of transcription factors: versatile regulators of stem and progenitor cell fate. *Cell Stem Cell.* 2013; 12:15-30.

Sarthy V. Collagen IV mRNA expression during development of the mouse retina: an in situ hybridization study. *Invest Ophthalmol Vis Sci.* 1993; 34:145-52.

Schedl A, Ross A, Lee M, Engelkamp D, Rashbass P, van Heyningen V, Hastie ND. Influence of PAX6 gene dosage on development: overexpression causes severe eye abnormalities. *Cell.* 1996; 86:71-82.

Schimmenti LA, Manligas GS, Sieving PA. Optic nerve dysplasia and renal insufficiency in a family with a novel PAX2 mutation, Arg115X: further ophthalmologic delineation of the renal-coloboma syndrome. *Ophthalmic Genet.* 2003; 24:191-202.

Schumann RG, Eibl KH, Zhao F, Scheerbaum M, Scheler R, Schaumberger MM, Wehnes H, Walch AK, Haritoglou C, Kampik A, Gandorfer A. Immunocytochemical and ultrastructural evidence of glial cells and hyalocytes in internal limiting membrane specimens of idiopathic macular holes. *Invest Ophthalmol Vis Sci.* 2011; 52:7822-34.

See J, Mamontov P, Ahn K, Wine-Lee L, Crenshaw EB 3rd, Grinspan JB. BMP signaling mutant mice exhibit glial cell maturation defects. *Mol Cell Neurosci*. 2007; 35:171-82.

Seemann P, Schwappacher R, Kjaer KW, Krakow D, Lehmann K, Dawson K, Stricker S, Pohl J, Plöger F, Staub E, Nickel J, Sebald W, Knaus P, Mundlos S. Activating and deactivating mutations in the receptor interaction site of GDF5 cause symphalangism or brachydactyly type A2. *J Clin Invest*. 2005; 115:2373-81.

Sehgal R, Karcavich R, Carlson S, Belecky-Adams TL. Ectopic Pax2 expression in chick ventral optic cup phenocopies loss of Pax2 expression. *Dev Biol*. 2008; 319:23-33.

Sehgal R, Sheibani N, Rhodes SJ, Belecky Adams TL. BMP7 and SHH regulate Pax2 in mouse retinal astrocytes by relieving TLX repression. *Dev Biol*. 2009; 332:429-43.

Semina E, Murray JC, Reiter R, Hrstka RF, Graw J. Deletion in the promotor region and altered expression of Pitx3 homeobox gene in aphakia mice. *Hum Mol Genet*. 2000; 9:1575–1585.

Semina EV, Brownell I, Mintz-Hittner HA, Murray JC, Jamrich M. Mutations in the human forkhead transcription factor FOXE3 associated with anterior segment ocular dysgenesis and cataracts. *Hum Mol Genet*. 2001; 10:231-6.

Semina EV, Ferrell RE, Mintz-Hittner HA, Bitoun P, Alward WL, Reiter RS, Funkhauser C, Daack-Hirsch S, Murray JC. A novel homeobox gene PITX3 is mutated in families with autosomal-dominant cataracts and ASMD. *Nat Genet*. 1998; 19:167-70.

Seo S, Singh HP, Lacal PM, Sasman A, Fatima A, Liu T, Schultz KM, Losordo DW, Lehmann OJ, Kume T. Forkhead box transcription factor FoxC1 preserves corneal transparency by regulating vascular growth. *Proc Natl Acad Sci U S A*. 2012; 109:2015-20.

Shaham O, Menuchin Y, Farhy C, Ashery-Padan R. Pax6: a multi-level regulator of ocular development. *Prog Retin Eye Res*. 2012; 31:351-76.

Shigeyasu C, Yamada M, Mizuno Y, Yokoi T, Nishina S, Azuma N. Clinical features of anterior segment dysgenesis associated with congenital corneal opacities. *Cornea*. 2012; 31:293-8.

Shimasaki S, Moore RK, Erickson GF, Otsuka F. The role of bone morphogenetic proteins in ovarian function. *Reprod Suppl*. 2003; 61:323-37.

Shukla S, Mishra R. Functional analysis of missense mutations G36A and G51A in PAX6, and PAX6 (5a) causing ocular anomalies. *Exp Eye Res*. 2011; 93:40-9.

Skarie JM, Link BA. FoxC1 is essential for vascular basement membrane integrity and hyaloid vessel morphogenesis. *Invest Ophthalmol Vis Sci*. 2009; 50:5026-34.

Smith RS, Zabaleta A, Kume T, Savinova OV, Kidson SH, Martin JE, Nishimura DY, Alward WL, Hogan BL, John SW. Haploinsufficiency of the transcription factors FOXC1 and FOXC2 results in aberrant ocular development. *Hum Mol Genet*. 2000; 9:1021-32.

Soto I, Oglesby E, Buckingham BP, Son JL, Roberson ED, Steele MR, Inman DM, Vetter ML, Horner PJ, Marsh-Armstrong N. Retinal ganglion cells downregulate gene expression and lose their axons within the optic nerve head in a mouse glaucoma model. *J Neurosci*. 2008; 28:548-61.

Soukkaieh C, Agius E, Soula C, Cochard P. Pax2 regulates neuronal-glial cell fate choice in the embryonic optic nerve. *Dev Biol*. 2007; 303:800-13.

Souza CJ, Campbell BK, McNeilly AS, Baird DT. Effect of bone morphogenetic protein 2 (BMP2) on oestradiol and inhibin A production by sheep granulosa cells, and localization of BMP receptors in the ovary by immunohistochemistry. *Reproduction*. 2002; 123:363-9.

Sowden JC. Molecular and developmental mechanisms of anterior segment dysgenesis. *Eye (Lond)*. 2007; 21:1310-8.

- Sowka J, Vollmer L, Falco L. Rapid onset phacolytic glaucoma. *Optometry*. 2004; 75(9):571-6.
- Srinivasan Y, Lovicu FJ, Overbeek PA. Lens-specific expression of transforming growth factor beta1 in transgenic mice causes anterior subcapsular cataracts. *J Clin Invest*. 1998; 101:625-34.
- Steinhart MR, Cone FE, Nguyen C, Nguyen TD, Pease ME, Puk O, Graw J, Oglesby EN, Quigley HA. Mice with an induced mutation in collagen 8A2 develop larger eyes and are resistant to retinal ganglion cell damage in an experimental glaucoma model. *Mol Vis*. 2012; 18:1093-106.
- Stone J, Dreher Z. Relationship between astrocytes, ganglion cells and vasculature of the retina. *J Comp Neurol*. 1987; 255:35-49.
- Surzenko N, Crowl T, Bachleda A, Langer L, Pevny L. SOX2 maintains the quiescent progenitor cell state of postnatal retinal Muller glia. *Development*. 2013; 140:1445-56.
- Tagami M, Honda S, Morioka I, Matsuo M, Negi A. Bilateral Optic Disc Anomalies Associated with PAX2 Mutation in a Case of Potter Sequence. *Case Report Ophthalmol*. 2010; 1:94-98.
- Tamimi Y, Skarie JM, Footz T, Berry FB, Link BA, Walter MA. FGF19 is a target for FOXC1 regulation in ciliary body-derived cells. *Hum Mol Genet*. 2006; 15:3229-40.
- Tholozan FM, Sanderson JM, Quinlan RA. Focus on molecules: FoxE3. *Exp Eye Res*. 2007; 84:799-800.
- Tindall AJ, Pownall ME, Morris ID, Isaacs HV. *Xenopus tropicalis* peroxidase gene is expressed within the developing neural tube and pronephric kidney. *Dev Dyn*. 2005; 232:377-84.
- Tomita K, Moriyoshi K, Nakanishi S, Guillemot F, Kageyama R. Mammalian achaete-scute and atonal homologs regulate neuronal versus glial fate determination in the central nervous system. *EMBO J*. 2000; 19:5460-72.
- Van Agtmael T, Schlötzer-Schrehardt U, McKie L, Brownstein DG, Lee AW, Cross SH, Sado Y,

Mullins JJ, Pöschl E, Jackson IJ. Dominant mutations of Col4a1 result in basement membrane defects which lead to anterior segment dysgenesis and glomerulopathy. *Hum Mol Genet.* 2005; 14:3161-8.

van Roy F, Berx G. The cell-cell adhesion molecule E-cadherin. *Cell Mol Life Sci.* 2008; 65:3756-88.

Vázquez-Chona FR, Swan A, Ferrell WD, Jiang L, Baehr W, Chien WM, Fero M, Marc RE, Levine EM. Proliferative reactive gliosis is compatible with glial metabolic support and neuronal function. *BMC Neurosci.* 2011; 12:98.

Vieira V, David G, Roche O, de la Houssaye G, Boutboul S, Arbogast L, Kobetz A, Orssaud C, Camand O, Schorderet DF, Munier F, Rossi A, Delezoide AL, Marsac C, Ricquier D, Dufier JL, Menasche M, Abitbol M. Identification of four new PITX2 gene mutations in patients with Axenfeld-Rieger syndrome. *Mol Vis.* 2006; 12:1448-60.

Vincent MC, Gallai R, Olivier D, Speeg-Schatz C, Flament J, Calvas P, Dollfus H. Variable phenotype related to a novel PAX 6 mutation (IVS4+5G>C) in a family presenting congenital nystagmus and foveal hypoplasia. *Am J Ophthalmol.* 2004; 138:1016-21.

Wan J, Zheng H, Xiao HL, She ZJ, Zhou GM. Sonic hedgehog promotes stem-cell potential of Müller glia in the mammalian retina. *Biochem Biophys Res Commun.* 2007; 363:347-54.

Watanabe T, Raff MC. Retinal astrocytes are immigrants from the optic nerve. *Nature.* 1988; 332:834-7.

Weisschuh N, Wolf C, Wissinger B, Gramer E. A novel mutation in the FOXC1 gene in a family with Axenfeld-Rieger syndrome and Peters' anomaly. *Clin Genet.* 2008; 74:476-80.

Weng J, Luo J, Cheng X, Jin C, Zhou X, Qu J, Tu L, Ai D, Li D, Wang J, Martin JF, Amendt BA, Liu M. Deletion of G protein-coupled receptor 48 leads to ocular anterior segment dysgenesis

(ASD) through down-regulation of Pitx2. *Proc Natl Acad Sci U S A.* 2008; 105:6081-6.

Weston CR, Wong A, Hall JP, Goad ME, Flavell RA, Davis RJ. JNK initiates a cytokine cascade that causes Pax2 expression and closure of the optic fissure. *Genes Dev.* 2003; 17:1271-80.

Wigle JT, Chowdhury K, Gruss P, Oliver G. Prox1 function is crucial for mouse lens-fibre elongation. *Nat Genet.* 1999; 21:318-22.

Wine-Lee L, Ahn KJ, Richardson RD, Mishina Y, Lyons KM, Crenshaw EB 3rd. Signaling through BMP type 1 receptors is required for development of interneuron cell types in the dorsal spinal cord. *Development.* 2004; 131:5393-403.

Wride MA. Lens fibre cell differentiation and organelle loss: many paths lead to clarity. *Philos Trans R Soc Lond B Biol Sci.* 2011; 366:1219-33.

Xiao J, Wang Y, Wu S, Li J, Zhang S. Inhibitory effect of tetrandrine on lens proteins-induced ocular inflammation in rabbits. *J Ocul Pharmacol.* 1992; 8:309-15.

Yahyavi M, Abouzeid H, Gawdat G, de Preux AS, Xiao T, Bardakjian T, Schneider A, Choi A, Jorgenson E, Baier H, El Sada M, Schorderet DF, Slavotinek AM. ALDH1A3 loss of function causes bilateral anophthalmia/microphthalmia and hypoplasia of the optic nerve and optic chiasm. *Hum Mol Genet.* 2013; 22:3250-8.

Yamada N, Kato M, ten Dijke P, Yamashita H, Sampath TK, Heldin CH, Miyazono K, Funahashi K. Bone morphogenetic protein type IB receptor is progressively expressed in malignant glioma tumours. *Br J Cancer.* 1996; 73:624-9.

Yamauchi K, Phan KD, Butler SJ. BMP type I receptor complexes have distinct activities mediating cell fate and axon guidance decisions. *Development.* 2008; 135:1119-28.

Yang Z, Ding K, Pan L, Deng M, Gan L. Math5 determines the competence state of retinal ganglion cell progenitors. *Dev Biol.* 2003; 264:240-54.

Yoon BS, Ovchinnikov DA, Yoshii I, Mishina Y, Behringer RR, Lyons KM. *Bmpr1a* and *Bmpr1b* have overlapping functions and are essential for chondrogenesis in vivo. *Proc Natl Acad Sci U S A*. 2005; 102:5062-7.

You L, Kruse FE, Pohl J, Völcker HE. Bone morphogenetic proteins and growth and differentiation factors in the human cornea. *Invest Ophthalmol Vis Sci*. 1999; 40:296-311.

Yuan A, Rao MV, Veeranna, Nixon RA. Neurofilaments at a glance. *J Cell Sci*. 2012; 125:3257-63.

Zahrani F, Aldahmesh MA, Alshammari MJ, Al-Hazzaa SA, Alkuraya FS. Mutations in *c12orf57* cause a syndromic form of colobomatous microphthalmia. *Am J Hum Genet*. 2013; 92:387-91.

Zeisberg M, Neilson EG. Biomarkers for epithelial-mesenchymal transitions. *J Clin Invest*. 2009; 119:1429-37.

Zhang W, Maric D, Fine HA. Epigenetic-mediated dysfunction of the bone morphogenetic protein pathway inhibits differentiation of glioblastoma-initiating cells. *Cancer Cell*. 2008; 13:69-80.

Zhang Y, Liu Y, Wildsoet CF. Bidirectional, optical sign-dependent regulation of *BMP2* gene expression in chick retinal pigment epithelium. *Invest Ophthalmol Vis Sci*. 2012; 53:6072-80.

Zhao J, Kawai K, Wang H, Wu D, Wang M, Yue Z, Zhang J, Liu YH. Loss of *Msx2* function down-regulates the *FoxE3* expression and results in anterior segment dysgenesis resembling Peters anomaly. *Am J Pathol*. 2012; 180:2230-9.

Zhao M, Harris SE, Horn D, Geng Z, Nishimura R, Mundy GR, Chen D. Bone morphogenetic protein receptor signaling is necessary for normal murine postnatal bone formation. *J Cell Biol*. 2002; 157:1049-60.

8. Abbreviations

ALDH1A3	Aldehyde dehydrogenase family 1, subfamily A3
AP2α	Transcription factor AP-2-alpha
ASD	Anterior segment dysgenesis
bHLH	basic helix-loop-helix
Barhl2	BarH-like homeobox 2
Beta igh3	Transforming growth factor-beta-induced gene
BMP	Bone morphogenetic protein
BR	Bmp receptors
Brn3	POU-domain transcription factors
Bmpr1a	Bone morphogenetic protein receptor, type Ia
Bmpr1b	Bone morphogenetic protein receptor, type Ib
BrdU	5-Bromo-2'-Deoxyuridine
C12orf57	Chromosome 12 open reading frame 57
cDNA	Complementary DNA
Chx10	Ceh-10 homeodomain containing homolog
CO₂	Carbon dioxide
COL	Collagen
CRALBP	Cellular retinaldehyde binding protein
Crybb1	β B1-Crystallin
DAPI	4', 6-diamidino-2-phenylindole
DEPC	Diethylpyrocarbonate

DIG	Digoxigenin
DiI	1, 1'-dioctadecyl-3, 3, 3', 3'-tetramethylindocarbocyanine perchlorate
DiO	3, 3'-Dioctadecyloxacarbocyanine perchlorate
DNA	Deoxyribonucleic acid
Dyl	Dysgenetic lens
dNTPs	Deoxyribonucleotide triphosphates
ECM	Extracellular matrix
EDTA	Ethylenediaminetetraacetic acid
EM	Electron microscopy
ENU	N-ethyl-N-nitrosourea
ERG	Electroretinography
ERM	Epiretinal membrane
FBS	Fetal bovine serum
FCS	Fetal calf serum
FGF19	Fibroblast growth factor-19
Foxc1	Forkhead box C1
Foxe3	Forkhead box protein E3
Foxn4	Forkhead box N4
GCL	Retinal ganglion cell layer
GDF-5	Growth and differentiation factor 5
GFAP	Glial fibrillary acidic protein
GMC	German mouse clinic
GPCRs	G protein-coupled receptors

Gpr48	G protein–coupled receptor 48
Grg4	Groucho/TLE family protein 4
GS	Glutamine synthetase.
HCl	Hydrochloric acid
Hes	Hairy and enhancer of split
HMGU	Helmholtz Center Munich or German Research Center for Environmental Health
IL	Interleukin
ILM	Inner limiting membrane
INL	Inner nuclear layer
INbL	Inner neuroblast layer
IPL	Inner plexiform layer
IPTG	Isopropylthio- β -galactoside
JNK	C-Jun NH ₂ -terminal kinase
KCl	Potassium chloride
LB	Lysogeny broth
LDL	Low-density lipoprotein
Lhx2	LIM homeodomain transcription factor
MAP2	Microtubule-associated protein
Mash1	Mammalian achaete-scute homolog 1
Math5	Helix-loop-helix protein mATH-5
MG50	MELANOMA-ASSOCIATED GENE 50
MIO-MI	Moorfields/Institute of Ophthalmology–Müller 1
MITF	Microphthalmia-associated transcription factor

MMP	Matrix metalloproteinases
Msx-2	Msh homeobox 2
NaCl	Sodium chloride
NaOH	Sodium hydroxide
NGF	Nerve growth factor
ODZ3	Odd Oz/ten-m homolog 3, a transmembrane protein
ONH	Optic nerve head
ONL	Outer nuclear layer
ONbL	Outer neuroblast layer
OPL	Outer plexiform layer
OS	Outer Segment
Otx2	Orthodenticle homeobox 2
Ox-LDL	Oxidized low-density lipoprotein
P21	Protein 21 or tumor protein 21
P27	Protein 27 or tumor protein 27
P53	Protein 53 or tumor protein 53
Pax2	Paired box gene 2
Pax6	Paired box 6
PBS	Phosphate buffered saline
PCR	Polymerase chain reaction
Pde6b	Beta- subunit of phosphodiesterase-6
PFA	Paraformaldehyde
Pitx2	Paired-like homeodomain 2

Pitx3	Paired-like homeodomain 3
PKC-α	Protein kinase C-alpha
Prox1	Prospero homeobox 1
PVR	Proliferative vitreous-retina diseases
PXDN	Peroxidasin
PXN	Peroxidasin (Drosophila)
qRT-PCR	quantitative reverse transcription PCR
RGC	Retinal ganglion cell
RNA	Ribonucleic acid
RPE	Retina pigmental epithelium
SD-OCT	Spectral domain optical coherence tomography
Shh	Sonic hedgehog
Sox2	SRY (sex determining region Y)-box 2
TGFβ1	Transforming growth factor beta 1
TMEM126A	Transmembrane protein 126A
TNF-α	Tumor necrosis factor alpha
TUBA8	Alpha-tubulin 8
VEP	Visually evoked potential
VPO1	Vascular peroxidase 1
VMT	Vitreomacular traction
vWF	Von Willebrand factor

5 Acknowledgements

First of all, I would like to express my deepest gratitude to my supervisor, Prof. Dr. Jochen Graw, for providing me with the opportunity to do my PhD work in the Institute of Developmental Genetics, Helmholtz Center Munich and I appreciate his support and guidance during the thesis work.

I would like to sincerely thank Prof. Dr. Anselm Kampik for providing me with an opportunity to study in the Department of Ophthalmology, LMU. I appreciate his support and guidance in clinical and research training during my fellowship there. I would like to thank Prof. Dr. Ernst Tamm for his guidance in the thesis committee meeting.

Moreover, I would like to sincerely thank Chinese Scholarship Council to provide me with the financial support during the PhD period. I would like to sincerely thank Prof. Dr. Alexander Baethmann and Dr. Matthias Hadesbeck for their support to apply for the CSC-LMU PhD programme.

I also would like to sincerely thank our collaborators for their significant and fruitful contributions in this work: Dr. Petrovski (Hungary) and Dr. Lumi (Slovenia) for their great help to provide ERM and ILM samples; Dr. Marion Horsch for her microarray experiments; Prof. Dr. Jan Kremers and Dr. Jenny Atorf for their VEP and ERG measurements.

Furthermore, I would like to thank all members of our group (Dr. Oliver Puk, Dr. Claudia Dalke, Dr. Naffees Ahmed, Dr. Mingxuan Sun, Mrs. Erika Bürkle, Mrs. Monika Stadler, Mrs. Maria Kulge, Mrs. Marija Ram) for having shared with me their experiences. I would like to thank all the colleagues in the institute for their kind help, especially to Prof. Dr. Wolfgang Wurst, the director of IDG, for creating a dynamic, international, scientific and friendly atmosphere.

I also would like to thank all the colleagues from Department of Ophthalmology, LMU for their kind help and sharing me with their clinical and research experiences during my fellowship there. Especially, I would like to sincerely thank Prof. Dr. Gerhild Wildner and Prof. Dr. Stephan Thureau for their guidance during my fellowship, and I would like to sincerely thank Dr. Maria Diedrichs-Möhring, Dr. Alice Yu and Dr. Armin Wolf for their care and help.

Finally, I especially thank my parents and my wife Chen for their unending love and support.